**Title**
Biogeography and Evolution of Montane Birds across Nuclear Central America



**Author**
Jimenez Barrios, Rosa Alicia

**Publication Date**
2021

Peer reviewed|Thesis/dissertation

# Biogeography and Evolution of Montane Birds across Nuclear Central America

By

Rosa A. Jimenez Barrios

A dissertation submitted in partial satisfaction of the

requirements for the degree of

Doctor of Philosophy

in

Integrative Biology

in the

Graduate Division

of the

University of California, Berkeley

Committee in charge:

Professor Rauri C. K. Bowie, Chair
Professor Jimmy A. McGuire
Associate Professor Ian J. Wang

Fall 2021

Abstract

Biogeography and Evolution of Montane Birds across Nuclear Central America

by

Rosa A. Jimenez Barrios

Doctor of Philosophy in Integrative Biology

University of California, Berkeley

Professor Rauri C. K. Bowie, Chair

This dissertation aims to understand the patterns and processes involved in the origin, maintenance, and diversification of montane birds in Nuclear Central America. Nuclear Central America, the region between the Isthmus of Tehuantepec and the Nicaraguan Depression, is an understudied tropical, but highly biodiverse region. We assemble genetic, morphological, and climatic datasets to uncover biogeographic and evolutionary processes across a spatial and temporal continuum. We report genomic data from 850 individuals representing ten bird species from the mountains of Nuclear Central America, and using these data we detect several new biogeographic breaks. This dissertation constitutes the first study incorporating genomic data to understand evolutionary processes underpinning bird diversity in Nuclear Central America.

Chapter 1 reveals that historical and contemporary processes have fueled *in situ* diversification within Nuclear Central America. We study *Lampornis viridipallens* and *L. sybillae* integrating phylogeography, landscape genetics, ecological niche modeling, and morphological measurements to understand diversification across the species-population interface. Mitochondrial and microsatellite data indicate that *L. viridipallens* and *L. sybillae* diverged in allopatry during the early Pleistocene on either side of the Honduras Depression. This divergence was followed or accompanied by ecological niche divergence. Within *L. viridipallens*, dry valleys that separate mountain ranges are geographic barriers promoting isolation in this hummingbird species restricted to cloud forests. Moreover, environmental variables are much more critical for facilitating gene flow and population connectivity than straight-line geographic distance.

Chapter 2 highlights the importance of assessing multiple processes to understand the origin and maintenance of biodiversity, especially in topographically complex regions such as the Neotropics. We investigate the phylogeography and genetic basis of phenotype-genotype discordance in *Atlapetes albinucha* across its geographic range, from Mexico to Colombia. We assemble mitochondrial and genomic data of 73 individuals, including the yellow and gray phenotypes of the species. Our analyses show that allopatric divergence results in high geographic genetic structure. Additionally, we included two individuals with intermediate phenotypes. Ours is the first report of hybridization between the two plumage color phenotypes. We describe the environment where the barrier between the yellow and gray phenotypes occurs

(biogeographic barrier east to Altos de Chiapas). We find that high precipitation and low elevation limit the geographic range of both phenotypes and provide a different environment in the hybrid zone. Furthermore, our genomic data suggests UDP-glucuronosyltransferase as a candidate gene explaining the presence-absence of yellow color in the ventral feathers of *A. albinucha*.

Chapter 3 investigates that the evolutionary and biogeographic history of *Saucerottia* hummingbirds and sets the biological stage for understanding the genetic basis of structural color variation in hummingbird plumage. We integrate mitochondrial and genomic data of 128 individuals, including representation from Mexico to Guyana, to understand phylogenetic relationships and the geographic distribution of genetic variation. Additionally, we examine and describe the physical structure of rufous, blue, and intermediately colored tail feathers. Our results demonstrate that shallow divergence and mixed ancestry in *Saucerottia* provide similar genetic backgrounds across species. Evolutionary labile tail coloration occurs across multiple species pairs differing mainly in structural coloration. Geographically detailed sampling within Nuclear Central America uncovers divergence consistent with the geographic distribution of tail color variants. We also identify various candidate genes related to the melanin biosynthesis pathway that may underlie variation in structural coloration.

Chapter 4 reports that the current mountain bird assemblage in Nuclear Central America results from common biogeographic history and species idiosyncratic evolutionary paths. Through a comparative phylogeographic approach, we examine mitochondrial and genomic data of 676 individuals comprising the bird species: *Lampornis viridipallens*, *L. sybillae*, *Henicorhina leucophrys*, *Basileuterus belli*, *Myioborus miniatus*, *Chlorospingus flavopectus*, and *Arremon brunneinucha*. Phylogenetic analyses support the role of Nuclear Central America as the interconnection between the avian fauna of North and South America. Additionally, high levels of population genetic structure among different mountain ranges within Nuclear Central America suggest *in situ* diversification. We show that the isolating effect of the Motagua-Polochic-Jocotán Fault System is not homogenous along its extent and that the biogeographic barrier east to Altos de Chiapas is essential to isolating montane populations from one another.

Resumen

Biogeografía y Evolución de Aves de Montaña en Centroamérica Nuclear

por

Rosa A. Jimenez Barrios

Doctora en Filosofía en Biología Integrativa

Universidad de California, Berkeley

Profesor Rauri C. K. Bowie, Asesor

Esta tesis tiene como objetivo comprender los patrones y procesos involucrados en el origen, mantenimiento y diversificación de las aves de montaña de Centroamérica Nuclear. Centroamérica Nuclear, la región entre el Istmo de Tehuantepec y la Depresión de Nicaragua, es una región tropical poco estudiada pero con una gran biodiversidad. Recopilamos datos genéticos, morfológicos y climáticos para descubrir procesos biogeográficos y evolutivos a través de un continuo espacial y temporal. Reportamos datos genómicos de 850 individuos que representan diez especies de aves de las montañas de Centroamérica Nuclear y usando estos datos detectamos varias barreras biogeográficas nuevas. Esta tesis constituye el primer estudio que incorpora datos genómicos para comprender los procesos evolutivos que sustentan la diversidad de aves en Centroamérica Nuclear.

El Capítulo 1 revela que procesos históricos y contemporáneos han impulsado la diversificación *in situ* dentro de Centroamérica Nuclear. Estudiamos a las especies *Lampornis viridipallens* y *L. sybillae* integrando filogeografía, genética del paisaje, modelado de nicho ecológico y morfología para comprender la diversificación en la interfaz especie-población. Los datos mitocondriales y de microsatélites indican que *L. viridipallens* y *L. sybillae* divergieron en alopatría durante el Pleistoceno temprano a ambos lados de la Depresión de Honduras. Esta divergencia fue seguida o acompañada por divergencia de nicho ecológico. Dentro de *L. viridipallens*, los valles secos que separan las cadenas montañosas son barreras geográficas que promueven el aislamiento de esta especie de colibrí restringida a los bosques nubosos. Además, las variables ambientales son mucho más críticas para facilitar el flujo de genes y la conectividad de las poblaciones en relación a la distancia geográfica.

El Capítulo 2 destaca la importancia de evaluar múltiples procesos para comprender el origen y mantenimiento de la biodiversidad, especialmente en regiones topográficamente complejas como el Neotrópico. Investigamos la filogeografía y la base genética de la discordancia fenotipo-genotipo en *Atlapetes albinucha* a lo largo de su área de distribución, desde México hasta Colombia. Recopilamos datos mitocondriales y genómicos de 73 individuos, incluyendo los dos fenotipos de la especie, amarillo y gris. Nuestros análisis muestran que la divergencia en alopatría da como resultado alta estructuración genética. Además, incluimos dos individuos con fenotipos intermedios entre el amarillo y el gris. Este constituye el primer reporte de hibridación

entre los dos fenotipos de coloración del plumaje. Describimos el ambiente donde ocurre la barrera entre los fenotipos amarillo y gris (barrera biogeográfica al este de los Altos de Chiapas). Encontramos que la alta precipitación y la baja elevación limitan el área de distribución de ambos fenotipos y a la vez proporcionan un ambiente diferente en donde ocurre una zona de hibridación. Además, nuestros datos genómicos sugieren que el gen que codifica la proteína UDP-glucuronosiltransferasa es un gen candidato que explica la presencia-ausencia de color amarillo en las plumas ventrales de *A. albinucha*.

El Capítulo 3 investiga la historia evolutiva y biogeográfica de los colibríes *Saucerottia* y establece el escenario biológico para comprender la base genética de la variación de color estructural en el plumaje de los colibríes. Integramos datos mitocondriales y genómicos de 128 individuos, incluyendo representación desde México hasta Guyana, para comprender las relaciones filogenéticas y la distribución geográfica de la variación genética. Además, examinamos y describimos la estructura física de las plumas de la cola de color rojizo, azul e intermedio. Nuestros resultados demuestran que la divergencia reciente y la ascendencia mixta en *Saucerottia* proporcionan una base genética similar en todas las especies. La coloración de la cola evolutivamente lábil ocurre en múltiples pares de especies que difieren principalmente en la coloración estructural. El muestreo geográficamente detallado dentro de Centroamérica Nuclear muestra divergencias consistentes con la distribución geográfica de las variantes del color de la cola. También identificamos varios genes candidatos relacionados con la ruta de biosíntesis de la melanina, los cuales pueden ser la base de la variación en la coloración estructural.

El Capítulo 4 informa que el ensamble actual de aves de montaña de Centroamérica Nuclear es el resultado de una historia biogeográfica común y de la evolución idiosincrática de las especies. Mediante un enfoque filogeográfico comparativo examinamos datos mitocondriales y genómicos de 676 individuos que comprenden las especies de aves: *Lampornis viridipallens*, *L. sybillae*, *Henicorhina leucophrys*, *Basileuterus belli*, *Myioborus miniatus*, *Chlorospingus flavopectus* y *Arremon brunneinucha*. Los análisis filogenéticos apoyan el papel de Centroamérica Nuclear en interconectar la avifauna de América del Norte y del Sur. Además, los altos niveles de estructura genética poblacional entre diferentes cadenas montañosas dentro de Centroamérica Nuclear sugieren diversificación *in situ*. Mostramos que el efecto de aislamiento que genera el Sistema de Fallas Motagua-Polochic-Jocotán no es homogéneo en toda su extensión y que la barrera biogeográfica al este de los Altos de Chiapas es fundamental para aislar las poblaciones de aves de montaña.

To the present and future generations of Biology students in Guatemala,
to motivate them to study our wonderful biodiversity.

A las presentes y futuras generaciones de estudiantes de Biología en Guatemala,
para motivarles a estudiar nuestra maravillosa biodiversidad.

Table of Contents

# Acknowledgments

Institutional and funding support: Universidad de San Carlos de Guatemala; Museum of Vertebrate Zoology and Department of Integrative Biology at the University of California, Berkeley; Faculty for the Future program of the Schlumberger Foundation; Fulbright-Laspau program of the United States Department of State; National Science Foundation; Center for Latin American Studies at the University of California, Berkeley.

Dissertation Committee: Dr. Rauri C. K. Bowie, Dr. Jimmy A. McGuire, Dr. Ian J. Wang.

Qualifying Exam Committee: Dr. Jimmy A. McGuire, Dr. Ian J. Wang, Dr. Eileen A. Lacey, Dr. Steven R. Beissinger.

This dissertation was possible thanks to the collaborative research and scientific collection of specimens in joint expeditions conducted by the Museum of Vertebrate Zoology, University of California, Berkeley; Escuela de Biología, Universidad de San Carlos de Guatemala; and Museo de Zoología "Alfonso R. Herrera", Universidad Nacional Autónoma de México.

Museum support through loans: American Museum of Natural History – AMNH; Burke Museum of Natural History and Culture – UWBM; Cornell University Museum of Vertebrates – CUMV; Field Museum of Natural History – FMNH; Instituto de Biología, Universidad Nacional Autónoma de México – IBUNAM; Kansas University, Natural History Museum – KU; Louisiana State University Museum of Natural Science – LSUMZ; Museum of Comparative Zoology, Harvard University – MCZ; Museum of Southern Biology – MSB; Museo de Zoología "Alfonso R. Herrera", Universidad Nacional Autónoma de México – MZFC; University of Alaska Museum – UAM; and Yale Peabody Museum of Natural History, Yale University – YPM.

Collaborators: Dr. Phred M. Benham, Dr. José Cerca, Dr. Ammon Corl, Dr. Zachary R. Hanna, Dr. Matthew D. Shawkey, M.Sc. María Fernanda Asturias.

Invaluable mentoring: Dr. Rauri C. K. Bowie and Dr. Carla Cicero.

Tireless support: Lydia Smith.

To the entire Museum of Vertebrate Zoology community for offering me a home away from home.

# Chapter 1

## Endemic Mountain-gem hummingbirds (*Lampornis*) highlight the biogeographic complexity of Nuclear Central America

## Introduction

The processes driving biological patterns occur in a continuum across space and time, and these determine the geographic range of a species, its phylogenetic relationships, and time of lineage divergence (Edwards et al. 2016). There is a positive relationship between the size of the geographic range and the level of biological organization within that area, with the form of this organization representing a nested hierarchy (i.e., population, species, genus, and above). A similar trend is observed when considering the timing of lineage divergence, with older divergence times typically characterized by higher hierarchical levels of biological organization (for example, populations within species are more recently diverged than are closely related species, and so on). However, despite that the evolutionary and ecological processes driving these patterns occurring in a continuum, certain processes can be more important at one particular level of biological organization than at others (e.g., gene flow within and among populations vs. between genera).

Extensive research has been conducted independently on population or species-level processes; however, integrative biogeographic studies of different spatial and temporal scales are scarce. Recent integrative studies highlight that recognizing evolutionary patterns at different geographic scales is necessary to develop hypotheses about the processes generating the fauna of a region (Elías et al. 2020). Additionally, understanding the interplay of historical and recent processes that generate diversity patterns of a particular biota is important (Rissler 2016), especially for endemic species with small geographic ranges that inhabit an ecosystem of conservation concern, such as naturally fragmented cloud forest habitats of the tropics. Here, we aim to study the processes operating across the population-species interface to better understand the drivers of variation in genetic diversity and population connectivity of two bird species restricted to the montane cloud forest ecosystem of Central America.

Biogeographic patterns involving historical processes generally emerge from changes in geology and climate that favor the origination and maintenance of isolating barriers. One such pattern is the geographic replacement of closely related species across space (Darwin 1859). Species that are isolated by geological barriers might have come to this stage by dispersal or through vicariant events, most often followed by allopatric speciation. Allopatric speciation, representing a continuous and usually neutral process of differentiation (Coyne and Orr 2004), can also be driven by adaptation to different environments, which might result in the divergence of ecological niches occupied by each species (Rato et al. 2014). These processes usually require extended periods of time, measured in millions of years. However, it is important to consider that geological features that represent barriers to dispersal at certain times in Earth's history might be easily overcome during others, such as with changes in climate that may be particularly pertinent to species inhabiting mountains (Chaves et al., 2011). The Quaternary glacial cycles are known for promoting population expansion and connectivity of montane species in the tropics during glacial periods and population contractions and fragmentation during interglacial periods

(Ramírez-Barahona and Eguiarte 2013); simulations of climate suggest that cloud forests shifted downslope during the Last Glacial Maximum (Still et al. 1999).

Population connectivity and gene flow drive patterns of population genetic structure. Physical landscape attributes (e.g., geological and environmental variables) influence the direction and extent of gene flow. Given the presence of gene flow and recent times of divergence between populations, population differentiation can be shallow and sometimes cryptic. Higher population connectivity and shallow divergence can result in the retention of ancestral polymorphisms that can be driven by gene flow or incomplete lineage sorting, which might be challenging to disentangle. However, assessing gene flow across multiple timescales can shed light on how important this process is across the species-population interface (Epps et al. 2013, Swaegers et al. 2014). Moreover, assessing population connectivity across the landscape provides valuable information about climatic variables that may facilitate or hinder gene flow. The changing environment also comes into play at these spatial and temporal scales, and it is essential to account for the effects of the Quaternary glacial cycles because ecosystem connectivity changes through time (Musher et al. 2020). For tropical montane species, the glacial cycles might have enhanced longer periods of climatic stability (warm periods) promoting population isolation, followed by brief periods of population connectivity (cold periods) (Soley-Guardia et al. 2019), which highlights the importance of considering the particularities of the species ranges across space and time.

Nuclear Central America (NCA) ranges from the Isthmus of Tehuantepec (IT) in southern Mexico to the Nicaraguan Depression (ND) in Nicaragua (**Figure 1**; Schuchert 1935). NCA is located over three tectonic plates (North American, Caribbean, and Cocos), which creates a complex topography with mountain ranges that have different origins and ages. The western side of NCA has rocks that date from the early Paleozoic and that were covered by ice during the Quaternary glacial cycles. Central NCA is comprised of uplifted volcanic rocks that date to the Carboniferous. The southern Pacific volcanic chain and eastern mountains of NCA emerged during the Tertiary and Quaternary, and include five active volcanoes (Schuchert 1935, Iturralde-Vinent 2006, Bergoeing 2015). Central America is recognized as the land bridge connecting North and South America that facilitated biotic interchange between these larger landmasses. However, recent work also highlights the importance of *in situ* diversification in NCA contributing to the diversity of the regional species pool (e.g., Hofmann and Townsend 2017, Beza-Beza et al. 2021). Twenty-two species of birds have geographic ranges restricted to the cloud forests of NCA. The complex geology and the dynamic climatic history during the Pleistocene glacial cycles set the stage for investigation of the diversification and origination of new lineages across the species-population interface.

The Motagua-Polochic-Jocotán Fault System (MPJFS) and the Honduras Depression (HD) are important barriers that have led to the structuring of the regional fauna, with the IT and the ND delimiting the northern and southern extent of the NCA region, respectively (Daza et al. 2010, snakes; Pérez Consuegra and Vázquez-Domínguez 2015, mammals; Rovito and Parra-Olea 2016, amphibians; Hofmann and Townsend 2017, lizards; Elías et al. 2020, fishes). The MPJFS is part of the suture zone between the North American and Caribbean plates (Ortega-Gutiérrez et al. 2007). The HD encompasses several rift valleys that create a continuous feature extending north to south from the Caribbean Sea to the Gulf of Fonseca (Schuchert 1935). The MPJFS and

the HD are currently dry lowland valleys that serve as barriers to the movement of montane species (Pérez Consuegra and Vázquez-Domínguez 2015, Firneno et al. 2020). The MPJFS is the most commonly reported geographic feature that isolates populations of different taxa; however, there is no consensus whether this barrier isolates taxa from north to south, or from east to west. This lack of consensus on the directionality of lineage isolation across the fault system may be the result of sparse geographic sampling of populations within the region, particularly for avian species/species complexes. Recent research with detailed and exhaustive geographic sampling (e.g., *Peromyscus mexicanus* voles, Pérez Consuegra and Vázquez-Domínguez 2015) has shown that NCA is more biogeographically complex than expected, considering only the overall area of the region. Therefore, to better understand the processes driving the accumulation of the rich biodiversity of the region, studies with more exhaustive and fine-scale sampling are needed in order detect additional phylogeographic breaks across NCA. In addition, very few studies have made use of spatially explicit analyses of contemporary environmental and topographic features to infer gene flow among populations across the region (e.g., Landaverde-González et al. 2017), with such analyses urgently needed to improve our understanding of how the remarkable fauna of NCA assembled.

Tropical montane cloud forests are defined by the presence of clouds throughout the year, rather than by particular vegetation type or elevational extent (Brown and Kappelle 2001). Cloud forests cover less than 1% of the land area in northern Mesoamerica and they harbor high levels of endemic plant and animal species (Ponce-Reyes et al. 2012, Rojas-Soto et al. 2012). Montane cloud forests are one of the most threatened ecosystems in the region, both from changes in land use and from changing global climate (Rojas-Soto et al. 2012). Among the endemic species of the NCA cloud forest, the mountain-gem hummingbird genus *Lampornis* represents an ideal exemplar of a species complex tightly associated with this ecosystem. The seven currently recognized species of *Lampornis* show a pattern of geographic replacement with larger geographic ranges occupied by the northern species and smaller ranges by the southern species, although some species coexist in sympatry (García-Moreno et al. 2006). Phylogenetic analyses have demonstrated that *Lampornis* is a genus of local Mesoamerican origin where diversification has taken place within the Central American land bridge (García-Moreno et al. 2006, McGuire et al. 2014). *Lampornis amethystinus* is the only species in the genus whose phylogeographic structure has been studied to date, being subdivided into four genetic groups, three restricted to the western side of the IT and one to the eastern side. The divergence across the IT within *L. amethystinus* dates back to the Pleistocene, between 2.39 – 0.57 million years before present (Ornelas et al. 2016).

Two species of *Lampornis* mountain-gems are endemic to Nuclear Central America, *L. viridipallens* and *L. sybillae* (Howell and Webb 1995). They are sister species (García-Moreno et al. 2006, McGuire et al. 2014) with allopatric geographic ranges situated on either side of the Honduras Depression, and no evidence of hybridization between them has been reported. The NCA mountain-gems represent an ideal system for studying montane biogeography at different spatial and temporal scales. The two species reside all year in montane cloud forests, and collectively they occupy the majority of montane highlands in NCA. *Lampornis viridipallens* ranges from the IT in southern Mexico to the HD in western Honduras. Four subspecies have been described within *L. viridipallens*: *L. v. amadoni* (Sierra Atravesada (SE Oaxaca), in S Mexico), *L. v. ovadensis* (highlands of SE Mexico (Chiapas) and NW Guatemala), *L. v.*

*viridipallens* (highlands of E Guatemala, extreme N El Salvador and W Honduras), and *L. v. nubivagus* (El Salvador (Santa Ana Volcano)) (Züchner and Boesman 2020). *Lampornis sybillae* is a monotypic species that replaces *L. viridipallens* from the eastern side of the HD extending its range to the highlands north of the ND (van Dort 2020).

Here, we investigate the patterns and processes driving diversification within NCA. We examine species-level processes operating between *L. viridipallens* and *L. sybillae* using mitochondrial and nuclear markers to estimate molecular differentiation and time of divergence. Additionally, we use species distribution models and a test of niche evolution to better understand the geographic template where the speciation process has occurred. We investigate intraspecific patterns and processes taking advantage of our exhaustive sampling within the range of *L. viridipallens*. We gather genetic and environmental data and perform spatially explicit analyses to understand the role of geographic and climatic barriers in enhancing population differentiation through limiting gene flow. Using the nuclear data, we estimated gene flow within *L. viridipallens* at two different timeframes, contemporary and historical. We discuss the geographic distribution of genetic clusters within the framework of previously known geographic barriers within NCA and the newly identified breaks discovered in this study. We conclude by discussing the taxonomic implications of our results.

## Methods

### Sampling and field procedures

For the molecular analysis, we sampled 183 hummingbirds of which we collected 140 from 17 localities between 2009 and 2017 (**Figure 2, Tables S1 and S2**). We conducted scientific collection of specimens in joint expeditions of the Museum of Vertebrate Zoology (MVZ), University of California, Berkeley (UC Berkeley); Escuela de Biología (EB), Universidad de San Carlos de Guatemala (USAC); and Museo de Zoología "Alfonso R. Herrera" (MZFC), Universidad Nacional Autónoma de México (UNAM). We sampled with the permission granted by the Consejo Nacional de Áreas Protegidas in Guatemala through research and collecting permits provided to EB-USAC, Mexico's Secretaría de Medio Ambiente y Recursos Naturales, Subsecretaría de Gestión para la Protección Ambiental, Dirección General de Vida Silvestre granted to UNAM, and ethical approval R317 granted by the UC Berkeley Institutional Animal Care and Use Committee. We preserved the captured individuals as voucher specimens (study skins and tissue samples) and deposited them in ornithological research collections at the MVZ-UC Berkeley, EB-USAC and MZFC-UNAM (**Table S2**). Our collections were supplemented with 26 samples obtained on loan from tissue collections (FMNH = Field Museum of Natural History; KU = Kansas University, Natural History Museum; UWBM = Burke Museum of Natural History and Culture; LSUMZ = Louisiana State University Museum of Natural Science), which included the species *L. viridipallens* and *L. sybillae*. We added 17 samples as outgroup taxa, nine samples from the MVZ tissue collection and eight sequences from GenBank (**Table S2**). The outgroup included the other five species of the genus *Lampornis*, two additional representative species of the clade of Mountain-gem hummingbirds (*Eugenes fulgens* and *Lamprolaima rhami*), one species from the Bee clade (*Calypte anna*), and one species from the Emeralds clade (*Hylocharis leucotis*). The species included in the outgroup sampling were selected following the most current hummingbird phylogeny (McGuire et al. 2014).

Unfortunately, it was not possible to include *Lampornis viridipallens – L. sybillae* samples from Honduras but we look forward to establishing collaborations with local biologists to further advance the study of the Central American regional fauna.

## Mitochondrial DNA sequencing

We extracted genomic DNA using the DNeasy blood and tissue extraction kit (Qiagen, Valencia, CA, USA), following the protocol recommended by the manufacturer. We PCR-amplified and sequenced three mtDNA genes: 1041 base pairs (bp) of NADH nicotinamide dehydrogenase subunit 2 (ND2), and 750 bp of ATPase 6 and ATPase 8. The amplification of ND2 was performed with primers L5204 and H6312 (Cicero and Johnson 2001), and for ATPase 6–8 we used L8929 (Sorenson et al. 1999) and H9929 (Mero et al. 2011). Polymerase chain reaction conditions for ND2 and ATPase included an initial denaturation at 94 °C for 1-(3) min; then 35 cycles at 94 °C for 30 s, 54 °C for 30 s, and 72 °C for 45-(60) s; and a final extension at 72 °C for 10 min. We sequenced PCR products in the forward and reverse directions using BigDye terminator chemistry (Applied Biosystems, Foster City, CA, USA) on an ABI 3730 automated sequencer (Applied Biosystems, Foster City, CA, USA) at the Evolutionary Genetics Lab in the Museum of Vertebrate Zoology (MVZ). We aligned the forward and reverse sequences using Geneious v. 5.1.7 (http://www.geneious.com).

## Mitochondrial summary statistics and haplotype network

The mitochondrial DNA sequences were aligned manually and checked for stop codons using MEGA v. 7.0.21 (Kumar et al. 2016). The complete mitochondrial dataset was examined for haplotype variation (*H*), segregating sites (*S*), haplotype diversity (*h*), and nucleotide diversity ($\pi$) per region (**Table S1**) using DnaSP v. 5.10.01 (Librado and Rozas 2009). We looked for signs of demographic change by calculating Tajima's D (Tajima 1989) and Fu's Fs (Fu 1997) in Arlequin 3.11 (Excoffier and Lischer 2010) with 1000 permutations. Mismatch distributions were calculated using the sudden expansion model of Schneider and Excoffier (1999) with 9000 bootstrap replicates. Positive values for D and Fs are indicative of mutation-drift equilibrium, which is typical of stable populations, whereas significant negative values (at the P = 0.05 level for Tajima's D and Fs tests; Excoffier and Lischer 2010) that result from an excess of rare haplotypes, indicate that populations have experienced a recent bottleneck followed by population demographic expansion. We calculated Harpending's raggedness index (Hri) and the sum squared deviation (SSD), which indicate deviations from the sudden expansion model and are higher in stable, non-expanding populations (Rogers and Harpending 1992).

We estimated, in Arlequin, the average number of pairwise differences between and within populations, and pairwise FST values between populations; the populations were grouped by mountain range for these analyses. Additionally, we carried out analyses of molecular variance (AMOVAs) in Arlequin; the populations were grouped by (A) species, and then within *Lampornis viridipallens* by (B) mountain range, (C) north and southwest of the MPJFS, (D) north and southeast of the MPJFS, and (E) southwest and southeast of the MPJFS, since the MPJFS is the most commonly reported physical barrier in the region. For the last three comparisons (C, D, and E), we excluded the populations from Sierra Atravesada, Altos de Chiapas, and Santa Ana and San Vicente volcanoes because they are located farther away from

MPJFS, and other topographic features seem to have a more significant effect on their isolation and divergence. An unrooted statistical parsimony haplotype network (Clement et al. 2000) was generated in POPART v. 1.7 (Leigh and Bryant 2015) using the combined mtDNA matrix (ND2 + ATPase).

## Phylogenetic analyses

To understand the phylogenetic relations of the studied species and populations, we reconstructed Bayesian inference (BI) trees using MRBAYES v. 3.2.6 (Huelsenbeck and Ronquist 2001, Ronquist and Huelsenbeck 2003). A first analysis was conducted with data partitioned by gene (tRNA) and each codon position within the coding genes (ND2, ATPase 6, and ATPase 8). Since there were only ND2 sequences available in GenBank to supplement the outgroup sampling, a second analysis was conducted exclusively for the gene ND2 partitioned by codon position. The substitution model for each partition was identified using jMODELTEST v. 2.1.10 (Guindon and Gascuel 2003, Darriba et al. 2012) and the corrected Akaike information criterion (AICc; **Table S3**). For both analyses, we executed simultaneously two parallel Markov chain Monte Carlo (MCMC) analyses, each with four chains; each was run for 20 million generations, sampling every 1000 generations. A majority consensus tree was calculated, retaining nodes with a posterior probability of 0.5 or greater. Bayesian posterior probabilities were calculated from the sampled trees remaining after a burn-in of 25%. The consensus trees were visualized in FIGTREE v. 1.2.3 (http://tree.bio.ed.ac.uk/software/figtree/).

## Divergence time estimation

The divergence time of the most recent common ancestor (TMRCA) of *Lampornis viridipallens* and *L. sybillae*, as well as the TMRCA of the different subclades within *L. viridipallens*, were estimated using BEAST v. 1.10.4 (Drummond and Rambaut 2007, Suchard and Rambaut 2009). Similar to phylogenetic analyses, we performed two different analyses: one using the complete mtDNA dataset partitioned by gene (ND2 and ATPase 6–8), and a second analysis for ND2 partitioned by codon position. The best-fit nucleotide substitution model (**Table S3**), empirical base frequencies, and an uncorrelated lognormal relaxed model were used. The coalescent model assuming constant population size was used to model the tree prior, as it has been suggested to offer a better fit for datasets that include mainly intraspecific variation (Ho et al. 2011). All the species of the Mountain-gem clade were grouped and constrained to be monophyletic (McGuire et al. 2014). To calibrate the tree we used the substitution rates estimated for the Hawaiian honeycreepers (Lerner et al. 2011), since they have been previously used in hummingbird studies (McGuire et al. 2014, Ornelas et al. 2016). Using a secondary calibration, the root of the tree was assigned the average 12.8 Ma (normal prior, SD 2.0, range 16.09–9.51 Ma) to reflect the divergence time for the split between the Mountain-gems and the Bee hummingbirds (Ornelas et al. 2016). For each time estimation analysis, we performed three independent runs of 10 million generations with random starting trees, sampling every 1000 steps, and discarding the first 10% of trees as burn-in. We assessed the results in TRACER v. 1.7.1 (Rambaut et al. 2018) to ensure that all the effective sample sizes (ESS) were higher than 200 and used LOGCOMBINER v. 1.10.4 to combine trees files. The trees were processed using TREEANNOTATOR v. 1.10.4, summarized as a maximum clade credibility tree with mean

divergence times and 95% highest posterior density (HPD) intervals of age estimates, and finally, visualized in FIGTREE.

**Microsatellite genotyping**

We genotyped samples from 153 *Lampornis viridipallens* and 13 *L. sybillae* at 13 polymorphic, unlinked, nuclear microsatellite loci. Eleven primer sets were designed for *L. viridipallens* (**Table S4**). Additionally, after testing for specific amplification and for the presence of polymorphisms in *L. viridipallens*, we included two further primer sets that were designed for other hummingbird species, one from *Selasphorus platycercus* (HumB6, Oyler-McCance et al. 2011) and one from *Campylopterus curvipennis* (Cacu16-1, Molecular Ecology Resources Primer Development Consortium et al. 2010). Fluorescently labeled fragments were scored using a 3730 automated DNA sequencer (Applied Biosystems) in the Evolutionary Genetics Lab in the MVZ. Allele peaks were visualized using GENEMAPPER v. 4.1 (Applied Biosystems) against an internal size standard (GeneScan-500 LIZ size standard; Applied Biosystems) and scored manually.

**Population structure assessed on microsatellite data**

We calculated the extent of linkage disequilibrium between pairs of loci and departures from Hardy-Weinberg (H-W) equilibrium within populations and loci using GENEPOP v. 4.7 (Raymond and Rousset 1997, Rousset 2008) with Bonferroni corrections applied (Rice 1989). We estimated observed versus expected heterozygosity of the different loci and tested for heterozygote deficiency using a t-test in the R package ADEgenet (Jombart 2008). Additionally, within *L. viridipallens*, we assessed population differentiation with FST implemented in the R package diveRsity (Keenan et al. 2013).

We assessed population genetic structure based on Bayesian clustering using STRUCTURE v. 2.3.4 (Pritchard et al. 2000). The complete dataset, which included *L. viridipallens* and *L. sybillae*, was analyzed under the admixture model with correlated allele frequencies without prior information on population origin. Ten independent replicates were run for each *K*, from *K* = 1 to 9. Convergence was achieved with 500,000 MCMC iterations after a burn-in of 100,000 steps. The most likely number of populations was determined by estimating DeltaK (Evanno et al. 2005) with Structure Harvester (Earl et al. 2012). Then, the same procedure was followed for determining the *K* value for *L. viridipallens*, and after determining the optimal value of *K*, a set of ten independent replicates were run for that *K* value, but this time with a prior of population information included.

We used discriminant analysis of principal components (DAPC) to compare clustering results with those obtained using STRUCTURE. DAPC does not assume Hardy-Weinberg equilibrium and optimizes the differences between groups (Jombart et al. 2010). We ran analyses for the dataset including both species (*L. viridipallens* and *L. sybillae*) and separately, for the *L. viridipallens* dataset. The DAPC analyses were conducted as implemented in ADEgenet, retaining axes that expressed 90 percent of the total variance of the data. Finally, in a similar way as for the mitochondrial data, we carried out analyses of molecular variance (AMOVAs) in Arlequin; the populations were grouped by (A) species, then, within *Lampornis viridipallens* by

(B) STRUCTURE clusters, (C) DAPC clusters, (D) north and southwest of the MPJFS, (E) north and southeast of the MPJFS, and (F) southwest and southeast of the MPJFS.

## Spatial genetic structure and barrier detection

We implemented spatially explicit analyses to try to understand the genetic structure in a landscape framework. We conducted spatial principal component analyses (sPCA) in ADEgenet using the microsatellite dataset. SPCA is a multivariate method that enables the assessment of spatial pattern of genetic variability using allele frequency data without the assumptions of Hardy-Weinberg or linkage equilibrium. This method has proved to be particularly useful as a means to study cryptic spatial patterns of genetic variability (Jombart et al. 2008). As in the previous analyses, we ran two independent analyses, one for the complete dataset (i.e., *L. viridipallens* and *L. sybillae*) and a second restricted to *L. viridipallens*. After loading the microsatellite data and geographic coordinates, we used the jitter function set to 0.01 to add a small amount of noise and accommodate samples with the same geographical coordinates. Then, we ran the analyses estimating a Gabriel connection network (type=2) and plotted the results as an interpolated map of individual scores using the lagged principal scores. Positive eigenvalues indicate global structures and negative eigenvalues represent local patterns, where actual structures result in more extreme eigenvalues (Jombart et al. 2008).

To discover which major geographic features promote population isolation, we ran the Bayesian model to detect landscape barriers implemented in the R package Geneland (Guillot et al. 2005). Geneland facilitates locating genetic discontinuities without *a priori* assumptions of population limits, estimates the number of populations, and has been shown to perform well when there are low levels of population differentiation (Guillot et al. 2005). Using the complete microsatellite dataset, we ran the analysis estimating the number of populations (from 1 to 10), assuming no spatial uncertainty in geographical coordinates, and following a correlated allele frequency model. We set five independent runs, each of 200,000 iterations, 100 thinning, and 20% burn-in. We selected the run with the highest posterior probability, plotted the maps of estimated population membership, and used them to determine correspondence with known landscape features from the region.

## Species distribution modeling and paleodistribution

To gain a better understanding of the geographic distribution of suitable habitat based on niche theory (Franklin 2013), we followed a species distribution modeling approach using the maximum entropy algorithm implemented in MAXENT v. 3.4.1 (Phillips et al. 2006, Phillips et al. 2017). We constructed species distribution models (SDM) using current environmental conditions and presence spatial points of *L. viridipallens* and *L. sybillae*. The presence data points of both species were derived from museum specimens with georeferenced records obtained through the Global Biodiversity Information Facility (GBIF; http://data.gbif.org) and our collection efforts. Additionally, since there are very few *L. sybillae* georeferenced specimens, we supplemented the presence dataset for this species with records from ebird (ebird.org) that included photos for confirmation of species identification. After removing duplicate presence points from the same locality, we obtained a total of 84 different records for *L. viridipallens* and 25 for *L. sybillae*. We extracted present climatic data, for each individual

presence point, from 19 bioclimatic layers downloaded from WorldClim (Hijmans et al. 2005, http://www.worldclim.org) at 30 arc-second resolution, and tested for correlation among these variables for each of the two species. Although MAXENT can deal with correlated variables, it is recommended to keep the environmental data simple and ecologically meaningful (Peterson et al. 2011). For each pair of correlated variables (> 0.9 Pearson correlation coefficient), we selected the most temporally inclusive variable. Eight variables were selected for *L. viridipallens* (BIO1 = annual average temperature, BIO2 = mean diurnal range, BIO3 = isothermality, BIO4 = temperature seasonality, BIO12 = annual precipitation, BIO15 = precipitation seasonality, BIO17 = precipitation of driest quarter, and BIO18 = precipitation of warmest quarter), and a slightly different set of eight variables was chosen for *L. sybillae* (BIO1, BIO2, BIO4, BIO7 = annual temperature range, BIO12, BIO15, BIO17, BIO18).

We constructed a SDM for each species using the default convergence threshold ($10^{-5}$) and 500 iterations (Pearson et al. 2007). Each analysis was set to randomly use 65% of the spatial points for training and 35% for testing the model. We used the AUC statistic to assess model performance (Mertz 1978). To obtain a general view of how Pleistocene glacial cycles might have altered the geographic distributions of our study hummingbird species, the models were projected to Pleistocene climatic scenarios developed by the Paleoclimate Modelling Intercomparison Project Phase II (Braconnot et al. 2007; downloaded from WorldClim, http://www.worldclim.org/past) at 30 arc-second resolution: the Last Glacial Maximum (LGM, 21,000–18,000 years ago) Model for Interdisciplinary Research on Climate (MIROC; Hasumi and Emori 2004) and the Last Interglacial (LIG, 140,000–120,000 years ago) scenario (Otto-Bliesner et al. 2006).

### ***Lampornis viridipallens – L. sybillae* niche evolution**

To assess whether the divergence between *L. viridipallens* and *L. sybillae* was driven by niche evolution in addition to the geographic barrier for by the Honduras Depression, we ran a MAXENT symmetric background test (Warren et al. 2008, Warren et al. 2019) in the R package ENMTools (Warren et al. 2010, Warren et al. 2019). The background or similarity test enables the comparison of the overlap between the ecological niche models of two species while correcting for the availability of habitat, informing if the observed similarity is significant given the total environmental and geographic space available to the species. Specifically, the symmetric background test is conducted against a null hypothesis generated from "species 1 background versus species 2 background" comparisons (Warren et al. 2019). We used the same presence spatial points from the SDM analysis and extracted 1000 background points from circles with a radius of 5 km that were drawn around the presence localities (buffer.type = "circles" in ENMTools). We set a radius of 5 km to create a feasible buffer since the known home range area for hummingbirds is ~1 $km^2$ (Volpe et al. 2016). As environmental data, we included the nine bioclimatic layers used in the SDM of *L. viridipallens* and *L. sybillae* (BIO1, BIO2, BIO3, BIO4, BIO7, BIO12, BIO15, BIO17, BIO18). Niche similarity is measured with the Schoener's *D* and Warren's *I* statistics (Warren et al. 2008), which range from 0 (no overlap) to 1 (niche models identical). The null hypothesis that the overlap of ecological niches of two species is explained by habitat availability is rejected if the observed value of niche similarity is lower (niches differ) or higher (niches resemble) than the 95% confidence limits of the null distribution (Warren et al. 2008).

**Contemporary and historical environmental connectivity in *Lampornis viridipallens***

Through a landscape genetics approach, we assessed whether environmental features are associated with connectivity and gene flow in populations of *Lampornis viridipallens*. We conducted least-cost path analyses (LCPA) to evaluate whether the costs of movement through potential dispersal corridors correlate with genetic distances (measured as FST). Using the R package gdistance (van Etten 2017), we estimated transition surfaces based on the SDM, LGM, and LIG projections generated in MAXENT. We also evaluated two suitable/non-suitable reclassifications for each of the three projections; one reclassification included the higher 90% of suitable habitat, and another one included the higher 50%. Additionally, to get a better understanding of the role different environmental variables might play in the movement of this species of hummingbird; we obtained independent transition matrices for each of the eight bioclimatic layers used to build the SDM (BIO1, BIO2, BIO3, BIO4, BIO12, BIO15, BIO17, BIO18). Matrices of the least-cost path and resistance distances were calculated for each transition surface, in addition to a matrix of straight-line distances for comparison (Isolation by Distance, IBD). Specifically for the contemporary SDM, we calculated topographically corrected least-cost paths and their distances using the topoLCP function of the R package topoDistance (Wang 2020).

We ran mantel tests to check how correlated were the geographic (straight line distance) and environmental (SDM, LGM, LIG, bioclimatic layers) distances with respect to the genetic distances (FST, **Table S5**). Additionally, we conducted a Multiple Matrix Regression with Randomization (MMRR) to quantify the effects of geographic and ecological isolation (Wang 2013). The MMRR analysis enabled us to quantify how genetic distances respond to changes in geographic and environmental distances (regression coefficients), the overall fit of the model (coefficient of determination), and the significance of each variable (*p* values). We ran this analysis in R using the code provided by Wang (2013). In this analysis, we included the genetic distance matrix (Y – FST), the geographic distance matrix ($X_1$ – straight line distance), and the environmental distance matrix ($X_2$ – topographically corrected SDM least-cost paths distances). Additionally, we tested for the correlation between the geographic distance ($X_1$) and the environmental distance ($X_2$) to discern whether both variables were correlated and driving MMRR results.

**Contemporary and historical gene flow across the Motagua-Polochic-Jocotán Fault System**

We assessed gene flow across the MPJFS using the microsatellite data. The MPJFS seems to be a permeable barrier for *Lampornis viridipallens* in contrast to other stronger geographic barriers detected in this study. To disentangle whether the evidence of admixture is the result of ongoing or historical gene flow, or a consequence of incomplete lineage sorting, we estimated migration rates on contemporary and historical timescales. For these analyses, we included 116 individuals subdivided into three groups: i) Sierra Atravesada + Altos de Chiapas (20 individuals, localities 1-3 in **Table S1**), ii) north of Motagua fault (49 individuals, localities 4-9 in **Table S1**), iii) southwest of MPJFS (47 individuals, localities 10-14 in **Table S1**). Using the Bayesian inference approach implemented in BAYESASS (Wilson and Rannala 2003), we estimated migration rates between populations within the last few generations (*m*). BAYESASS was initially run with default parameters, and then, with subsequent runs, we adjusted the delta values for allelic

frequency (*A*), migration rate (*M*), and inbreeding (*F*). Adjusted final delta values used were $\Delta A = 0.4$ (34% acceptance rate), $\Delta M = 0.2$ (33%), and $\Delta F = 0.4$ (23%). Once we selected the parameters, we performed five independent short runs (10 million iterations and 1-million burn-in) and compared the results looking for consistency. We analyzed the trace file with TRACER to ensure proper mixing and burn-in. We report the results of a final run that was increased to 30 million iterations with a 3 million burn-in.

Then, we used the coalescent approach implemented in MIGRATE v. 4.4.3 (Beerli et al. 2019) to estimate asymmetrical gene flow between pairs of populations over the long term. We ran MIGRATE incorporating Bayesian inference analyses and a Brownian-motion model with a constant mutation rate and FST to estimate θ. After finding suitable priors through several short runs, MIGRATE was run with three long chains, with an MCMC of 10 million steps and burn-in of 1-million. A static four-chain heating scheme at temperatures of 1, 1.5, 3, and 1000000 was implemented to increase the efficiency of the MCMC. We tested the similarity between contemporary and historical values of *m* with a Mantel test. For this analysis, we used the *m* values generated by BAYESASS and estimated *m* from values of *M* ($M = m/\mu$) generated by MIGRATE using the estimated microsatellite mutation rate of $5 \times 10^{-4}$ (Chiucchi and Gibbs 2010). We also estimated the number of migrants per generation (Nem).

**Morphological variation within *Lampornis viridipallens***

Six body measurements were taken from 111 *Lampornis viridipallens*, the measurements were as follows: bill length, bill width, wing length, length of the tail feathers 1 and 5 from the right side, and mass. Following previously described protocols (Bowie et al. 2004) RAJ took five of the six measurements using a dial caliper with a precision of 0.1 mm and a wing rule with a precision of 1mm. The mass was obtained from the specimen labels. The final dataset included 88 hummingbirds with the complete set of measurements. All the measured hummingbirds were included in the genetic analysis.

The dataset was subdivided by sex as there is evidence of sexual dimorphism in *L. viridipallens*, resulting in measurements from 41 females and 47 males. Based on the geographic locality of each specimen, the individuals were assigned to one of five different groups: (i) Sierra Atravesada – Altos de Chiapas, (ii) north of Polochic Fault, (iii) between Polochic and Motagua Faults, (iv) southwest of the Motagua Fault, and (v) southeast of the Motagua Fault (**Table S2**). To control for allometry, we estimated the ratio between five measurements (mass, bill length, bill width, and length of the tail feathers 1 and 5 from the right side) and the wing length. We tested for the homogeneity of variances for the measurements of each ratio estimate with a Levene's test. After corroborating the homogeneity of variances, we conducted a two-way ANOVA for each variable followed by Tukey's posthoc-test. In these analyses, we considered the effect of the sex, the population, and the interaction between them. These analyses were conducted using the software Past 4.02 (Hammer et al. 2001).

## Results

### Genetic diversity and phylogenetics

In general, genetic diversity levels were high in both species of mountain-gem hummingbirds (**Table S6**). Mitochondrial haplotype diversity (*h*) in *L. viridipallens* ranged from 0.79 in the Sierra de los Cuchumatanes to 0.91 in Altos de Chiapas, two populations that are geographically located in adjacent mountain ranges. Most populations of *L. viridipallens* had more than one haplotype, with the exception of populations on four volcanos: Tecuamburro (n = 10), Suchitán (n = 2), Santa Ana (n = 2), and San Vicente (n = 5), which shared the same mitochondrial haplotype (ND2 + ATPase). Haplotype diversity was high in *L. sybillae* (0.94): we recovered nine different haplotypes among the 13 individuals we sampled from Cordillera Dariense. Neutrality test values (Tajima's D and Fu's F) revealed that most populations are demographically stable, although the populations of Sierra Atravesada and Sierra de los Cuchumatanes have undergone recent expansions. However, for the population of Sierra de los Cuchumatanes, the analysis of mismatch distributions was consistent with a demographically stable population (SSD positive and significant value).

Mitochondrial structure between species *L. viridipallens* and *L. sybillae*, and within *L. viridipallens*, was evident (pairwise differences, FST, and AMOVAs – **Tables S7 and S8**). *Lampornis sybillae* was clearly identified as a different group from *L. viridipallens*, being ~5% divergent in mtDNA. Within *L. viridipallens*, the most highly differentiated groups were the populations from southeast of the MPJFS, followed by the Pacific Volcanic Chain. Interestingly, the AMOVA showed that the percentage of variation among groups increased when the population from southeast of the MPJFS is compared either to populations to the north of the MPJFS or to the southwest of the MPJFS. The same pattern was not observed when contrasting the haplotype frequencies of populations north of the MPJFS against those of populations from southwest of the MPJFS.

The mitochondrial haplotype network, phylogenetic and dating analyses confirmed that *L. sybillae* represents a different lineage from *L. viridipallens* (**Figures 2, 3, 4**, **Table 1**), both lineages being recovered as reciprocally monophyletic groups, consistent with McGuire et al. (2014). However, the position of *L. sybillae* in the phylogenetic tree built with ND2 showed discrepancies with respect to that using the whole mtDNA dataset (ND2 + ATPase). The ND2-phylogenetic tree recovered *L. sybillae* as the sister species of *L. viridipallens* with an estimation of 2.1 my of divergence; whereas the ND2 + ATPase tree recovered the group *L. castaneoventris* / *L. calolaemus* as the sister lineage to *L. viridipallens* (divergence time: 2.28 my) and *L. sybillae* as the sister group to those four species (divergence time: 2.57 my).

Within *L. viridipallens*, three main clades were consistently recovered by the haplotype network and the trees (clades A, B, and C in **Figures 3, 4**). The most differentiated clade (C) included populations from the southeast of the MPJFS region and a few individuals from north of the faults. This lineage showed the oldest divergence time within the species, close to 480k-500k years (**Table 1**). The other two lineages (A and B) were more geographically intermixed. These patterns are typical of either incomplete lineage sorting or gene flow. However, one of the clades was exclusively from the region located south of the Polochic fault. Additionally, we recovered a

shallow sub-clade restricted primarily to Altos de Chiapas and the area north of the Polochic fault. The divergence time between the clades A and B was estimated at 308k-372k years.

The analyzed microsatellite loci were not linked and did not depart from Hardy Weinberg equilibrium after sequential Bonferroni corrections, both by locus and population. In general, across the 13 loci, the observed heterozygosity was lower than the expected heterozygosity (**Figure S1**), both in the complete dataset (166 samples, $t = 3.231$, $p = 0.007$) and the *L. viridipallens* dataset (153 samples, $t = 2.949$, $p = 0.012$).

Three genetic groups were detected by the Structure analysis of the microsatellite data of *L. viridipallens* and *L. sybillae* (DeltaK = 3; **Figures 5, S2**). The three groups were: 1) *L. sybillae*, and within *L. viridipallens*, 2) the populations from southeast of the MPJFS and Tecuamburro, Santa Ana, and San Vicente Volcanoes, 3) the remaining populations of *L. viridipallens*. The DAPC analysis supported the Structure results (**Figure S3**), although it suggested that K = 6. PC1 separated the two species, *L. sybillae* - *L. viridipallens*, PC2 differentiated the *L. viridipallens* population from southeast of the MPJFS from the remaining populations, and PC3 set Tecuamburro, Santa Ana, and San Vicente Volcanoes as one group different from the rest of the range. The AMOVA also suggested the highest percentage of variation among groups was recovered when both species were contrasted (**Table S9**).

The Structure analysis restricted to only *L. viridipallens* suggested four clusters (DeltaK = 4; **Figures 5, S2**), whereas the DAPC analysis recognized five (**Figure S4**). The four most clearly differentiated groups were: 1) populations southeast of the MPJFS (corresponded with PC1), 2) Tecuamburro, Santa Ana, and San Vicente Volcanoes (corresponded with PC2), 3) Sierra Atravesada and Altos de Chiapas (corresponded with PC3), and 4) populations southwest of the MPJFS. The K = 4 Structure analysis run while including a prior on population origin, confirmed the four previously detected groups and suggested that the populations from north of the Polochic Fault and those from between branches of the MPJFS represent a zone of admixture between 3) Sierra Atravesada and Altos de Chiapas, and 4) populations southwest of the MPJFS. The peculiarities of DAPC analysis differentiated the admixed populations as a different group. Consistent with the mitochondrial AMOVAs, the highest percentage of variation among population groups of *L. viridipallens* was recovered when contrasting the southeastern populations against either those to the north or the southwest of the MPJFS (**Table S9**).

## Spatial patterns of genetic diversity and barrier detection

The sPCAs of the microsatellite data revealed high positive eigenvalues supporting a well-defined pattern of global population structure (**Figure S5**). For the complete dataset, the results were similar to those of Structure and DAPC (**Figures 6, S6**). In this particular analysis, PC1 captured the variation between species, and PC2 differentiated the populations from southeast of the MPJFS and Tecuamburro, Santa Ana, and San Vicente Volcanoes (which corresponded to PC2 and PC3 of DAPC) from the remaining western populations. For the *L. viridipallens* dataset, PC1 differentiated the populations from southeast of the MPJFS and Tecuamburro, Santa Ana, and San Vicente Volcanoes from the remaining populations (PC1 and PC2 from the corresponding DAPC) and PC2, recognized Sierra Atravesada and Altos de Chiapas (PC3 from DAPC) as a separate group (**Figures 7, S6**).

Barrier analyses using Geneland identified seven different groups (**Figure 8**). The additional group detected by this analysis came from the subdivision of Santa Ana and San Vicente Volcanoes from Tecuamburro Volcano. The barriers detected are spatially concordant with known topographic systems that isolate different mountain ranges such as the Honduras Depression and the MPJFS. Other geographic barriers that correspond with the analyses are the geographic limits between Altos de Chiapas and Sierra de los Cuchumatanes, the boundary between the Ipala and the Chortis blocks, and the island-effect inhabiting volcanoes can induce on highland species.

## Species distribution modeling and niche evolution

The contemporary species distribution models had AUC values above 0.9, suggesting good fits to the data. The *Lampornis viridipallens* SDM predicted suitable habitat along the montane region between the Isthmus of Tehuantepec and the Honduras Depression, corresponding with the known geographic range of the species (**Figure 9**). In contrast, the *L. sybillae* SDM predicted suitable habitat across a wider range than the actual current distribution of the species. In addition to the area inhabited by *L. sybillae*, which are the mountain ranges between the Honduras and Nicaraguan Depressions, the SDM also suggested the availability of suitable habitat in some mountains in Guatemala and western Honduras where this species is presently absent (**Figure 9**).

Neither of the two models (*L. viridipallens* and *L. sybillae*) completely cross-predicted the suitable habitat of the other species. Additionally, the symmetric background test showed that the ecological niches of the two species are more divergent than expected given what is environmentally and geographically available (Schoener's $D = 0.53$, $p = 0.04$; Warren's $I = 0.79$, $p = 0.02$). However, the climatic variables that had a higher percent contribution to the SDM were shared between *L. viridipallens* and *L. sybillae*: annual mean temperature (79.2% and 61.6%, respectively) and mean diurnal temperature range (11.7% and 24.5%). The climatic variables with lower percent contribution to demarcating the niche space occupied by both species were temperature seasonality (0.6% and 0%) and precipitation of the warmest quarter (0.1% and 0%).

The paleodistribution models for the LGM and LIG (**Figure 9**) revealed that the suitable habitat for both species has remained fairly stable during the past ~120k years. The geographic areas that currently represent isolated mountain ranges could have been separated for at least the same amount of years; for instance, *L. viridipallens* populations from the southeastern area of the MPJFS and Santa Ana and San Vicente Volcanoes. However, the habitat connectivity for *L. viridipallens* north and southwest of the MPJFS could have been enhanced during the LIG.

## Contemporary and historical landscape connectivity and gene flow in *Lampornis viridipallens*

Most of the geographic and environmental models and variables compared to genetic distances showed a significant positive correlation (**Table 2**). The correlation between the geographic and genetic distances was fairly high ($r = 0.64$). However, the correlation between the SDM-based least-cost path distances (with and without topographic correction) and genetic distances was the

highest ($r$ = 0.76), followed by the correlation of the 50% SDM reclassification ($r$ = 0.74). These results suggest that while a component of genetic distances can be explained by geographic distance itself, the environmental models that consider landscape resistance have a larger association with genetic differentiation (**Figure S7**). The climatic variables that were more highly correlated with genetic distances were the precipitation of the warmest quarter ($r$ = 0.71) and temperature seasonality ($r$ = 0.70). The genetically studied populations are located where there is high precipitation during the warmest quarter and small temperature changes across the year (**Figure S8**). The resistance matrices calculated for the LGM and LIG correlated with the genetic distances to a similar degree to the correlation found for the SDM (LGM: $r$ = 0.71 and LIG: $r$ = 0.72; **Table 2**). The MMRR analysis suggested a clear and strong pattern of isolation by environment ($\beta_E$ = 0.748, $p$ = 0.004) without a significant contribution of the straight geographic distance (i.e., Isolation by distance: $\beta_D$ = 0.0145, $p$ = 0.973). However, the straight geographic distance and the environmental distance were highly correlated ($r$ = 0.844, $p$ = 0.001).

BayesAss analysis of the *L. viridipallens* populations that showed signs of admixture with the Structure analyses indicated low estimates of contemporary gene flow (**Table 3**). The highest migration rate value was obtained when the source population was to the southwest of the MPJFS, and the recipient population was to the north of the MPJFS ($m$ = 0.16). Long-term migration rates estimated with Migrate-n did not show a significant correlation with the contemporary rates (Mantel test: $r$ = -0.15, $p$ = 0.67). For the historical migration rates, the two highest scores involved bidirectional gene flow between the populations from Sierra Atravesada + Altos de Chiapas and those southwest of the MPJFS (**Table 3**). However, in general, for long-term gene flow, the number of migrants per generation (*Nem*) was less than 1.0, ranging from 0.01 to 0.18. Interestingly, the lowest contemporary and historical migration rates were found when the source population was to the north of MPJFS, having confidence intervals that included zero estimates in all the comparisons (**Table 3**).

**Morphological variation within *Lampornis viridipallens***

Females were significantly differentiated from males for all five morphological variables (**Figure 10, Table S10**). Compared to males, females are less heavy, had larger and wider bills, longer central tail feathers, and shorter external tail feathers. When contrasting the populations, the population from the southwest of MPJFS had significantly longer tails. The analyses on the interaction of sex and population revealed that the bill length was the morphological variable most differentiated between females and males in four of the five populations considered.

## Discussion

Our study shows that the genetic diversity and geographic structure of the endemic mountain-gem hummingbirds of Nuclear Central America are the result of historical and contemporary processes that drove *in situ* diversification. Mitochondrial and microsatellite data indicated that *Lampornis viridipallens* and *L. sybillae* diverged in allopatry on either side of the Honduras Depression, an event that occurred during the early Pleistocene. Their geographic and genetic isolation was followed or accompanied by ecological niche divergence. Within *Lampornis viridipallens*, the genetic breaks corresponded with dry valleys that separate the mountain ranges; especially those associated with the Motagua-Polochic-Jocotán Fault System. The

boundary between the Ipala and Chortis blocks, and the break between Altos de Chiapas and Sierra de los Cuchumatanes were also revealed to be barriers to gene flow in *L. viridipallens*. The divergence times between lineages of *L. viridipallens* were between 500 and 370 ky, suggesting divergence events older than the LGM and LIG. Analyses of population connectivity showed that environmental distances are more important than geographic distances in limiting gene flow, although both environmental and geographic distances are highly correlated. We demonstrate that exhaustive and robust geographic sampling of the differently aged mountain ranges in NCA is necessary to understand its biogeographic complexity.

**Historical patterns and processes – species level**

Our findings demonstrate that *Lampornis viridipallens* and *L. sybillae* are genetically highly differentiated in response to geographic isolation and ecological divergence. The level of genetic divergence (5% in mtDNA) corresponds with what has been reported in other montane neotropical species (Zamudio-Beltrán and Hernández-Baños 2015, Cadena et al. 2019), highlighting the importance of climatic stability during the Pleistocene in enabling species persistence and the accumulation of species through time (García-Rodríguez et al. 2021, Morales-Barbero et al. 2021). The effect of the isolating barriers is remarkable in keeping the two species apart and preventing hybridization and interspecific gene flow, a process that is common in hummingbirds (Grant and Grant 1992), even between highly diverged species (Ottenburghs et al. 2015). The association that the two species have with the naturally fragmented montane forests (Züchner and Boesman 2020, van Dort 2020) and their ecological niche divergence suggest that these hummingbirds have limited mobility among different mountain ranges and are locally adapted to the environment that they occupy. However, detailed sampling across the Honduras Depression remains necessary to completely factor out the presence of interspecific hybridization.

**Contemporary patterns and processes – intraspecific level**

Our genetic and spatial data analyses show that environmental and landscape variables, in addition to climate stability during the LGM and LIG, are the main drivers of population differentiation within *Lampornis viridipallens*. The genetic breaks that we uncover align with dry valleys situated between mountain ranges. Dry valleys are widely known to act as barriers limiting gene flow and isolating populations of species restricted to montane habitats (Soley-Guardia et al. 2019), especially for species that live in cloud forest ecosystems (Zamudio-Beltrán and Hernández-Baños 2015, Ornelas et al. 2016, Cadena et al. 2019). We found higher genetic structure analyzing microsatellite data when compared to mitochondrial DNA, although the larger patterns coincide between the two types of genetic markers. Mito-nuclear concordance is a general pattern when populations are demographically stable and geographically isolated (Toews and Brelsford 2012), although microsatellites may recover additional population structure than the mitochondria given their nature as neutral markers and expected high substitution rates (Ornelas et al. 2016).

To our surprise, we discovered with the microsatellite dataset that populations to the north of the Motagua-Polochic-Jocotán region represent a zone of admixture between populations inhabiting the Sierra Atravesada-Altos de Chiapas and those from the southwest of the MPJFS. However,

north of MPJFS was recognized as a separate genetic group with the geographically explicit analysis (**Figure 7**) and contemporary and historical migration rates across the MPJFS indicated low estimates of gene flow. The low estimates of contemporary gene flow across the MPJFS point to incomplete lineage sorting as an alternative to introgression in explaining the shared alleles. Additionally, *L. viridipallens* and *L. sybillae* are species restricted to montane forests and it is reported that hummingbirds would choose to fly longer distances inside the forest rather than adventuring into non-forested habitats (Volpe et al. 2016), both characteristics that would promote low levels of gene flow. However, we suggest these results be interpreted with caution since it has been suggested that microsatellite data can show different patterns of introgression from nuclear markers sampled more broadly across the genome (Bradbury et al. 2015), even when both types of genetic markers tend to show correspondence in population structure (Sunde et al. 2020). We look forward to better understanding the relative roles of gene flow and genetic introgression between populations with our future research endeavors centered in using a SNP dataset.

## Biogeography of Nuclear Central America

Our detailed and exhaustive geographic sampling along with genetic and spatially explicit analyses revealed more genetic groups than any other avian study has reported for Nuclear Central America (Jiménez and Ornelas 2016, Rodríguez-Gómez et al. 2021), highlighting the biogeographic complexity of the region. The role of the Honduras Depression in promoting allopatric speciation has also been documented in toads (Firneno et al. 2020), reptiles (Hofmann and Townsend 2017), and voles (Pérez Consuegra and Vázquez-Domínguez 2015). We speculate that similar high genetic diversity might be present in other bird species from NCA, but that the sparse geographic sampling of previous studies has not enabled its recovery. It is also important to consider that in addition to the geologic origin and history of the region, its topography and geographic location (e.g., within the Neotropics, land bridge connecting North and South America, and in between the Pacific Ocean and the Caribbean Sea) creates a variety of different climates and habitats that can enhance diversification through niche evolution, as it is exemplified here with *L. viridipallens* and *L. sybillae*. All these facts raise the question of how much we can still discover about the diversification of life in this little-studied region, especially if we delve into studying local adaptation.

One of the most interesting biogeographic findings from our research was that within *L. viridipallens* the most differentiated genetic group was from the southeastern side of the MPJFS. The genetic break coincides with the recently defined border between the Ipala and the Chortis blocks (Ellis et al. 2019). As far as we are aware, just one previous study with comprehensive geographic sampling found a genetic break matching this same area (Pérez Consuegra and Vázquez-Domínguez 2015). However, distinct morphological groups have been described in different families of beetles that correspond with this geographic boundary (Passalidae – Schuster 2000, Cano et al. 2018; Curculionidae – Barrios-Izás 2020). Furthermore, recent genetic studies of amphibians and reptiles, with sparser sampling on the Guatemalan side of the break, suggest a similar pattern (Hofmann et al. 2017, Firneno et al. 2020).

Another important biogeographic consideration that results from our study is that the MPJFS does not represent the geographic break with a higher impact on genetic discontinuities. We

caution researchers in concluding that the MPJFS is the main driver of population isolation within NCA when the available geographic sampling is sparse. As we show here, there are many other geographic barriers in the region that isolate montane fragments. For instance, the lowland region between Altos de Chiapas and the Sierra de los Cuchumatanes, as well as the lowland region that isolates different volcanoes within the Pacific Volcanic Chain. Future research will discern the relative importance of these barriers in isolating populations of other taxa.

**Taxonomical analysis of the subspecies of *Lampornis viridipallens***

Our genetic analyses show groups that do not correspond precisely with the described subspecies of *L. viridipallens*. The known geographic distribution of the subspecies *L. v. amadoni* is within the Sierra Atravesada; however, the genetic group to which individuals from this area belong also included populations from Altos de Chiapas, which we recovered as one genetic group: Sierra Atravesada + Altos de Chiapas. The reported subspecies inhabiting the highlands from Altos de Chiapas is *L. v. ovadensis* and not *L. v. amadoni*. The subspecies reported for northwestern Guatemala is also *L. v. ovadensis*, which corresponds to the groups we recovered from the region north and southwest of the MPJFS. The nominate subspecies *L. v. viridipallens* matches perfectly to the most differentiated group in the southeastern area of the MPJFS. The fourth subspecies, *L. v. nubivagus*, is known from Santa Ana Volcano in El Salvador, although our analyses showed that individuals from San Vicente Volcano also belong to this taxon. Morphological measurements evidenced that sexual dimorphism was greater than divergence among any of the subspecies.

**Conclusions**

Our work on *Lampornis* hummingbirds reveals that historical and contemporary processes have fueled *in situ* diversification within Nuclear Central America. Dry valleys separating mountain ranges are important geographic barriers promoting isolation for species inhabiting cloud forest ecosystems. Environmental stability during the Pleistocene has played an essential role in interspecific ecological divergence and in limiting intraspecific population connectivity through time. The rich geology, climate, and topography of Nuclear Central America results in a region with high levels of biological diversity that is still one of the less studied areas within the American continent. Our findings highlight the need for future research involving detailed and exhaustive sampling in NCA to better understand its high biodiversity, and the ecological and evolutionary processes that have driven the diversification of this remarkable fauna.

## Tables and figures

**Table 1.** Time to the most recent common ancestor estimates for *Lampornis viridipallens* and *L. sybillae* based on mtDNA.

| Lineages | Age (my) | 95% HPD |
|---|---|---|
| ND2 tree | | |
| (*L. viridipallens* – *L. sybillae*) – (CR-Pan) | 2.598 | 1.971-3.279 |
| *L. viridipallens* – *L. sybillae* | 2.175 | 1.581-2.772 |
| *L. viridipallens* (A – B) – C | 0.500 | 0.320-0.711 |
| *L. viridipallens* A – B | 0.372 | 0.239-0.529 |
| ND2 + ATPase tree | | |
| (*L. viridipallens* – (CR-Pan)) – *L. sybillae* | 2.571 | 2.053-3.119 |
| *L. viridipallens* – (CR-Pan) | 2.288 | 1.781-2.783 |
| *L. viridipallens* (A – B) – C | 0.480 | 0.322-0.639 |
| *L. viridipallens* A – B | 0.308 | 0.199-0.409 |

CR-Pan: *Lampornis* species from Costa Rica and Panama – *L. castaneoventris*, *L. calolaemus*.

**Table 2.** Mantel tests for geographic (straight line distance) and environmental (SDM, LGM, LIG, bioclimatic layers) distances with respect to microsatellite genetic distances (FST) for *Lampornis viridipallens*.

| Geographic and environmental models and variables | *r* statistic | *p* value |
|---|---|---|
| Straight distance (IBD) | 0.643 | 0.001* |
| Species distribution model (SDM) | 0.757 | 0.001* |
| SDM 90% | 0.531 | 0.023* |
| SDM 50% | 0.739 | 0.001* |
| SDM + topographic correction | 0.758 | 0.001* |
| Last glacial maximum (LGM) | 0.709 | 0.001* |
| LGM 90% | 0.471 | 0.063 |
| LGM 50% | 0.612 | 0.002* |
| Last interglacial (LIG) | 0.716 | 0.001* |
| LIG 90% | 0.488 | 0.017* |
| LIG 50% | 0.671 | 0.002* |
| Annual mean temperature (bio 1) | 0.587 | 0.001* |
| Mean diurnal range (bio 2) | 0.672 | 0.001* |
| Isothermality (bio 3) | 0.637 | 0.001* |
| Temperature seasonality (bio 4) | 0.704 | 0.001* |
| Annual precipitation (bio 12) | 0.655 | 0.001* |
| Precipitation seasonality (bio 15) | 0.611 | 0.001* |
| Precipitation of driest quarter (bio 17) | 0.687 | 0.001* |
| Precipitation of warmest quarter (bio 18) | 0.707 | 0.001* |

*: significant *p* value.

**Table 3.** BAYESASS and MIGRATE estimates of contemporary and historical migration rates (95% confidence intervals), respectively, based on microsatellites data between populations of *Lampornis viridipallens* hummingbirds. The recipient (sink) populations are shown in the left side, and the source (donor) populations are across the top.

| | **Source population** | | |
|---|---|---|---|
| **Recipient population** | **Sierra Atravesada – Altos de Chiapas** | **North of Motagua-Polochic Faults** | **Southwest of Motagua-Polochic Faults** |
| BAYESASS | | | |
| Contemporary migration rates (*m*) | | | |
| Sierra Atravesada – Altos de Chiapas | – | 0.03 (0.00–0.06) | 0.06 (0.02–0.09) |
| North of Motagua-Polochic Faults | 0.05 (0.03–0.08) | – | 0.16 (0.11–0.22) |
| Southwest of Motagua-Polochic Faults | 0.01 (0.00–0.02) | 0.01 (0.00–0.02) | – |
| MIGRATE | | | |
| Historical migration rates (*M*) | | | |
| Sierra Atravesada – Altos de Chiapas | – | 0.09 (0.00–0.18) | 1.88 (1.09–2.69) |
| North of Motagua-Polochic Faults | 1.25 (0.17–1.78) | – | 1.09 (0.00–3.08) |
| Southwest of Motagua-Polochic Faults | 2.78 (0.73–4.82) | 0.15 (0.00–0.52) | – |
| Number of migrants per generation ($N_em$) | | | |
| Sierra Atravesada – Altos de Chiapas | – | 0.01 (0.00–0.01) | 0.13 (0.08–0.19) |
| North of Motagua-Polochic Faults | 0.10 (0.01–0.14) | – | 0.09 (0.00–0.24) |
| Southwest of Motagua-Polochic Faults | 0.18 (0.05–0.32) | 0.01 (0.00–0.03) | – |
| Migration rates (*m*) | | | |
| Sierra Atravesada – Altos de Chiapas | – | 0.00005 | 0.00094 |
| North of Motagua-Polochic Faults | 0.00062 | – | 0.00054 |
| Southwest of Motagua-Polochic Faults | 0.00139 | 0.00007 | – |

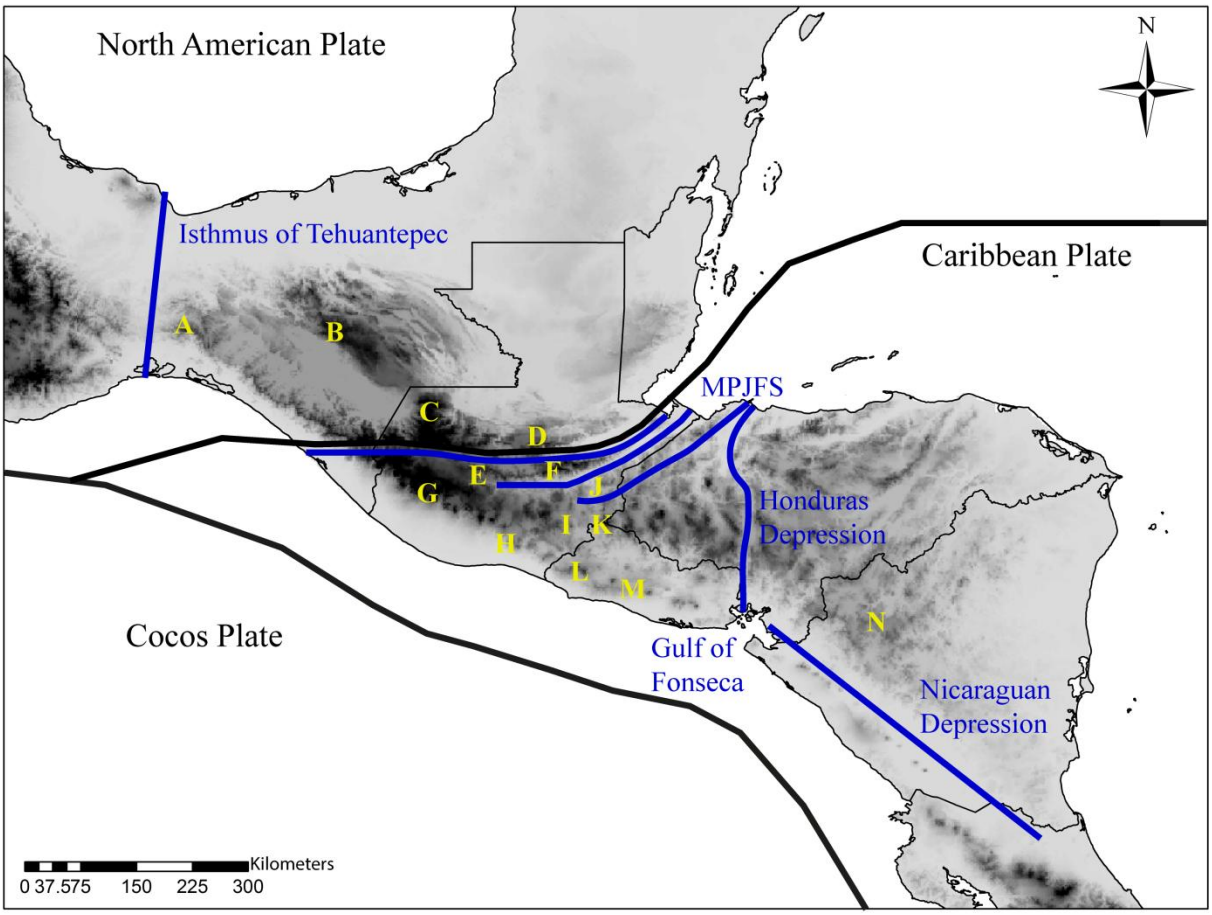


**Figure 1.** Nuclear Central America (NCA) and geographic features in the region. NCA is located over three tectonic plates: North American, Caribbean, and Cocos. NCA is limited to the north by the Isthmus of Tehuantepec and to the south by the Nicaraguan Depression. Biogeographic barriers recognized within Nuclear Central America are the Motagua-Polochic-Jocotán Fault System (MPJFS), and the Honduras Depression that extends from the Caribbean Sea to the Gulf of Fonseca. The map shows the elevation in grayscale, with the lighter tones representing lower elevations and the higher dark, high elevations. Montane ranges and volcanoes labeled on the map are: A – Sierra Atravesada; B – Altos de Chiapas; C – Sierra de los Cuchumatanes; D – Sierra de Chamá; E – Sierra de Chuacús; F – Sierra de las Minas; G – Pacific Volcanic Chain (southwest of the MPJFS); H – Tecuamburro Volcano; I – Suchitán Volcano; J – La Unión, Zacapa (southeast of the MPJFS); K – Cerro Montecristo (southeast of the MPJFS); L – Santa Ana Volcano; M – San Vicente Volcano; N – Cordillera Dariense.

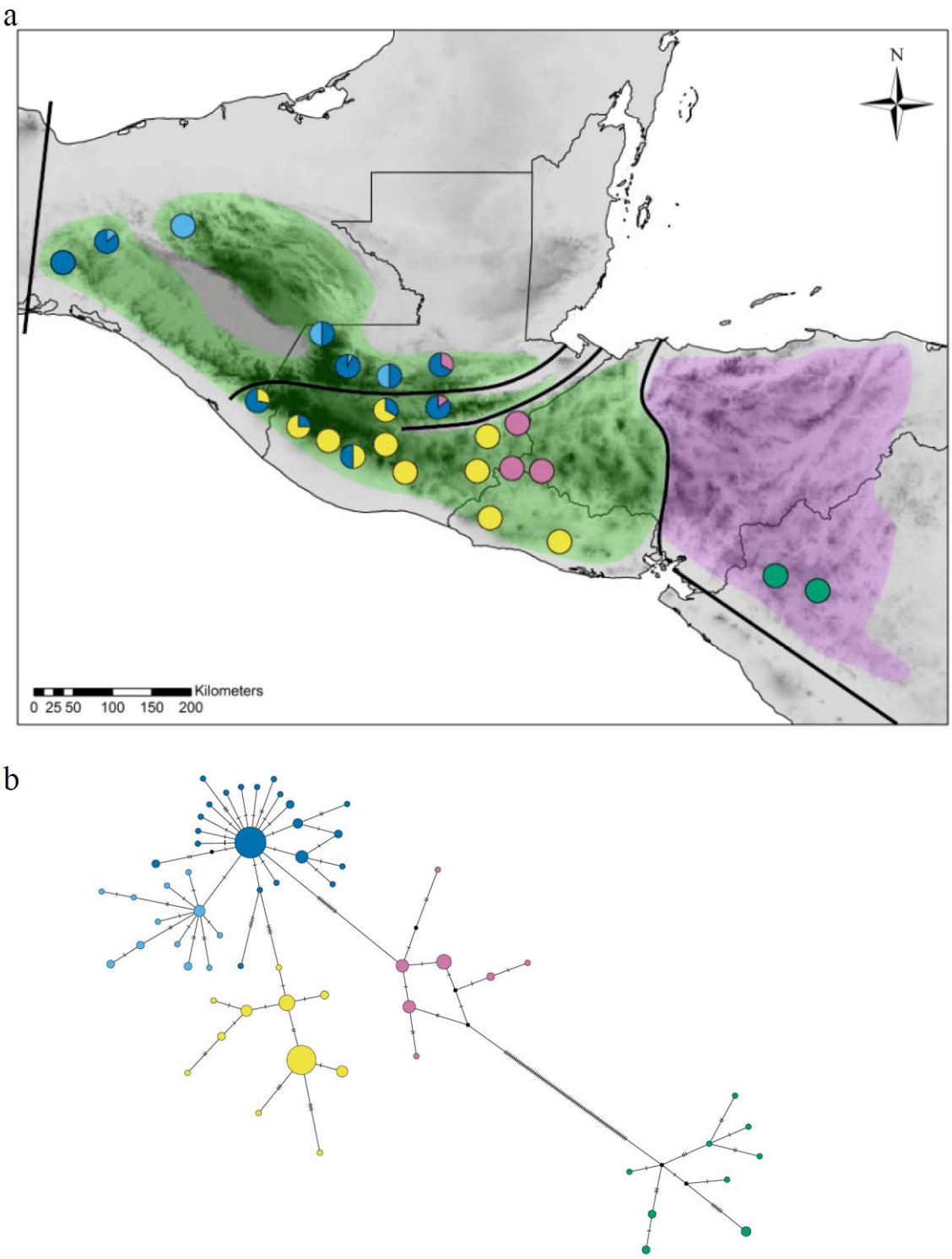


**Figure 2.** Sampling localities and mitochondrial groups within *Lampornis viridipallens* and *L. sybillae*. a) Map depicting geographic distribution of mitochondrial groups. The circle pies on the map show the haplotype groups in each locality. b) Mitochondrial haplotype network of genes ND2 and ATPase.

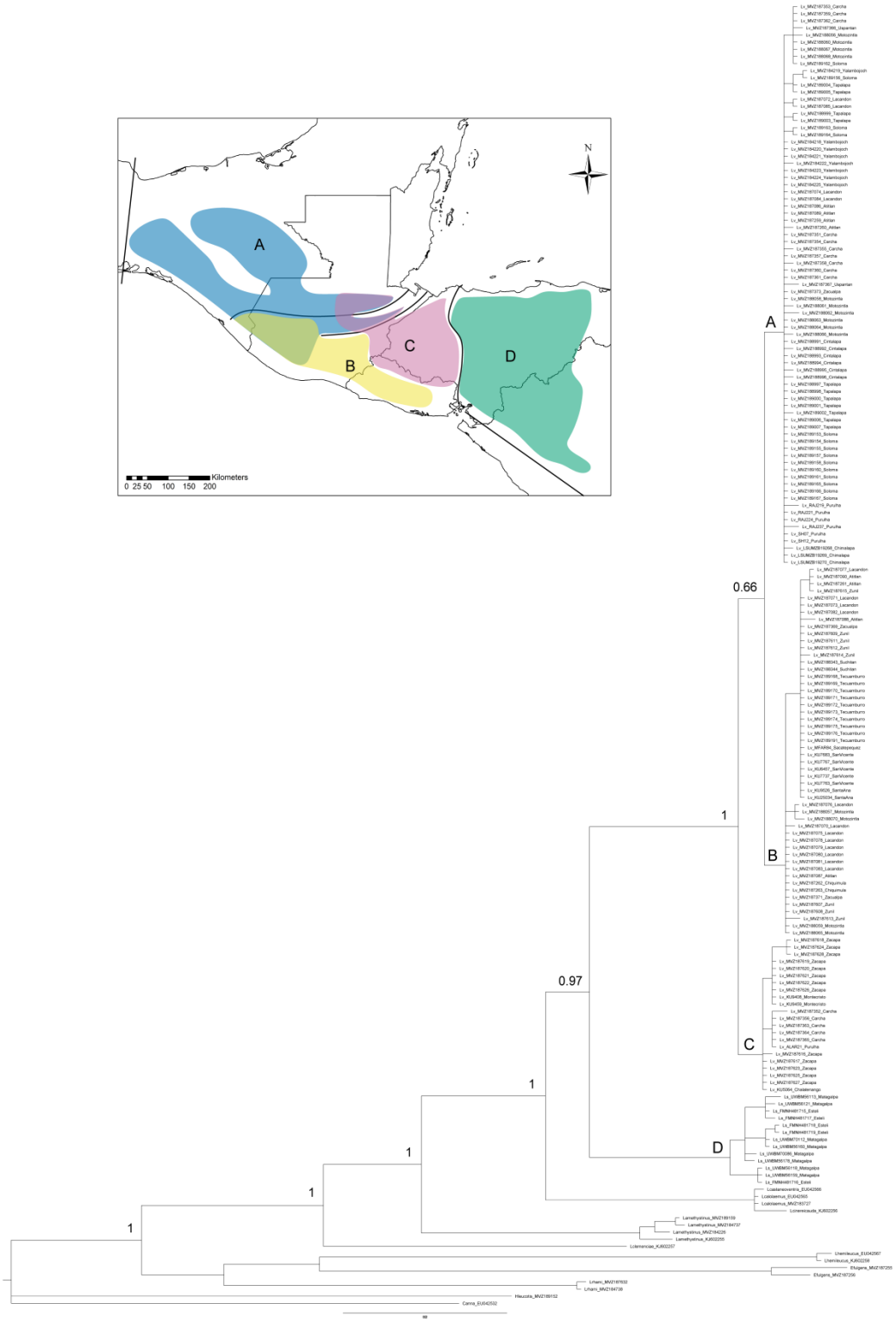


**Figure 3.** Bayesian inference phylogeny of *Lampornis viridipallens* and *L. sybillae* based on mitochondrial gene ND2. The numbers on the nodes are posterior probabilities. The insert map shows the geographic distribution of groups A, B, C, and D as indicated on the phylogeny. Groups A, B, and C correspond to *L. viridipallens* and group D, to *L. sybillae*. Posterior probabilities of groups: A = 0.66; B = 1; C = 0.70; D = 1.

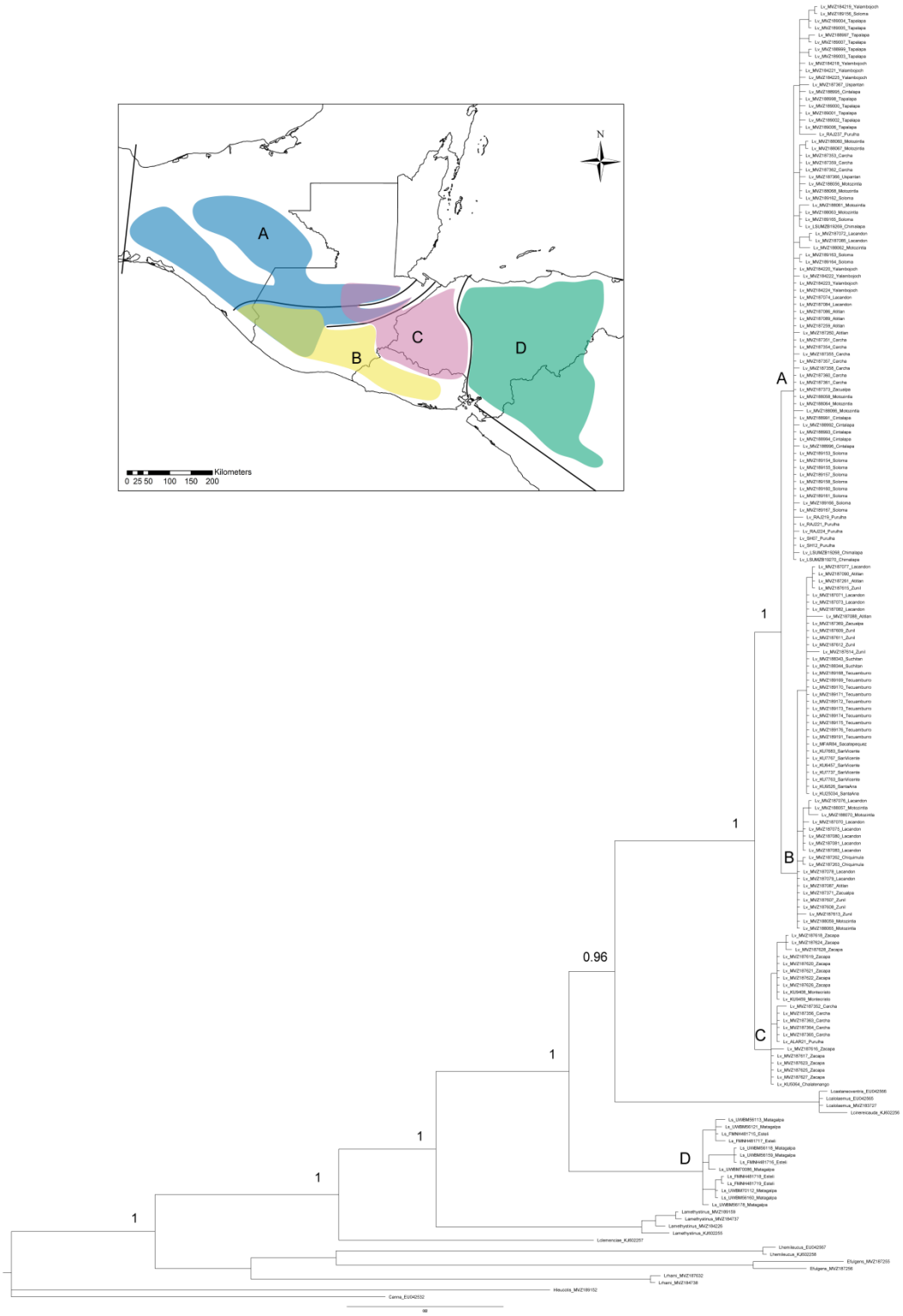


**Figure 4.** Bayesian inference phylogeny of *Lampornis viridipallens* and *L. sybillae* based on mitochondrial genes ND2 and ATPase. The numbers on the nodes are posterior probabilities. The insert map shows the geographic distribution of groups A, B, C, and D as indicated on the phylogeny. Groups A, B, and C correspond to *L. viridipallens* and group D, to *L. sybillae*. Posterior probabilities of groups: A = 0.98; B = 1; C = 0.75; D = 1.

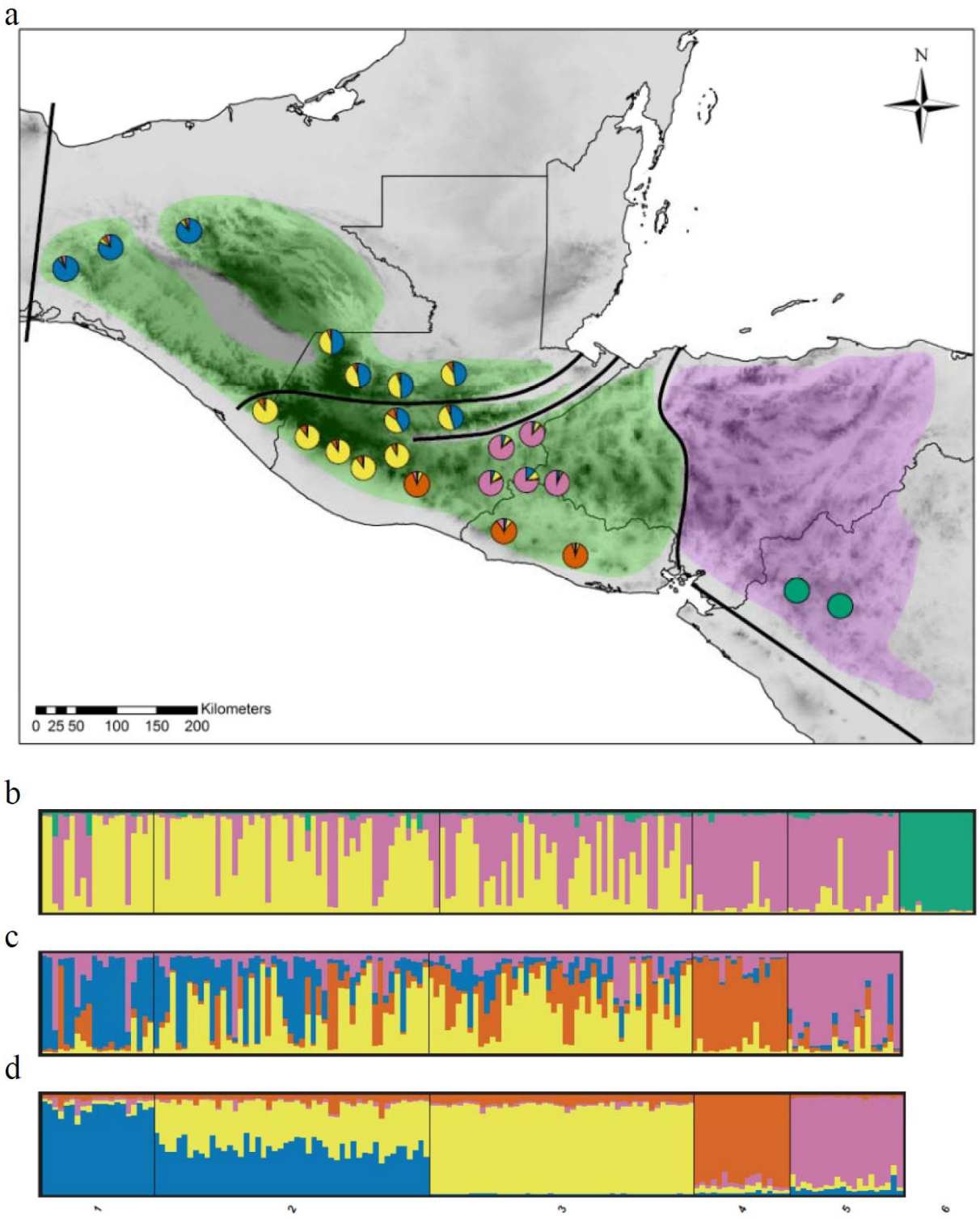


**Figure 5.** Sampling localities and microsatellite groups within *Lampornis viridipallens* and *L. sybillae*. a) Map depicting geographic distribution of genetic groups. The circle pies on the map show the microsatellite groups in each locality. b) Structure analysis of *Lampornis viridipallens* and *L. sybillae*, K = 3. c) Structure analysis of *L. viridipallens*, K = 4. d) Structure analysis of *L. viridipallens* with population prior information, K = 4.

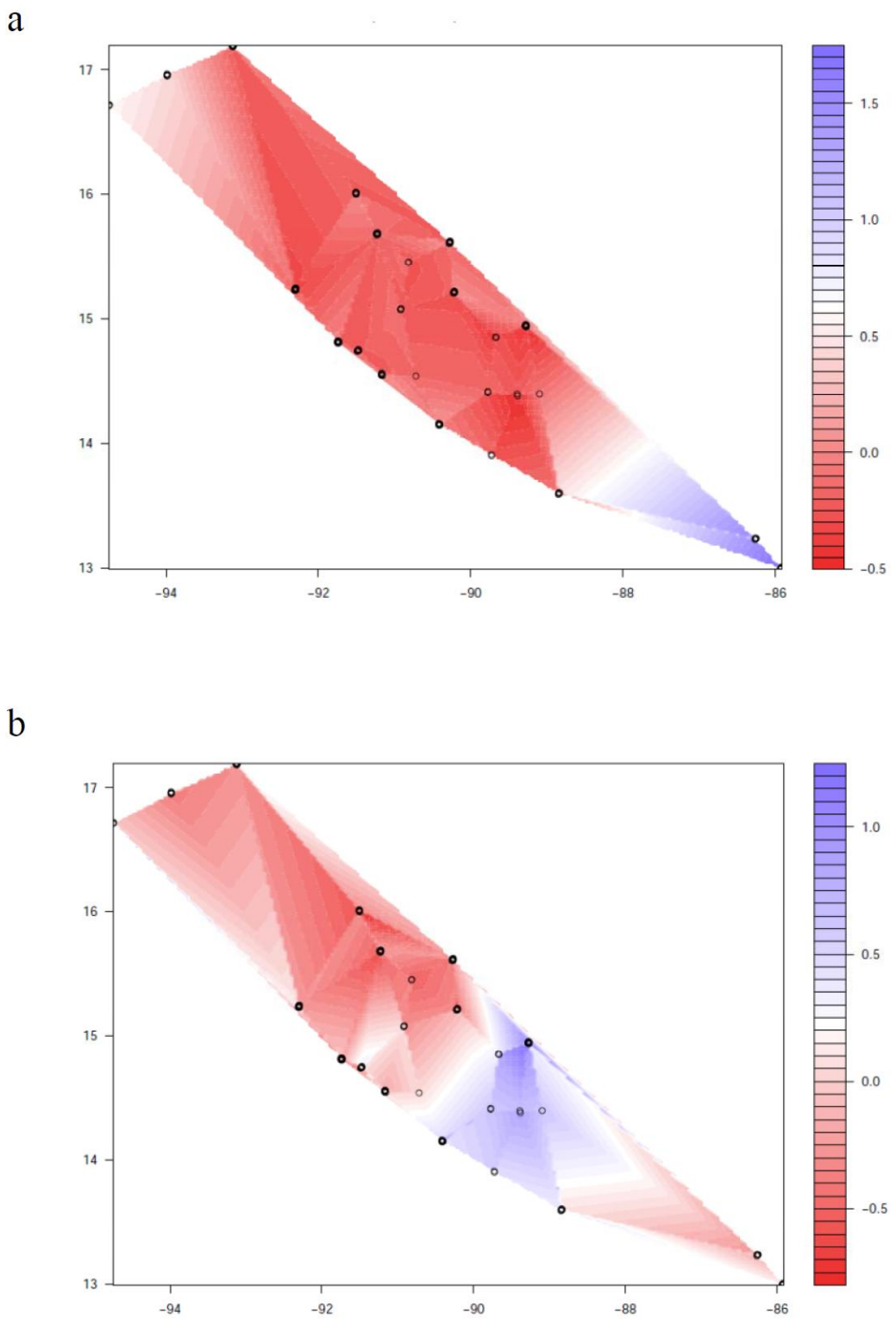


**Figure 6.** Spatial Principal Component Analysis (sPCA) of *Lampornis viridipallens* and *L. sybillae*, 166 samples. a) Interpolated map of individual scores, ls1. b) Interpolated map of individual scores, ls2.

a

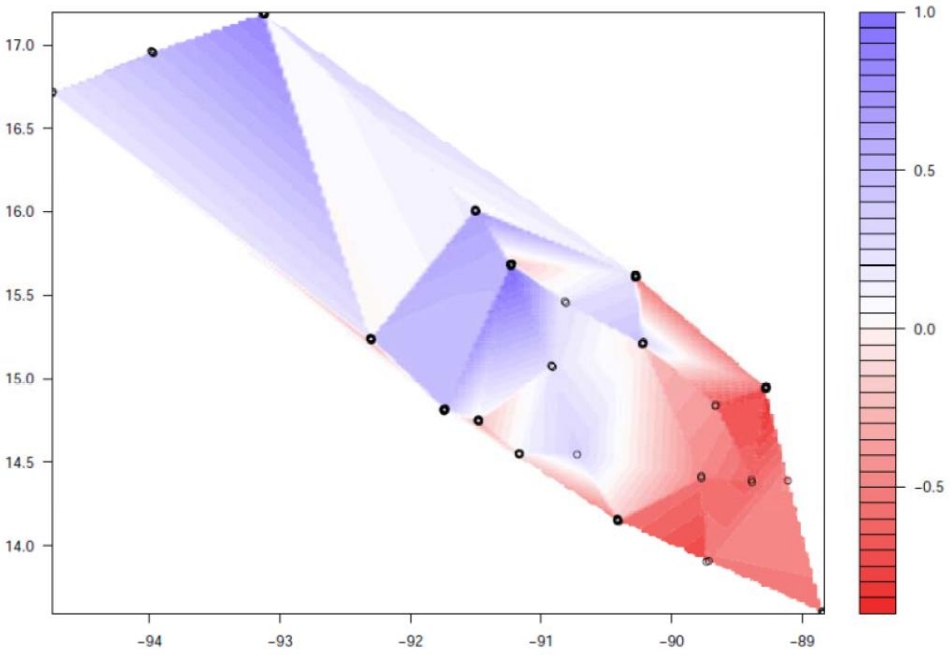


b

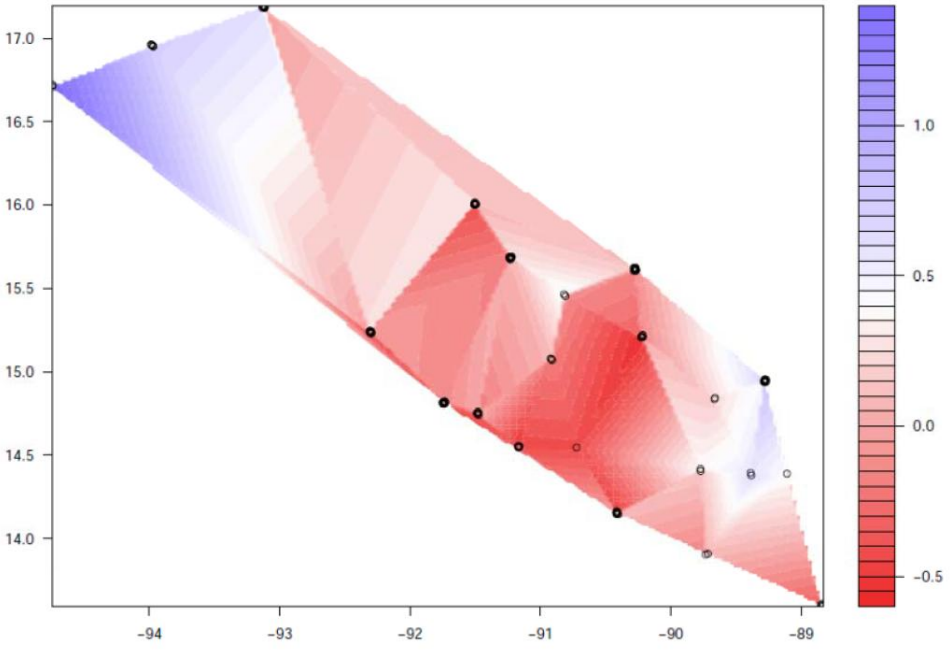


**Figure 7.** Spatial Principal Component Analysis (sPCA) of *Lampornis viridipallens*, 153 samples. a) Interpolated map of individual scores, ls1. b) Interpolated map of individual scores, ls2.

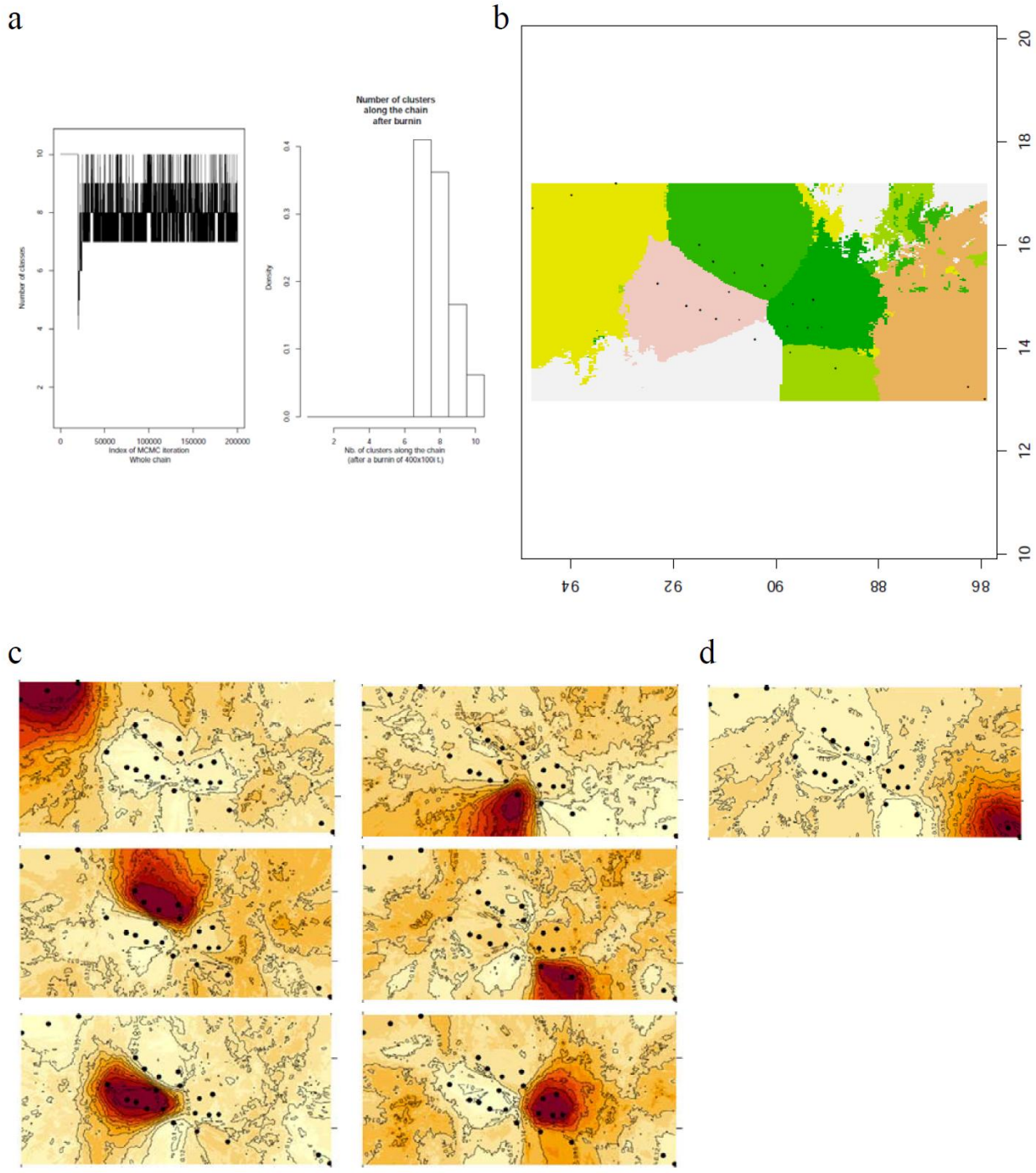


**Figure 8.** Barrier detection analysis of *Lampornis viridipallens* and *L. sybillae* based on 13 microsatellite loci (n = 166). a) Number of clusters. c) Estimated cluster membership. c) Maps of posterior probabilities to belong to a cluster within *L. viridipallens*. d) Map of posterior probabilities to belong to the cluster of *L. sybillae*.

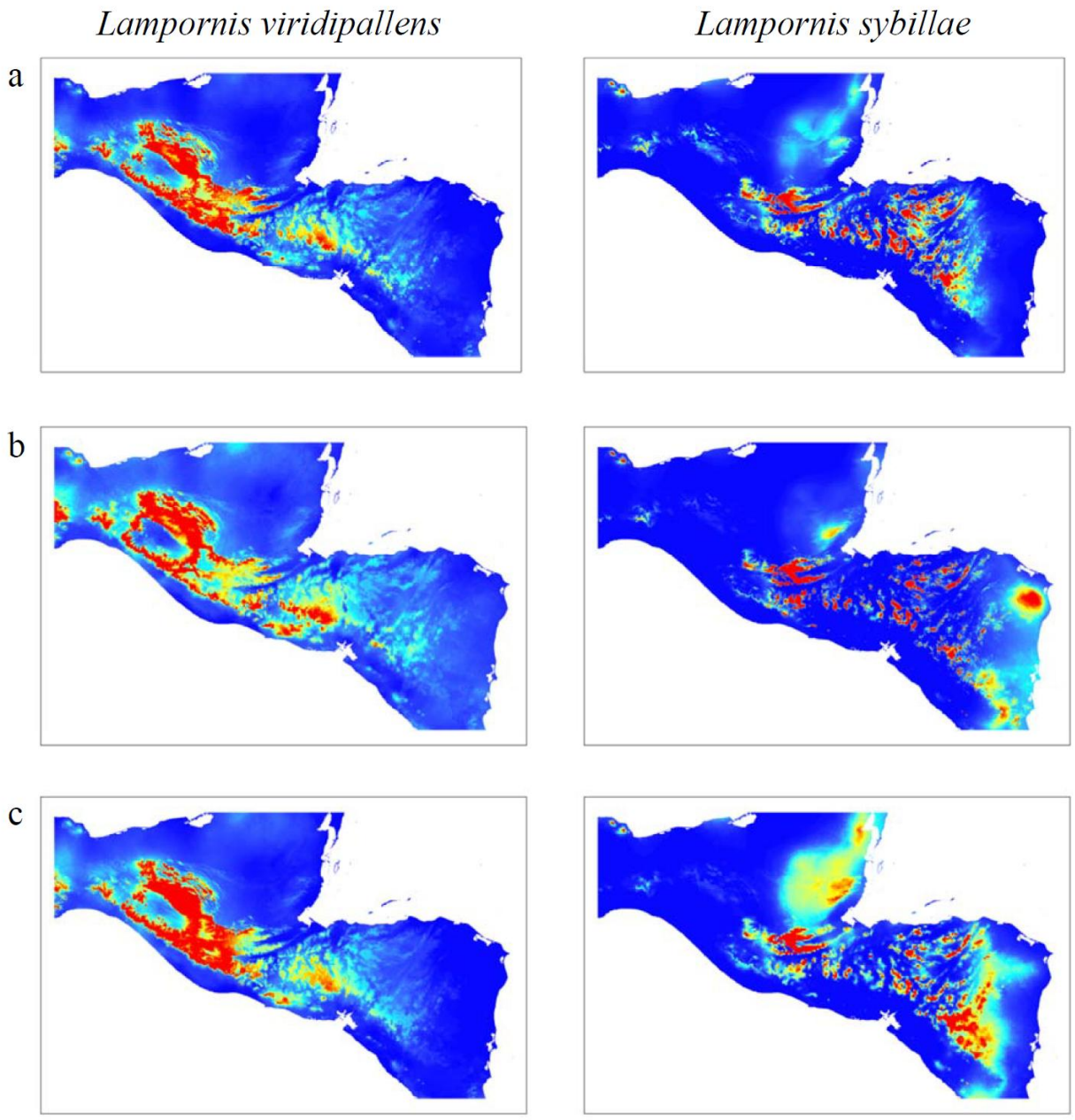


**Figure 9.** Species distribution modeling and paleodistribution models of *Lampornis viridipallens* and *L. sybillae*. a) Present. b) Last Glacial Maximum (21,000 - 18,000 years ago). c) Last Interglacial (140,000 - 120,000 years ago).

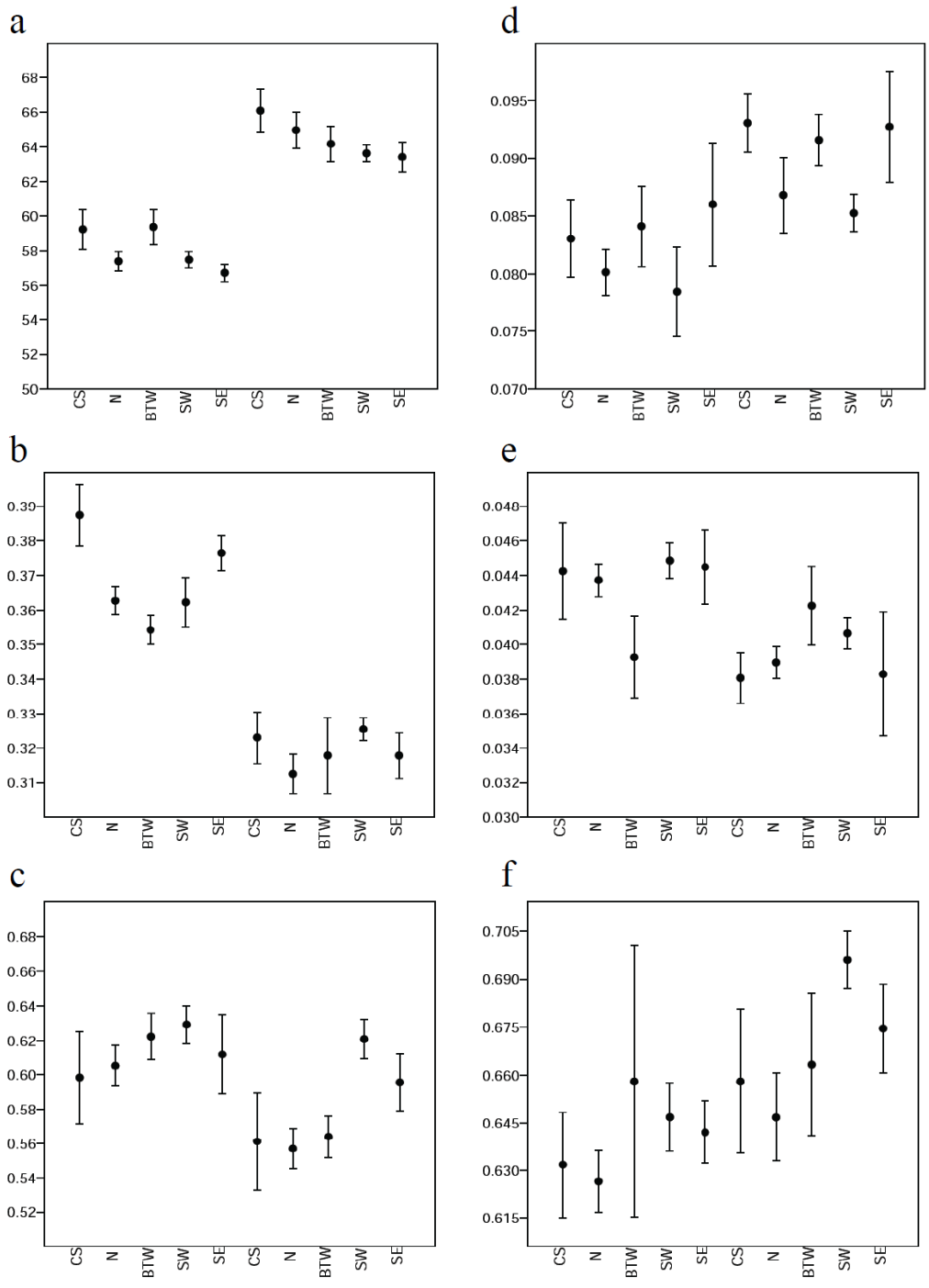


**Figure 10.** Morphological variation within *Lampornis viridipallens*. a) Wing length. b) Bill length – wing length ratio. c) Tail feather R1 – wing length ratio. d) Mass – wing length ratio. e) Bill width – wing length ratio. f) Tail feather R5 – wing length ratio. CS: Sierra Atravesada and Altos de Chiapas. N: North of Motagua-Polochic-Jocotán Fault System (MPJFS). BTW: Between MPJFS. SW: Southwest of MPJFS. SE: Southeast of MPJFS. Females are at the left of each graph, and males are at the right. The black dot represents the mean and the whiskers, the standard error.

## References


Barrios-Izás, M. A. (2020). Taxonomy of the weevil genus *Plumolepilius* Barrios-Izás amp; Anderson (Coleoptera: Curculionidae: Molytinae: Conotrachelini): new species from Central America. Zootaxa, 4768(2).

Beerli, P., Mashayekhi, S., Sadeghi, M., Khodaei, M., & Shaw, K. (2019). Population genetic inference with MIGRATE. Current protocols in bioinformatics, 68(1).

Bergoeing, J. P. (2015). Geomorphology of Central America: A Syngenetic Perspective. Elsevier.

Beza-Beza, C. F., Jiménez-Ferbans, L., & McKenna, D. D. (2021). Historical biogeography of New World passalid beetles (Coleoptera, Passalidae) reveals Mesoamerican tropical forests as a centre of origin and taxonomic diversification. Journal of Biogeography.

Bowie, R. C., Fjeldså, J., Hackett, S. J., & Crowe, T. M. (2004). Systematics and biogeography of double-collared sunbirds from the Eastern Arc Mountains, Tanzania. The Auk, 121(3), 660-681.

Bradbury, I. R., Hamilton, L. C., Dempson, B., Robertson, M. J., Bourret, V., Bernatchez, L., & Verspoor, E. (2015). Transatlantic secondary contact in Atlantic Salmon, comparing microsatellites, a single nucleotide polymorphism array and restriction-site associated DNA sequencing for the resolution of complex spatial structure. Molecular Ecology, 24(20), 5130-5144.

Braconnot, P., Otto-Bliesner, B., Harrison, S., Joussaume, S., Peterchmitt, J. Y., Abe-Ouchi, A., ... & Zhao, Y. (2007). Results of PMIP2 coupled simulations of the Mid-Holocene and Last Glacial Maximum–Part 2: feedbacks with emphasis on the location of the ITCZ and mid-and high latitudes heat budget. Climate of the Past, 3(2), 279-296.

Brown, A.D., & Kappelle, M. (2001).Introducción a los bosques nublados del neotrópico: una síntesis regional. In: M. Kappelle & A. D. Brown (Eds.) Bosques nublados del neotrópico. Costa Rica: INBio, 25-40.

Cadena, C. D., Pérez-Emán, J. L., Cuervo, A. M., Céspedes, L. N., Epperly, K. L., & Klicka, J. T. (2019). Extreme genetic structure and dynamic range evolution in a montane passerine bird: implications for tropical diversification. Biological Journal of the Linnean Society, 126(3), 487-506.

Cano, E. B., Schuster, J. C., & Morrone, J. J. (2018). Phylogenetics of *Ogyges kaup* and the biogeography of Nuclear Central America (Coleoptera, Passalidae). ZooKeys, (737), 81.

Chaves, J. A., Weir, J. T., & Smith, T. B. (2011). Diversification in *Adelomyia* hummingbirds follows Andean uplift. Molecular Ecology, 20(21), 4564-4576.

Chiucchi, J. E., & Gibbs, H. L. (2010). Similarity of contemporary and historical gene flow among highly fragmented populations of an endangered rattlesnake. Molecular Ecology, 19(24), 5345-5358.

Cicero, C., & Johnson, N. K. (2001). Higher-level phylogeny of New World vireos (Aves: Vireonidae) based on sequences of multiple mitochondrial DNA genes. Molecular Phylogenetics and Evolution, 20(1), 27-40.

Clement, M., Posada, D., & Crandall, K. A. (2000). TCS: a computer program to estimate gene genealogies. Molecular Ecology, 9(10):1657-1659.

Coyne, J. A., & Orr, H. A. (2004). Speciation. Sinauer Associates.

Darriba, D., Taboada, G. L., Doallo, R., & Posada, D. (2012). jModelTest 2: more models, new heuristics and parallel computing. Nature Methods, 9(8), 772-772.

Darwin, C. (1859). On the origin of species by means of natural selection. London.
Daza, J. M., Castoe, T. A., & Parkinson, C. L. (2010). Using regional comparative phylogeographic data from snake lineages to infer historical processes in Middle America. Ecography, 33(2), 343-354.
Drummond, A. J., & Rambaut, A. (2007). BEAST: Bayesian evolutionary analysis by sampling trees. BMC evolutionary biology, 7(1), 1-8.
Earl, D. A., & VonHoldt, B. M. (2012). STRUCTURE HARVESTER: a website and program for visualizing STRUCTURE output and implementing the Evanno method. Conservation Genetics Resources, 4(2), 359-361.
Edwards, S. V., Potter, S., Schmitt, C. J., Bragg, J. G., & Moritz, C. (2016). Reticulation, divergence, and the phylogeography–phylogenetics continuum. Proceedings of the National Academy of Sciences, 113(29), 8025-8032.
Elías, D. J., McMahan, C. D., Matamoros, W. A., Gómez-González, A. E., Piller, K. R., & Chakrabarty, P. (2020). Scale (s) matter: Deconstructing an area of endemism for Middle American freshwater fishes. Journal of Biogeography, 47(11), 2483-2501.
Ellis, A., DeMets, C., McCaffrey, R., Briole, P., Cosenza Muralles, B., Flores, O., ... & Tikoff, B. (2019). GPS constraints on deformation in northern Central America from 1999 to 2017, Part 2: Block rotations and fault slip rates, fault locking and distributed deformation. Geophysical Journal International, 218(2), 729-754.
Epps, C. W., Wasser, S. K., Keim, J. L., Mutayoba, B. M., & Brashares, J. S. (2013). Quantifying past and present connectivity illuminates a rapidly changing landscape for the African elephant. Molecular Ecology, 22(6), 1574-1588.
Evanno, G., Regnaut, S., & Goudet, J. (2005). Detecting the number of clusters of individuals using the software STRUCTURE: a simulation study. Molecular Ecology, 14(8), 2611-2620.
Excoffier, L., & Lischer, H. E. (2010). Arlequin suite ver 3.5: a new series of programs to perform population genetics analyses under Linux and Windows. Molecular Ecology Resources, 10(3), 564-567.
Firneno Jr, T. J., O'Neill, J. R., Portik, D. M., Emery, A. H., Townsend, J. H., & Fujita, M. K. (2020). Finding complexity in complexes: Assessing the causes of mitonuclear discordance in a problematic species complex of Mesoamerican toads. Molecular Ecology, 29(18), 3543-3559.
Franklin, J. (2013). Species distribution models in conservation biogeography: developments and challenges. Diversity and Distributions 19: 1217-1223.
Fu, Y. X. (1997). Statistical tests of neutrality of mutations against population growth, hitchhiking and background selection. Genetics, 147(2), 915-925.
García-Moreno, J., Cortés, N., García-Deras, G. M., & Hernández-Baños, B. E. (2006). Local origin and diversification among *Lampornis* hummingbirds: a Mesoamerican taxon. Molecular Phylogenetics and Evolution, 38(2), 488-498.
García-Rodríguez, A., Velasco, J. A., Villalobos, F., & Parra-Olea, G. (2021). Effects of evolutionary time, speciation rates and local abiotic conditions on the origin and maintenance of amphibian montane diversity. Global Ecology and Biogeography, 30(3), 674-684.
Grant, P. R., & Grant, B. R. (1992). Hybridization of bird species. Science 256, 193-197.
Guillot, G., Mortier, F., & Estoup, A. (2005). GENELAND: a computer package for landscape genetics. Molecular Ecology Notes, 5(3), 712-715.

Guindon, S., & Gascuel, O. (2003). A simple, fast, and accurate algorithm to estimate large phylogenies by maximum likelihood. Systematic Biology, 52(5), 696-704.
Hammer, Ø., Harper, D. A., & Ryan, P. D. (2001). PAST: Paleontological statistics software package for education and data analysis. Palaeontologia Electronica, 4(1), 9.
Hasumi, H., & Emori, S. (2004). Coupled GCM (MIROC) description. Center for Climate System Research, University of Tokyo.
Hijmans, R. J., Cameron, S. E., Parra, J. L., Jones, P. G., & Jarvis, A. (2005). Very high resolution interpolated climate surfaces for global land areas. International Journal of Climatology: A Journal of the Royal Meteorological Society, 25(15), 1965-1978.
Ho, S. Y., Lanfear, R., Bromham, L., Phillips, M. J., Soubrier, J., Rodrigo, A. G., & Cooper, A. (2011). Time-dependent rates of molecular evolution. Molecular Ecology, 20(15), 3087-3101.
Hofmann, E. P., & Townsend, J. H. (2017). Origins and biogeography of the *Anolis crassulus* subgroup (Squamata: Dactyloidae) in the highlands of Nuclear Central America. BMC Evolutionary Biology, 17(1), 1-14.
Howell, S. N., & Webb, S. (1995). A guide to the birds of Mexico and northern Central America. Oxford University Press.
Huelsenbeck, J. P., & Ronquist, F. R. (2001). MRBAYES: Bayesian inference of phylogeny. Bioinformatics, 17, 754-755.
Iturralde-Vinent, M.A. (2006). El Origen Paleogrográfico de la Biota de Guatemala. In: E. B. Cano (Ed.) Biodiversidad de Guatemala Vol. I. Universidad del Valle de Guatemala.
Jiménez, R. A., & Ornelas, J. F. (2016). Historical and current introgression in a Mesoamerican hummingbird species complex: a biogeographic perspective. PeerJ, 4, e1556.
Jombart, T., Devillard, S., & Balloux, F. (2010). Discriminant analysis of principal components: a new method for the analysis of genetically structured populations. BMC genetics, 11(1), 1-15.
Jombart, T., Devillard, S., Dufour, A. B., & Pontier, D. (2008). Revealing cryptic spatial patterns in genetic variability by a new multivariate method. Heredity, 101(1), 92-103.
Jombart, T. (2008). adegenet: a R package for the multivariate analysis of genetic markers. Bioinformatics, 24(11), 1403-1405.
Keenan, K., McGinnity, P., Cross, T. F., Crozier, W. W., & Prodöhl, P. A. (2013). diveRsity: An R package for the estimation and exploration of population genetics parameters and their associated errors. Methods in Ecology and Evolution, 4(8), 782-788.
Kumar, S., Stecher, G., & Tamura, K. (2016). MEGA7: molecular evolutionary genetics analysis version 7.0 for bigger datasets. Molecular Biology and Evolution, 33(7), 1870-1874.
Landaverde-González, P., Enríquez, E., Ariza, M. A., Murray, T., Paxton, R. J., & Husemann, M. (2017). Fragmentation in the clouds? The population genetics of the native bee Partamona bilineata (Hymenoptera: Apidae: Meliponini) in the cloud forests of Guatemala. Conservation Genetics, 18(3), 631-643.
Leigh, J. W., & Bryant, D. (2015). popart: full-feature software for haplotype network construction. Methods in Ecology and Evolution, 6(9), 1110-1116.
Lerner, H. R., Meyer, M., James, H. F., Hofreiter, M., & Fleischer, R. C. (2011). Multilocus resolution of phylogeny and timescale in the extant adaptive radiation of Hawaiian honeycreepers. Current Biology, 21(21), 1838-1844.
Librado, P., & Rozas, J. (2009). DnaSP v5: a software for comprehensive analysis of DNA polymorphism data. Bioinformatics, 25(11), 1451-1452.

McGuire, J. A., Witt, C. C., Remsen Jr, J. V., Corl, A., Rabosky, D. L., Altshuler, D. L., & Dudley, R. (2014). Molecular phylogenetics and the diversification of hummingbirds. Current Biology, 24(8), 910-916.

Melo, M., Warren, B. H., & Jones, P. J. (2011). Rapid parallel evolution of aberrant traits in the diversification of the Gulf of Guinea white-eyes (Aves, Zosteropidae). Molecular Ecology, 20(23), 4953-4967.

Metz, C. E. (1978, October). Basic principles of ROC analysis. In Seminars in nuclear medicine (Vol. 8, No. 4, pp. 283-298). WB Saunders.

Molecular Ecology Resources Primer Development Consortium, Abdoullaye, D., Acevedo, I., Adebayo, A. A., Behrmann-Godel, J. A. S. M. I. N. C. A., Benjamin, R. C., ... & ZHOU, Y. (2010). Permanent genetic resources added to molecular ecology resources database 1 August 2009–30 September 2009. Molecular Ecology Resources, 10(1), 232-236.

Morales-Barbero, J., Gouveia, S. F., & Martinez, P. A. (2021). Historical climatic instability predicts the inverse latitudinal pattern in speciation rate of modern mammalian biota. Journal of Evolutionary Biology, 34(2), 339-351.

Musher, L. J., Galante, P. J., Thom, G., Huntley, J. W., & Blair, M. E. (2020). Shifting ecosystem connectivity during the Pleistocene drove diversification and gene-flow in a species complex of Neotropical birds (Tityridae: *Pachyramphus*). Journal of Biogeography, 47(8), 1714-1726.

Ornelas, J. F., González, C., Hernández-Baños, B. E., & García-Moreno, J. (2016). Molecular and iridescent feather reflectance data reveal recent genetic diversification and phenotypic differentiation in a cloud forest hummingbird. Ecology and Evolution, 6(4), 1104-1127.

Ortega-Gutiérrez, F., Solari, L. A., Ortega-Obregon, C., Elias-Herrera, M., Martens, U., Moran-Ical, S., ... & Schaaf, P. (2007). The Maya-Chortís boundary: a tectonostratigraphic approach. International Geology Review, 49(11), 996-1024.

Ottenburghs, J., Ydenberg, R. C., Van Hooft, P., Van Wieren, S. E., & Prins, H. H. (2015). The Avian Hybrids Project: gathering the scientific literature on avian hybridization. Ibis, 157(4), 892-894.

Otto-Bliesner, B. L., Hewitt, C. D., Marchitto, T. M., Brady, E., Abe-Ouchi, A., Crucifix, M., ... & Weber, S. L. (2007). Last Glacial Maximum ocean thermohaline circulation: PMIP2 model intercomparisons and data constraints. Geophysical Research Letters, 34(12).

Oyler-McCance, S. J., Fike, J. A., Talley-Farnham, T., Engelman, T., & Engelman, F. (2011). Characterization of ten microsatellite loci in the Broad-tailed Hummingbird (Selasphorus platycercus). Conservation Genetics Resources, 3(2), 351-353.

Pearson, R. G., Raxworthy, C. J., Nakamura, M., & Townsend Peterson, A. (2007). Predicting species distributions from small numbers of occurrence records: a test case using cryptic geckos in Madagascar. Journal of Biogeography, 34(1), 102-117.

Pérez Consuegra, S. G., & Vázquez-Domínguez, E. (2015). Mitochondrial diversification of the *Peromyscus mexicanus* species group in Nuclear Central America: biogeographic and taxonomic implications. Journal of Zoological Systematics and Evolutionary Research, 53(4), 300-311.

Peterson, A. T., Soberón, J., Pearson, R. G., Anderson, R. P., Martínez-Meyer, E., Nakamura, M., & Araújo, M. B. (2011). Ecological niches and geographic distributions (MPB-49). Princeton University Press.

Phillips, S. J., Anderson, R. P., & Schapire, R. E. (2006). Maximum entropy modeling of species geographic distributions. Ecological modelling, 190(3-4), 231-259.

Phillips, S. J., Dudík, M., & Schapire, R. E. (2017). Maxent software for modeling species niches and distributions (Version 3.4. 1). Biodiversity Informatics.
Ponce-Reyes, R., Reynoso-Rosales, V. H., Watson, J. E., VanDerWal, J., Fuller, R. A., Pressey, R. L., & Possingham, H. P. (2012). Vulnerability of cloud forest reserves in Mexico to climate change. Nature Climate Change, 2(6), 448-452.
Pritchard, J. K., Stephens, M., & Donnelly, P. (2000). Inference of population structure using multilocus genotype data. Genetics, 155(2), 945-959.
Rambaut, A., Drummond, A. J., Xie, D., Baele, G., & Suchard, M. A. (2018). Posterior summarization in Bayesian phylogenetics using Tracer 1.7. Systematic Biology, 67(5), 901.
Ramírez-Barahona, S., & Eguiarte, L. E. (2013). The role of glacial cycles in promoting genetic diversity in the Neotropics: the case of cloud forests during the Last Glacial Maximum. Ecology and Evolution, 3(3), 725-738.
Rato, C., Harris, D. J., Perera, A., Carvalho, S. B., Carretero, M. A., & Rödder, D. (2015). A combination of divergence and conservatism in the niche evolution of the Moorish gecko, *Tarentola mauritanica* (Gekkota: Phyllodactylidae). PLoS One, 10(5), e0127980.
Raymond, M. (1995). GENEPOP (version 1.2): population genetics software for exact tests and ecumenicism. Journal of Heredity, 86, 248-249.
Rice, W. R. (1989). Analyzing tables of statistical tests. Evolution, 43(1), 223-225.
Rissler, L. J. (2016). Union of phylogeography and landscape genetics. Proceedings of the National Academy of Sciences, 113(29), 8079-8086.
Rodríguez-Gómez, F., Licona-Vera, Y., Silva-Cárdenas, L., & Ornelas, J. F. (2021). Phylogeography, morphology and ecological niche modelling to explore the evolutionary history of Azure-crowned Hummingbird (*Amazilia cyanocephala*, Trochilidae) in Mesoamerica. Journal of Ornithology, 162(2), 529-547.
Rogers, A. R., & Harpending, H. (1992). Population growth makes waves in the distribution of pairwise genetic differences. Molecular Biology and Evolution, 9(3), 552-569.
Rojas-Soto, O. R., Sosa, V., & Ornelas, J. F. (2012). Forecasting cloud forest in eastern and southern Mexico: conservation insights under future climate change scenarios. Biodiversity and Conservation, 21(10), 2671-2690.
Ronquist, F., & Huelsenbeck, J. P. (2003). MrBayes 3: Bayesian phylogenetic inference under mixed models. Bioinformatics, 19(12), 1572-1574.
Rousset, F. (2008). A complete re-implementation of the GENEPOP software for teaching and research. Molecular Ecology Resources, 8, 103-106.
Rovito, S. M., & Parra-Olea, G. (2016). Neotropical plethodontid biogeography: insights from molecular phylogenetics. Copeia, 104(1), 222-232.
Schneider, S., & Excoffier, L. (1999). Estimation of past demographic parameters from the distribution of pairwise differences when the mutation rates vary among sites: application to human mitochondrial DNA. Genetics, 152(3), 1079-1089.
Schuchert, C. (1935). Historical geology of the Antillean-Caribbean region. John Wiley and Sons.
Schuster, J. C., Cano, E. B., & Cardona, C. (2000). Un método sencillo para priorizar la conservación de los bosques nubosos de Guatemala, usando Passalidae (Coleoptera) como organismos indicadores. Acta Zoológica Mexicana, (80), 197-209.
Soley-Guardia, M., Carnaval, A. C., & Anderson, R. P. (2019). Sufficient versus optimal climatic stability during the Late Quaternary: using environmental quality to guide

phylogeographic inferences in a Neotropical montane system. Journal of Mammalogy, 100(6), 1783-1807.
Sorenson, M. D., Ast, J. C., Dimcheff, D. E., Yuri, T., & Mindell, D. P. (1999). Primers for a PCR-based approach to mitochondrial genome sequencing in birds and other vertebrates. Molecular Phylogenetics and Evolution, 12(2), 105-114.
Still, C. J., Foster, P. N., & Schneider, S. H. (1999). Simulating the effects of climate change on tropical montane cloud forests. Nature, 398(6728), 608-610.
Suchard, M. A., & Rambaut, A. (2009). Many-core algorithms for statistical phylogenetics. Bioinformatics, 25(11), 1370-1376.
Sunde, J., Yıldırım, Y., Tibblin, P., & Forsman, A. (2020). Comparing the performance of microsatellites and RADseq in population genetic studies: Analysis of data for pike (*Esox lucius*) and a synthesis of previous studies. Frontiers in genetics, 11, 218.
Swaegers, J., Mergeay, J., Therry, L., Bonte, D., Larmuseau, M. H. D., & Stoks, R. (2014). Unravelling the effects of contemporary and historical range expansion on the distribution of genetic diversity in the damselfly *Coenagrion scitulum*. Journal of Evolutionary Biology, 27(4), 748-759.
Tajima, F. (1989). Statistical method for testing the neutral mutation hypothesis by DNA polymorphism. Genetics, 123, 585-595.
Toews, D. P., & Brelsford, A. (2012). The biogeography of mitochondrial and nuclear discordance in animals. Molecular Ecology, 21(16), 3907-3930.
van Dort J. (2020). Green-breasted Mountain-gem (*Lampornis sybillae*), version 1.0. In Birds of the World (Schulenberg TS, Editor). Cornell Lab of Ornithology, Ithaca, NY, USA.
van Etten J (2017). "R Package gdistance: Distances and Routes on Geographical Grids." Journal of Statistical Software, 76(13), 21. doi: 10.18637/jss.v076.i13.
Volpe, N. L., Robinson, W. D., Frey, S. J., Hadley, A. S., & Betts, M. G. (2016). Tropical forest fragmentation limits movements, but not occurrence of a generalist pollinator species. PLoS One, 11(12), e0167513.
Wang, I. J. (2013). Examining the full effects of landscape heterogeneity on spatial genetic variation: a multiple matrix regression approach for quantifying geographic and ecological isolation. Evolution, 67(12), 3403-3411.
Wang, I. J. (2020). Topographic path analysis for modelling dispersal and functional connectivity: calculating topographic distances using the topoDistance r package. Methods in Ecology and Evolution, 11(2), 265-272.
Warren, D. L., Glor, R. E., & Turelli, M. (2008). Environmental niche equivalency versus conservatism: quantitative approaches to niche evolution. Evolution: International Journal of Organic Evolution, 62(11), 2868-2883.
Warren, D. L., Glor, R. E., & Turelli, M. (2010). ENMTools: a toolbox for comparative studies of environmental niche models. Ecography, 33(3), 607-611.
Warren, D. L., Matzke, N., Cardillo, M., Baumgartner, J., Beaumont, L., Huron, N., ... & Dinnage, R. (2019). ENMTools (Software Package). URL: https://github. com/danlwarren/ENMTools. doi, 10.
Wilson, G. A., & Rannala, B. (2003). Bayesian inference of recent migration rates using multilocus genotypes. Genetics, 163(3), 1177-1191.
Zamudio-Beltrán, L. E., & Hernández-Baños, B. E. (2015). A multilocus analysis provides evidence for more than one species within *Eugenes fulgens* (Aves: Trochilidae). Molecular Phylogenetics and Evolution, 90, 80-84.

Züchner,T, Boesman PFD. (2020). Green-throated Mountain-gem (*Lampornis viridipallens*), version 1.0. In Birds of the World (del Hoyo J, Elliott A, Sargatal J, Christie DA, de Juana E, Editors). Cornell Lab of Ornithology, Ithaca, NY, USA.

## Supplementary tables and figures

**Table S1.** Collection localities for *Lampornis viridipallens* and *L. sybillae.* Region according to the mountain range where the specific locality lays on, in parenthesis, geographic position with respect to the Motagua-Polochic Fault System used in Molecular Analysis of Variance. Subspecies according to geography: *Lampornis viridipallens* (*amadoni*, *ovandensis*, *viridipallens*, *nubivagus*), *L. sybillae* (monotypic). *n* = sample size; MX = Mexico, GT = Guatemala, ES = El Salvador, NI = Nicaragua.

| Locality | Region | Subspecies | *n* |
|---|---|---|---|
| MX: Oaxaca, San Miguel Chimalapa | Sierra Atravesada | *amadoni* | 3 |
| MX: Oaxaca, Cintalapa de Figueroa | Sierra Atravesada | *amadoni* | 6 |
| MX: Chiapas, Tapalapa | Altos de Chiapas | *ovandensis* | 11 |
| GT: Huehuetenango, Yalambojoch | Sierra de los Cuchumatanes (N) | *ovandensis* | 8 |
| GT: Huehuetenango, Soloma | Sierra de los Cuchumatanes (N) | *ovandensis* | 14 |
| GT: Quiché, Uspantán | Sierra de los Cuchumatanes (N) | *ovandensis* | 2 |
| GT: Alta Verapaz, San Pedro Carchá | Sierra de Chamá (N) | *viridipallens* | 15 |
| GT: Quiché, Zacualpa | Sierra de Chuacús | *viridipallens* | 3 |
| GT: Baja Verapaz, Purulhá | Sierra de las Minas | *viridipallens* | 7 |
| MX: Chiapas, Motozintla | Cadena Volcánica del Pacífico (SW) | *viridipallens* | 14 |
| GT: Quetzaltenango, Volcán Lacandón | Cadena Volcánica del Pacífico (SW) | *viridipallens* | 16 |
| GT: Quetzaltenango, Volcán Zunil | Cadena Volcánica del Pacífico (SW) | *viridipallens* | 8 |
| GT: Suchitepéquez, Volcán Atitlán | Cadena Volcánica del Pacífico (SW) | *viridipallens* | 8 |
| GT: Sacatepéquez, San Cristóbal El Alto | Cadena Volcánica del Pacífico (SW) | *viridipallens* | 1 |
| GT: Santa Rosa, Volcán Tecuamburro | Cadena Volcánica del Pacífico (SW) | *viridipallens* | 10 |
| ES: Santa Ana, Volcán Santa Ana | Cadena Volcánica del Pacífico (SW) | *nubivagus* | 2 |
| ES: San Vicente, Volcán San Vicente | Cadena Volcánica del Pacífico (SW) | *nubivagus* | 5 |
| GT: Jutiapa, Volcán Suchitán | E Guatemala (SE) | *viridipallens* | 2 |
| GT: Chiquimula, Cerro El Gigante | E Guatemala (SE) | *viridipallens* | 2 |
| GT: Zacapa, La Unión | E Guatemala (SE) | *viridipallens* | 13 |
| ES: Santa Ana, Cerro Montecristo | NW El Salvador (SE) | *viridipallens* | 2 |
| ES: Chalatenango, Cerro El Pital | NW El Salvador (SE) | *viridipallens* | 1 |
| NI: Estelí | Cordillera Dariense | *sybillae* | 5 |
| NI: Matagalpa | Cordillera Dariense | *sybillae* | 8 |
| **TOTAL** | | | **166** |

**Table S2.** Species names, voucher information, and localities of origin for the specimens examined genetically and morphologically in this study. Museum abbreviations used in voucher numbers: MVZ = Museum of Vertebrate Zoology, University of California, Berkeley; USAC = Escuela de Biología, Universidad de San Carlos de Guatemala; FMNH = Field Museum of Natural History; KU = Kansas University, Natural History Museum; UWBM = Burke Museum of Natural History and Culture; LSUMZ = Louisiana State University Museum of Natural Science. MX = Mexico, GT = Guatemala, ES = El Salvador, NI = Nicaragua.

| No. | Species | Museum | Voucher number | Locality | Microsatellites/ Morphological measurements |
|---|---|---|---|---|---|
| 1 | *Lampornis viridipallens* | LSUMZ | B-19268 | MX: Oaxaca, San Miguel Chimalapa | X |
| 2 | *Lampornis viridipallens* | LSUMZ | B-19269 | MX: Oaxaca, San Miguel Chimalapa | X |
| 3 | *Lampornis viridipallens* | LSUMZ | B-19270 | MX: Oaxaca, San Miguel Chimalapa | X |
| 4 | *Lampornis viridipallens* | MVZ | 188991 | MX: Oaxaca, Cintalapa de Figueroa | X |
| 5 | *Lampornis viridipallens* | MVZ | 188992 | MX: Oaxaca, Cintalapa de Figueroa | X/X |
| 6 | *Lampornis viridipallens* | MVZ | 188993 | MX: Oaxaca, Cintalapa de Figueroa | X |
| 7 | *Lampornis viridipallens* | MVZ | 188994 | MX: Oaxaca, Cintalapa de Figueroa | X/X |
| 8 | *Lampornis viridipallens* | MVZ | 188995 | MX: Oaxaca, Cintalapa de Figueroa | X |
| 9 | *Lampornis viridipallens* | MVZ | 188996 | MX: Oaxaca, Cintalapa de Figueroa | X/X |
| 10 | *Lampornis viridipallens* | MVZ | 188997 | MX: Chiapas, Tapalapa | X |
| 11 | *Lampornis viridipallens* | MVZ | 188998 | MX: Chiapas, Tapalapa | X/X |
| 12 | *Lampornis viridipallens* | MVZ | 188999 | MX: Chiapas, Tapalapa | X/X |
| 13 | *Lampornis viridipallens* | MVZ | 189000 | MX: Chiapas, Tapalapa | X |
| 14 | *Lampornis viridipallens* | MVZ | 189001 | MX: Chiapas, Tapalapa | X |
| 15 | *Lampornis viridipallens* | MVZ | 189002 | MX: Chiapas, Tapalapa | X |
| 16 | *Lampornis viridipallens* | MVZ | 189003 | MX: Chiapas, Tapalapa | X/X |
| 17 | *Lampornis viridipallens* | MVZ | 189004 | MX: Chiapas, Tapalapa | X/X |
| 18 | *Lampornis viridipallens* | MVZ | 189005 | MX: Chiapas, Tapalapa | X/X |
| 19 | *Lampornis viridipallens* | MVZ | 189006 | MX: Chiapas, Tapalapa | X |
| 20 | *Lampornis viridipallens* | MVZ | 189007 | MX: Chiapas, Tapalapa | X/X |
| 21 | *Lampornis viridipallens* | MVZ | 184218 | GT: Huehuetenango, Yalambojoch | X/X |
| 22 | *Lampornis viridipallens* | MVZ | 184219 | GT: Huehuetenango, Yalambojoch | X/X |
| 23 | *Lampornis viridipallens* | MVZ | 184220 | GT: Huehuetenango, Yalambojoch | X/X |
| 24 | *Lampornis viridipallens* | MVZ | 184221 | GT: Huehuetenango, Yalambojoch | X/X |
| 25 | *Lampornis viridipallens* | MVZ | 184222 | GT: Huehuetenango, Yalambojoch | X/X |
| 26 | *Lampornis viridipallens* | MVZ | 184223 | GT: Huehuetenango, Yalambojoch | X/X |
| 27 | *Lampornis viridipallens* | MVZ | 184224 | GT: Huehuetenango, Yalambojoch | X/X |
| 28 | *Lampornis viridipallens* | MVZ | 184225 | GT: Huehuetenango, Yalambojoch | X/X |
| 29 | *Lampornis viridipallens* | MVZ | 189153 | GT: Huehuetenango, Soloma | X/X |
| 30 | *Lampornis viridipallens* | MVZ | 189154 | GT: Huehuetenango, Soloma | X/X |
| 31 | *Lampornis viridipallens* | MVZ | 189155 | GT: Huehuetenango, Soloma | X/X |
| 32 | *Lampornis viridipallens* | MVZ | 189156 | GT: Huehuetenango, Soloma | X/X |
| 33 | *Lampornis viridipallens* | MVZ | 189157 | GT: Huehuetenango, Soloma | X/X |
| 34 | *Lampornis viridipallens* | MVZ | 189158 | GT: Huehuetenango, Soloma | X/X |
| 35 | *Lampornis viridipallens* | MVZ | 189160 | GT: Huehuetenango, Soloma | X/X |
| 36 | *Lampornis viridipallens* | MVZ | 189161 | GT: Huehuetenango, Soloma | X/X |
| 37 | *Lampornis viridipallens* | MVZ | 189162 | GT: Huehuetenango, Soloma | X/X |
| 38 | *Lampornis viridipallens* | MVZ | 189163 | GT: Huehuetenango, Soloma | X/X |
| 39 | *Lampornis viridipallens* | MVZ | 189164 | GT: Huehuetenango, Soloma | X/X |
| 40 | *Lampornis viridipallens* | MVZ | 189165 | GT: Huehuetenango, Soloma | X/X |
| 41 | *Lampornis viridipallens* | MVZ | 189166 | GT: Huehuetenango, Soloma | X/X |
| 42 | *Lampornis viridipallens* | MVZ | 189167 | GT: Huehuetenango, Soloma | X/X |
| 43 | *Lampornis viridipallens* | MVZ | 187366 | GT: Quiché, Uspantán | X |
| 44 | *Lampornis viridipallens* | MVZ | 187367 | GT: Quiché, Uspantán | X |
| 45 | *Lampornis viridipallens* | MVZ | 187351 | GT: Alta Verapaz, San Pedro Carchá | X |
| 46 | *Lampornis viridipallens* | MVZ | 187352 | GT: Alta Verapaz, San Pedro Carchá | X |

| | | | | | |
|---|---|---|---|---|---|
| 47 | *Lampornis viridipallens* | MVZ | 187353 | GT: Alta Verapaz, San Pedro Carchá | X |
| 48 | *Lampornis viridipallens* | MVZ | 187354 | GT: Alta Verapaz, San Pedro Carchá | X |
| 49 | *Lampornis viridipallens* | MVZ | 187355 | GT: Alta Verapaz, San Pedro Carchá | X |
| 50 | *Lampornis viridipallens* | MVZ | 187356 | GT: Alta Verapaz, San Pedro Carchá | X |
| 51 | *Lampornis viridipallens* | MVZ | 187357 | GT: Alta Verapaz, San Pedro Carchá | X |
| 52 | *Lampornis viridipallens* | MVZ | 187358 | GT: Alta Verapaz, San Pedro Carchá | X |
| 53 | *Lampornis viridipallens* | MVZ | 187359 | GT: Alta Verapaz, San Pedro Carchá | X |
| 54 | *Lampornis viridipallens* | MVZ | 187360 | GT: Alta Verapaz, San Pedro Carchá | X |
| 55 | *Lampornis viridipallens* | MVZ | 187361 | GT: Alta Verapaz, San Pedro Carchá | X |
| 56 | *Lampornis viridipallens* | MVZ | 187362 | GT: Alta Verapaz, San Pedro Carchá | X |
| 57 | *Lampornis viridipallens* | MVZ | 187363 | GT: Alta Verapaz, San Pedro Carchá | X |
| 58 | *Lampornis viridipallens* | MVZ | 187364 | GT: Alta Verapaz, San Pedro Carchá | X |
| 59 | *Lampornis viridipallens* | MVZ | 187365 | GT: Alta Verapaz, San Pedro Carchá | X/X |
| 60 | *Lampornis viridipallens* | MVZ | 187369 | GT: Quiché, Zacualpa | X/X |
| 61 | *Lampornis viridipallens* | MVZ | 187371 | GT: Quiché, Zacualpa | X/X |
| 62 | *Lampornis viridipallens* | MVZ | 187373 | GT: Quiché, Zacualpa | X/X |
| 63 | *Lampornis viridipallens* | USAC | RAJ219 | GT: Baja Verapaz, Purulhá | X/X |
| 64 | *Lampornis viridipallens* | USAC | RAJ221 | GT: Baja Verapaz, Purulhá | X/X |
| 65 | *Lampornis viridipallens* | USAC | RAJ224 | GT: Baja Verapaz, Purulhá | X/X |
| 66 | *Lampornis viridipallens* | USAC | RAJ237 | GT: Baja Verapaz, Purulhá | X/X |
| 67 | *Lampornis viridipallens* | USAC | SH7 | GT: Baja Verapaz, Purulhá | X/X |
| 68 | *Lampornis viridipallens* | USAC | SH12 | GT: Baja Verapaz, Purulhá | X/X |
| 69 | *Lampornis viridipallens* | USAC | ALAR21 | GT: Baja Verapaz, Purulhá | X |
| 70 | *Lampornis viridipallens* | MVZ | 188056 | MX: Chiapas, Motozintla | X |
| 71 | *Lampornis viridipallens* | MVZ | 188057 | MX: Chiapas, Motozintla | X |
| 72 | *Lampornis viridipallens* | MVZ | 188058 | MX: Chiapas, Motozintla | X |
| 73 | *Lampornis viridipallens* | MVZ | 188059 | MX: Chiapas, Motozintla | X |
| 74 | *Lampornis viridipallens* | MVZ | 188060 | MX: Chiapas, Motozintla | X/X |
| 75 | *Lampornis viridipallens* | MVZ | 188061 | MX: Chiapas, Motozintla | X/X |
| 76 | *Lampornis viridipallens* | MVZ | 188062 | MX: Chiapas, Motozintla | X |
| 77 | *Lampornis viridipallens* | MVZ | 188063 | MX: Chiapas, Motozintla | X |
| 78 | *Lampornis viridipallens* | MVZ | 188064 | MX: Chiapas, Motozintla | X |
| 79 | *Lampornis viridipallens* | MVZ | 188065 | MX: Chiapas, Motozintla | X |
| 80 | *Lampornis viridipallens* | MVZ | 188066 | MX: Chiapas, Motozintla | X |
| 81 | *Lampornis viridipallens* | MVZ | 188067 | MX: Chiapas, Motozintla | X/X |
| 82 | *Lampornis viridipallens* | MVZ | 188068 | MX: Chiapas, Motozintla | X |
| 83 | *Lampornis viridipallens* | MVZ | 188070 | MX: Chiapas, Motozintla | X/X |
| 84 | *Lampornis viridipallens* | MVZ | 187070 | GT: Quetzaltenango, Volcán Lacandón | X |
| 85 | *Lampornis viridipallens* | MVZ | 187071 | GT: Quetzaltenango, Volcán Lacandón | X/X |
| 86 | *Lampornis viridipallens* | MVZ | 187072 | GT: Quetzaltenango, Volcán Lacandón | X/X |
| 87 | *Lampornis viridipallens* | MVZ | 187073 | GT: Quetzaltenango, Volcán Lacandón | X |
| 88 | *Lampornis viridipallens* | MVZ | 187074 | GT: Quetzaltenango, Volcán Lacandón | X/X |
| 89 | *Lampornis viridipallens* | MVZ | 187075 | GT: Quetzaltenango, Volcán Lacandón | X/X |
| 90 | *Lampornis viridipallens* | MVZ | 187076 | GT: Quetzaltenango, Volcán Lacandón | X |
| 91 | *Lampornis viridipallens* | MVZ | 187077 | GT: Quetzaltenango, Volcán Lacandón | X/X |
| 92 | *Lampornis viridipallens* | MVZ | 187078 | GT: Quetzaltenango, Volcán Lacandón | X |
| 93 | *Lampornis viridipallens* | MVZ | 187079 | GT: Quetzaltenango, Volcán Lacandón | X/X |
| 94 | *Lampornis viridipallens* | MVZ | 187080 | GT: Quetzaltenango, Volcán Lacandón | X |
| 95 | *Lampornis viridipallens* | MVZ | 187081 | GT: Quetzaltenango, Volcán Lacandón | X |
| 96 | *Lampornis viridipallens* | MVZ | 187082 | GT: Quetzaltenango, Volcán Lacandón | X/X |
| 97 | *Lampornis viridipallens* | MVZ | 187083 | GT: Quetzaltenango, Volcán Lacandón | X |
| 98 | *Lampornis viridipallens* | MVZ | 187084 | GT: Quetzaltenango, Volcán Lacandón | X |
| 99 | *Lampornis viridipallens* | MVZ | 187085 | GT: Quetzaltenango, Volcán Lacandón | X/X |
| 100 | *Lampornis viridipallens* | MVZ | 187607 | GT: Quetzaltenango, Volcán Zunil | X/X |
| 101 | *Lampornis viridipallens* | MVZ | 187608 | GT: Quetzaltenango, Volcán Zunil | X/X |
| 102 | *Lampornis viridipallens* | MVZ | 187609 | GT: Quetzaltenango, Volcán Zunil | X/X |
| 103 | *Lampornis viridipallens* | MVZ | 187611 | GT: Quetzaltenango, Volcán Zunil | X/X |
| 104 | *Lampornis viridipallens* | MVZ | 187612 | GT: Quetzaltenango, Volcán Zunil | X/X |
| 105 | *Lampornis viridipallens* | MVZ | 187613 | GT: Quetzaltenango, Volcán Zunil | X/X |

| | | | | | |
|---|---|---|---|---|---|
| 106 | *Lampornis viridipallens* | MVZ | 187614 | GT: Quetzaltenango, Volcán Zunil | X/X |
| 107 | *Lampornis viridipallens* | MVZ | 187615 | GT: Quetzaltenango, Volcán Zunil | X/X |
| 108 | *Lampornis viridipallens* | MVZ | 187086 | GT: Suchitepéquez, Volcán Atitlán | X |
| 109 | *Lampornis viridipallens* | MVZ | 187087 | GT: Suchitepéquez, Volcán Atitlán | X/X |
| 110 | *Lampornis viridipallens* | MVZ | 187088 | GT: Suchitepéquez, Volcán Atitlán | X/X |
| 111 | *Lampornis viridipallens* | MVZ | 187089 | GT: Suchitepéquez, Volcán Atitlán | X/X |
| 112 | *Lampornis viridipallens* | MVZ | 187090 | GT: Suchitepéquez, Volcán Atitlán | X/X |
| 113 | *Lampornis viridipallens* | MVZ | 187259 | GT: Suchitepéquez, Volcán Atitlán | X/X |
| 114 | *Lampornis viridipallens* | MVZ | 187260 | GT: Suchitepéquez, Volcán Atitlán | X/X |
| 115 | *Lampornis viridipallens* | MVZ | 187261 | GT: Suchitepéquez, Volcán Atitlán | X/X |
| 116 | *Lampornis viridipallens* | MVZ | MFAR84 | GT: Sacatepéquez, San Cristóbal El Alto | X |
| 117 | *Lampornis viridipallens* | MVZ | 189168 | GT: Santa Rosa, Volcán Tecuamburro | X/X |
| 118 | *Lampornis viridipallens* | MVZ | 189169 | GT: Santa Rosa, Volcán Tecuamburro | X/X |
| 119 | *Lampornis viridipallens* | MVZ | 189170 | GT: Santa Rosa, Volcán Tecuamburro | X/X |
| 120 | *Lampornis viridipallens* | MVZ | 189171 | GT: Santa Rosa, Volcán Tecuamburro | X |
| 121 | *Lampornis viridipallens* | MVZ | 189172 | GT: Santa Rosa, Volcán Tecuamburro | X |
| 122 | *Lampornis viridipallens* | MVZ | 189173 | GT: Santa Rosa, Volcán Tecuamburro | X/X |
| 123 | *Lampornis viridipallens* | MVZ | 189174 | GT: Santa Rosa, Volcán Tecuamburro | X |
| 124 | *Lampornis viridipallens* | MVZ | 189175 | GT: Santa Rosa, Volcán Tecuamburro | X |
| 125 | *Lampornis viridipallens* | MVZ | 189176 | GT: Santa Rosa, Volcán Tecuamburro | X/X |
| 126 | *Lampornis viridipallens* | MVZ | 189191 | GT: Santa Rosa, Volcán Tecuamburro | X/X |
| 127 | *Lampornis viridipallens* | MVZ | 188343 | GT: Jutiapa, Volcán Suchitán | X/X |
| 128 | *Lampornis viridipallens* | MVZ | 188344 | GT: Jutiapa, Volcán Suchitán | X/X |
| 129 | *Lampornis viridipallens* | KU | 9526 | ES: Santa Ana, Volcán Santa Ana | X |
| 130 | *Lampornis viridipallens* | KU | 25034 | ES: Santa Ana, Volcán Santa Ana | X |
| 131 | *Lampornis viridipallens* | KU | 6457 | ES: San Vicente, Volcán San Vicente | X |
| 132 | *Lampornis viridipallens* | KU | 7683 | ES: San Vicente, Volcán San Vicente | X |
| 133 | *Lampornis viridipallens* | KU | 7737 | ES: San Vicente, Volcán San Vicente | X |
| 134 | *Lampornis viridipallens* | KU | 7763 | ES: San Vicente, Volcán San Vicente | X |
| 135 | *Lampornis viridipallens* | KU | 7767 | ES: San Vicente, Volcán San Vicente | X |
| 136 | *Lampornis viridipallens* | MVZ | 187262 | GT: Chiquimula, Cerro El Gigante | X/X |
| 137 | *Lampornis viridipallens* | MVZ | 187263 | GT: Chiquimula, Cerro El Gigante | X/X |
| 138 | *Lampornis viridipallens* | MVZ | 187616 | GT: Zacapa, La Unión | X/X |
| 139 | *Lampornis viridipallens* | MVZ | 187617 | GT: Zacapa, La Unión | X |
| 140 | *Lampornis viridipallens* | MVZ | 187618 | GT: Zacapa, La Unión | X/X |
| 141 | *Lampornis viridipallens* | MVZ | 187619 | GT: Zacapa, La Unión | X/X |
| 142 | *Lampornis viridipallens* | MVZ | 187620 | GT: Zacapa, La Unión | X/X |
| 143 | *Lampornis viridipallens* | MVZ | 187621 | GT: Zacapa, La Unión | X/X |
| 144 | *Lampornis viridipallens* | MVZ | 187622 | GT: Zacapa, La Unión | X |
| 145 | *Lampornis viridipallens* | MVZ | 187623 | GT: Zacapa, La Unión | X/X |
| 146 | *Lampornis viridipallens* | MVZ | 187624 | GT: Zacapa, La Unión | X |
| 147 | *Lampornis viridipallens* | MVZ | 187625 | GT: Zacapa, La Unión | X/X |
| 148 | *Lampornis viridipallens* | MVZ | 187626 | GT: Zacapa, La Unión | X/X |
| 149 | *Lampornis viridipallens* | MVZ | 187627 | GT: Zacapa, La Unión | X/X |
| 150 | *Lampornis viridipallens* | MVZ | 187628 | GT: Zacapa, La Unión | X/X |
| 151 | *Lampornis viridipallens* | KU | 9408 | ES: Santa Ana, Cerro Montecristo | X |
| 152 | *Lampornis viridipallens* | KU | 9459 | ES: Santa Ana, Cerro Montecristo | X |
| 153 | *Lampornis viridipallens* | KU | 5064 | ES: Chalatenango, Cerro El Pital | X |
| 154 | *Lampornis sybillae* | FMNH | 481715 | NI: Estelí | X |
| 155 | *Lampornis sybillae* | FMNH | 481716 | NI: Estelí | X |
| 156 | *Lampornis sybillae* | FMNH | 481717 | NI: Estelí | X |
| 157 | *Lampornis sybillae* | FMNH | 481718 | NI: Estelí | X |
| 158 | *Lampornis sybillae* | FMNH | 481719 | NI: Estelí | X |
| 159 | *Lampornis sybillae* | UWBM | 56113 | NI: Matagalpa | X |
| 160 | *Lampornis sybillae* | UWBM | 56118 | NI: Matagalpa | X |
| 161 | *Lampornis sybillae* | UWBM | 56121 | NI: Matagalpa | X |
| 162 | *Lampornis sybillae* | UWBM | 56159 | NI: Matagalpa | X |
| 163 | *Lampornis sybillae* | UWBM | 56160 | NI: Matagalpa | X |
| 164 | *Lampornis sybillae* | UWBM | 56178 | NI: Matagalpa | X |

| | | | | | |
|---|---|---|---|---|---|
| 165 | *Lampornis sybillae* | UWBM | 70086 | NI: Matagalpa | X |
| 166 | *Lampornis sybillae* | UWBM | 70112 | NI: Matagalpa | X |
| 167 | *Lampornis calolaemus* | MVZ | 183727 | | |
| 168 | *Lampornis calolaemus* | | | From GenBank: EU042565 | |
| 169 | *Lampornis castaneiventris* | | | From GenBank: EU042566 | |
| 170 | *Lampornis cinereicauda* | | | From GenBank: KJ602256 | |
| 171 | *Lampornis amethystinus* | MVZ | 184226 | | |
| 172 | *Lampornis amethystinus* | MVZ | 184737 | | |
| 173 | *Lampornis amethystinus* | MVZ | 189159 | | |
| 174 | *Lampornis amethystinus* | | | From GenBank: KJ602255 | |
| 175 | *Lampornis clemenciae* | | | From GenBank: KJ602257 | |
| 176 | *Lampornis hemileucus* | | | From GenBank: EU042567 | |
| 177 | *Lampornis hemileucus* | | | From GenBank: KJ602258 | |
| 178 | *Lamprolaima rhami* | MVZ | 184738 | | |
| 179 | *Lamprolaima rhami* | MVZ | 187632 | | |
| 180 | *Eugenes fulgens* | MVZ | 187255 | | |
| 181 | *Eugenes fulgens* | MVZ | 187256 | | |
| 182 | *Calypte anna* | | | From GenBank: EU042532 | |
| 183 | *Hylocharis leucotis* | MVZ | 189152 | | |

**Table S3.** Frequency and number of base pairs (bp), variable sites, and parsimony informative sites for the gene partitions, and DNA substitution models applied to each partition.

| Partition | Included bp | Frequency of variable sites | Frequency of parsimony informative sites | DNA substitution model AICc | AIC |
|---|---|---|---|---|---|
| ATPase6, 8, tRNA | 750 | 0.249 (187) | 0.197 (148) | HKY + I | HKY + I |
| ND2 | 1041 | 0.318 (331) | 0.242 (252) | GTR + G | GTR + G |
| TOTAL | 1791 | 0.289 (518) | 0.223 (400) | | |
| tRNA | 51 | 0.098 (5) | 0.059 (3) | GTR + I | K80 + I |
| ATPase6 | 541 | 0.248 (134) | 0.200 (108) | HKY + I | HKY + I |
| ATPase8 | 168 | 0.286 (48) | 0.220 (37) | HKY + I | HKY + I |
| ND2 | 1041 | 0.318 (331) | 0.242 (252) | GTR + G | GTR + G |
| TOTAL | 1801 | 0.288 (518) | 0.222 (400) | | |
| tRNA | 51 | 0.098 (5) | 0.059 (3) | GTR + I | K80 + I |
| ND2pos1 | 347 | 0.250 (87) | 0.176 (61) | JC | HKY + G |
| ND2pos2 | 347 | 0.072 (25) | 0.035 (12) | JC | GTR + I |
| ND2pos3 | 347 | 0.631 (219) | 0.516 (179) | JC | GTR + I + G |
| ATPase6pos1 | 181 | 0.116 (21) | 0.088 (16) | GTR + I | GTR + I |
| ATPase6pos2 | 180 | 0.039 (7) | 0.028 (5) | HKY | HKY |
| ATPase6pos3 | 180 | 0.589 (106) | 0.483 (87) | HKY + I | HKY + I |
| ATPase8pos1 | 56 | 0.250 (14) | 0.214 (12) | GTR + I | HKY + I |
| ATPase8pos2 | 56 | 0.161 (9) | 0.125 (7) | GTR + G | HKY |
| ATPase8pos3 | 56 | 0.446 (25) | 0.321 (18) | GTR + G | HKY + G |
| TOTAL | 1801 | 0.288 (518) | 0.222 (400) | | |

**Table S4**. Summary statistics of microsatellite loci isolated from the Green-throated Mountain-gem (*Lampornis viridipallens*).

| | | | | N MPJFS (Alta Verapaz) | | | | | S MPJFS (Quetzaltenango) | | | | |
|---|---|---|---|---|---|---|---|---|---|---|---|---|---|
| **Locus** | **Primer sequence (5'-3') and dye label** | **Repeat motif** | **$T_a$(°C)** | ***N*** | ***$N_A$*** | **Allele size range (bp)** | ***$H_O$*** | ***$H_E$*** | ***N*** | ***$N_A$*** | **Allele size range (bp)** | ***$H_O$*** | ***$H_E$*** |
| Lvi14 | F: TTCTGGTCCATTTTACTTTAATACCA (HEX)<br>R: TGTTCTGTGTGAGGCTAACGA | (ATCT)6 | 56 | 15 | 5 | 179 - 203 | 0.47 | 0.79 | 15 | 4 | 175 - 191 | 0.67 | 0.73 |
| Lvi17 | F: TCCTCAGAAATTTAGCTGCTACC (FAM)<br>R: CCAACTTTTAGGTGGGTGGA | (ATCT)5 | 61 | 15 | 6 | 119 - 151 | 0.67 | 0.80 | 15 | 6 | 123 - 151 | 0.73 | 0.79 |
| Lvi51 | F: TGATAAGGACTGACCTGCAAGA (HEX)<br>R: GAATCTGATTTGGATATAAGTCACC | (TATC)11 | 57 | 15 | 6 | 128 - 148 | 0.60 | 0.70 | 15 | 5 | 128 - 144 | 0.73 | 0.71 |
| Lvi76 | F: AATGCATTGGGACTCAGC (FAM)<br>R: ATCTGCAATTGAGACACAGCA | (TATC)12 | 57 | 15 | 8 | 129 - 161 | 0.87 | 0.86 | 15 | 7 | 129 - 153 | 0.47 | 0.80 |
| Lvi82 | F: GCAAAATAAATTTGAGGCAAATAA (HEX)<br>R: CTGTTTAATTTTGAAGCTAGAGATTTT | (ATAC)5 | 56 | 15 | 2 | 139 - 147 | 0.27 | 0.33 | 15 | 2 | 139 - 147 | 0.53 | 0.46 |
| Lvi86 | F: CTCCGAAGCTGACAGTAGCC (FAM)<br>R: CAACTGACAGCTCTATAATAAATGAAG | (TATC)6 | 58 | 15 | 2 | 153 - 161 | 0.13 | 0.13 | 15 | 2 | 161 - 165 | 0.07 | 0.07 |
| Lvi98 | F: TGTCACCTTAGGGGGTAGGA (FAM)<br>R: TGGCAGGGATAAAAGATGGA | (GATA)11 | 62 | 15 | 6 | 128 - 140 | 0.73 | 0.74 | 15 | 7 | 132 - 156 | 0.73 | 0.74 |
| Lvi102 | F: GGTTGCTATGTGTATAAGCTATCAAAA (HEX)<br>R: TGGTGAACTTGTGACCACTCA | (TACA)5 | 56 | 15 | 1 | 150 | 0.00 | 0.00 | 15 | 2 | 142 - 150 | 0.07 | 0.07 |
| Lvi111 | F: TGCTGAAACTTATATGTTGTGTATTGA (FAM)<br>R: TCTCATCTTGCCAACAGTGC | (AGAT)4 | 56 | 15 | 1 | 190 | 0.00 | 0.00 | 15 | 2 | 186 - 190 | 0.13 | 0.13 |
| Lvi151 | F: TTTCAAAGCCAGTTCTTTTCA (HEX)<br>R: GCCAATTCAGTGTTTTCCTCTT | (GA)12 | 60 | 15 | 7 | 161 - 173 | 0.87 | 0.73 | 15 | 4 | 161 - 169 | 0.73 | 0.62 |
| Lvi172 | F: AGTCCCCTGACACCCCTTAC (FAM)<br>R: TTCTGTGACTTGCTGGAACG | (AC)6 | 60 | 15 | 3 | 163 - 167 | 0.60 | 0.48 | 15 | 2 | 163 - 165 | 0.07 | 0.07 |

$T_a$: optimized annealing temperature; *N*: number of individuals genotyped; $N_A$: number of alleles; $H_O$: observed heterozygosity; $H_E$: expected heterozygosity.
No loci showed significant deviation from Hardy-Weinberg equilibrium and no loci were linked in either population, after Bonferroni correction ($p > 0.002$)

**Table S5.** Population differentiation of *Lampornis viridipallens* based on microsatellite data. Pairwise FST values between populations.

| | **1** | **2** | **3** | **4** | **5** | **6** | **7** | **8** | **9** | **10** | **11** | **12** | **13** | **14** | **15** | **16** |
|---|---|---|---|---|---|---|---|---|---|---|---|---|---|---|---|---|
| **1** | ----- | 0.051 | 0.053 | 0.096 | 0.123 | 0.156 | 0.118 | 0.178 | 0.148 | 0.182 | 0.174 | 0.155 | 0.245 | 0.279 | 0.185 | 0.152 |
| **2** | | ----- | 0.045 | 0.027 | 0.048 | 0.073 | 0.023 | 0.135 | 0.063 | 0.069 | 0.078 | 0.049 | 0.128 | 0.164 | 0.140 | 0.089 |
| **3** | | | ----- | 0.016 | 0.030 | 0.073 | 0.010 | 0.106 | 0.072 | 0.067 | 0.059 | 0.073 | 0.157 | 0.149 | 0.113 | 0.058 |
| **4** | | | | ----- | -0.005 | 0.021 | 0.000 | 0.023 | 0.031 | 0.017 | 0.026 | 0.013 | 0.150 | 0.151 | 0.121 | 0.088 |
| **5** | | | | | ----- | 0.012 | 0.017 | 0.028 | 0.018 | 0.020 | 0.034 | 0.009 | 0.124 | 0.154 | 0.093 | 0.061 |
| **6** | | | | | | ----- | 0.033 | 0.022 | 0.025 | 0.032 | 0.052 | 0.011 | 0.100 | 0.119 | 0.091 | 0.054 |
| **7** | | | | | | | ----- | 0.008 | 0.025 | 0.015 | 0.004 | -0.001 | 0.078 | 0.078 | 0.067 | 0.034 |
| **8** | | | | | | | | ----- | 0.058 | 0.055 | 0.054 | 0.018 | 0.172 | 0.176 | 0.099 | 0.091 |
| **9** | | | | | | | | | ----- | 0.001 | 0.031 | -0.001 | 0.069 | 0.119 | 0.098 | 0.063 |
| **10** | | | | | | | | | | ----- | 0.017 | -0.006 | 0.077 | 0.127 | 0.105 | 0.093 |
| **11** | | | | | | | | | | | ----- | 0.002 | 0.110 | 0.163 | 0.081 | 0.075 |
| **12** | | | | | | | | | | | | ----- | 0.087 | 0.145 | 0.084 | 0.065 |
| **13** | | | | | | | | | | | | | ----- | 0.156 | 0.152 | 0.143 |
| **14** | | | | | | | | | | | | | | ----- | 0.186 | 0.175 |
| **15** | | | | | | | | | | | | | | | ----- | -0.018 |
| **16** | | | | | | | | | | | | | | | | ----- |

Sierra Atravesada: 1 – San Miguel Chimalapa. 2 – Cintalapa de Figueroa. Altos de Chiapas: 3 – Tapalapa. Sierra de los Cuchumatanes: 4 – Yalambojoch, 5 – Soloma. Sierra de Chamá: 6 – San Pedro Carchá. Sierra de Chuacús: 7 – Zacualpa. Sierra de las Minas: 8 – Purulhá. Cadena Volcánica del Pacífico: 9 – Motozintla, 10 – Volcán Lacandón, 11 – Volcán Zunil, 12 – Volcán Atitlán, 13 – Volcán Tecuamburro, 14 – Volcán San Vicente. Southeast of the Motagua-Polochic Faults: 15 – La Unión, 16 – Montecristo.

**Table S6.** Summary statistics, neutrality tests and population expansion tests for populations of *Lampornis viridipallens* and *L. sybillae* based on mtDNA. Number of individuals sequenced (*n*), number of haplotypes (*H*), number of segregating sites (*S*), *h* = haplotype diversity, $\pi$ = nucleotide diversity, Tajima's *D*, Fu's *F*s. Positive values for *D* and $F_S$ are indicative of mutation-drift equilibrium, which is typical of stable populations, whereas significant negative values (at the $P = 0.05$ level for Tajima's *D* and for *Fs* tests; Excoffier and Lischer 2010) that result from an excess of rare haplotypes, indicate that populations have experienced a recent bottleneck followed by population expansion. Significant ($P = 0.05$) Hri and SSD values indicate deviations from the sudden expansion model. Significant values are shown in bold (*$P < 0.05$).

| Mountain range / Region | *n* | *H* | *S* | *h* | $\pi$ | Tajima's *D* | Fu's *Fs* | Hri | SSD |
|---|---|---|---|---|---|---|---|---|---|
| ***Lampornis viridipallens*** | | | | | | | | | |
| North of Polochic Fault | | | | | | | | | |
| Sierra Atravesada | 9 | 6 | 6 | 0.833±0.127 | 0.001 | **-1.728*** | **-3.329*** | 0.145 | 0.016 |
| Altos de Chiapas | 11 | 7 | 9 | 0.909±0.066 | 0.001 | -0.771 | 0.802 | 0.078 | 0.027 |
| Sierra de los Cuchumatanes | 24 | 12 | 14 | 0.793±0.085 | 0.001 | **-1.770*** | **-7.122*** | 0.029 | **0.109*** |
| Sierra de Chamá | 15 | 6 | 19 | 0.819±0.064 | 0.004 | 1.186 | 3.230 | 0.091 | 0.106 |
| Between Polochic - Motagua Faults | | | | | | | | | |
| Sierras de Chuacús y de las Minas | 10 | 7 | 26 | 0.867±0.107 | 0.004 | -1.241 | 0.240 | 0.168 | 0.051 |
| South of Motagua Fault | | | | | | | | | |
| Cadena Volcánica del Pacífico (SW of Motagua-Polochic) | 64 | 20 | 35 | 0.835±0.040 | 0.003 | -0.893 | -3.153 | 0.025 | 0.016 |
| E Guatemala and NW El Salvador (SE of Motagua-Polochic) | 20 | 7 | 24 | 0.821±0.059 | 0.004 | -0.010 | 2.825 | 0.042 | 0.040 |
| ***Lampornis sybillae*** | | | | | | | | | |
| Cordillera Dariense | 13 | 9 | 22 | 0.936±0.051 | 0.004 | 0.117 | -0.688 | 0.034 | 0.015 |

**Table S7.** Genetic differentiation between populations of *Lampornis viridipallens* and *L. sybillae* based on mtDNA. Above diagonal: average number of pairwise differences between the populations. Diagonal: average number of pairwise differences within populations. Below the diagonal: pairwise FST values between populations; significant values are shown in bold.

| | **Sierra Atravesada** | **Altos de Chiapas** | **Sierra de los Cuchumatanes** | **Sierra de Chamá** | **Sierras de Chuacús y de las Minas** | **Pacific Volcanic Chain** | **E Guatemala and NW El Salvador** | **Cordillera Dariense** |
|---|---|---|---|---|---|---|---|---|
| Sierra Atravesada | 7.964 | 5.535 | **5.530** | **10.224** | **9.091** | **11.808** | **18.191** | **92.678** |
| Altos de Chiapas | **0.140** | 1.333 | 1.602 | 5.800 | 4.844 | **7.368** | **13.767** | **88.436** |
| Sierra de los Cuchumatanes | **0.173** | -0.006 | 1.855 | **6.089** | **5.150** | **7.697** | **14.100** | **88.603** |
| Sierra de Chamá | **0.243** | **0.187** | **0.267** | 7.543 | 8.000 | **10.388** | **10.900** | **88.010** |
| Sierras de Chuacús y de las Minas | **0.144** | 0.068 | **0.146** | 0.054 | 7.600 | **8.005** | **13.460** | **89.692** |
| Pacific Volcanic Chain | **0.478** | **0.437** | **0.477** | **0.409** | **0.222** | 5.374 | **14.170** | **91.072** |
| E Guatemala and NW El Salvador | **0.602** | **0.650** | **0.707** | **0.347** | **0.473** | **0.588** | 6.747 | **88.269** |
| Cordillera Dariense | **0.918** | **0.945** | **0.958** | **0.916** | **0.917** | **0.937** | **0.921** | 7.282 |

*Lampornis viridipallens*: Sierra Atravesada, Altos de Chiapas, Sierra de los Cuchumatanes, Sierra de Chamá, Sierras de Chuacús y de las Minas, Pacific Volcanic Chain, E Guatemala and NW El Salvador.
*Lampornis sybillae*: Cordillera Dariense.

**Table S8.** Results of analyses of molecular variance of *Lampornis viridipallens* and *L. sybillae* populations based on mtDNA. The populations were grouped (A) by species: *L. viridipallens* vs. *L. sybillae*, (B) within *L. viridipallens*, by mountain range, and (C, D, E) within *L. viridipallens*, by location north vs. south of the Motagua-Polochic system of faults. * $p < 0.05$.

| Source of variation | d.f. | Sum of squares | Variance components | Percentage of variation | Fixation indices |
|---|---|---|---|---|---|
| (A) *Lampornis viridipallens* vs. *L. sybillae* | | | | | |
| Among groups | 1 | 1043.90 | 42.76 | 90.70 | $F_{CT} = 0.91$* |
| Among populations within groups | 22 | 404.26 | 2.43 | 5.15 | $F_{SC} = 0.55$* |
| Within populations | 142 | 277.71 | 1.96 | 4.15 | $F_{ST} = 0.96$* |
| Total | 165 | 1725.87 | 47.15 | | |
| (B) *Lampornis viridipallens* by mountain range | | | | | |
| Among groups | 6 | 279.50 | 1.75 | 37.39 | $F_{CT} = 0.37$* |
| Among populations within groups | 15 | 123.21 | 1.13 | 24.21 | $F_{SC} = 0.39$* |
| Within populations | 131 | 235.27 | 1.80 | 38.39 | $F_{ST} = 0.62$* |
| Total | 152 | 637.98 | 4.68 | | |
| (C) *Lampornis viridipallens* N vs. SW Motagua-Polochic | | | | | |
| Among groups | 1 | 77.98 | 1.44 | 33.77 | $F_{CT} = 0.34$* |
| Among populations within groups | 8 | 69.12 | 0.73 | 17.11 | $F_{SC} = 0.26$* |
| Within populations | 86 | 180.63 | 2.10 | 49.12 | $F_{ST} = 0.51$* |
| Total | 95 | 327.73 | 4.27 | | |
| (D) *Lampornis viridipallens* N vs. SE Motagua-Polochic | | | | | |
| Among groups | 1 | 97.38 | 3.00 | 47.96 | $F_{CT} = 0.48$* |
| Among populations within groups | 7 | 71.59 | 1.61 | 25.74 | $F_{SC} = 0.49$* |
| Within populations | 50 | 82.15 | 1.64 | 26.30 | $F_{ST} = 0.74$* |
| Total | 58 | 251.12 | 6.25 | | |
| (E) *Lampornis viridipallens* SW vs. SE Motagua-Polochic | | | | | |
| Among groups | 1 | 120.89 | 3.51 | 50.91 | $F_{CT} = 0.51$* |
| Among populations within groups | 9 | 102.96 | 1.54 | 22.42 | $F_{SC} = 0.46$* |
| Within populations | 66 | 121.25 | 1.83 | 26.67 | $F_{ST} = 0.73$* |
| Total | 76 | 345.09 | 6.89 | | |

**Table S9.** Results of analyses of molecular variance of *Lampornis viridipallens* and *L. sybillae* populations based on microsatellites. The populations were grouped (A) by species: *L. viridipallens* vs. *L. sybillae*, (B) within *L. viridipallens*, by Structure, (C) within *L. viridipallens*, by DAPC excluding intermediate group from north of the Polochic fault and between Polochic and Motagua faults, and (D, E, F) within *L. viridipallens*, by location north vs. south of the Motagua-Polochic system of faults. * $p < 0.05$.

| Source of variation | d.f. | Sum of squares | Variance components | Percentage of variation | Fixation indices |
|---|---|---|---|---|---|
| (A) *Lampornis viridipallens* vs. *L. sybillae* | | | | | |
| Among groups | 1 | 32.793 | 0.524 | 12.07 | $F_{CT}$ = 0.121* |
| Among populations within groups | 21 | 160.316 | 0.290 | 6.68 | $F_{SC}$ = 0.076* |
| Within populations | 309 | 1090.295 | 3.528 | 81.25 | $F_{ST}$ = 0.188* |
| Total | 331 | 1283.404 | 4.343 | | |
| (B) *Lampornis viridipallens* by Structure | | | | | |
| Among groups | 3 | 54.635 | 0.248 | 6.42 | $F_{CT}$ = 0.064* |
| Among populations within groups | 11 | 58.545 | 0.155 | 4.01 | $F_{SC}$ = 0.043* |
| Within populations | 193 | 666.652 | 3.454 | 89.57 | $F_{ST}$ = 0.104* |
| Total | 207 | 779.832 | 3.857 | | |
| (C) *Lampornis viridipallens* by DAPC | | | | | |
| Among groups | 4 | 69.386 | 0.192 | 4.92 | $F_{CT}$ = -0.049* |
| Among populations within groups | 16 | 86.441 | 0.142 | 3.64 | $F_{SC}$ = 0.038* |
| Within populations | 285 | 1013.745 | 3.557 | 91.44 | $F_{ST}$ = 0.086* |
| Total | 305 | | | | |
| (D) *Lampornis viridipallens* N vs. SW Motagua-Polochic | | | | | |
| Among groups | 1 | 13.238 | 0.077 | 2.09 | $F_{CT}$ = 0.021* |
| Among populations within groups | 8 | 43.275 | 0.107 | 2.92 | $F_{SC}$ = 0.030* |
| Within populations | 182 | 635.727 | 3.493 | 95.00 | $F_{ST}$ = 0.050* |
| Total | 191 | 692.240 | 3.677 | | |
| (E) *Lampornis viridipallens* N vs. SE Motagua-Polochic | | | | | |
| Among groups | 1 | 20.386 | 0.286 | 7.03 | $F_{CT}$ = 0.070* |
| Among populations within groups | 6 | 27.814 | 0.075 | 1.85 | $F_{SC}$ = 0.020* |
| Within populations | 110 | 407.334 | 3.703 | 91.11 | $F_{ST}$ = 0.089* |
| Total | 117 | 455.534 | 4.064 | | |
| (F) *Lampornis viridipallens* SW vs. SE Motagua-Polochic | | | | | |
| Among groups | 1 | 20.456 | 0.246 | 6.55 | $F_{CT}$ = 0.066* |
| Among populations within groups | 8 | 41.001 | 0.125 | 3.33 | $F_{SC}$ = 0.036* |
| Within populations | 144 | 487.303 | 3.384 | 90.12 | $F_{ST}$ = 0.099* |
| Total | 153 | 548.760 | 3.755 | | |

**Table S10.** Morphological variation within *Lampornis viridipallens* . * $p < 0.05$.

| | **Mass - WL ratio** | **Bill length - WL ratio** | **Bill width - WL ratio** | **Tail R1 - WL ratio** | **Tail R5 - WL ratio** |
|---|---|---|---|---|---|
| Levene's test for homogeneity of variance | 0.2499 | 0.2674 | 0.05428 | 0.3802 | 0.7949 |
| Two-way ANOVA | | | | | |
| Sex | **0.0019*** | **<0.0001*** | **<0.0001*** | **0.0167*** | **0.0001*** |
| Population | 0.1141 | **0.0391*** | 0.9143 | **0.0086*** | **0.0090*** |
| Interaction | 0.9654 | **0.0289*** | 0.1727 | 0.4158 | 0.4977 |
| Tukey's post-hoc | | | | | |
| Sex | F/M **0.0018*** | F/M **<0.0001*** | F/M **<0.0001*** | F/M **0.0165*** | F/M **0.0001*** |
| Population | NA | NA | NA | CS/SW **0.0358*** N/SW **0.0177*** | N/SW **0.0033*** |
| Interaction | NA | F-CS/M-CS **<0.0001*** F-N/M-N **<0.0001*** F-SW/M-SW **<0.0001*** F-SE/M-SE **<0.0001*** | NA | M-N/M-SW **0.0106*** | M-N/M-SW **0.0424*** F-SW/M-SW **0.0234*** |

WL: wing length; F: female; M: male; CS: Sierra Atravesada + Altos de Chiapas; N: north of the Motagua-Polochic Faults; SW: southwest of the Motagua-Polochic Faults.

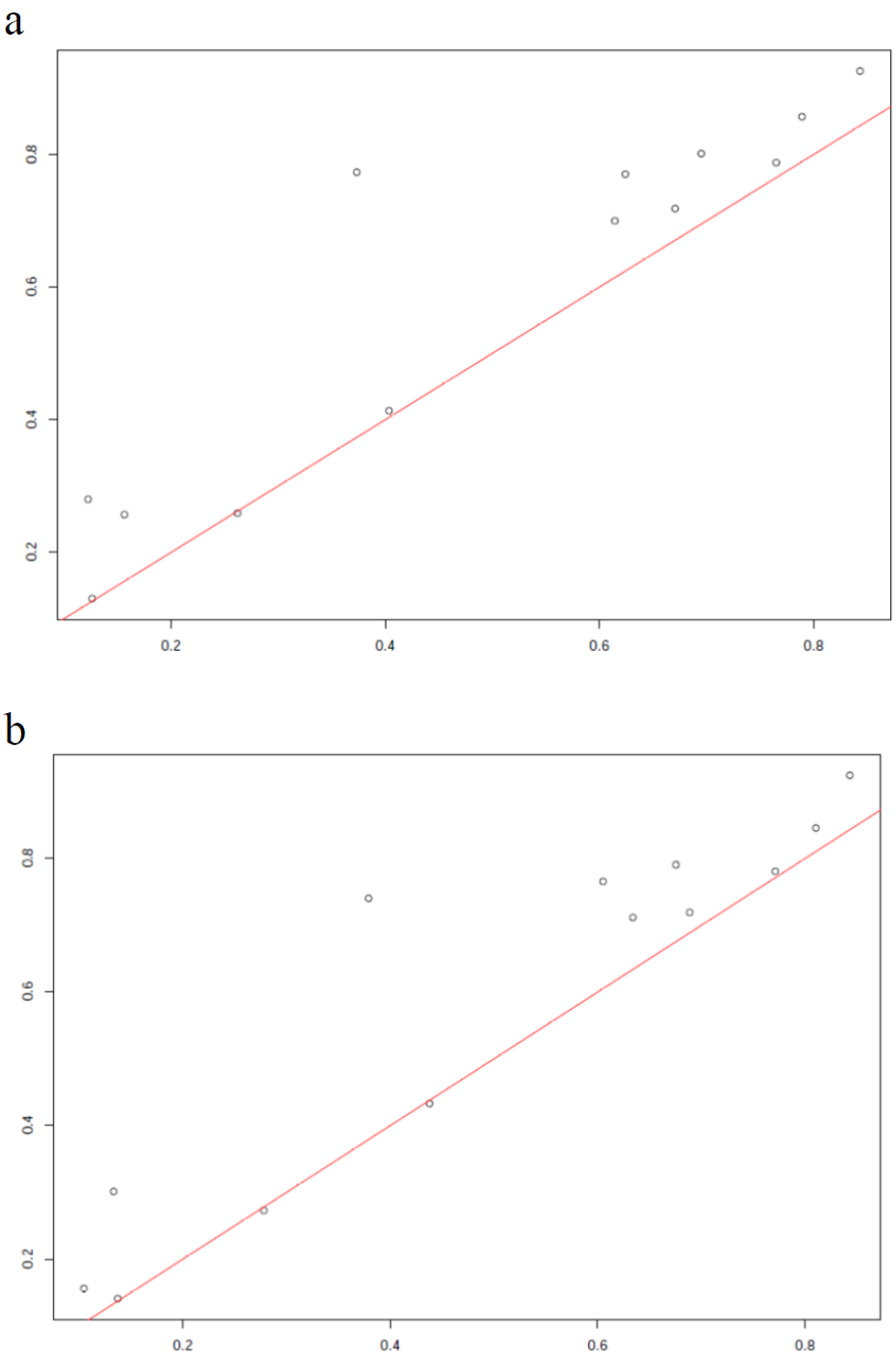


**Figure S1.** Observed versus expected heterozygosity. a) Complete dataset, *Lampornis viridipallens* and *L. sybillae* (166 samples). b) *Lampornis viridipallens* (153 samples).

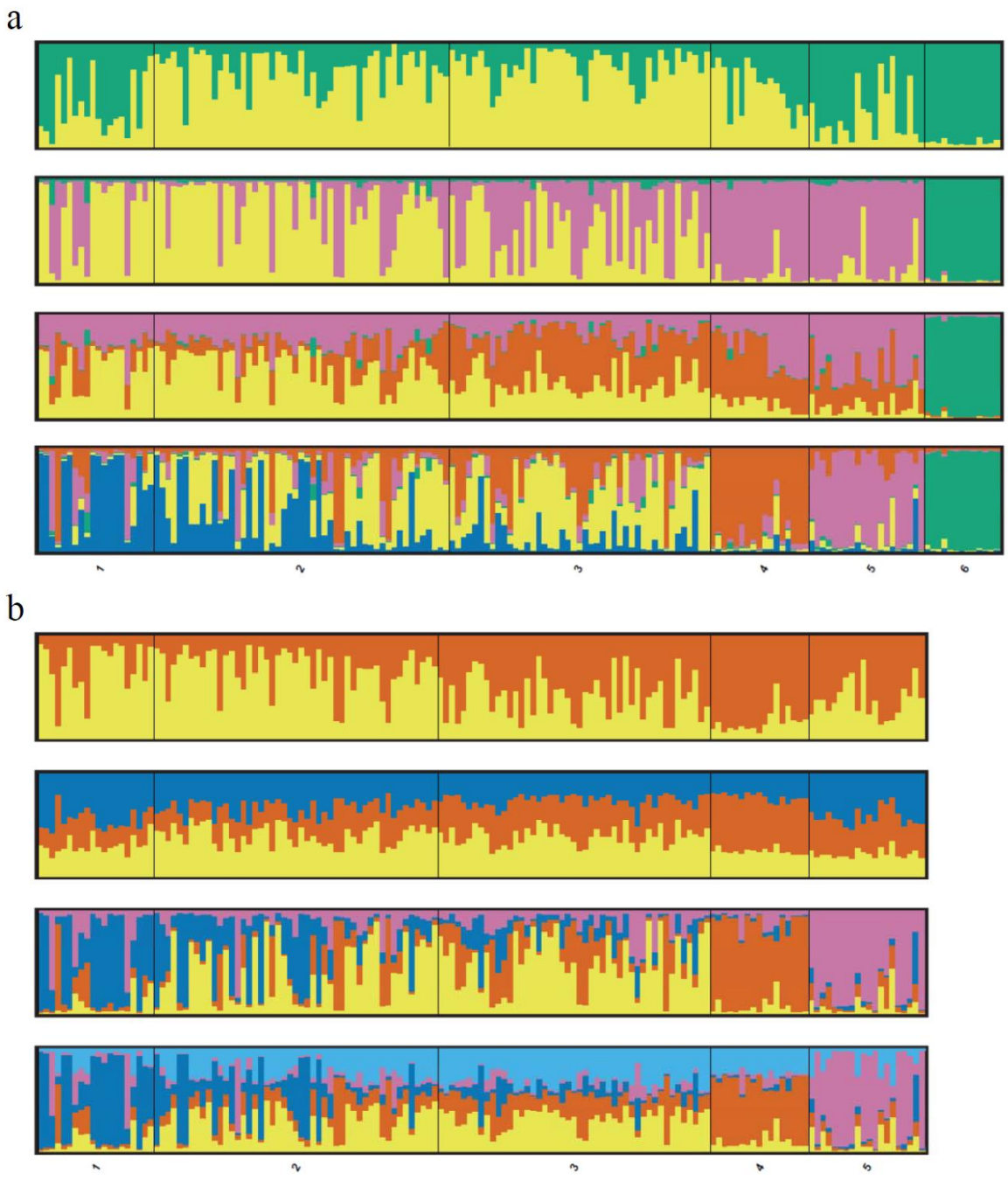


**Figure S2.** Structure analysis of *Lampornis viridipallens* and *L. sybillae* based on microsatellite data. a) Structure analysis of *L. viridipallens* and *L. sybillae* from K = 2 to K = 5. b) Structure analysis of *L. viridipallens* from K = 2 to K = 5.

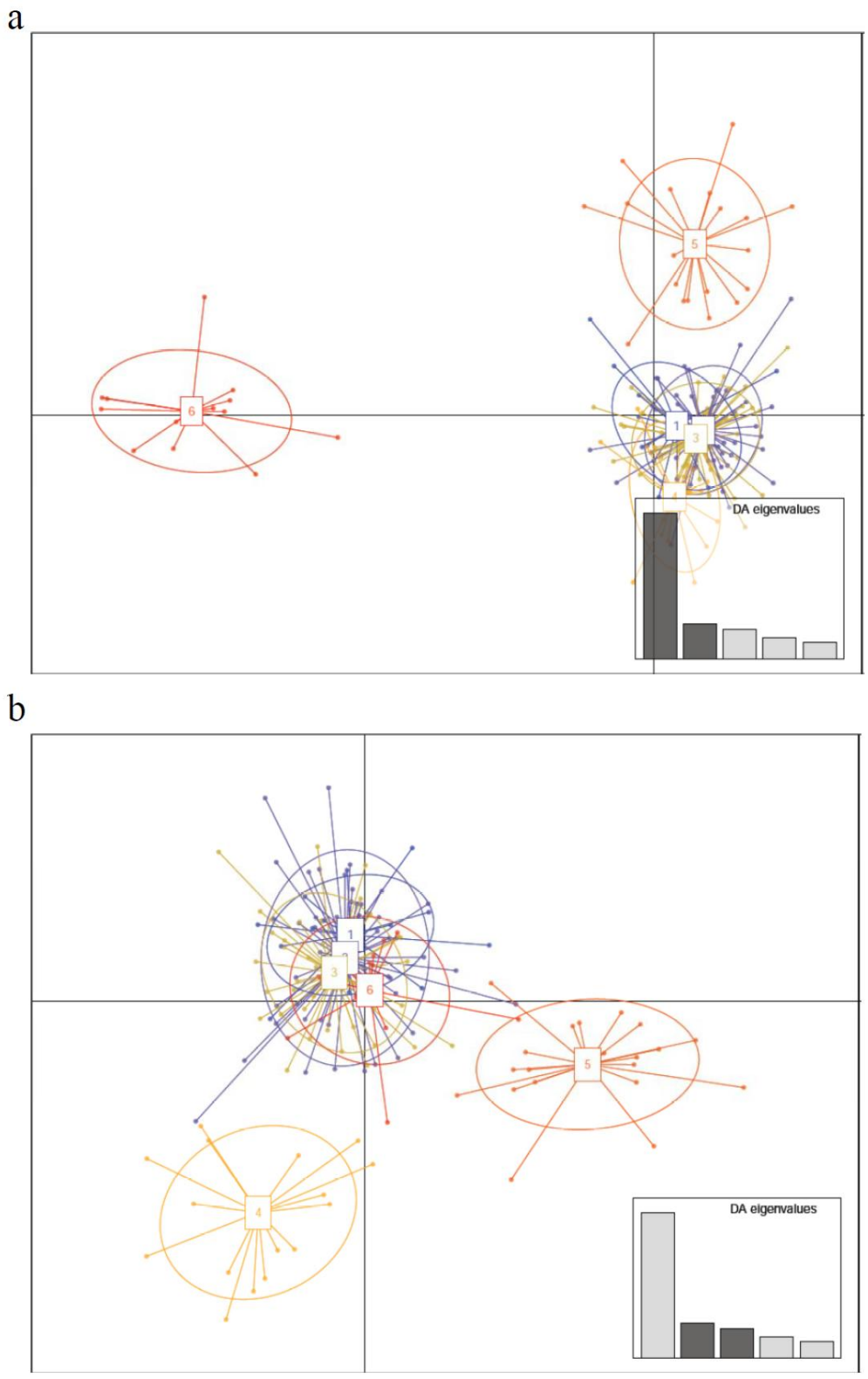


**Figure S3.** Discriminant Analysis of Principas Components (DAPC) of the complete dataset, *Lampornis viridipallens* and *L. sybillae* (166 samples). a) Axes 1 and 2. b) Axes 2 and 3.

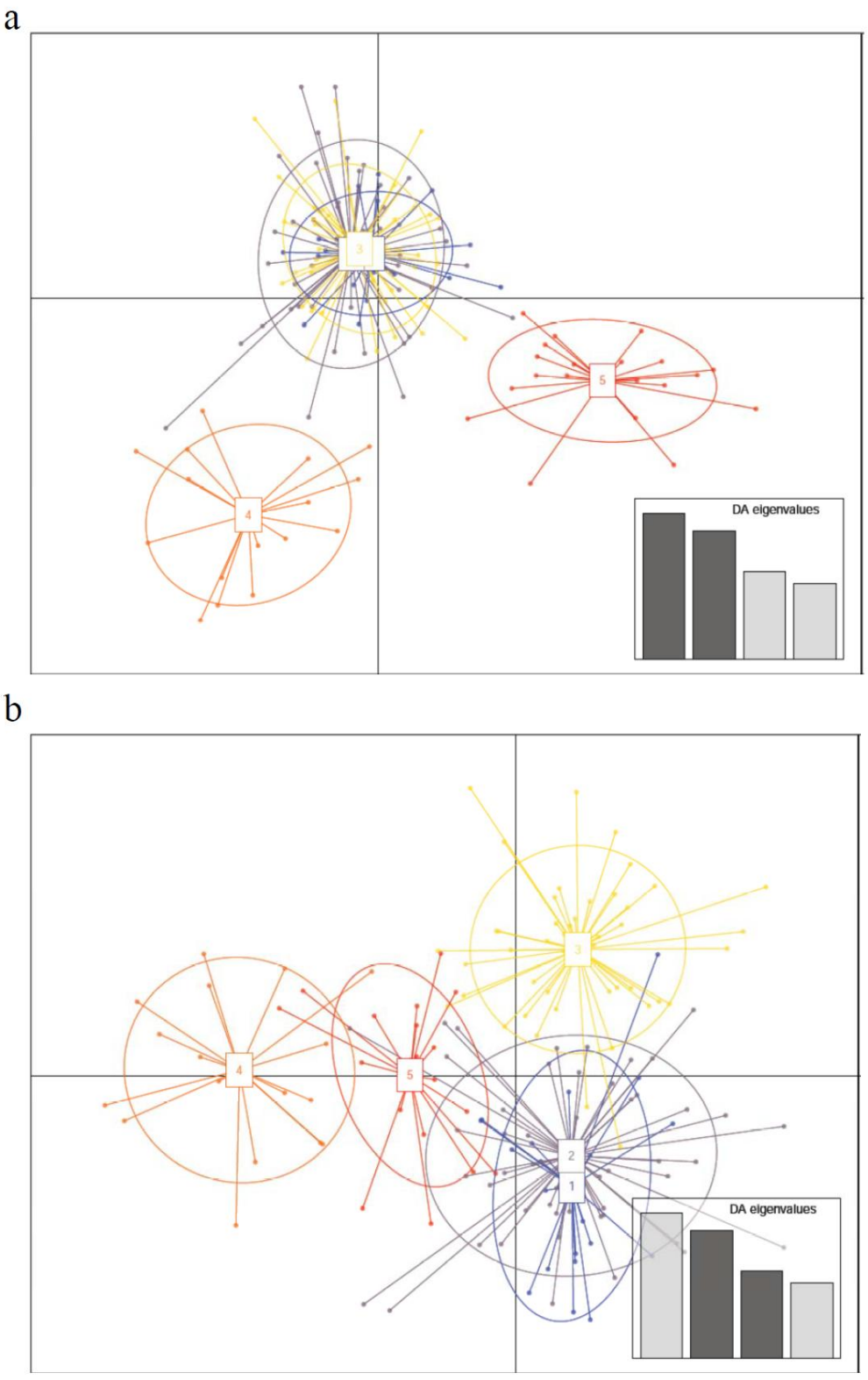


**Figure S4.** Discriminant Analysis of Principas Components (DAPC) of the complete dataset, *Lampornis viridipallens* (153 samples). a) Axes 1 and 2. b) Axes 2 and 3.

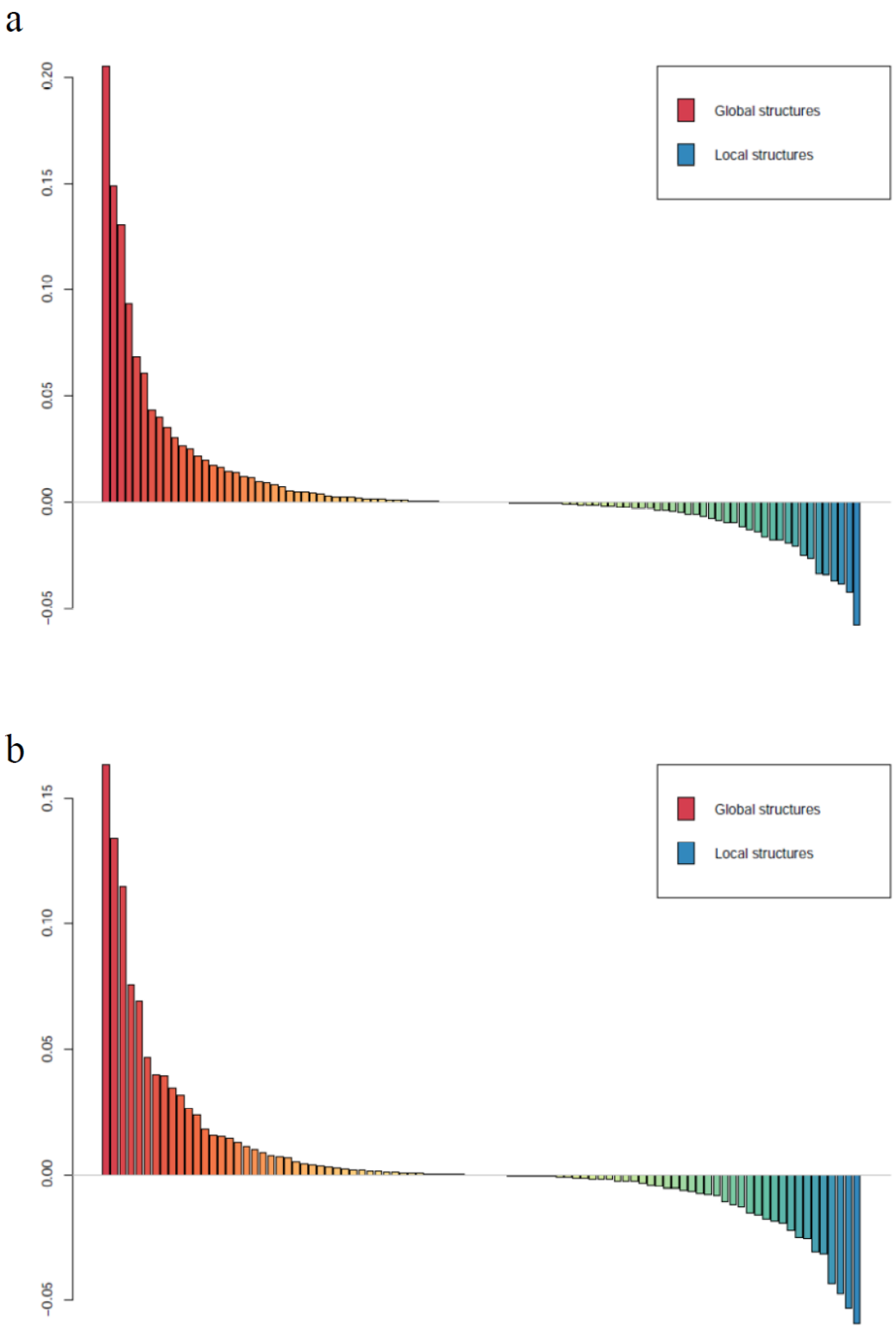


**Figure S5.** Eigenvalues of Spatial Principal Components Analysis (sPCA). a) Complete dataset, *Lampornis viridipallens* and *L. sybillae* (166 samples). b) *L. viridipallens* (153 samples).

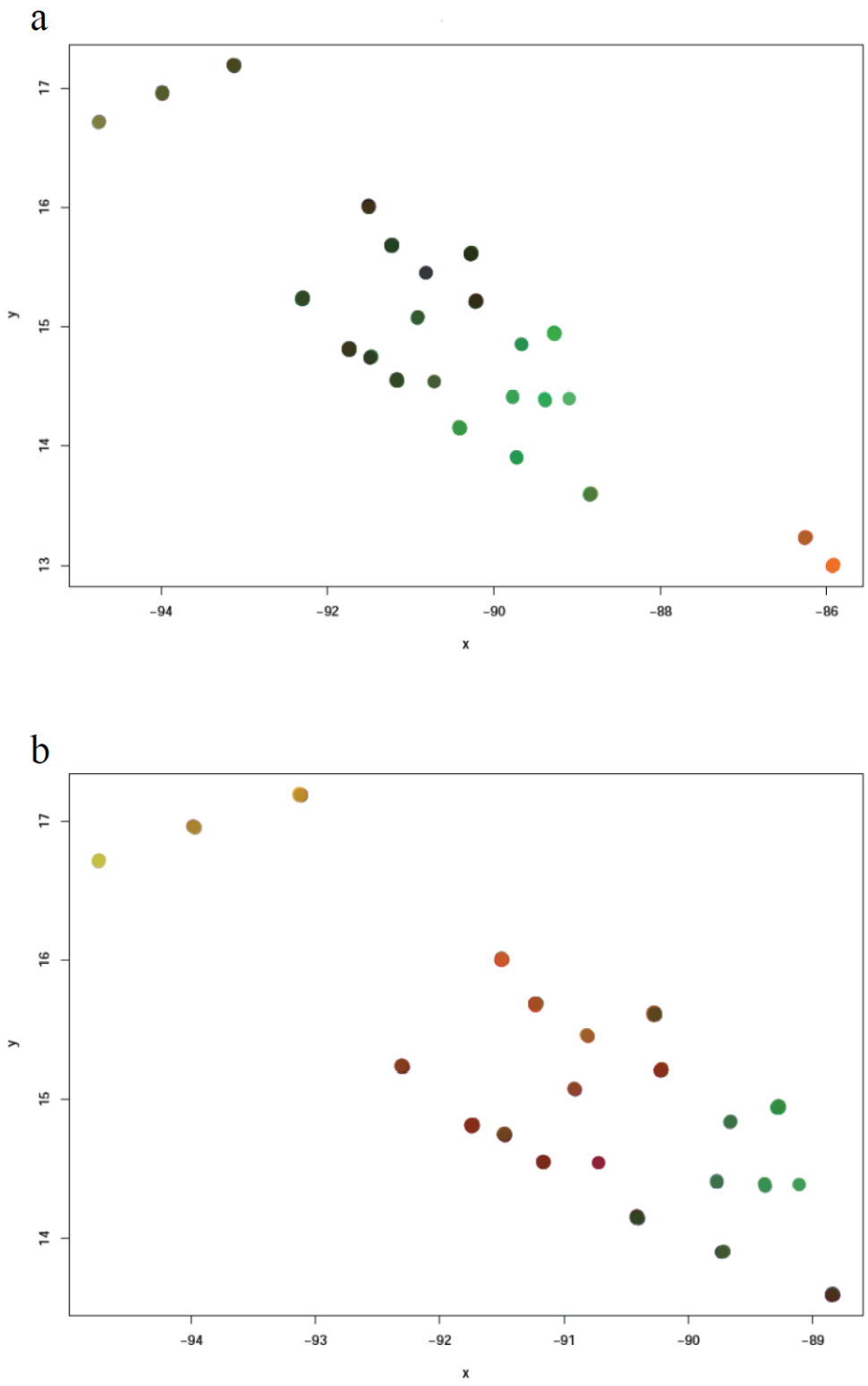


**Figure S6.** Colorplot of Spatial Principal Components Analysis (sPCA), axes 1 and 2. a) Complete dataset, *Lampornis viridipallens* and *L. sybillae* (166 samples). b) *L. viridipallens* (153 samples).

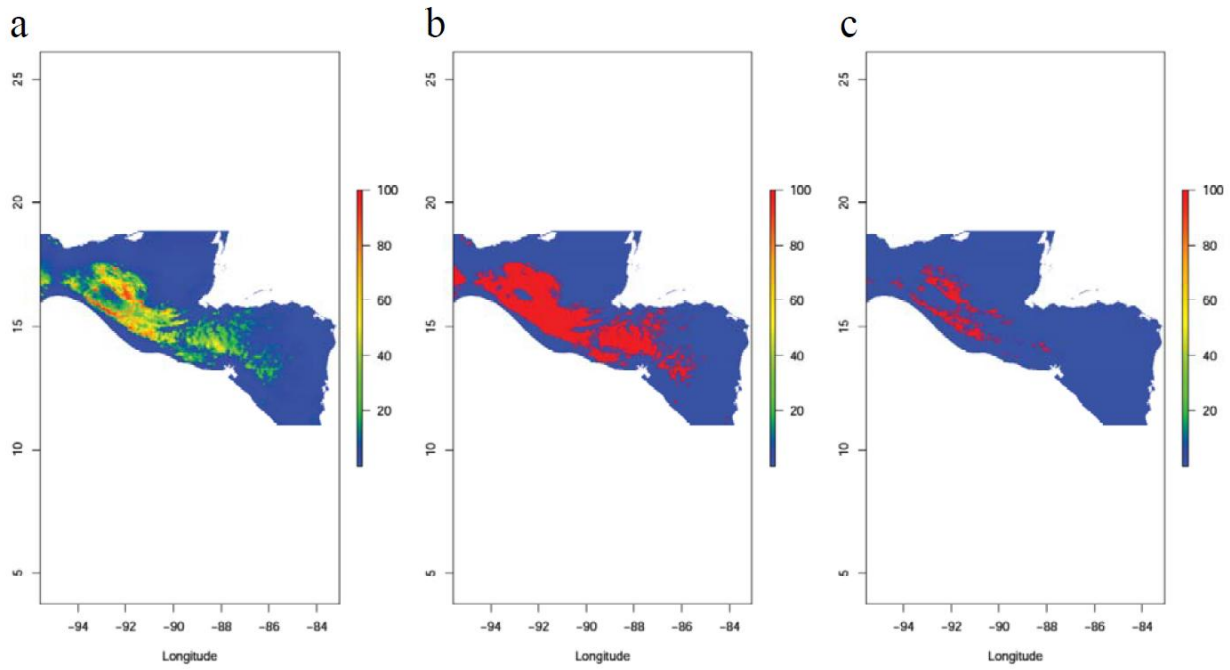


**Figure S7.** Species Distribution Model and reclassifications used in connectivity analysis. a) Species Distribution Model (SDM). b) Reclassification of the 90% probability of presence in SDM. c) Reclassification of the 50% probability of presence in SDM.

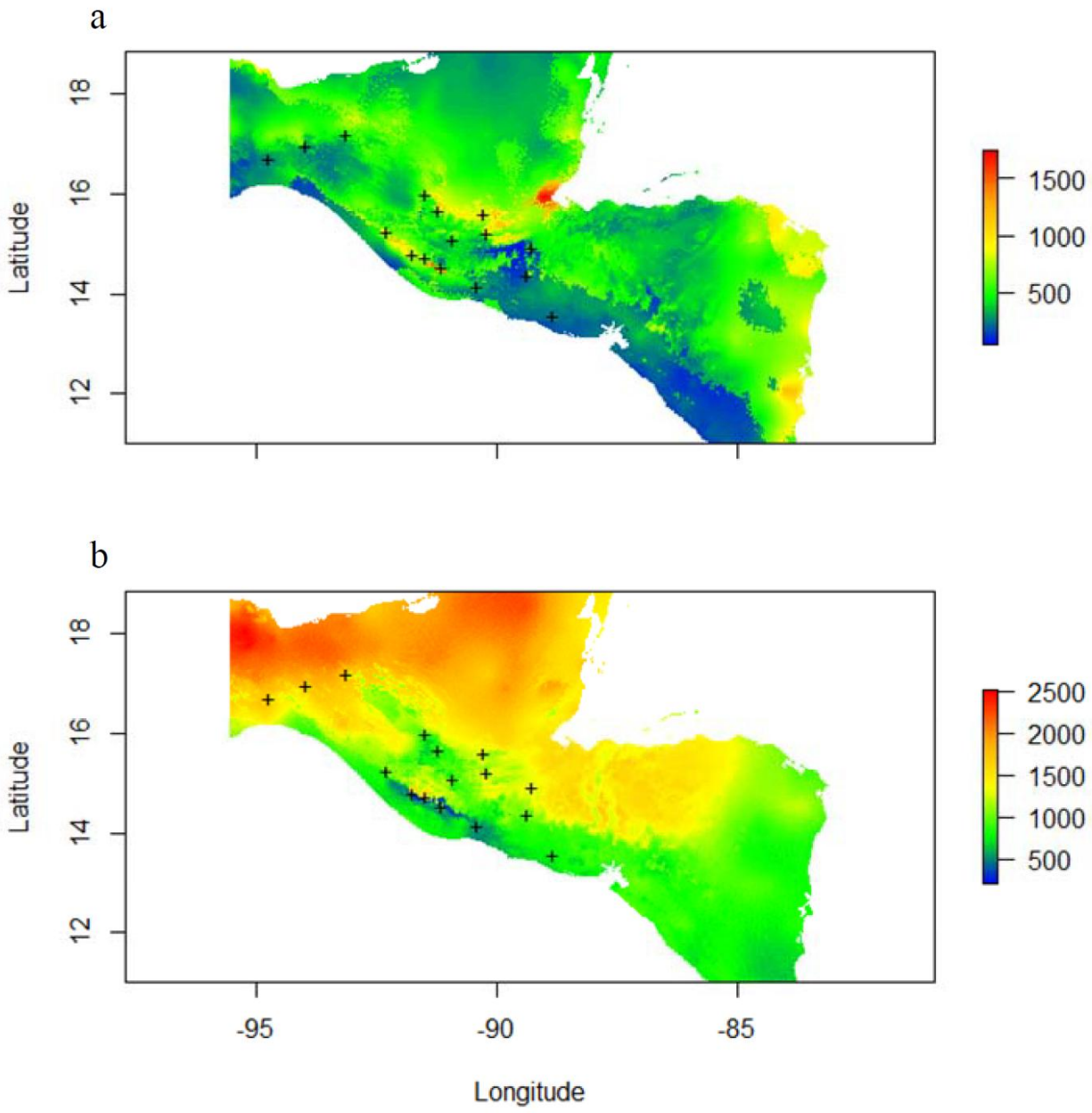


**Figure S8.** Bioclimatic variables with stronger correlation with genetic distances. a) Precipitation of the warmest quarter, scale in millimeters of rain. b) Temperature seasonality, scale in Celsius degrees multiplied by 100.

# Chapter 2

## Elucidation of the phylogeography and genetic basis of phenotype-genotype discordance in the White-naped Brushfinch (*Atlapetes albinucha*) across its geographic range

### Introduction

The origin and maintenance of montane tropical biodiversity results from a complex interaction comprising the evolutionary history of lineages, habitat persistence, and ecological filtering among other processes, which act at the genotypic and phenotypic levels (Graham et al. 2014, Antonelli et al. 2018, Rahbek et al. 2019, Rull and Carnaval 2020). The genotypes of individuals within populations typically diverge when they are geographically isolated from contiguous populations, a process known as allopatric divergence (Coyne and Orr 2004). The level of genetic divergence depends on how permeable the barriers separating populations are and the time since population isolation, although selection can also promote divergence when the environment is heterogeneous (Wang and Bradburd 2014). Populations experiencing greater genetic change with neighboring populations, or those more recently isolated, show more genetic similarity (Slatkin 1987). Genetic similarity can result from incomplete lineage sorting or genetic introgression, processes that can be hard to disentangle (Rheindt and Scott 2011). However, examining molecular markers with different inheritance patterns and substitution rates, like mitochondrial and nuclear DNA, can help elucidate the different evolutionary processes involved (Toews et al. 2016, Wogan et al. 2020).

The phenotype, as a product of the genotype and interactions with the environment, can obscure the actual genetic diversity within species (e.g., cryptic lineages, Chesser et al. 2020), and the processes generating such genetic diversity (e.g., cryptic genetic introgression or divergence). Changes in the phenotype can be solely the consequence of neutral processes, although the role of selective processes (natural and sexual selection) is often invoked in lineage divergence where selection either leads to conserved or divergent phenotypes (Coyne and Orr 2004, Price 2008). For instance, in the Neotropics, birds tend to have conserved plumage coloration despite high genetic divergence (Cadena et al. 2019, Chesser et al. 2020), which could be indicative of selective forces acting to constrain phenotype, although genomic introgression can also be related to stasis in plumage divergence (Winger 2017). However, plumage divergence is usually associated with genetic divergence (Winger 2017); therefore, the observance of intraspecific variation in the phenotype is typically indicative of lineage divergence. Further, the presence of individuals with intermediate phenotypes alerts us to likely hybridization and introgression between morphologically diagnostic parental lineages.

Species with broad geographic ranges, several disjunct populations and intraspecific phenotype differences represent excellent systems with which to study how a combination of evolutionary and ecological processes generate and maintain biological diversity. One such system is *Atlapetes albinucha*, the White-naped Brushfinch. This species inhabits the mountains from eastern Mexico to Colombia (Rising 2020), a topographically and climatically complex region within the Neotropics. Most phylogeographic work on bird species from this region has centered on mitochondrial markers and in some cases, a few nuclear markers. Major geographic breaks for montane species have been evidenced through this prior research, and include the Isthmus of

Tehuantepec, the Motagua-Polochic-Jocotan Fault System, the Nicaraguan Depression, and the Isthmus of Panama (**Figure 1**; e.g., snakes, Daza et al. 2010; mammals, Pérez Consuegra and Vázquez-Domínguez 2015; amphibians, Rovito and Parra-Olea 2016; birds, Jiménez and Ornelas 2016, Rodríguez-Gómez et al. 2021). In order to determine whether these barriers detected primarily in non-volant vertebrates also pertain to birds generally, and to determine whether there are additional biogeographic breaks within the region, we focus on resolving the phylogeography of this widespread brushfinch species using a combination of mitochondrial DNA sequences, double digest restriction-site associated DNA (ddRAD), and exome capture data.

*Atlapetes albinucha* diverged from its sister species *A. pileatus* about 1.73 million years ago (Sánchez-González et al. 2015), during the Pleistocene. A previous study on mitochondrial DNA and geographic sampling from northern Chiapas to Colombia reported incomplete genetic differentiation and shallow phylogeographic structure (Rocha-Méndez et al. 2018). Ecological niche models suggest that the Isthmus of Tehuantepec (IT), the Nicaraguan Depression (ND), and the Isthmus of Panama (IP) formed isolating barriers for *A. albinucha* during interglacials, but that these barriers were likely permeable during glacial cycles when montane forests expanded to lower elevations (Rocha-Méndez et al. 2018). No additional geographic barriers have been uncovered for *A. albinucha*, although the Grijalva River has been suggested as a barrier separating the populations of northern Chiapas from southern Chiapas (Paynter 1978). The Grijalva River along with the IT, ND, and IP correspond with low-elevation and low-precipitation valleys.

*Atlapetes albinucha* is the only species in the genus (~30 species) with two well-differentiated phenotypes where the underpart colors of birds in different parts of the geographic range are either yellow or gray. However, the reciprocal monophyly of the two different phenotypes has not been recovered in molecular phylogenetic analyses, although both phenotypes have been included in these phylogenetic hypotheses (Sánchez-González et al. 2015, Rocha-Méndez et al. 2018). Eight subspecies have been proposed based on plumage coloration, one subspecies with yellow underparts (*A. a. albinucha*) and seven subspecies with gray underparts (Rising 2020). No other phenotypic traits differ between the yellow and gray populations, including a lack of divergence in song, a cultural trait in oscine passerine birds (Boesman 2016). Interestingly, the switch between yellow and gray ventral plumage coloration is widespread among the 30 species in the genus *Atlapetes*, where species with yellow underparts are often sister to species with gray underparts (Sánchez-González et al. 2015). In the Andes of South America, interspecific competition has been proposed as a hypothesis to explain why yellow *A. rufinucha* inhabits lower elevations than another yellow species (*A. tricolor*) and a gray species (*A. schistaceus*) that inhabit higher elevations (Remsen and Graves 1995), suggesting a putative role for signal communication in these ventral color patches.

The yellow phenotype of *A. albinucha* is found in two disjunct areas on both sides of the Isthmus of Tehuantepec, from Puebla and Veracruz to Oaxaca on the eastern side of the isthmus, and in northern Chiapas (Altos de Chiapas) on the western side. The gray phenotype ranges from southern Mexico to Colombia (Rising 2020). The geographic range of the yellow population in northern Chiapas does not overlap with that of the gray phenotype in southern Mexico and western Guatemala, and previous to our study, no intermediate phenotypes had been reported.

Yellow coloration in birds results from the deposition of carotenoids in feathers, in particular lutein (Johnson and Brush 1972). Recent research has shown that genes related to carotenoid uptake, processing, and degradation are important for carotenoid coloration (Price-Waldman and Stoddard 2021). Understanding the genomic basis of the phenotype, in this case of the yellow-gray plumage coloration, can illuminate our understanding of the diversification processes within *A. albinucha*, and more generally, in the genus *Atlapetes*.

Here, we investigate the patterns and processes driving the evolution of *Atlapetes albinucha* across its geographic range. Our geographic sampling is comprehensive and includes both intraspecific plumage phenotypes as well as individuals with intermediate phenotypes from the highlands of western Guatemala. Using a phylogeographic approach, we examine the genetic structure of *A. albinucha* and identify associated geographic barriers based on mitochondrial sequences, ddRAD, and exome capture data. We assess morphological variation and plumage coloration. We also incorporate exome capture data to disentangle the genomic basis of the two plumage color phenotypes, yellow and gray. We investigate hybridization and introgression between the two plumage color phenotypes. We fit geographic clines to the different molecular markers and analyze environmental data to understand the role of geographic and environmental barriers in isolating the yellow and gray phenotypes. We discuss the high genetic structure uncovered with genomic data and document the discovery of new geographic barriers in northern Central America. We conclude by highlighting the need to integrate data on multiple processes (allopatric divergence, plumage color evolution, introgression, geographic and environmental breaks) if we are to understand the origin and maintenance of Neotropical montane biodiversity.

## Methods

### Sampling and field procedures

For the molecular analysis, we generated a dataset comprising 73 individuals that consisted of 65 *Atlapetes albinucha* and eight individuals of seven related species as the outgroup taxa (**Figure 1, Table S1**). Our sampling makes this study the most comprehensive to date, both in number of *A. albinucha* individuals included and in geographic representation, particularly with respect to Nuclear Central America, as well as the amount of molecular sequence data generated. We collected 30 ingroup individuals from nine localities between 2009 and 2013. Two individuals came from the region where the yellow and the gray phenotypes abut in western Guatemala, each having a different intermediate phenotype (**Figure 5**). We conducted scientific collection of specimens in joint expeditions of the Museum of Vertebrate Zoology (MVZ), University of California, Berkeley (UC Berkeley); Escuela de Biología (EB), Universidad de San Carlos de Guatemala (USAC); and Museo de Zoología "Alfonso R. Herrera" (MZFC), Universidad Nacional Autónoma de México (UNAM). We sampled with the permission granted by the Consejo Nacional de Áreas Protegidas in Guatemala through research and collecting permits provided to EB-USAC, the Mexico's Secretaría de Medio Ambiente y Recursos Naturales, Subsecretaría de Gestión para la Protección Ambiental, Dirección General de Vida Silvestre granted to UNAM, and ethical approval granted by the UC Berkeley Institutional Animal Care and Use Committee (R317). We preserved the captured individuals as voucher specimens (study skins and tissue samples) and deposited the specimens in ornithological research collections at the MVZ-UC Berkeley, EB-USAC, and MZFC-UNAM (**Table S1**).

Our collections were supplemented with 29 ingroup individuals obtained on loan from tissue collections (Burke Museum of Natural History and Culture – UWBM; Field Museum of Natural History – FMNH; Kansas University, Natural History Museum – KU; Louisiana State University Museum of Natural Science – LSUMZ; and MZFC-UNAM). We also included six mitochondrial sequences from GenBank since we could not obtain tissue loans from Colombian birds (**Table S1**). We only included GenBank data from Colombian birds recently sequenced in Colombia and with the complete 1,041 bp of the ND2 region (Rocha-Méndez et al. 2018). We decided not to include additional GenBank sequences because we found discrepancies between sample identification and locality of origin of previously published sequences. For instance, ND2 was obtained from the individual FMNH 394151 and associated with the accession code GU377054 in Barber and Klicka (2010). The database of the FMNH collection indicates that FMNH 394151 was collected in Chiapas, Mexico, with the collector code BMM-083. That same sample was included later in Klicka et al. (2014) although the accession code is not provided for this particular sample. However, a later study, Sánchez-González et al. (2015), which supposedly included five individuals of *A. albinucha*, showed some inconsistencies. The authors included the individual referred as BMM-083 with the collection locality of Chiapas, Mexico, and provided a new GenBank accession code KM360518. Additionally, they included the sample 394151A with the collection locality of Risaralda, Colombia, and the GenBank accession code GU377054. These incompatibilities were carried over to a subsequent publication (Carantón-Ayala et al. 2018), which included the same individual three times: (i) FMNH 394151 from Klicka et al. (2014), (ii) BMM-083 – KM360518, and (iii) 394151A – GU377054. Fortunately, the main conclusions of their paper were not affected, although the phylogeographic patterns of the species may have been obscured.

We added eight individuals as outgroup species, three individuals from the MVZ tissue collection and five individuals from LSUMZ. The outgroup sampling included: the sister species *A. pileatus*, and two more distantly related species, *A. pallidinucha* and *A. rufinucha*. Additionally, we included other related species from different genera: *Pezopetes capitalis*, *Melozone fusca*, *Melozone biarcuata*, and *Pipilo chlorurus*. The species included in the outgroup sampling were selected following a recent New World sparrow phylogeny (Family Passerellidae, Klicka et al. 2014).

## Mitochondrial DNA sequencing

We extracted genomic DNA using the DNeasy blood and tissue extraction kit (Qiagen, Valencia, CA, USA), following the protocol recommended by the manufacturer. We PCR-amplified and sequenced 1041 base pairs (bp) of NADH nicotinamide dehydrogenase subunit 2 (ND2). The amplification of ND2 was performed with primers L5204 and H6312 (Cicero and Johnson 2001). Polymerase chain reaction conditions included an initial denaturation at 94 °C for 1 min; followed by 35 cycles at 94 °C for 30 s, 54 °C for 30 s, and 72 °C for 45 s; and a final extension at 72 °C for 10 min. We sequenced PCR products in both directions using BigDye terminator chemistry (Applied Biosystems, Foster City, CA, USA) on an ABI 3730 automated sequencer (Applied Biosystems, Foster City, CA, USA). We generated consensus sequences and ensured that the sequences contained no stop codons using Geneious v. 5.1.7 (http://www.geneious.com).

## ddRAD sequencing and SNP calling

We followed the protocol for double digest restriction site-associated DNA sequencing (ddRAD) described by Peterson et al. (2012). Briefly, 500 ng of genomic DNA, quantified with Qubit (Thermo Fisher Scientific), were digested over three hours using the restriction enzymes EcoRI and SphI-HF (NEB). After digestion and bead clean-up, each sample was labeled by the ligation of one of 24 different adapters. Adapter ligation was followed by pooling sets of up to 24 samples (two pools of 24 and one pool of 19 resulting in three libraries) and two consecutive bead clean-ups. The cleaned product was PCR-amplified and indexed during ten cycles using the Phusion DNA polymerase (NEB). After bead clean-up and qPCR, the three libraries were combined in an equimolar manner. The combined final library was subject to size selection through PippinPrep, targeting the fragment sizes from 350 to 550 bp (200 to 400 bp without the adapters). The excised library was run on one lane of the Illumina NovaSeq S1 to generate 100 bp paired-end sequence reads. Due to clustering issues on the sequencing lane that did not allow for the recovery of the individual barcode in 50% of the sequence reads, the excised library was subsequently run a second time on one lane of the Illumina NovaSeq SP to generate 150 bp paired-end sequence reads to supplement the previous set of reads. The sequencing was carried at the QB3 Vincent J. Coates Genomic Sequencing Laboratory at UC Berkeley.

Raw sequence reads from both runs were demultiplexed, combined, and trimmed to the same length using the process_radtags program in Stacks (Catchen et al. 2013). Clean sequences from each individual were mapped to the reference genome of *Zonotrichia albicollis*, which is available through NCBI (GenBank assembly accession: GCA_000385455.1). The sequence reads were mapped to the genome using the software BWA (Li and Durbin 2009) and then converted to BAM files with SAMtools (Li et al. 2009). We used the gstacks program from Stacks to create loci and build a catalog using the BAM files as input. We then used the populations program from Stacks to assign 60% as the minimum percentage of individuals in a population required to process a locus and to generate a file in Variant Call Format (VCF). Then, we performed additional filtering steps in VCFtools (Danecek et al. 2011). We included only sites with a minor allele frequency parameter set to 0.01 (--maf 0.01), and with mean depth values greater than or equal to 3 (--min-meanDP 3) and less than or equal to 10 (--max-meanDP 10). We aimed to remove the individuals with 30% or more missing data, but none of the samples fell into this category; therefore, we continued the analysis with the 59 *Atlapetes albinucha* individuals from which we sequenced genomic data. We proceeded to prune sites with evidence of linkage disequilibrium creating a BED file and estimating r2 in Plink v1.9 (Purcell et al. 2007). This dataset included the 59 *A. albinucha* individuals and was used for downstream population analysis. We obtained a separate catalog of variant sites that included the ingroup (59 *A. albinucha*) and the outgroup taxa (eight individuals), which was used for phylogenetic analysis.

## Exome capture and SNP calling

We used a custom target capture probe set designed for the family Passerellidae by Benham et al. (unpubl. data) in order to: (i) attempt to discern the genetic basis of the variation in underpart color, and (ii) to understand the extent of hybridization within the two *A. albinucha* phenotypes (i.e., gray vs. yellow). For this dataset, we included a total of 24 *A. albinucha* individuals that

spanned the two extreme phenotypes and the putative hybrids. Our sampling consisted of 11 individuals with completely yellow underparts, 11 individuals with a yellow throat and gray breast and belly, and the two putative hybrids with phenotypes intermediate between yellow and gray (**Table S1**). We targeted the capture of DNA from 56,533 exons representing 13,813 genes and 3,443 non-genic regions.

We followed standard library prep procedures. Briefly, we sheared 1 µg of genomic DNA through sonication on a qSonica for 5 minutes at an amplitude of 40%. We expected fragments centered around 350 bp, therefore, following the sonication, we performed a double-sided size selection with low-ratio SPRI (Sera-Mag) beads, 0.5x for the right side and 0.65x for the left side. Then, we prepped the DNA samples for probe hybridization with consecutive steps of end repair, A-tailing, and adapter ligation. After cleaning the DNA one more time with beads, we proceeded with an indexing PCR using a combination of unique P5 and P7 indexing oligos for each individual. In addition to the oligo mix, we used Kapa 2x Ready Mix and amplified the DNA during six cycles. We followed the amplification with bead clean-up and quality control, which consisted of DNA quantification on an Agilent Bioanalyzer to verify that no adapter dimer was present. This step was followed by the pooling of all individuals using equal concentrations of DNA. Target capture was performed using the Roche NimbleGen SeqCap EZ Library SR protocol with an incubation time of 72 hours. Following the same Roche protocol, the libraries were washed with capture beads, and PCR amplified during six cycles. After post-PCR cleaning and quality control steps, the libraries were sequenced at the QB3 Vincent J. Coates Genomic Sequencing Laboratory at UC Berkeley.

We proceeded to demultiplex and check the quality of the reads with FastQC (Andrews 2010). We trimmed adapter contamination and low-quality reads and removed PCR duplicates. We mapped the reads to the reference genome of *Zonotrichia albicollis* (GenBank assembly accession: GCA_000385455.1). After calling variants, we created a VCF file and filtered the data in VCFtools (Danecek et al. 2011). First, we included only bi-allelic sites (--max-alleles 2 --min-alleles 2) with mean depth values greater than or equal to 1 (--min-meanDP 1) and with a quality value above 20 (--minQ 20). We also removed indels. In the second step of filtering, we included the sites with a number of alleles less than or equal to 2 (--max-alleles 2), genotypes greater than or equal to the value 5 (--minDP 5), and less than or equal to the value 250 (--maxDP 250). We determined Hardy-Weinberg Equilibrium using a p-value of 0.01 (--hwe 0.01), and did not allow for missing data (--max-missing 1).

## Morphological measurements

Using a dial caliper with a precision of 0.1 mm and a wing rule with a precision of 1 mm, RAJ took body measurements from 36 *Atlapetes albinucha* specimens deposited in the Museum of Vertebrate Zoology (MVZ-UC Berkeley). The measured specimens included representation of most of the geographic range of the species, from southern Mexico to Colombia, and 16 of these individuals were included in the genetic analyses (**Table S2**). We followed previously described protocols (Bowie et al. 2004) to obtain the following six measurements: bill length, bill width, bill depth, tarsus length, wing length, and tail length. It was not possible to measure bill depth from five specimens because the specimens were dried with the bill opened, and one additional

specimen had the tail feathers worn and hence it was not possible to measure tail length accurately.

To quantify the yellow coloration of the underparts, we recorded, as a percentage, the extent between the chin and vent of the underparts that were yellow. We acknowledge that the precise value of the extent of yellow may be dependent on the preparation of each specimen; however, the range of the value for both phenotypes (yellow vs. gray) is distinct with no overlap. We are also aware that plumage color can fade with time and interfere with precise color measurements (Burns et al. 2018). However, we only assessed the presence of the color yellow in the underparts, not quantitative color variables. Additionally, we recorded the collection year of the specimens.

**Population structure and differentiation**

We aligned the mitochondrial DNA sequences and looked for stop codons using MEGA v. 7.0.21 (Kumar et al. 2016). For the mitochondrial dataset, we estimated haplotype variation (*H*), segregating sites (*S*), haplotype diversity (*h*), and nucleotide diversity ($\pi$), for each geographic region delineated in **Figure 1** using DnaSP v. 5.10.01 (Librado and Rozas 2009). We looked for signs of demographic changes by calculating Tajima's D (Tajima 1989) and Fu's Fs (Fu 1997) in Arlequin 3.11 (Excoffier and Lischer 2010) with 1000 permutations. Mismatch distributions were calculated using the sudden expansion model of Schneider and Excoffier (1999) with 9000 bootstrap replicates. Positive values for D and Fs are indicative of mutation-drift equilibrium, which is typical of stable populations. In contrast, significant negative values (at the P = 0.05 level for Tajima's D and Fs tests) that result from an excess of rare haplotypes indicate that populations have experienced a recent bottleneck followed by population demographic expansion. We calculated Harpending's raggedness index (Hri) and the sum squared deviation (SSD), which indicate deviations from the sudden expansion model and are higher in stable, non-expanding populations (Rogers and Harpending 1992).

We estimated with the mitochondrial DNA dataset in DnaSP the average number of pairwise differences between and within populations, and in Arlequin the pairwise FST values between populations. Additionally, we carried out analyses of molecular variance (AMOVAs) in Arlequin; the populations were organized in separate analyses as follows: (A) four groups separated by major geographic breaks (i.e., Isthmus of Tehuantepec, Nicaraguan Depression, Isthmus of Panama), (B) groups defined by the ddRAD admixture analysis, and (C) groups defined by the ddRAD PCA. An unrooted statistical parsimony haplotype network (Clement et al. 2000) was generated in POPART v. 1.7 (Leigh and Bryant 2015) using the ND2 mtDNA matrix.

To assess population genetic structure and ancestry with the genomic data, we conducted Principal Component Analysis (PCA) and maximum-likelihood ancestry analysis. Clustering analyses, including approaches such as PCA, help understand the spatial distribution of the data without the restrictions imposed by the assumptions of other genetic analyses (e.g., Hardy-Weinberg equilibrium and Linkage Disequilibrium). We conducted a PCA as implemented in ADEgenet (Jombart 2008), and recorded the eigenvalues for the first four principal components. We run a PCA with the ddRAD data and another PCA with the exome capture data. The ancestry

analysis was run using the software ADMIXTURE v1.3 (Alexander et al. 2009). This ancestry analysis enables estimation of individual ancestries from SNP data; it can also be used to estimate the number of populations through a cross-validation procedure. The most suitable number of populations is the one that minimizes the estimated prediction error. Therefore, using the ddRAD data, we ran ADMIXTURE with a variable number of populations, from K1 to K10, and plotted the cross-validation error.

To analyze the morphological data and look for any geographic differentiation, we started by calculating the ratio of the measurements (bill length, bill width, wing length, tail length, and extent of yellow on the underparts) against the tarsus length. We excluded bill depth since it was not possible to score this measurement from 14% of the samples. We also excluded the individual from which we were unable to measure tail length (MVZ 86544). We ended up with a final matrix of 35 specimens with data for five traits. To look for clustering patterns, we conducted two PCAs, one PCA with the complete final matrix and another PCA excluding the yellow extension trait. Based on the obtained results, we did not proceed with more detailed analysis of the morphological data.

**Phylogenetic analyses**

We conducted phylogenetic reconstructions using either mitochondrial DNA or nuclear DNA. Mitochondrial DNA and nuclear DNA are inherited in different ways, have different population sizes, and recombination rates. For these reasons as well as the possibility of incomplete sorting, analyses of mitochondrial and nuclear DNA can support distinct phylogenetic relationships. The distinct topologies between mitochondrial and nuclear DNA are expected in hybridizing populations and represent relevant evidence for hybridization and introgression, although incomplete lineage sorting should not be discounted. Using the mitochondrial DNA dataset (ND2 matrix), we conducted maximum likelihood (ML) phylogenetic analyses in RAxML v8.2 (Stamatakis 2014), and Bayesian inference (BI) in MRBAYES v. 3.2.6 (Huelsenbeck and Ronquist 2001, Ronquist and Huelsenbeck 2003). For the ML analysis, we used the model of nucleotide substitutions GTRCAT for the mitochondrial dataset and obtained node support by running rapid bootstrapping with 100 iterations. For BI, we implemented the GTR+G substitution model for ND2, as identified by the corrected Akaike information criterion in jMODELTEST v. 2.1.10 (Guindon and Gascuel 2003, Darriba et al. 2012). The BI was executed with two simultaneous parallel Markov chain Monte Carlo (MCMC) runs and four chains; and was run for 20 million generations, sampling every 1000 generations. Bayesian posterior probabilities were calculated from the sampled trees remaining after a burn-in of 25%. A majority consensus tree was calculated, showing nodes with a posterior probability of 0.5 or greater. Using the ddRAD nuclear dataset, we performed a maximum likelihood analysis in RAxML. We used the model of nucleotide substitutions GTRCAT for the complete SNP set and obtained node support by running rapid bootstrapping with 100 iterations. The consensus trees were visualized in FIGTREE v. 1.2.3 (http://tree.bio.ed.ac.uk/software/figtree/).

**Identification of outlier loci associated with the yellow-gray plumage coloration**

We identified outlier SNPs using the exome capture dataset and estimated FST between yellow- and gray-bellied phenotypes. We included the 14 samples with a more similar genetic

background (as determined by close proximity in the PCA, **Figure S1a**), nine with the yellow phenotype from Altos de Chiapas and five with the gray phenotype from southern Mexico – western Guatemala. First, we filtered out the SNPs that were not segregating in the two phenotypic groups. Then, we calculated both Weir and Cockerham FST (Weir and Cockerham 1984) and Hudson FST (Hudson et al. 1992). We plotted a comparison of the two different FST estimates (**Figure S1b**) and used Weir and Cockerham FST for subsequent analysis because the two measures of FST showed similar results. Methods based only on FST can have a high false discovery rate (Lotterhos and Whitlock 2015); therefore, we set a very stringent threshold of five standard deviations from the mean. Then, we intersected the outliers with the genomic coordinates of our custom target probe to identify the putative loci that may underlie the observed phenotypic differences in belly color.

We examined the outliers from the coding regions that had a Weir and Cockerham FST higher than 0.8. For the list of outlier SNPs, after alignment to the reference genome we looked for information on the genes function and the pathway that the encoded proteins may belong to. After that, we looked for additional outliers in the same gene and on the same scaffold that was differentially fixed in the two groups (yellow-bellied from Altos de Chiapas vs. gray-bellied from southern Mexico and western Guatemala; FST = 1). We obtained the genotypes of all the outlier SNPs within that scaffold for the 14 initial samples, the hybrid individuals, and the other eight samples included in the exome capture essay. We drew a figure with the genotypes and assigned different colors to each kind of homozygote and heterozygote.

**Geographic cline analysis**

We conducted cline analyses to describe patterns of genetic introgression between the yellow and gray phenotypes. Specifically, we fitted molecular genetic data from the intermixing groups (yellow-bellied from Altos de Chiapas, hybrids, and gray-bellied from southern Mexico and western Guatemala) to cline models using the Metropolis-Hastings Markov chain Monte Carlo (MCMC) algorithm implemented in the R package HZAR (Derryberry et al. 2014). We tested models for 13 genetic markers: mitochondrial DNA dataset, admixture q-value for the ddRAD dataset, and 11 outlier SNPs from the scaffold NW_005082739.1. The estimated parameters for cline shape can be compared to look for concordance or patterns of differential introgression, the latter through looking at the skew of the clines to either side of a general cline pattern, in this case, the one based on the ddRAD dataset. The parameters can also provide information on the strength of selection against hybrids; very steep clines being indicative of strong selection against heterozygotes or the presence of a strong barrier to dispersal (Slatkin 1973).

We tested three different models for each of the 13 genetic markers: 1) fixed trait interval and no fitting of tails, 2) observed trait interval and no fitting of tails, 3) observed trait interval and fitting of both tails. We tested the three models for the 13 genetic markers for two different estimates of geographic distance among sampled populations. The hybrid zone is located in a region with high topographic complexity, and Euclidean geographic distance alone can misrepresent the actual distance between two places. Therefore, we measured Euclidean geographic distance in addition to a measurement that considered the geographic breaks (**Figure S2**), for example, the Grijalva River valley in central Chiapas, a reported strong barrier between yellow and gray morphotypes (Paynter 1978). We compared the models using the corrected

Akaike information criterion (AICc) and selected the models with the lowest AICc score as the best-fitting model. We did not fit a cline for plumage coloration since one outlier SNP correlates completely with this trait.

## Geographic and environmental barriers isolating the yellow and gray phenotypes

We analyzed geographic (elevation, downloaded from WorldClim) and environmental variables (19 bioclimatic layers from WorldClim) at 30 arc-second resolution (Hijmans et al. 2005, http://www.worldclim.org) to try to understand if there are barriers that promote isolation between the yellow and gray phenotypes in addition to the Grijalva River in southern Mexico. First, we extracted the values from the elevation and bioclimatic layers corresponding to the collection sites of the 73 individuals included in the genetic analyses. We proceeded to run a PCA on the dataset to check the spatial distribution of the geographic and environmental data of the locations where the birds live. We conducted a PCA on the 73 individual dataset, and another analysis focused on the intermixing phenotypic groups: yellow-bellied from Altos de Chiapas, hybrids, and gray-bellied from southern Mexico and western Guatemala. We noted the variables that had the greatest loading on the PCs.

Second, to detect a plausible barrier, we looked at the environmental variation geographically available for the intermixing groups to occupy (yellow-bellied from Altos de Chiapas, hybrids, and gray-bellied from southern Mexico and western Guatemala). To do this, we drew a rectangle that cut across the region (**Figure 7a**) and randomly selected 10,000 points within the rectangle. We extracted the values of the 10,000 points from the variables that contributed the most to the PCA: annual precipitation (bio_12) and elevation (hdem). We plotted the extracted values against latitude to obtain a profile of the background environmental variation. To check if there was an environmental discontinuity matching the geographic distribution of the yellow and gray phenotypes and the hybrids, we overlapped the collection points of the specimens with the background environmental profile.

## Results

The sampling of individuals from which we obtained mitochondrial DNA sequences encompasses the entire geographic range of *Atlapetes albinucha*, from central Mexico to Colombia. We included complete ND2 sequences (1041 bp) for 73 individuals, 67 sequenced by us, and six additional sequences downloaded from GenBank (**Table S1**). We obtained ddRAD genomic data from 59 individuals of *A. albinucha*, ranging from central Mexico to Panama. After building the loci catalog, the mean coverage was 20.6 (4.5 – 34.6), and the final number of variant sites called was 26,589 (after filtering and pruning). For the dataset that included the outgroup taxa, we called 281,813 variant sites. Lastly, from the exome capture dataset we obtained 1,662,727 SNPs, which included 100,284 non-coding SNPs and 1,562,443 SNPs from coding regions. The average coverage of the exome capture data was 36.5 (28.2 – 54.9).

## Population structure and differentiation

The mitochondrial genetic diversity in *Atlapetes albinucha* was moderate. Haplotype diversity was higher than 0.538 in seven of the nine regions studied (**Table S3**). However, the other two

regions showed haplotype diversity of zero; with each individual sampled from these regions sharing an identical ND2 haplotype (eastern Guatemala and eastern Honduras – Nicaragua). Nucleotide diversity of ND2 ranged from 0.000 to 0.005. Interestingly, the higher nucleotide diversity was recorded for the region identified as a putative hybrid zone. Neutrality tests and analysis of mismatch distributions were consistent with demographically stable populations.

*Atlapetes albinucha* showed high geographic structure for both the mitochondrial DNA and nuclear DNA. For the mitochondrial DNA, pairwise FST values (**Table 1**), AMOVAs (**Table S4**), and the haplotype network (**Figure 2**) supported four highly differentiated groups separated by the geographic barriers of the Isthmus of Tehuantepec, the Nicaraguan Depression, and the Isthmus of Panama. The highest percentage of mitochondrial DNA variation among groups was obtained when the groups were defined by the ddRAD PCA groups (62.58%), followed by the groups separated by major geographic breaks (61.45%). The most common haplotype was shared from southern Mexico to Nicaragua.

The haplotype network for ND2, in addition to supporting four genetic groups, showed that the genetic structure does not match the plumage coloration. The haplotypes from Altos de Chiapas (yellow phenotype) were grouped with the samples from southern Mexico to Nicaragua (gray phenotype) instead of with the samples from west of the Isthmus of Tehuantepec (yellow phenotype). Furthermore, the individuals identified as hybrids shared haplotypes or were closely linked to haplotypes from the southern area of the putative hybrid zone (gray phenotype), regardless of their plumage coloration. The haplotypes of three individual sampled from Altos de Chiapas (yellow phenotype) were linked to haplotypes from southern Mexico and western Guatemala (gray phenotype) and not with other haplotypes from Altos de Chiapas (yellow phenotype), which formed a slightly differentiated haplotype group.

The ddRAD genomic data showed more geographic genetic structure than the mitochondrial dataset. The PC1 showed two main clusters, one from each side of the Motagua Valley; the PC2 also showed two clusters, one from each side of the Isthmus of Tehuantepec. It was the PC3 that uncovered stronger genetic structure across the geographic range of *A. albinucha*. The PCA revealed seven clusters: west of the Isthmus of Tehuantepec, Altos de Chiapas, southern Mexico – western Guatemala, eastern Guatemala, El Salvador – western Honduras, eastern Honduras – Nicaragua, and Costa Rica – Panama. Additionally, the putative hybrids were intermediate between Altos de Chiapas and southern Mexico – western Guatemala (**Figures 2 and S3a**). The PCA based on the exome capture data recovered the same pattern (**Figure S3b**). The same barriers as identified in the mitochondrial DNA dataset were also recovered in the ddRAD data, but with the inclusion of a much greater number of loci further geographic barriers were identified for *A. albinucha*: the Altos de Chiapas-Cuchumatanes boundary area, Motagua Valley, the Ipala-Chortis blocks limit, and the Honduras Depression.

The ADMIXTURE ancestry analyses, along with the cross-validation error (0.414), supported two genetic clusters (**Figures 3 and S4**). The two clusters corresponded with PC1, separating the samples to the north and south of the Motagua Valley. The two groups are not consistent with delimitation of plumage coloration, and there are signs of admixture in areas adjacent to the Motagua Valley. Although $K$=3 was not the optimal value of $K$ (0.447), the assignment of three clusters was geographically meaningful. The assignment for $K$=3 confirmed the mixed ancestry

of the individuals we designated as putative hybrids (probably F1s), while maintaining the differentiation imposed by the Motagua Valley. Further, the assignment of individuals into three clusters was consistent with plumage coloration, separating the yellow from the gray phenotypes, although the admixed zone at the Motagua Valley region remains cryptic.

The analyses on the morphological data revealed that the plumage coloration, gray and yellow, is the only trait differentiating the specimens into two groups (**Figure S5**). None of the bill, wing, and tail measurements separated the specimens into distinct clusters.

**Phylogenetic analyses**

The mitochondrial and nuclear phylogenetic analyses confirmed the monophyly of *Atlapetes albinucha* (**Figures 4 and S6**). The mitochondrial and nuclear phylogenies were consistent in showing that plumage coloration, yellow versus gray, is not associated with a monophyletic group. However, the topologies of the mitochondrial DNA and nuclear DNA were incongruent, especially for the hybrid individuals.

Specifically for the mitochondrial data, both the maximum likelihood and the Bayesian inference recovered similar topologies, with a lack of supported nodes among clades within *A. albinucha*. The individuals from Costa Rica – Panamá were always grouped with the individuals from Colombia. Similar to the haplotype network, the hybrid individuals were grouped more closely to southern Mexico – western Guatemala region. Additionally, some individuals sampled from Altos de Chiapas clustered with those from the southern Mexico – western Guatemala region.

The maximum likelihood analysis of the genomic SNP data supported a well-resolved phylogeny with a clear geographic structure. The first divergence within *A. albinucha* resulted in two groups, each one on either side of the Isthmus of Tehuantepec. Following that divergence, the phylogeny suggests divergence across the Motagua Valley, within the group on the eastern side of the Isthmus of Tehuantepec. The clade with a geographic range north of the Motagua Valley follows a diversification pattern in a northerly direction and includes individuals with yellow and gray phenotypes. The hybrid individuals clustered within the clade north of the Motagua Valley and were more closely related to the yellow phenotype birds from Altos de Chiapas. The clade located south of the Motagua Valley follows a diversification pattern in a southerly direction, and therefore the more recently diverged groups are located in southern Central America; this clade only includes individuals with gray phenotypes.

**Genomic basis of plumage coloration**

We detected 2,269 outlier SNPs among 1,180,857 variant sites analyzed when contrasting nine individuals with the yellow phenotype from Altos de Chiapas and five individuals with the gray phenotype from southern Mexico – western Guatemala. Only 34 of the outlier SNPs had a Weir and Cockerham FST higher than 0.8, and these 34 SNPs were distributed across 23 genes (**Table S5**). Three of those 23 genes are of interest to understanding the genomic basis of plumage coloration: LOC102074020, which codes for the protein UDP-glucuronosyltransferase 1-1-like, DCT that codes for the protein dopachrome tautomerase, and LOC102071381 that codes for the keratin-associated protein 6-5-like.

One single SNP was differentially fixed between the two phenotypic groups (yellow versus gray) among the three genes mentioned above. The fixed SNP was located in the gene LOC102074020. Seven additional outlier SNPs were located in the same gene. Another three SNPs were located within the same scaffold (NW_005082739.1), one SNP in each of three genes: LOC102073677, LOC102073846, and LOC102074190. These three genes code for different mRNA variants of the UDP-glucuronosyltransferase 1-1-like protein. Within the gene LOC102074020 (**Figure 5**), the outlier SNPs show a high degree of correspondence with the phenotype color; the nine yellow individuals have one or two copies of the yellow allele in all of the outlier positions, and the five gray individuals have one or two copies of the gray allele. Heterozygous positions are present in eight of nine yellow individuals, four of five gray-bellied individuals, and the two hybrid individuals, a pattern indicative of hybridization and introgression. However, none of above fixed SNPs putatively pertaining to phenotype color are fixed among the eight individuals collected outside of the hybrid zone from which exome capture data was obtained (**Figure S7**).

## Hybridization and introgression

Geographic cline analyses revealed that the models that incorporated a distance measurement that considered topography provided a better fit to the genetic data than those incorporating Euclidean geographic distance (**Table 2, Figures 6 and S8**). Using this distance metric, the patterns of introgression were variable among genetic markers. The mitochondrial DNA cline showed a pattern of introgression from the gray phenotype into the yellow phenotype, a pattern that overlapped with the outlier SNP in Gene 3 – 21695. The majority of outlier SNPs (6 of 11) showed a contrasting pattern, in which introgression was mainly from the yellow phenotype into the gray phenotype. Additionally, one of the outlier SNPs, the SNP with FST = 1 when comparing both groups (Gene 3 – 21839), had a cline with a center coincident with the ddRAD dataset cline (center Gene 3 – 21839: 217.47; center ddRAD: 224.51).

The mean cline center of the 13 genetic markers (226.98 km) that underpin phenotype, closely matched the collection sites of the two hybrids included in the study (214.81 – 217.41 km). Most of the clines had gradual slopes encompassing a broad geographic area, supported by a high mean width (195.56 km). Only the cline of the outlier SNP FST = 1 (Gene 3 – 21839) was very steep (width 1.61 km).

## Geographic and environmental barriers isolating the yellow and gray phenotypes

The PCA of the elevation and environmental variables showed that the two phenotypes, yellow and gray, occupy similar geographic and environmental regions (**Figure S9**). Annual precipitation and elevation are variables that explain most of the variation. The environmental space where the gray phenotype inhabits is broader than the environmental space of the yellow phenotype. The yellow phenotype is restricted to moderate levels of precipitation (Altos de Chiapas: 1,129 to 1,962 mm of annual precipitation). In contrast, the gray phenotype expands into areas with higher precipitation (southern Mexico and western Guatemala: 960 to 2,879 mm of annual precipitation). There is a similar pattern in the elevational distribution; with the yellow phenotype occupying a narrower mountain belt (Altos de Chiapas samples range from 1,900 to

2,400 m asl) than the gray phenotype (southern Mexico and western Guatemala samples range from 750 to 3,098 m asl).

The analysis of the available environmental background revealed an increase in annual precipitation and a decrease in elevation in the area where the yellow and gray phenotypes abut (**Figure 7b**). Annual precipitation increases significantly in the area where the phenotypic and geographic break occurs, reaching values higher than 5,000 mm. Interestingly, the hybrid individuals were collected at sites where annual precipitation (1840 – 2650 mm) overlaps with the values for the gray phenotype, which are geographically close to the areas with the highest precipitation. The geographic break is also very evident in elevation; there is an abrupt decrease in elevation separating the ranges of the yellow and gray phenotypes. The hybrids were collected at lower elevation than either parental phenotype.

**Discussion**

Our study highlights how the interplay of multiple processes drives the diversification of an avian species, *Atlapetes albinucha*. Divergence in allopatry explains the strong geographic structure detected with mitochondrial and genomic (ddRAD and exome capture data) markers within the species. Genetic groups correspond with different mountain ranges and volcanoes separated by low-elevation areas: Isthmus of Tehuantepec, Altos de Chiapas-Cuchumatanes boundary area, Motagua Valley, Ipala-Chortis blocks boundary, Honduras Depression, Nicaraguan Depression, and Isthmus of Panama. Hybridization between the yellow phenotype from northern Chiapas and the gray phenotype from western Guatemala enhances genetic introgression between the two groups. The phenotypes are fixed on either side of the hybrid zone in spite of introgression, which suggests that some selective force may be acting to maintain the two plumage coloration variants. Additionally, the hybrid zone occurs in a narrow area with higher precipitation and lower elevation than the parental environments. A steep cline associated with the plumage color phenotype suggests that selection might be acting against the hybrids. Outlier SNPs of the exome capture data point to a protein (UDP-glucuronosyltransferase 1-1-like) involved in carotenoid degradation, specifically in the lutein cycle, as a candidate to explain the differences between the yellow and the gray phenotypes in northern Central America. We uncovered new biogeographic breaks and complex evolution across the landbridge connecting North and South America.

**Phylogeography of *Atlapetes albinucha***

Our findings show that the high genetic structure in *A. albinucha* is driven by divergence in allopatry promoted by geographical isolating barriers. Most of the isolating barriers that we detected (Isthmus of Tehuantepec, Motagua Valley, Honduras Depression, Nicaraguan Depression, and Isthmus of Panama) correspond with commonly reported barriers for montane species in the region (snakes, Daza et al. 2010; mammals, Pérez Consuegra and Vázquez-Domínguez 2015; amphibians, Rovito and Parra-Olea 2016; birds, Jiménez and Ornelas 2016, Rodríguez-Gómez et al. 2021). Our detailed sampling in northern Central America and genomic data allowed us to uncover new geographic breaks associated with genetic divergence, the Altos de Chiapas-Cuchumatanes boundary area, and the Ipala-Chortis blocks boundary. The Altos de Chiapas-Cuchumatanes boundary area separates the yellow and gray phenotypes of *A.*

*albinucha* and agrees with suggested limits between areas of endemism of beetles (Schuster et al. 2000). The boundary between the Ipala and Chortis blocks was recently described based on geological research (Ellis et al. 2019). The Ipala-Chortis blocks boundary is located in eastern Guatemala and western El Salvador; future studies will show whether it represents a barrier for other species in the region.

This study is the first instance to demonstrate hybridization between the yellow and gray phenotypes of *A. albinucha*. Previous studies report that the yellow and gray phenotypes do not interbreed because they are allopatric, with the Grijalva River separating the phenotypes in central Chiapas (Paynter 1978, Rocha-Méndez et al. 2018). However, those studies seem to ignore the close geographic proximity of both phenotypes between northern Chiapas and western Guatemala, where we collected hybrid individuals. Our mtDNA analyses suggest that hybridization and genetic introgression are better explanations for the geography-genetic discordance observed in the area where the yellow and gray phenotypes abut, rather than incomplete lineage sorting, as previously proposed (Rocha-Méndez et al. 2018).

## Genomic basis of the two color morphotypes within *Atlapetes albinucha*

Exome capture data and outlier analysis suggest UDP-glucuronosyltransferase as a candidate to explain the presence-absence of yellow color in feathers. One SNP from the gene encoding for the UDP-glucuronosyltransferase was fixed for the color differences (yellow vs. gray) in Altos de Chiapas and southern Mexico – western Guatemala. UDP-glucuronosyltransferase is a protein within the route of carotenoid processing and excretion, including lutein (Hill and Johnson 2012). UDP-glucuronosyltransferase has also been recognized as important in eggshell pigmentation (Bai et al. 2019). However, when we looked at the genotypes of populations outside this region, the pattern of correspondence between the completely fixed SNP and plumage coloration is not as strong; two yellow and six gray individuals were heterozygous for the yellow and gray alleles, and two other gray individuals were homozygous for the yellow allele. A similar pattern has been found in melanin pigmentation in other species of birds, and it has been attributed to multiple gene interactions rather than one locus of large effect forming the genomic basis of plumage coloration (Uy et al. 2016). Since the two *A. albinucha* hybrids that we collected are genetically intermediate and have different degrees of yellow-gray coloration, the possibility of multiple mutations interacting to produce the observed plumage color variation observed in this species seems likely.

## Hybridization and introgression within *Atlapetes albinucha*

We discovered cryptic genetic introgression across the hybrid zone between the yellow phenotype from northern Chiapas and the gray phenotype from southern Mexico and western Guatemala. Cryptic genetic introgression and the fixed phenotypes on either side of the hybrid zone suggest selection plays a role in maintaining the two differentiated plumage color variants. Our findings have similarities and differences when compared to other avian hybrid zones in Central America (manakins, Stein and Uy 2006; jacanas, Lipshutz et al. 2019). Similarly, we found differential introgression for distinct regions of the genome, but genetic introgression in *A. albinucha* is cryptic and not visually evident as in manakins (Stein and Uy 2006) and jacanas (Lipshutz et al. 2019). Future research should look into disentangling the regions of the genome

with higher and lower introgression, in order to uncover the regions involved in maintaining the two plumage phenotypes (Lamichhaney et al. 2020).

Through detailed geographic and climatic analyses we uncovered the precipitation and elevation break that isolates the two phenotypes. Barriers established by differences in elevation are common for montane species in northern Central America. To our knowledge, breaks associated with high precipitation rates are not commonly described, however; rain is thought to be a strong abiotic selective pressure in tropical species (Boyle et al. 2020). We recommend paying particular attention to precipitation regimes in the study of tropical hybrid zones, especially in regions with complex topography.

Environmental and geographic differences in precipitation and elevation demarcate the position and width of the hybrid zone. The position of a hybrid zone usually correlates with ecological factors (Price 2008), which seems to be the case in our study. The width of a hybrid zone provides information about the strength of selection against the hybrids (Alexandrino et al. 2005). For *A. albinucha*, the abrupt environmental break and the steep cline associated with color phenotype suggest strong selection against the hybrids. Whether the hybrids have lower or higher fitness in the environment where they live remains to be directly tested. However, the discovery of this geographic break and associated hybrid zone opens up new possibilities for exciting research in the area.

## Conclusions

Our work highlights the importance of assessing multiple processes if we are to improve our understanding of the drivers of origin and maintenance of biodiversity, particularly in geographical and topographical complex regions such as the Neotropics. The evolution of *Atlapetes albinucha*, an avian species restricted to mountain ranges extending from eastern Mexico to Colombia, involves a diverse set of processes. Divergence in allopatry given geographic breaks results in strong genetic structure. Selective forces maintain two plumage color phenotypes, yellow and gray, despite hybridization and genetic introgression. Differential cryptic introgression is evidenced across distinct regions of the genome. High precipitation and low elevation limit the geographic range of the yellow and gray phenotypes in northern Chiapas and western Guatemala, while at the same time, provide a different environment where a hybrid zone occurs. Our genomic data suggests UDP-glucuronosyltransferase as a candidate gene explaining the presence-absence of yellow color in feathers. Examining this gene in other *Atlapetes* species, and other birds in general, might help to understand the genomic basis of carotenoid-based plumage coloration. Finally, our study uncovers new biogeographic breaks in northern Central America (Altos de Chiapas-Cuchumatanes boundary and Ipala-Chortis blocks boundary), important knowledge needed to understand the complex evolution of lineages residing on the landbridge connecting North and South America, as well as for use in setting conservation priorities.

## Tables and figures

**Table 1.** Genetic differentiation between populations of *Atlapetes albinucha* based on mtDNA. Above diagonal: average number of pairwise differences between the populations. Diagonal: average number of pairwise differences within populations. Below the diagonal: pairwise FST values between populations; significant values are shown in bold.

| | **W Isthmus of Tehuantepec** | **Altos de Chiapas** | **Hybrids** | **S Mexico – W Guatemala** | **E Guatemala** | **El Salvador – W Honduras** | **E Honduras – Nicaragua** | **Costa Rica – Panamá** | **Colombia** |
|---|---|---|---|---|---|---|---|---|---|
| W Isthmus of Tehuantepec | 2.000 | 7.564 | 9.833 | 7.491 | 7.333 | 8.000 | 7.333 | 8.619 | 12.000 |
| Altos de Chiapas | 0.719 | 2.154 | 6.192 | 4.146 | 3.923 | 4.564 | 3.923 | 5.934 | 8.897 |
| Hybrids | 0.690 | 0.579 | 5.000 | 3.289 | 2.500 | 3.167 | 2.500 | 8.357 | 11.167 |
| S Mexico – W Guatemala | **0.705** | **0.467** | 0.113 | 2.257 | 1.421 | 2.088 | 1.421 | 6.015 | 8.825 |
| E Guatemala | **0.907** | **0.626** | 0.473 | 0.060 | 0.000 | 0.667 | 0.000 | 5.857 | 8.667 |
| El Salvador – W Honduras | **0.808** | **0.593** | 0.268 | **0.104** | -0.034 | 1.333 | 0.667 | 6.524 | 9.333 |
| E Honduras – Nicaragua | **0.889** | **0.606** | 0.384 | 0.030 | 0.000 | -0.081 | 0.000 | 5.857 | 8.667 |
| Costa Rica – Panamá | **0.848** | **0.706** | **0.792** | **0.688** | **0.894** | **0.819** | **0.883** | 1.048 | 8.524 |
| Colombia | **0.872** | **0.788** | **0.818** | **0.772** | **0.915** | **0.857** | **0.905** | **0.862** | 1.333 |

**Table 2.** Parameter estimates for best fitting geographic clines for mitochondrial DNA, ddRAD data, and 11 outlier SNPs within scaffold NW_005082739.1 (Gene 1 – LOC102073677, Gene 2 – LOC102073846, Gene 3 – LOC102074020, Gene 4 – LOC102074190). Cline center (c), cline width (w), trait interval (pMin/pMax), log-likelihood scores, and AICc. Euclidean distances (non-shaded rows) and distances considering topography and geographic barriers (shaded rows).

| Dataset / Locus | Best model | c | w | pMin | pMax | Log-likelihood | AICc |
|---|---|---|---|---|---|---|---|
| mtDNA | pMin/pMax free, no tails | 91.37 (39.46 – 181.21) | 100.62 (0.07 – 255.90) | 0.15 | 1 | -5.10 | 19.59 |
| | pMin/pMax fixed, no tails | 176.66 (89.19 – 252.19) | 319.17 (190.11 – 409.98) | 0 | 1 | -5.63 | 15.65 |
| ddRAD-seq | pMin/pMax fixed, no tails | 151.88 (105.11 – 186.13) | 97.41 (41.71 – 211.34) | 0 | 1 | -3.87 | 12.13 |
| | pMin/pMax fixed, no tails | 224.51 (152.16 – 269.33) | 73.01 (18.07 – 206.32) | 0 | 1 | -0.08 | 4.54 |
| Gene 1 – 7038 | pMin/pMax fixed, no tails | 208.77 (125.68 – 355.05) | 244.07 (98.53 – 409.93) | 0 | 1 | -4.21 | 13.34 |
| | pMin/pMax fixed, no tails | 259.80 (164.54 – 379.48) | 227.60 (89.88 – 409.95) | 0 | 1 | -2.61 | 10.15 |
| Gene 2 – 12871 | pMin/pMax fixed, no tails | 237.63 (172.27 – 379.99) | 157.74 (47.40 – 409.98) | 0 | 1 | -1.35 | 7.62 |
| | pMin/pMax fixed, no tails | 310.83 (218.72 – 380.00) | 219.32 (73.02 – 409.96) | 0 | 1 | -1.45 | 7.82 |
| Gene 3 – 21505 | pMin/pMax fixed, no tails | 94.27 (-14.09 – 189.70) | 255.24 (113.27 – 409.99) | 0 | 1 | -318 | 11.28 |
| | pMin/pMax fixed, no tails | 109.54 (-3.13 – 222.02) | 290.95 (126.42 – 410.00) | 0 | 1 | -2.54 | 10.00 |
| Gene 3 – 21589 | pMin/pMax fixed, no tails | 290.82 (169.74 – 379.87) | 378.20 (126.80 – 409.98) | 0 | 1 | -5.21 | 15.34 |
| | pMin/pMax fixed, no tails | 306.67 (239.85 – 379.76) | 76.57 (22.11 – 409.95) | 0 | 1 | -1.39 | 7.70 |
| Gene 3 – 21663 | pMin/pMax fixed, no tails | 135.84 (23.52 – 248.81) | 391.12 (163.39 – 410.00) | 0 | 1 | -3.15 | 11.22 |
| | pMin/pMax fixed, no tails | 162.29 (47.23 – 284.96) | 379.12 (174.22 – 409.97) | 0 | 1 | -2.02 | 8.95 |
| Gene 3 – 21691 | pMin/pMax fixed, no tails | 153.37 (80.72 – 248.61) | 188.38 (87.63 – 409.88) | 0 | 1 | -1.82 | 8.57 |
| | pMin/pMax fixed, no tails | 190.15 (92.17 – 311.42) | 261.85 (124.53 – 409.98) | 0 | 1 | -1.77 | 8.46 |
| Gene 3 – 21695 | pMin/pMax fixed, no tails | 146.00 (41.93 – 265.13) | 310.80 (139.72 – 410.00) | 0 | 1 | -3.08 | 11.08 |
| | pMin/pMax fixed, no tails | 176.22 (66.20 – 300.11) | 313.06 (149.98 – 409.94) | 0 | 1 | -1.77 | 8.47 |
| Gene 3 – 21715 | pMin/pMax fixed, no tails | 184.47 (73.94 – 356.53) | 135.07 (0.00 – 409.99) | 0.25 | 1 | -1.72 | 8.36 |
| | pMin/pMax fixed, no tails | 256.04 (103.84 – 379.89) | 147.38 (0.09 – 410.00) | 0.25 | 1 | -0.53 | 5.98 |
| Gene 3 – 21839 | pMin/pMax fixed, no tails | 177.81 (116.63 – 244.50) | 120.07 (43.45 – 392.43) | 0 | 1 | -3.49 | 11.90 |
| | pMin/pMax fixed, no tails | 217.47 (175.84 – 278.38) | 1.61 (0.54 – 225.86) | 0 | 1 | -0.01 | 4.93 |
| Gene 3 – 22431 | pMin/pMax fixed, no tails | 204.32 (128.87 – 346.01) | 211.54 (84.19 – 409.85) | 0 | 1 | -3.73 | 12.38 |
| | pMin/pMax fixed, no tails | 262.39 (178.57 – 348.20) | 135.16 (48.03 – 409.84) | 0 | 1 | -0.91 | 6.75 |
| Gene 4 – 23950 | pMin/pMax fixed, no tails | 243.65 (97.16 – 379.86) | 279.32 (0.09 – 410.00) | 0.25 | 1 | -3.33 | 11.58 |
| | pMin/pMax fixed, no tails | 298.22 (193.65 – 379.96) | 97.52 (0.03 – 409.91) | 0.25 | 1 | -0.93 | 6.78 |

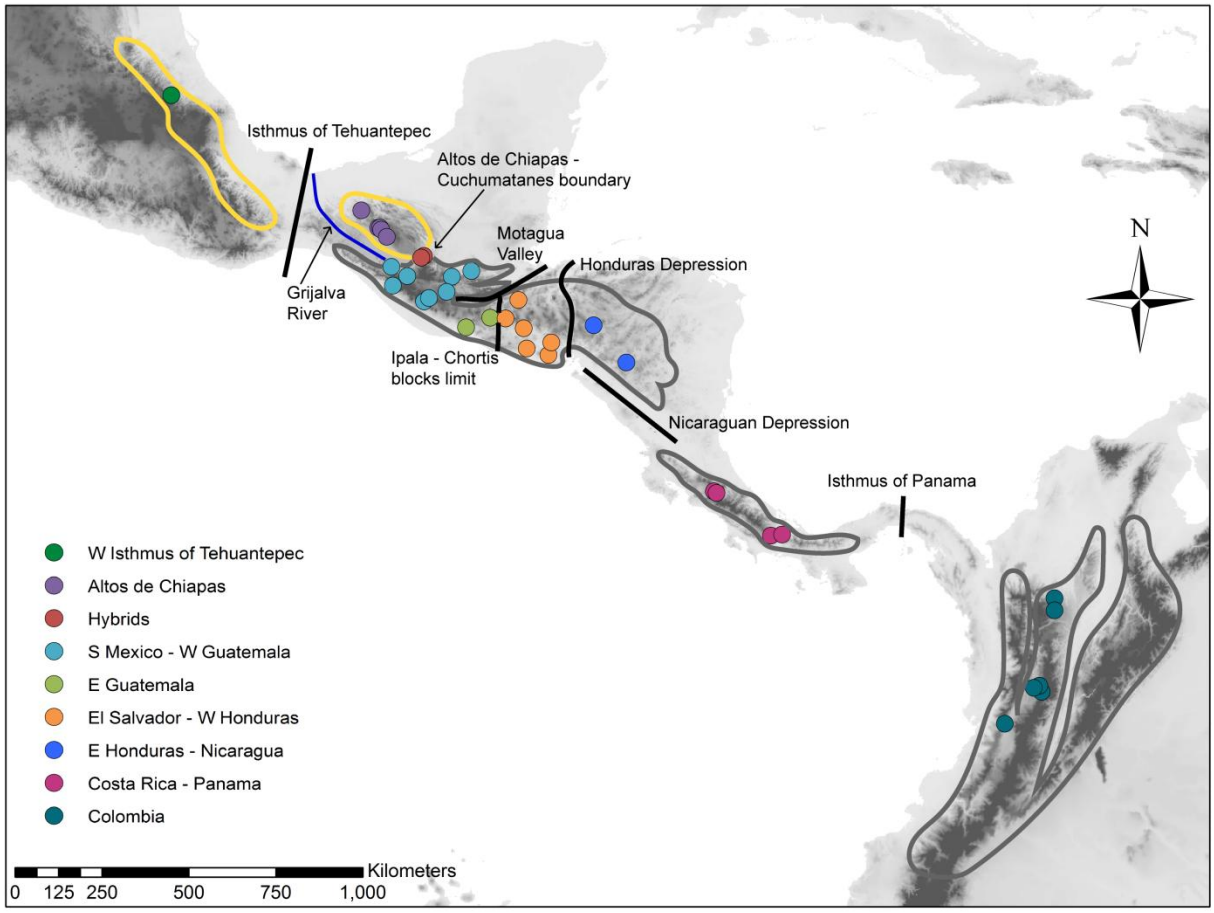


**Figure 1.** Geographic range of the two plumage color phenotypes of *Atlapetes albinucha*, main geographic barriers in the region, and localities where the samples analyzed genetically were collected. The yellow polygons represent the geographic range of the yellow phenotype and the gray polygons, the range of the gray phenotype.

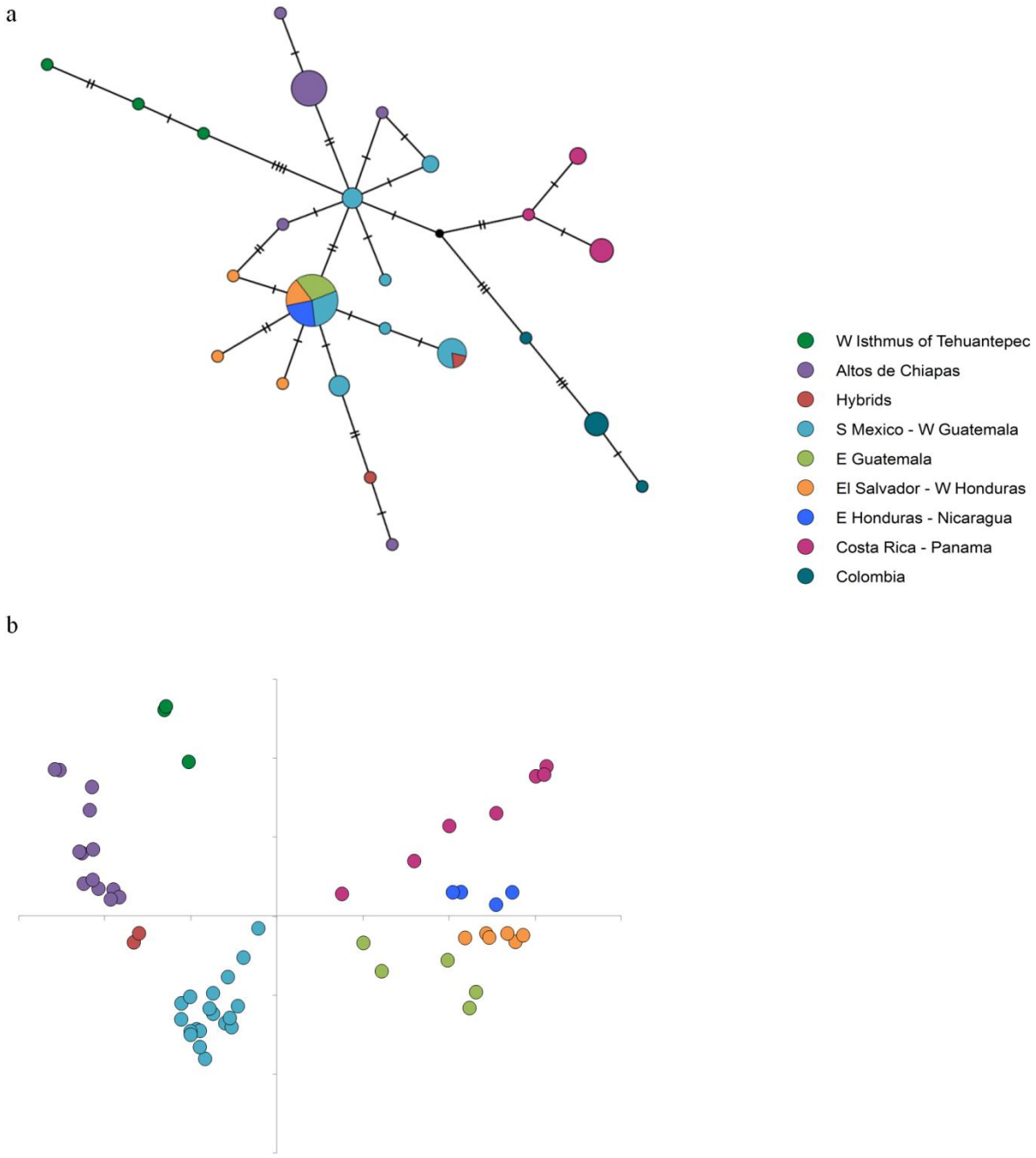


**Figure 2.** Mitochondrial and nuclear genetic structure in *Atlapetes albinucha*. a) Haplotype network of mitochondrial ND2. b) Principal Component Analysis of the genomic ddRAD data. Percentage of variation in PC1: 9.3, and PC3: 3.6.

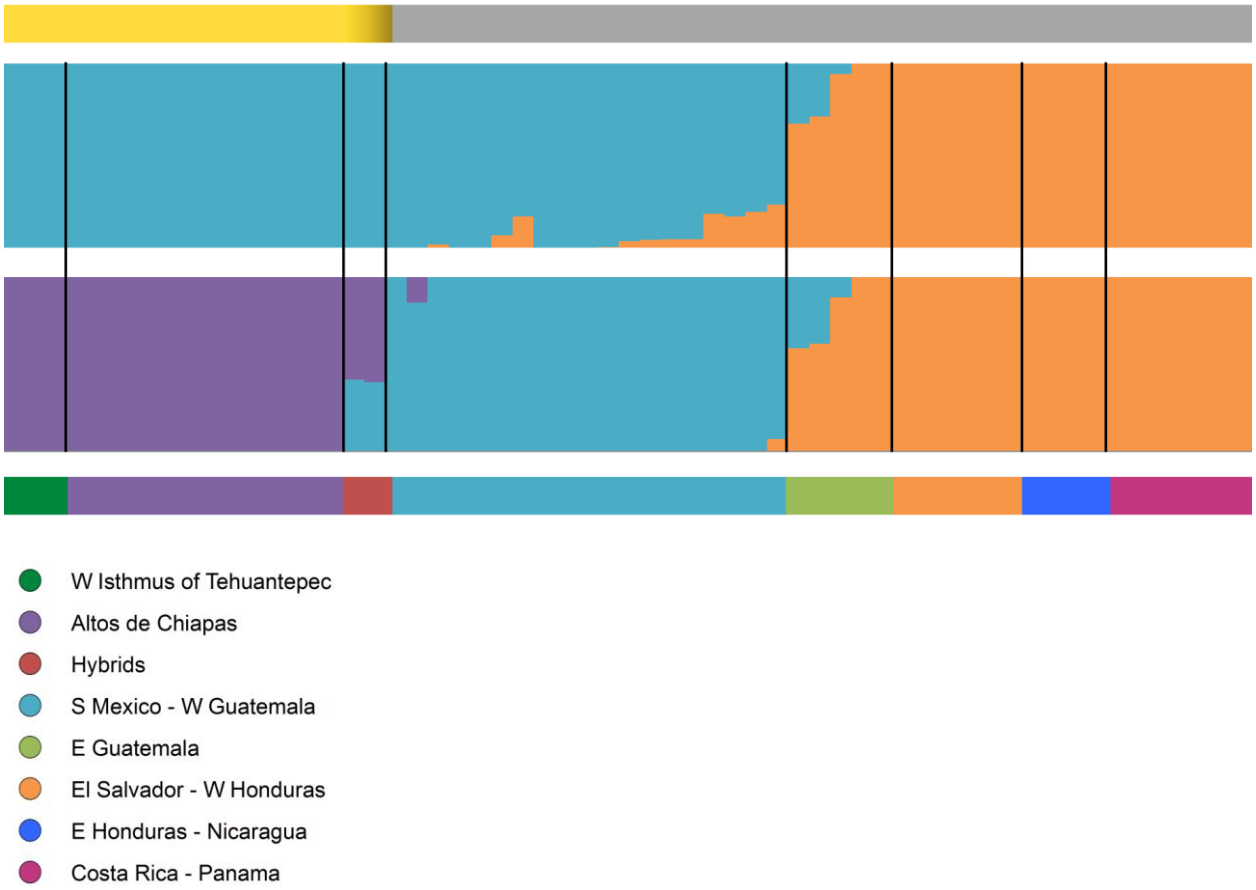


**Figure 3.** Phenotype, genotype, and geographic distribution of *Atlapetes albinucha*. The upper bar shows the plumage color phenotype, yellow-bellied and gray-bellied individuals. The second and third bars show the results of ADMIXTURE analysis for K=2 and K=3, respectively. ADMIXTURE analyses were done using the ddRAD-seq data. The lower bar shows the color assigned to different geographic populations.

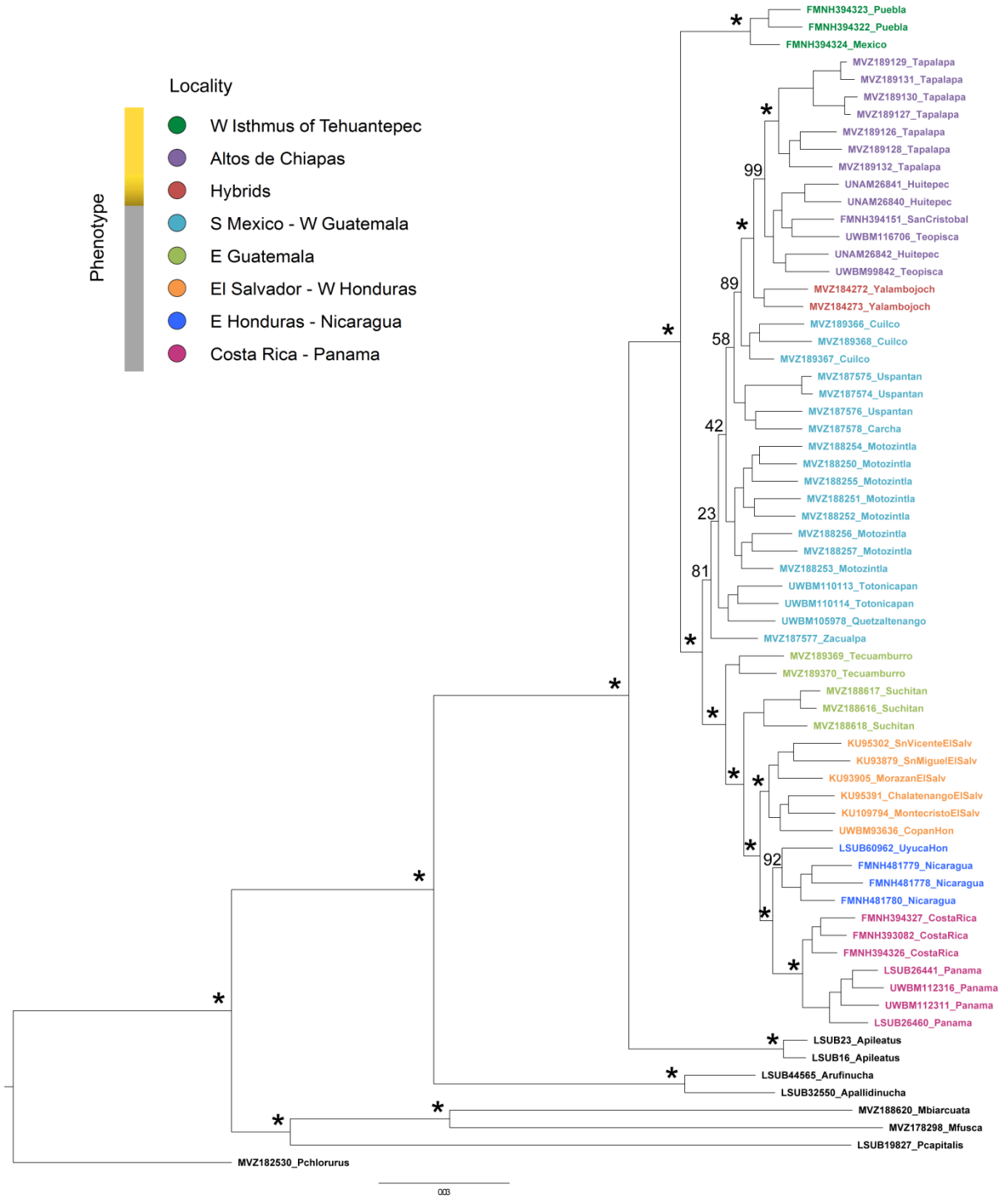


**Figure 4.** Maximum Likelihood phylogeny of *Atlapetes albinucha* based on ddRAD data. Node support was estimated with 100 iterations of rapid bootstrapping, asterisks at nodes represent a support value of 100.


| Gene | | Gene 1 | Gene 2 | Gene 3 | | | | | | | | Gene 4 |
|---|---|---|---|---|---|---|---|---|---|---|---|---|
| Position within the scaffold | | 7038 | 12871 | 21505 | 21589 | 21663 | 21691 | 21695 | 21715 | 21839 | 22431 | 23950 |
| Fst (9 Yellow vs. 5 Gray) | | 0.7352 | 0.5254 | 0.6516 | 0.6451 | 0.5909 | 0.6669 | 0.6669 | 0.6682 | 1.0000 | 0.8389 | 0.5545 |
| | | C | T | T | T | C | C | G | C | C | G | T |
| Sample/Region | | T | C | C | A | T | T | A | T | T | A | A |
| MZFC26841 | AChis | | | | | | | | | | | |
| FMNH394151 | AChis | | | | | | | | | | | |
| UWBM116706 | AChis | | | | | | | | | | | |
| MVZ189128 | AChis | | | | | | | | | | | |
| MVZ189129 | AChis | | | | | | | | | | | |
| MVZ189127 | AChis | | | | | | | | | | | |
| MVZ189131 | AChis | | | | | | | | | | | |
| UNAM26840 | AChis | | | | | | | | | | | |
| UNAM26842 | AChis | | | | | | | | | | | |
| USAC823 | Hybrid-Yellow | | | | | | | | | | | |
| MVZ184272 | Hybrid-Gray | | | | | | | | | | | |
| MVZ187574 | SMxWGt | | | | | | | | | | | |
| MVZ189367 | SMxWGt | | | | | | | | | | | |
| MVZ189368 | SMxWGt | | | | | | | | | | | |
| MVZ188254 | SMxWGt | | | | | | | | | | | |
| MVZ188250 | SMxWGt | | | | | | | | | | | |

Gene 1: LOC102073677
Gene 2: LOC102073846
Gene 3: LOC102074020
Gene 4: LOC102074190

**Figure 5.** Genotypes for outlier SNPs within the four genes on scaffold NW_005082739.1. Yellow and gray colors were used to represent the homozygote positions, and the samples collected in allopatry for either of both phenotypes. The brick red color represents the heterozygote positions, and the hybrid individuals.

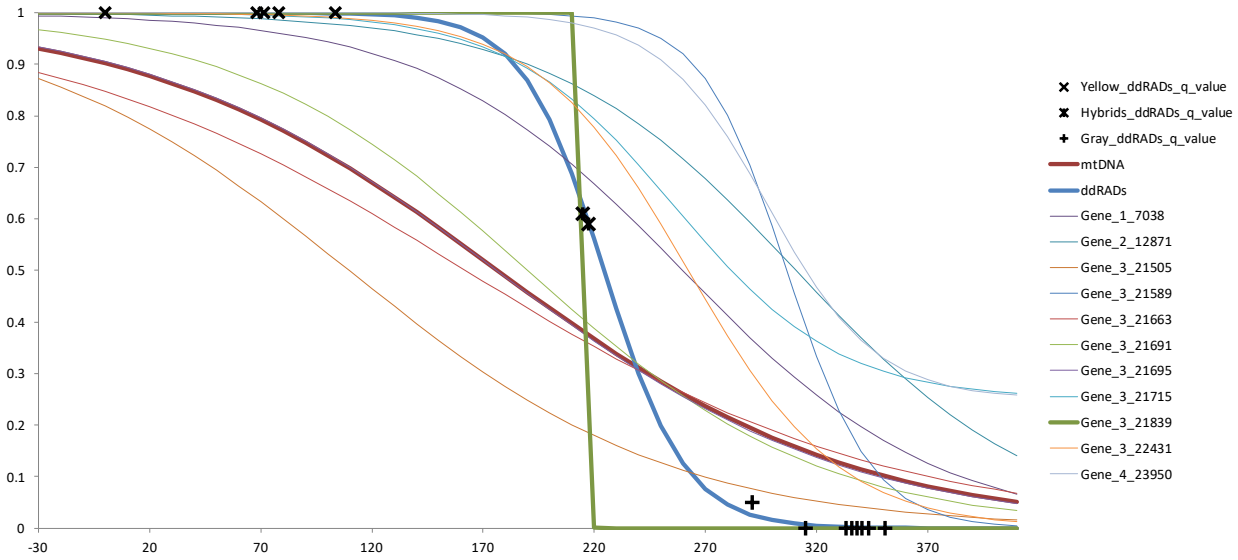


**Figure 6.** Geographic clines fitted for the mitochondrial DNA, ddRAD data, and SNPs within scaffold NW_005082739.1. The geographic distance used for this analysis was corrected to account for geographic barriers. The "x" axis represents the distance in kilometers and the "y" axis represents allelic frequencies.

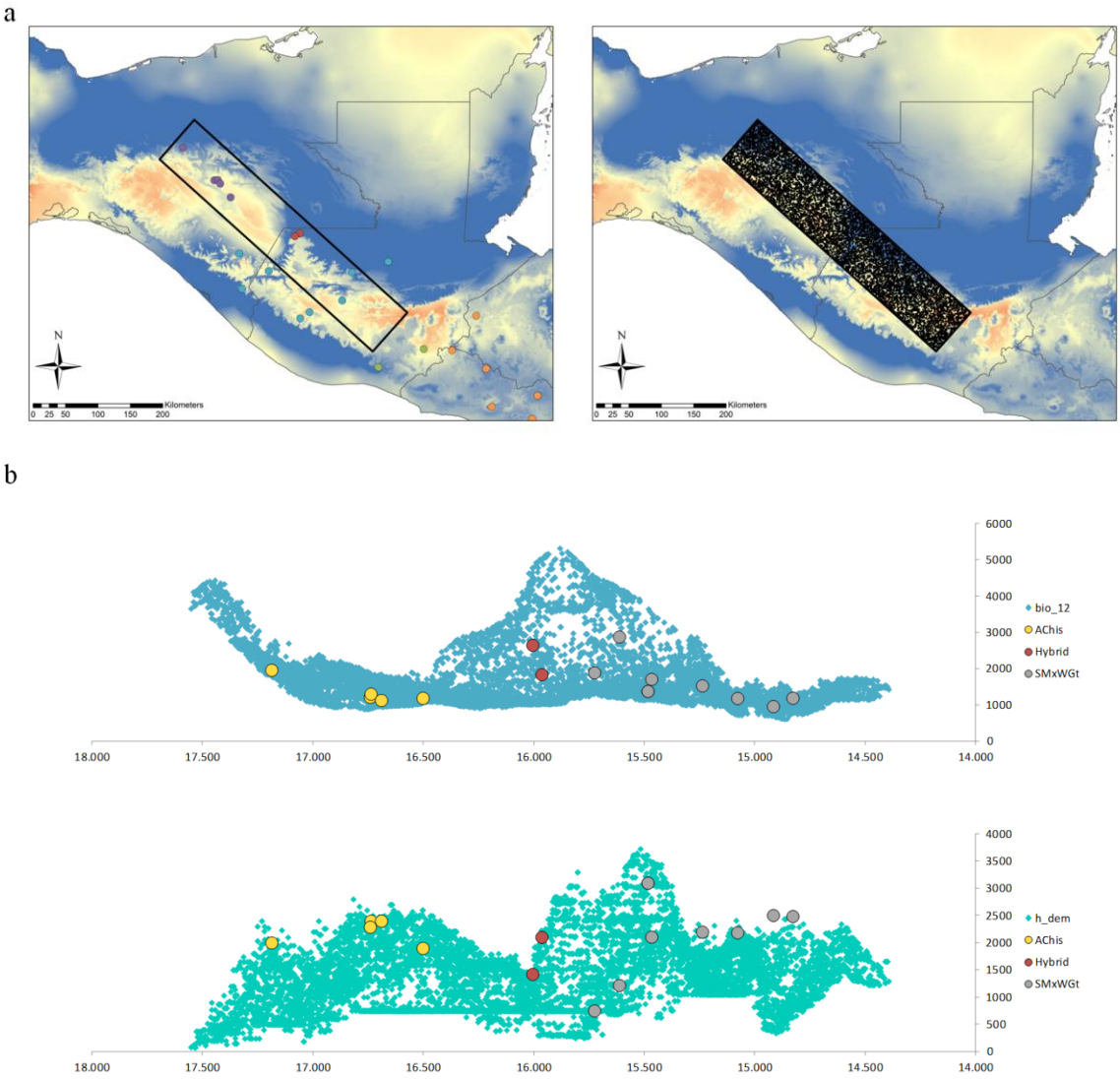


**Figure 7.** Geographic and environmental barriers isolating the yellow and gray phenotypes of *Atlapetes albinucha*. a) The maps show the regions involved in the hybridization between the two phenotypes. The background in the maps is based on annual precipitation (BioClim "bio_12"), blue represents wetter areas and red, drier areas. Left map: the black rectangle was drawn on the geographic area where the yellow and gray phenotypes abut. Rigth map: 10,000 random points were generated within the rectangle. b) Overlap between background environmental and geographic variables and sample collection localities. The "x" axis represents the latitude and the "y" axis represents the values of the analyzed variable. Upper graph: overlap between background annual precipitation (values from the 10,000 random points) and annual precipitation in the localities where the samples were collected. Annual precipitation is measured in millimeters per year ("y" axis). Lower graph: overlap between background elevation (values from the 10,000 random points) and elevation in the localities where the samples were collected. Elevation is measured in meters above sea level ("y" axis).

## References


Alexander, D. H., Novembre, J., & Lange, K. (2009). Fast model-based estimation of ancestry in unrelated individuals. Genome research, 19(9), 1655-1664.

Alexandrino, J., Baird, S. J., Lawson, L., Macey, J. R., Moritz, C., & Wake, D. B. (2005). Strong selection against hybrids at a hybrid zone in the Ensatina ring species complex and its evolutinary implications. Evolution, 59(6), 1334-1347.

Andrews, S. (2017). FastQC: a quality control tool for high throughput sequence data. 2010. Available online at: http://www.bioinformatics.babraham.ac.uk/projects/fastqc/

Antonelli, A., Ariza, M., Albert, J., Andermann, T., Azevedo, J., Bacon, C., ... & Edwards, S. V. (2018). Conceptual and empirical advances in Neotropical biodiversity research. PeerJ, 6, e5644.

Bai, D. P., Lin, X. Y., Wu, Y., Zhou, S. Y., Huang, Z. B., Huang, Y. F., ... & Huang, X. H. (2019). Isolation of blue-green eggshell pigmentation-related genes from Putian duck through RNA-seq. BMC genomics, 20(1), 1-12.

Barber, B. R., & Klicka, J. (2010). Two pulses of diversification across the Isthmus of Tehuantepec in a montane Mexican bird fauna. Proceedings of the Royal Society B: Biological Sciences, 277(1694), 2675-2681.

Boesman P. (2016). Notes on the vocalizations of White-naped Brush-finch (*Atlapetes albinucha*). HBW Alive Ornithological Note 364. In: Handbook of the Birds of the World Alive. Lynx Edicions, Barcelona. Doi: 10.2173/bow-on.100364.

Bowie, R. C., Fjeldså, J., Hackett, S. J., & Crowe, T. M. (2004). Systematics and biogeography of double-collared sunbirds from the Eastern Arc Mountains, Tanzania. The Auk, 121(3), 660-681.

Boyle, W. A., Shogren, E. H., & Brawn, J. D. (2020). Hygric niches for tropical endotherms. Trends in Ecology & Evolution.

Burns, K. J., McGraw, K. J., Shultz, A. J., Stoddard, M. C., & Thomas, D. B. (2017). Advanced Methods for Studying Pigments and Coloration Using Avian Specimens. In M. S. Webster (Ed.) The extended specimen: emerging frontiers in collections-based ornithological research (pp. 23-56). CRC Press.

Cadena, C. D., Pérez-Emán, J. L., Cuervo, A. M., Céspedes, L. N., Epperly, K. L., & Klicka, J. T. (2019). Extreme genetic structure and dynamic range evolution in a montane passerine bird: implications for tropical diversification. Biological Journal of the Linnean Society, 126(3), 487-506.

Carantón-Ayala, D., Avendaño, J. E., & Cadena, C. D. (2018). Hybridization in brushfinches (*Atlapetes*, Emberizidae) from the southeast Andes of Colombia: a consequence of habitat disturbance? Journal of Ornithology, 159(3), 713-722.

Catchen, J., Hohenlohe, P. A., Bassham, S., Amores, A., & Cresko, W. A. (2013). Stacks: an analysis tool set for population genomics. Molecular Ecology, 22(11), 3124-3140.

Chesser, R. T., Isler, M. L., Cuervo, A. M., Cadena, C. D., Galen, S. C., Bergner, L. M., ... & Hosner, P. A. (2020). Conservative plumage masks extraordinary phylogenetic diversity in the *Grallaria rufula* (Rufous Antpitta) complex of the humid Andes. The Auk, 137(3), ukaa009.

Cicero, C., & Johnson, N. K. (2001). Higher-level phylogeny of New World vireos (Aves: Vireonidae) based on sequences of multiple mitochondrial DNA genes. Molecular Phylogenetics and Evolution, 20(1), 27-40.

Clement, M., Posada, D., & Crandall, K. A. (2000). TCS: a computer program to estimate gene genealogies. Molecular Ecology, 9(10):1657-1659.
Coyne, J. A., & Orr, H. A. (2004). Speciation. Sinauer Associates.
Darriba, D., Taboada, G. L., Doallo, R., & Posada, D. (2012). jModelTest 2: more models, new heuristics and parallel computing. Nature methods, 9(8), 772-772.
Danecek, P., Auton, A., Abecasis, G., Albers, C. A., Banks, E., DePristo, M. A., ... & 1000 Genomes Project Analysis Group. (2011). The variant call format and VCFtools. Bioinformatics, 27(15), 2156-2158.
Daza, J. M., Castoe, T. A., & Parkinson, C. L. (2010). Using regional comparative phylogeographic data from snake lineages to infer historical processes in Middle America. Ecography, 33(2), 343-354.
Derryberry, E. P., Derryberry, G. E., Maley, J. M., & Brumfield, R. T. (2014). HZAR: hybrid zone analysis using an R software package. Molecular Ecology Resources, 14(3), 652-663.
Ellis, A., DeMets, C., McCaffrey, R., Briole, P., Cosenza Muralles, B., Flores, O., ... & Tikoff, B. (2019). GPS constraints on deformation in northern Central America from 1999 to 2017, Part 2: Block rotations and fault slip rates, fault locking and distributed deformation. Geophysical Journal International, 218(2), 729-754.
Excoffier, L., & Lischer, H. E. (2010). Arlequin suite ver 3.5: a new series of programs to perform population genetics analyses under Linux and Windows. Molecular Ecology Resources, 10(3), 564-567.
Fu, Y. X. (1997). Statistical tests of neutrality of mutations against population growth, hitchhiking and background selection. Genetics, 147(2), 915-925.
Graham, C. H., Carnaval, A. C., Cadena, C. D., Zamudio, K. R., Roberts, T. E., Parra, J. L., ... & Sanders, N. J. (2014). The origin and maintenance of montane diversity: integrating evolutionary and ecological processes. Ecography, 37(8), 711-719.
Guindon, S., & Gascuel, O. (2003). A simple, fast, and accurate algorithm to estimate large phylogenies by maximum likelihood. Systematic Biology, 52(5), 696-704.
Hijmans, R. J., Cameron, S. E., Parra, J. L., Jones, P. G., & Jarvis, A. (2005). Very high resolution interpolated climate surfaces for global land areas. International Journal of Climatology: A Journal of the Royal Meteorological Society, 25(15), 1965-1978.
Hill, G. E., & Johnson, J. D. (2012). The vitamin A–redox hypothesis: a biochemical basis for honest signaling via carotenoid pigmentation. The American Naturalist, 180(5), E127-E150.
Hudson, R. R., Slatkin, M., & Maddison, W. P. (1992). Estimation of levels of gene flow from DNA sequence data. Genetics, 132(2), 583-589.
Huelsenbeck, J. P., & Ronquist, F. (2001). MRBAYES: Bayesian inference of phylogenetic trees. Bioinformatics, 17(8), 754-755.
Jiménez, R. A., & Ornelas, J. F. (2016). Historical and current introgression in a Mesoamerican hummingbird species complex: a biogeographic perspective. PeerJ, 4, e1556.
Jombart, T. (2008). adegenet: a R package for the multivariate analysis of genetic markers. Bioinformatics, 24(11), 1403-1405.
Johnson, N. K., & Brush, A. H. (1972). Analysis of polymorphism in the Sooty-capped Bush Tanager. Systematic Zoology, 21(3), 245-262.
Klicka, J., Barker, F. K., Burns, K. J., Lanyon, S. M., Lovette, I. J., Chaves, J. A., & Bryson Jr, R. W. (2014). A comprehensive multilocus assessment of sparrow (Aves: Passerellidae) relationships. Molecular Phylogenetics and Evolution, 77, 177-182.

Kumar, S., Stecher, G., & Tamura, K. (2016). MEGA7: molecular evolutionary genetics analysis version 7.0 for bigger datasets. Molecular Biology and Evolution, 33(7), 1870-1874.
Lamichhaney, S., Han, F., Webster, M. T., Grant, B. R., Grant, P. R., & Andersson, L. (2020). Female-biased gene flow between two species of Darwin's finches. Nature Ecology & Evolution, 4(7), 979-986.
Leigh, J. W., & Bryant, D. (2015). popart: full-feature software for haplotype network construction. Methods in Ecology and Evolution, 6(9), 1110-1116.
Li, H., & Durbin, R. (2009). Fast and accurate short read alignment with Burrows–Wheeler transform. bioinformatics, 25(14), 1754-1760.
Li, H., Handsaker, B., Wysoker, A., Fennell, T., Ruan, J., Homer, N., ... & Durbin, R. (2009). The sequence alignment/map format and SAMtools. Bioinformatics, 25(16), 2078-2079.
Librado, P., & Rozas, J. (2009). DnaSP v5: a software for comprehensive analysis of DNA polymorphism data. Bioinformatics, 25(11), 1451-1452.
Lipshutz, S. E., Meier, J. I., Derryberry, G. E., Miller, M. J., Seehausen, O., & Derryberry, E. P. (2019). Differential introgression of a female competitive trait in a hybrid zone between sex-role reversed species. Evolution, 73(2), 188-201.
Lotterhos, K. E., & Whitlock, M. C. (2015). The relative power of genome scans to detect local adaptation depends on sampling design and statistical method. Molecular Ecology, 24(5), 1031-1046.
Paynter, R. A. (1978). Biology and evolution of the avian genus *Atlapetes* (Emberizinae). Bulletin of the Museum of Comparative Zoology, 148(7), 323-369.
Pérez Consuegra, S. G., & Vázquez-Domínguez, E. (2015). Mitochondrial diversification of the *Peromyscus mexicanus* species group in Nuclear Central America: biogeographic and taxonomic implications. Journal of Zoological Systematics and Evolutionary Research, 53(4), 300-311.
Peterson, B. K., Weber, J. N., Kay, E. H., Fisher, H. S., & Hoekstra, H. E. (2012). Double digest RADseq: an inexpensive method for de novo SNP discovery and genotyping in model and non-model species. PloS one, 7(5), e37135.
Price, T. (2008). Speciation in birds. Roberts and Company.
Price-Waldman, R., & Stoddard, M. C. (2021). Avian Coloration Genetics: Recent Advances and Emerging Questions. Journal of Heredity.
Purcell, S., Neale, B., Todd-Brown, K., Thomas, L., Ferreira, M. A., Bender, D., ... & Sham, P. C. (2007). PLINK: a tool set for whole-genome association and population-based linkage analyses. The American Journal of Human Genetics, 81(3), 559-575.
Rahbek, C., Borregaard, M. K., Antonelli, A., Colwell, R. K., Holt, B. G., Nogues-Bravo, D., ... & Fjeldså, J. (2019). Building mountain biodiversity: Geological and evolutionary processes. Science, 365(6458), 1114-1119.
Remsen Jr, J. V., & Graves IV, W. S. (1995). Distribution patterns and zoogeography of *Atlapetes* brush-finches (Emberizinae) of the Andes. The Auk, 112(1), 210-224.
Rheindt, F. E., & Edwards, S. V. (2011). Genetic introgression: an integral but neglected component of speciation in birds. The Auk, 128(4), 620-632.
Rising JD. (2020). White-naped Brushfinch (*Atlapetes albinucha*), version 1.0. In Birds of the World (del Hoyo J, Elliott A, Sargatal J, Christie DA, de Juana E, Editors). Cornell Lab of Ornithology, Ithaca, NY, USA. Doi: 10.2173/bow.wnbfin1.01
Rocha-Méndez, A., Sánchez-González, L. A., Arbeláez-Cortés, E., & Navarro-Sigüenza, A. G. (2018). Phylogeography indicates incomplete genetic divergence among phenotypically

differentiated montane forest populations of *Atlapetes albinucha* (Aves, Passerellidae). ZooKeys, (809), 125.
Rodríguez-Gómez, F., Licona-Vera, Y., Silva-Cárdenas, L., & Ornelas, J. F. (2021). Phylogeography, morphology and ecological niche modelling to explore the evolutionary history of Azure-crowned Hummingbird (*Amazilia cyanocephala*, Trochilidae) in Mesoamerica. Journal of Ornithology, 162(2), 529-547.
Rogers, A. R., & Harpending, H. (1992). Population growth makes waves in the distribution of pairwise genetic differences. Molecular Biology and Evolution, 9(3), 552-569.
Ronquist, F., & Huelsenbeck, J. P. (2003). MrBayes 3: Bayesian phylogenetic inference under mixed models. Bioinformatics, 19(12), 1572-1574.
Rovito, S. M., & Parra-Olea, G. (2016). Neotropical plethodontid biogeography: insights from molecular phylogenetics. Copeia, 104(1), 222-232.
Rull V, Carnaval AC. (Eds.). (2020). Neotropical Diversification: Patterns and Processes. Springer.
Sánchez-González, L. A., Navarro-Sigüenza, A. G., Krabbe, N. K., Fjeldså, J., & García-Moreno, J. (2015). Diversification in the Andes: the *Atlapetes* brush-finches. Zoologica Scripta, 44(2), 135-152.
Schneider, S., & Excoffier, L. (1999). Estimation of past demographic parameters from the distribution of pairwise differences when the mutation rates vary among sites: application to human mitochondrial DNA. Genetics, 152(3), 1079-1089.
Schuster, J. C., Cano, E. B., & Cardona, C. (2000). Un método sencillo para priorizar la conservación de los bosques nubosos de Guatemala, usando Passalidae (Coleoptera) como organismos indicadores. Acta Zoológica Mexicana, (80), 197-209.
Slatkin, M. (1973). Gene flow and selection in a cline. Genetics, 75(4), 733-756.
Slatkin, M. (1987). Gene flow and the geographic structure of natural populations. Science, 236(4803), 787-792.
Stamatakis, A. (2014). RAxML Version 8: A tool for Phylogenetic Analysis and Post-Analysis of Large Phylogenies. Bioinformatics, 30(9), 1312-1313.
Stein, A. C., & Uy, J. A. C. (2006). Unidirectional introgression of a sexually selected trait across an avian hybrid zone: a role for female choice? Evolution, 60(7), 1476-1485.
Toews, D. P., Campagna, L., Taylor, S. A., Balakrishnan, C. N., Baldassarre, D. T., Deane-Coe, P. E., ... & Winger, B. M. (2016). Genomic approaches to understanding population divergence and speciation in birds. The Auk: Ornithological Advances, 133(1), 13-30.
Tajima, F. (1989). Statistical method for testing the neutral mutation hypothesis by DNA polymorphism. Genetics, 123, 585-595.
Uy, J. A. C., Cooper, E. A., Cutie, S., Concannon, M. R., Poelstra, J. W., Moyle, R. G., & Filardi, C. E. (2016). Mutations in different pigmentation genes are associated with parallel melanism in island flycatchers. Proceedings of the Royal Society B: Biological Sciences, 283(1834), 20160731.
Wang, I. J., & Bradburd, G. S. (2014). Isolation by environment. Molecular Ecology, 23(23), 5649-5662.
Weir, B. S., & Cockerham, C. C. (1984). Estimating F-statistics for the analysis of population structure. Evolution, 1358-1370.
Winger, B. M. (2017). Consequences of divergence and introgression for speciation in Andean cloud forest birds. Evolution, 71(7), 1815-1831.

Wogan, G. O., Voelker, G., Oatley, G., & Bowie, R. C. (2020). Biome stability predicts population structure of a southern African aridland bird species. Ecology and Evolution, 10(9), 4066-4081.

**Supplementary tables and figures**

**Table S1.** Species names, voucher information, and localities of origin of the specimens examined genetically in this study. Museum abbreviations used in voucher numbers: MVZ = Museum of Vertebrate Zoology, University of California, Berkeley; USAC = Escuela de Biología, Universidad de San Carlos de Guatemala; FMNH = Field Museum of Natural History; KU = Kansas University, Natural History Museum; UWBM = Burke Museum of Natural History and Culture; LSUMZ = Louisiana State University Museum of Natural Science; MZFC = Museo de Zoología "Alfonso R. Herrera", Universidad Nacional Autónoma de México. MX = México, GT = Guatemala, ES = El Salvador, HO = Honduras, NI = Nicaragua, CR = Costa Rica, PA = Panamá, CO = Colombia, PE = Perú, USA = United States of America.

| Species | Museum | Voucher number | Locality | Latitude | Longitude | Morphotype | ddRAD / exon capture |
|---|---|---|---|---|---|---|---|
| *Atlapetes albinucha* | FMNH | 394322 | MX: Puebla, Huauchinango | 20.17333° | -98.045° | Yellow | X / X |
| *Atlapetes albinucha* | FMNH | 394323 | MX: Puebla, Huauchinango | 20.17333° | -98.045° | Yellow | X |
| *Atlapetes albinucha* | FMNH | 394324 | MX: Mexico | | | Yellow | X / X |
| *Atlapetes albinucha* | MVZ | 189126 | MX: Chiapas, Tapalapa | 17.187556° | -93.123174° | Yellow | X |
| *Atlapetes albinucha* | MVZ | 189127 | MX: Chiapas, Tapalapa | 17.187556° | -93.123174° | Yellow | X / X |
| *Atlapetes albinucha* | MVZ | 189128 | MX: Chiapas, Tapalapa | 17.187556° | -93.123174° | Yellow | X / X |
| *Atlapetes albinucha* | MVZ | 189129 | MX: Chiapas, Tapalapa | 17.187556° | -93.123174° | Yellow | X / X |
| *Atlapetes albinucha* | MVZ | 189130 | MX: Chiapas, Tapalapa | 17.187556° | -93.123174° | Yellow | X |
| *Atlapetes albinucha* | MVZ | 189131 | MX: Chiapas, Tapalapa | 17.187556° | -93.123174° | Yellow | X / X |
| *Atlapetes albinucha* | MVZ | 189132 | MX: Chiapas, Tapalapa | 17.187556° | -93.123174° | Yellow | X |
| *Atlapetes albinucha* | MZFC | 26840 | MX: Chiapas, Cerro Huitepec | 16.738056° | -92.688056° | Yellow | X / X |
| *Atlapetes albinucha* | MZFC | 26841 | MX: Chiapas, Cerro Huitepec | 16.738056° | -92.688056° | Yellow | X / X |
| *Atlapetes albinucha* | MZFC | 26842 | MX: Chiapas, Cerro Huitepec | 16.738056° | -92.688056° | Yellow | X / X |
| *Atlapetes albinucha* | FMNH | 394151 | MX: Chiapas, San Cristóbal de las Casas | 16.741354° | -92.63865° | Yellow | X / X |
| *Atlapetes albinucha* | UWBM | 99842 | MX: Chiapas, Teopisca | 16.69108° | -92.60593° | Yellow | X |
| *Atlapetes albinucha* | UWBM | 116706 | MX: Chiapas, Teopisca | 16.502667° | -92.461333° | Yellow | X / X |
| *Atlapetes albinucha* | MVZ | 184272 | GT: Huehuetenango, Yalambojoch | 16.005943° | -91.499862° | Hybrid | X / X |
| *Atlapetes albinucha* | USAC | 823 | GT: Huehuetenango, Yalambojoch | 15.964617° | -91.568423° | Hybrid | X / X |
| *Atlapetes albinucha* | MVZ | 187574 | GT: Quiché, Uspantán | 15.46773° | -90.777083° | Gray | X / X |
| *Atlapetes albinucha* | MVZ | 187575 | GT: Quiché, Uspantán | 15.46773° | -90.777083° | Gray | X |
| *Atlapetes albinucha* | MVZ | 187576 | GT: Quiché, Uspantán | 15.46773° | -90.777083° | Gray | X |
| *Atlapetes albinucha* | MVZ | 187578 | GT: Alta Verapaz, San Pedro Carchá | 15.613624° | -90.273532° | Gray | X |
| *Atlapetes albinucha* | MVZ | 189366 | GT: Huehuetenango, Cuilco | 15.48427° | -91.93246° | Gray | X |
| *Atlapetes albinucha* | MVZ | 189367 | GT: Huehuetenango, Cuilco | 15.48427° | -91.93246° | Gray | X / X |
| *Atlapetes albinucha* | MVZ | 189368 | GT: Huehuetenango, Cuilco | 15.48427° | -91.93246° | Gray | X / X |
| *Atlapetes albinucha* | MVZ | 187577 | GT: Quiché, Zacualpa | 15.0784° | -90.9115° | Gray | X |
| *Atlapetes albinucha* | MVZ | 188250 | MX: Chiapas, Motozintla | 15.725967° | -92.34153° | Gray | X /X |
| *Atlapetes albinucha* | MVZ | 188251 | MX: Chiapas, Motozintla | 15.725967° | -92.34153° | Gray | X |
| *Atlapetes albinucha* | MVZ | 188252 | MX: Chiapas, Motozintla | 15.725967° | -92.34153° | Gray | X |
| *Atlapetes albinucha* | MVZ | 188253 | MX: Chiapas, Motozintla | 15.725967° | -92.34153° | Gray | X |

| | | | | | | | |
|---|---|---|---|---|---|---|---|
| *Atlapetes albinucha* | MVZ | 188254 | MX: Chiapas, Motozintla | 15.725967° | -92.34153° | Gray | X / X |
| *Atlapetes albinucha* | MVZ | 188255 | MX: Chiapas, Motozintla | 15.725967° | -92.34153° | Gray | X |
| *Atlapetes albinucha* | MVZ | 188256 | MX: Chiapas, Motozintla | 15.23776° | -92.303378° | Gray | X |
| *Atlapetes albinucha* | MVZ | 188257 | MX: Chiapas, Motozintla | 15.23776° | -92.303378° | Gray | X |
| *Atlapetes albinucha* | UWBM | 105978 | GT: Quetzaltenango, Quetzaltenango | 14.828333° | -91.495° | Gray | X |
| *Atlapetes albinucha* | UWBM | 110113 | GT: Totonicapán, Totonicapán | 14.916667° | -91.366667° | Gray | X |
| *Atlapetes albinucha* | UWBM | 110114 | GT: Totonicapán, Totonicapán | 14.916667° | -91.366667° | Gray | X |
| *Atlapetes albinucha* | MVZ | 189369 | GT: Santa Rosa, Volcán Tecuamburro | 14.15393° | -90.41051° | Gray | X |
| *Atlapetes albinucha* | MVZ | 189370 | GT: Santa Rosa, Volcán Tecuamburro | 14.15393° | -90.41051° | Gray | X / X |
| *Atlapetes albinucha* | MVZ | 188616 | GT: Jutiapa, Volcán Suchitán | 14.40648° | -89.780126° | Gray | X |
| *Atlapetes albinucha* | MVZ | 188617 | GT: Jutiapa, Volcán Suchitán | 14.40648° | -89.780126° | Gray | X / X |
| *Atlapetes albinucha* | MVZ | 188618 | GT: Jutiapa, Volcán Suchitán | 14.40648° | -89.780126° | Gray | X |
| *Atlapetes albinucha* | KU | 109794 | ES: Santa Ana, Parque Nacional Montecristo | 14.38767° | -89.38655° | Gray | X |
| *Atlapetes albinucha* | KU | 95391 | ES: Chalatenango, La Laguna | 14.13300° | -88.91300° | Gray | X |
| *Atlapetes albinucha* | KU | 95302 | ES: San Vicente, Volcán San Vicente | 13.60800° | -88.83700° | Gray | X / X |
| *Atlapetes albinucha* | KU | 93879 | ES: San Miguel, Volcán San Miguel | 13.44200° | -88.27200° | Gray | X |
| *Atlapetes albinucha* | KU | 93905 | ES: Morazán, Cerro Cacahuatique | 13.76200° | -88.20000° | Gray | X |
| *Atlapetes albinucha* | UWBM | 93636 | HO: Copán, Copán Ruinas | 14.86667° | -89.05° | Gray | X |
| *Atlapetes albinucha* | LSUMZ | B-60962 | HO: Francisco Morazán, Cerro Uyuca | 14.208263° | -87.101232° | Gray | X |
| *Atlapetes albinucha* | FMNH | 481778 | NI: Estelí, Reserva Natural Miraflor | 13.2464° | -86.2524° | Gray | X |
| *Atlapetes albinucha* | FMNH | 481779 | NI: Estelí, Reserva Natural Miraflor | 13.2464° | -86.2524° | Gray | X |
| *Atlapetes albinucha* | FMNH | 481780 | NI: Estelí, Reserva Natural Miraflor | 13.2464° | -86.2524° | Gray | X / X |
| *Atlapetes albinucha* | FMNH | 393082 | CR: Cartago, Tres Ríos | 9.907172° | -83.986461° | Gray | X / X |
| *Atlapetes albinucha* | FMNH | 394326 | CR: Cartago, El Radio | 9.863809° | -83.916194° | Gray | X |
| *Atlapetes albinucha* | FMNH | 394327 | CR: Cartago, El Radio | 9.863809° | -83.916194° | Gray | X / X |
| *Atlapetes albinucha* | LSUMZ | B-26441 | PA: Chiriquí, Gualaca | 8.754382° | -82.507098° | Gray | X |
| *Atlapetes albinucha* | LSUMZ | B-26460 | PA: Chiriquí, Bugaba | 8.754382° | -82.507098° | Gray | X |
| *Atlapetes albinucha* | UWBM | 112311 | PA: Bocas del Toro, Chiriquí Grande | 8.784167° | -82.214° | Gray | X |
| *Atlapetes albinucha* | UWBM | 112316 | PA: Bocas del Toro, Chiriquí Grande | 8.784167° | -82.214° | Gray | X |
| *Atlapetes albinucha* | GenBank | MH938483 | CO: GenBank – Rocha-Méndez et al. 2018 | 4.709233° | -75.4907° | Gray | |
| *Atlapetes albinucha* | GenBank | MH938485 | CO: GenBank – Rocha-Méndez et al. 2018 | 3.87975° | -76.443° | Gray | |
| *Atlapetes albinucha* | GenBank | MH938486 | CO: GenBank – Rocha-Méndez et al. 2018 | 4.8675° | -75.54666° | Gray | |
| *Atlapetes albinucha* | GenBank | MH938487 | CO: GenBank – Rocha-Méndez et al. 2018 | 7.135444° | -75.15527° | Gray | |
| *Atlapetes albinucha* | GenBank | MH938488 | CO: GenBank – Rocha-Méndez et al. 2018 | 6.8235° | -75.15527° | Gray | |
| *Atlapetes albinucha* | GenBank | MH938490 | CO: GenBank – Rocha-Méndez et al. 2018 | 4.814278° | -75.69455° | Gray | |
| *Atlapetes pileatus* | LSUMZ | B-16 | MX: Veracruz | | | | X |
| *Atlapetes pileatus* | LSUMZ | B-23 | MX: Puebla | | | | X |
| *Atlapetes pallidinucha* | LSUMZ | B-32550 | PE: Cajamarca | | | | X |
| *Atlapetes rufinucha* | LSUMZ | B-44565 | PE: San Martín | | | | X |
| *Pezopetes capitalis* | LSUMZ | B-19827 | CR: San José | | | | X |
| *Melozone fusca* | MVZ | 178298 | USA: Oklahoma | | | | X |
| *Melozone biarcuata* | MVZ | 188620 | GT: Jutiapa | | | | X |
| *Pipilo chlorurus* | MVZ | 182530 | USA: California | | | | X |

**Table S2.** Species names, voucher information, and localities of origin for the specimens examined morphologically in this study. Museum abbreviations used in voucher numbers: MVZ = Museum of Vertebrate Zoology, University of California, Berkeley. MX = México, GT = Guatemala, ES = El Salvador, HO = Honduras, CR = Costa Rica, CO = Colombia.

| Species | Museum | Voucher number | Locality | Latitude | Longitude | Collection year | Morphotype |
|---|---|---|---|---|---|---|---|
| *Atlapetes albinucha albinucha* | MVZ | 189126 | MX: Chiapas, Tapalapa | 17.187556° | -93.123174° | 2013 | Yellow |
| *Atlapetes albinucha albinucha* | MVZ | 189128 | MX: Chiapas, Tapalapa | 17.187556° | -93.123174° | 2013 | Yellow |
| *Atlapetes albinucha albinucha* | MVZ | 189131 | MX: Chiapas, Tapalapa | 17.187556° | -93.123174° | 2013 | Yellow |
| *Atlapetes albinucha albinucha* | MVZ | 189132 | MX: Chiapas, Tapalapa | 17.187556° | -93.123174° | 2013 | Yellow |
| *Atlapetes albinucha albinucha* | MVZ | 155369 | MX: Chiapas, San Cristóbal de las Casas | 16.736667° | -92.683889° | 1965 | Yellow |
| *Atlapetes albinucha albinucha* | MVZ | 121507 | MX: Chiapas, San Cristóbal de las Casas | 16.674444° | -92.573333° | 1950 | Yellow |
| *Atlapetes albinucha albinucha* | MVZ | 121508 | MX: Chiapas, San Cristóbal de las Casas | 16.674444° | -92.573333° | 1950 | Yellow |
| *Atlapetes albinucha albinucha* | MVZ | 121509 | MX: Chiapas, San José | 16.094444° | -91.739167° | 1950 | Yellow |
| *Atlapetes albinucha griseipectus* | MVZ | 184272 | GT: Huehuetenango, Yalambojoch | 16.005943° | -91.499862° | 2009 | Hybrid |
| *Atlapetes albinucha griseipectus* | MVZ | 187576 | GT: Quiché, Uspantán | 15.46773° | -90.777083° | 2011 | Gray |
| *Atlapetes albinucha griseipectus* | MVZ | 189367 | GT: Huehuetenango, Cuilco | 15.48427° | -91.93246° | 2013 | Gray |
| *Atlapetes albinucha griseipectus* | MVZ | 189368 | GT: Huehuetenango, Cuilco | 15.48427° | -91.93246° | 2013 | Gray |
| *Atlapetes albinucha griseipectus* | MVZ | 187577 | GT: Quiché, Zacualpa | 15.0784° | -90.9115° | 2011 | Gray |
| *Atlapetes albinucha griseipectus* | MVZ | 165763 | GT: Baja Verapaz | 15.14862° | -90.06711° | 1978 | Gray |
| *Atlapetes albinucha griseipectus* | MVZ | 188250 | MX: Chiapas, Motozintla | 15.725967° | -92.34153° | 2012 | Gray |
| *Atlapetes albinucha griseipectus* | MVZ | 188252 | MX: Chiapas, Motozintla | 15.725967° | -92.34153° | 2012 | Gray |
| *Atlapetes albinucha griseipectus* | MVZ | 188253 | MX: Chiapas, Motozintla | 15.725967° | -92.34153° | 2012 | Gray |
| *Atlapetes albinucha griseipectus* | MVZ | 188257 | MX: Chiapas, Motozintla | 15.23776° | -92.303378° | 2012 | Gray |
| *Atlapetes albinucha griseipectus* | MVZ | 189369 | GT: Santa Rosa, Volcán Tecuamburro | 14.15393° | -90.41051° | 2013 | Gray |
| *Atlapetes albinucha griseipectus* | MVZ | 188617 | GT: Jutiapa, Volcán Suchitán | 14.40648° | -89.780126° | 2011 | Gray |
| *Atlapetes albinucha griseipectus* | MVZ | 188618 | GT: Jutiapa, Volcán Suchitán | 14.40648° | -89.780126° | 2011 | Gray |
| *Atlapetes albinucha griseipectus* | MVZ | 24667 | GT: Guatemala | ----- | ----- | ----- | Gray |
| *Atlapetes albinucha griseipectus* | MVZ | 86545 | ES: Santa Ana, Cerro El Aguila | 13.89167° | -89.69694° | 1942 | Gray |
| *Atlapetes albinucha griseipectus* | MVZ | 86544 | ES: Santa Ana, Cerro de los Naranjos | 13.86667° | -89.66845° | 1942 | Gray |
| *Atlapetes albinucha fuscipygius* | MVZ | 86546 | ES: Morazán, Cacaguatique | 13.76667° | -88.21667° | 1942 | Gray |
| *Atlapetes albinucha fuscipygius* | MVZ | 86539 | HO: Ocotepeque, Cerro El Pital | 14.38306° | -89.12899° | 1942 | Gray |
| *Atlapetes albinucha fuscipygius* | MVZ | 86541 | HO: Ocotepeque, Cerro El Pital | 14.38306° | -89.12899° | 1942 | Gray |
| *Atlapetes albinucha fuscipygius* | MVZ | 86542 | HO: Ocotepeque, Cerro El Pital | 14.38306° | -89.12899° | 1942 | Gray |
| *Atlapetes albinucha parvirostris* | MVZ | 162242 | CR: Cartago, Volcán Irazú | 9.98333° | -83.85° | 1966 | Gray |
| *Atlapetes albinucha parvirostris* | MVZ | 155711 | CR: San José, Desamparados | 9.86483° | -84.0312° | 1965 | Gray |
| *Atlapetes albinucha gutturalis* | MVZ | 139122 | CO: Valle del Cauca, San Antonio | 3.3° | -76.533333° | 1958 | Gray |
| *Atlapetes albinucha gutturalis* | MVZ | 139121 | CO: Valle del Cauca, San Antonio | 3.25° | -76.583333° | 1958 | Gray |
| *Atlapetes albinucha gutturalis* | MVZ | 154934 | CO: Valle del Cauca, San Antonio | 3.216667° | -76.65° | 1965 | Gray |
| *Atlapetes albinucha gutturalis* | MVZ | 139119 | CO: Cauca, Popoyán | 2.666667° | -76.583333° | 1958 | Gray |
| *Atlapetes albinucha gutturalis* | MVZ | 139120 | CO: Cauca, Popoyán | 2.666667° | -76.583333° | 1958 | Gray |
| *Atlapetes albinucha gutturalis* | MVZ | 160239 | CO: Cauca, Popoyán | 2.5° | -76.583333° | 1967 | Gray |

**Table S3.** Summary statistics, neutrality tests and population expansion tests for populations of *Atlapetes albinucha* based on mtDNA. Number of individuals analyzed (*n*), number of haplotypes (*H*), number of segregating sites (*S*), *h* = haplotype diversity, $\pi$ = nucleotide diversity, Tajima's *D*, Fu's *F*s. Positive values for *D* and $F_S$ are indicative of mutation-drift equilibrium, which is typical of stable populations, whereas significant negative values (at the $P = 0.05$ level for Tajima's *D* and for *Fs* tests; Excoffier and Lischer 2010) that result from an excess of rare haplotypes, indicate that populations have experienced a recent bottleneck followed by population expansion. Significant ($P = 0.05$) Hri and SSD values indicate deviations from the sudden expansion model. Significant values are shown in bold ($P < 0.05$).

| Region | *n* | *H* | *S* | *h* | $\pi$ | Tajima's *D* | Fu's *Fs* | Hri | SSD |
|---|---|---|---|---|---|---|---|---|---|
| West – Isthmus of Tehuantepec | 3 | 3 | 3 | 1.000±0.272 | 0.00192 | 0.00000 | -0.69315 | 0.22222 | 0.04206 |
| Altos de Chiapas | 13 | 5 | 11 | 0.538±0.161 | 0.00207 | -1.58607 | 0.11677 | 0.23997 | **0.37147** |
| Hybrids | 2 | 2 | 5 | 1.000±0.500 | 0.00480 | 0.00000 | 1.60944 | ----- | ----- |
| Southern Mexico – Western Guatemala | 19 | 7 | 7 | 0.865±0.042 | 0.00217 | 0.42420 | -0.94813 | 0.02267 | 0.00114 |
| Eastern Guatemala | 5 | 1 | 0 | 0.000±0.000 | 0.00000 | 0.00000 | ----- | ----- | ----- |
| El Salvador – Western Honduras | 6 | 4 | 4 | 0.800±0.172 | 0.00128 | -1.29503 | -1.25217 | 0.09333 | 0.00511 |
| Eastern Honduras – Nicaragua | 4 | 1 | 0 | 0.000±0.000 | 0.00000 | 0.00000 | ----- | ----- | ----- |
| Costa Rica – Panamá | 7 | 3 | 2 | 0.667±0.160 | 0.00101 | 1.16843 | 0.10980 | 0.15646 | 0.02755 |
| Colombia | 6 | 3 | 4 | 0.600±0.215 | 0.00128 | -1.29503 | 0.29690 | 0.20444 | **0.50667** |

**Table S4.** Results of analyses of molecular variance of *Atlapetes albinucha* populations based on mtDNA. The populations were organized in (A) four groups separated by major geographic breaks (i.e., Isthmus of Tehuantepec, Nicaraguan Depression, Isthmus of Panama), (B) groups defined by the ddRAD admixture analysis, and (C) groups defined by the ddRAD PCA. * $p < 0.05$.

| Source of variation | d.f. | Sum of squares | Variance components | Percentage of variation | Fixation indices |
|---|---|---|---|---|---|
| (A) Groups separated by major geographic breaks | | | | | |
| Among groups | 3 | 76.55 | 2.36 | 61.45 | $F_{CT}$ = 0.61* |
| Among populations within groups | 4 | 25.77 | 0.66 | 17.20 | $F_{SC}$ = 0.45* |
| Within populations | 55 | 45.05 | 0.82 | 21.35 | $F_{ST}$ = 0.79* |
| Total | 62 | 147.37 | 3.84 | | |
| (B) Groups defined by ddRAD admixture analysis | | | | | |
| Among groups | 3 | 61.63 | 0.11 | 3.98 | $F_{CT}$ = 0.04 |
| Among populations within groups | 4 | 40.69 | 1.77 | 65.63 | $F_{SC}$ = 0.68* |
| Within populations | 55 | 45.05 | 0.82 | 30.39 | $F_{ST}$ = 0.70* |
| Total | 62 | 147.37 | 2.70 | | |
| (C) Groups defined by ddRAD PCA | | | | | |
| Among groups | 8 | 105.81 | 1.67 | 62.58 | $F_{CT}$ = 0.63* |
| Among populations within groups | 8 | 15.13 | 0.32 | 12.14 | $F_{SC}$ = 0.32* |
| Within populations | 48 | 32.42 | 0.68 | 25.28 | $F_{ST}$ = 0.75* |
| Total | 64 | 153.35 | 2.67 | | |

**Table S5.** Genes, proteins, and protein function that had outliers with Weir and Cockerham FST higher than 0.8.

| Gene name | Protein name | Function | FST |
|---|---|---|---|
| LOC102074020 | UDP-glucuronosyltransferase 1-1-like (1 SNP Fst 1, 1 SNP Fst 0.8389) | Glucuronidation reactions (involved in carotenoid pathways, including lutein) | 1.0000 |
| LOC102066495 | C-factor like (2 SNPs) | | 0.9241 |
| ABCC2 | ATP binding cassette subfamily C member 2 | Binds and hydrolyzes ATP | 0.8513 |
| KCND2 | potassium voltage-gated channel subfamily D member 2 | Transmembrane potassium channel | 0.8513 |
| PHETA2 | PH domain containing endocytic trafficking adaptor 2 | Protein homodimerization | 0.8513 |
| SPSB3 | splA/ryanodine receptor domain and SOCS box containing 3 | May be a substrate recognition component of a SCF-like ECS E3 ubiquitin-protein ligase | 0.8513 |
| ETV1 | ETS variant transcription factor 1 | Transcription factor | 0.8389 |
| SLC25A28 | solute carrier family 25 member 28 | Mitochondrial iron transporter | 0.8389 |
| DNAJC2 | DnaJ heat shock protein family (Hsp40) member C2 | Chaperone in the cytosol and chromatin regulator in the nucleus | 0.8389 |
| CDH18 | cadherin 18 (2 SNPs) | Cell adhesion | 0.8389 |
| PHETA2 | PH domain containing endocytic trafficking adaptor 2 (2 SNPs) | Endocytic traffic | 0.8389 |
| PKP3 | plakophilin 3 (2 SNPs) | Link cadherins to cytoskeleton | 0.8389 |
| PITPNM1 | phosphatidylinositol transfer protein membrane associated 1 (3 SNPs) | Transfer phosphatidylinositol, cytoskeleton remodeling | 0.8389 |
| LOC102071381 | keratin-associated protein 6-5-like | Keratinization | 0.8389 |
| MAP2K2 | mitogen-activated protein kinase kinase 2 | Catalyzes phosphorylation of threonine and tyrosine residue | 0.8389 |
| F8 | coagulation factor VIII, procoagulant component (3 SNPs) | Blood coagulation factor | 0.8320 |
| DGKH | diacylglycerol kinase eta | Converts diacylglycerol into phosphatidic acid/phosphatidate | 0.8320 |
| DCT | dopachrome tautomerase | Participates in melanin biosynthesis | 0.8320 |
| MINDY2 | MINDY lysine 48 deubiquitinase 2 | Hydrolisis | 0.8320 |
| LOC102060630 | glutamate receptor-interacting protein 2 | Participates in the glutamato binding pathway | 0.8320 |
| NAGA | alpha-N-acetylgalactosaminidase | Removes terminal alpha-N-acetylgalactosamine residues | 0.8320 |
| CEND1 | cell cycle exit and neuronal differentiation 1 | Involved in neuronal differentiation | 0.8320 |
| LARP4 | La ribonucleoprotein 4 (2 SNPs) | RNA binding protein, binds to the poly-A tract of mRNA molecules | 0.8320 |

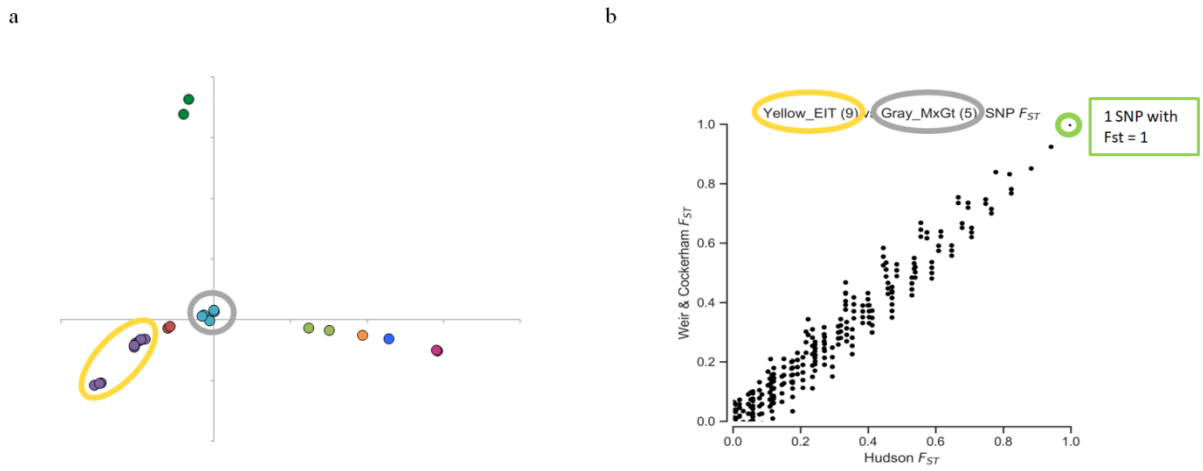


**Figure S1.** Analyses on the exome capture dataset of *Atlapetes albinucha*. a) Principal Component Analysis highlighting the 14 samples included in the outlier analysis, yellow and gray phenotypes. b) Comparison of Weir and Cockerham FST and Hudson FST values.

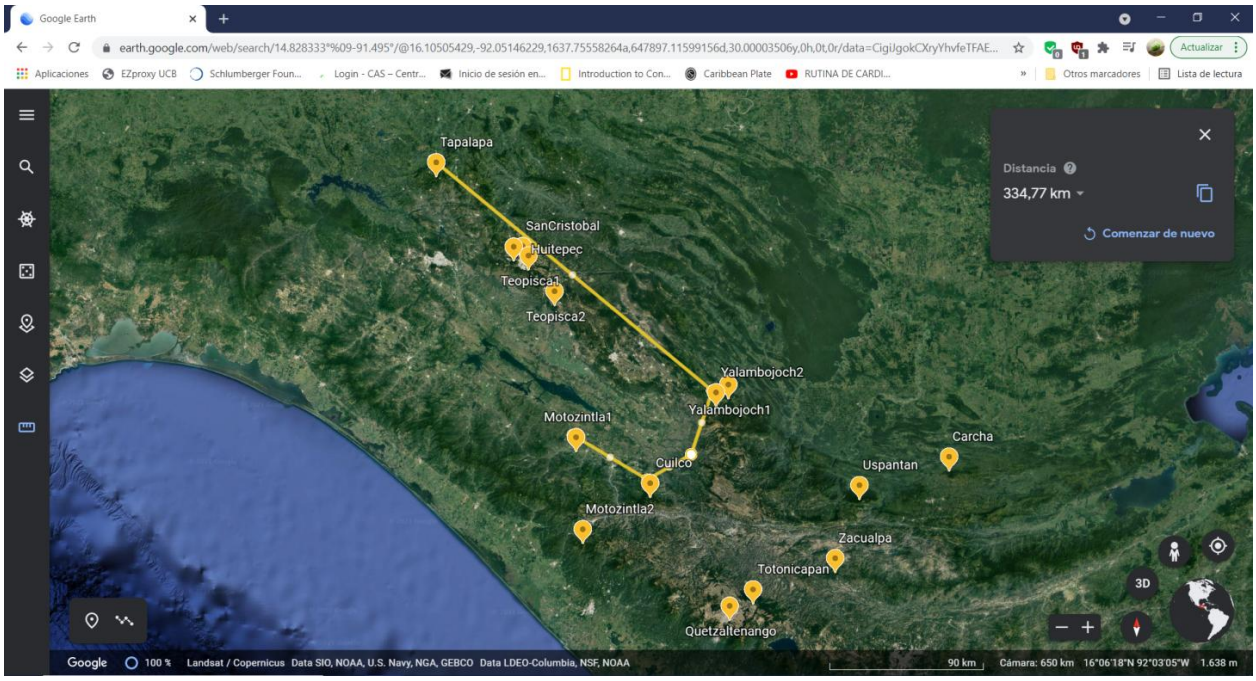


**Figure S2.** Example of geographic distance that considers geographic barriers, in this case the geographic barrier, Grijalva River, separates Tapalapa from Motozintla1. Image from Google Earth.

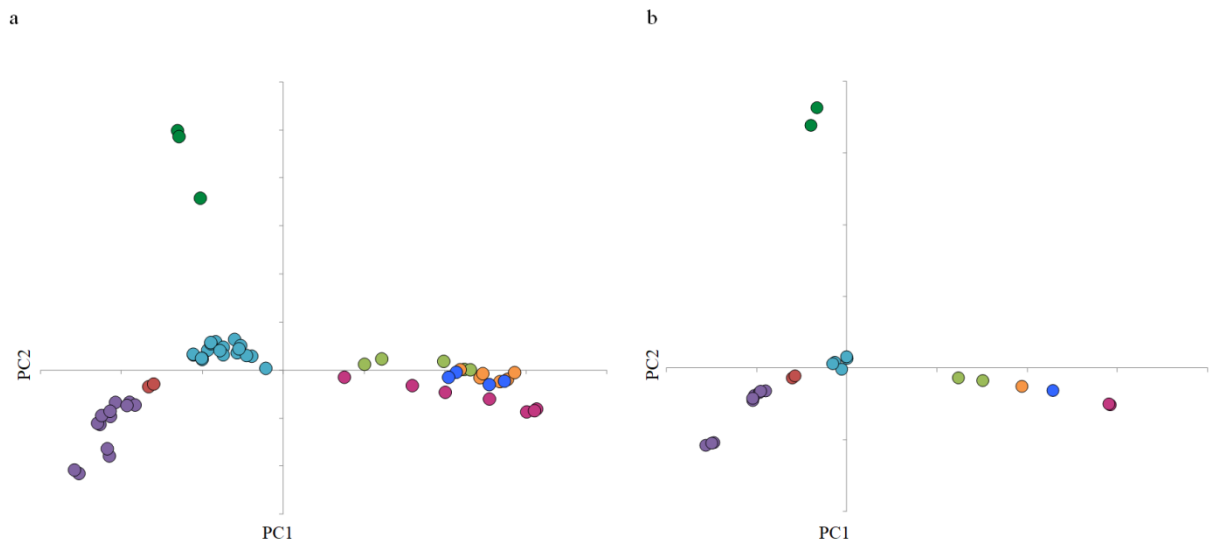


**Figure S3.** Principal Component Analyses on genomic data of *Atlapetes albinucha*. a) ddRAD data. b) Exome capture data.

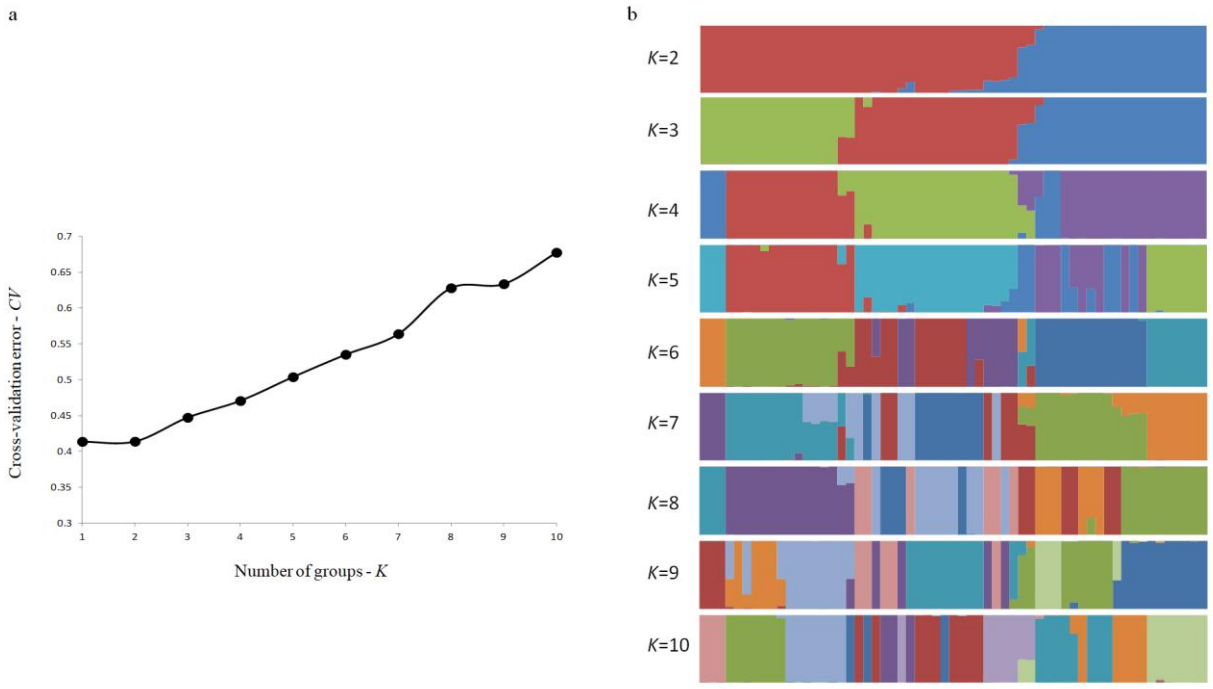


**Figure S4.** ADMIXTURE analysis – ddRAD data. a) Cross-validation error suggests K=2. b) ADMIXTURE plots for K=2 to K=10.

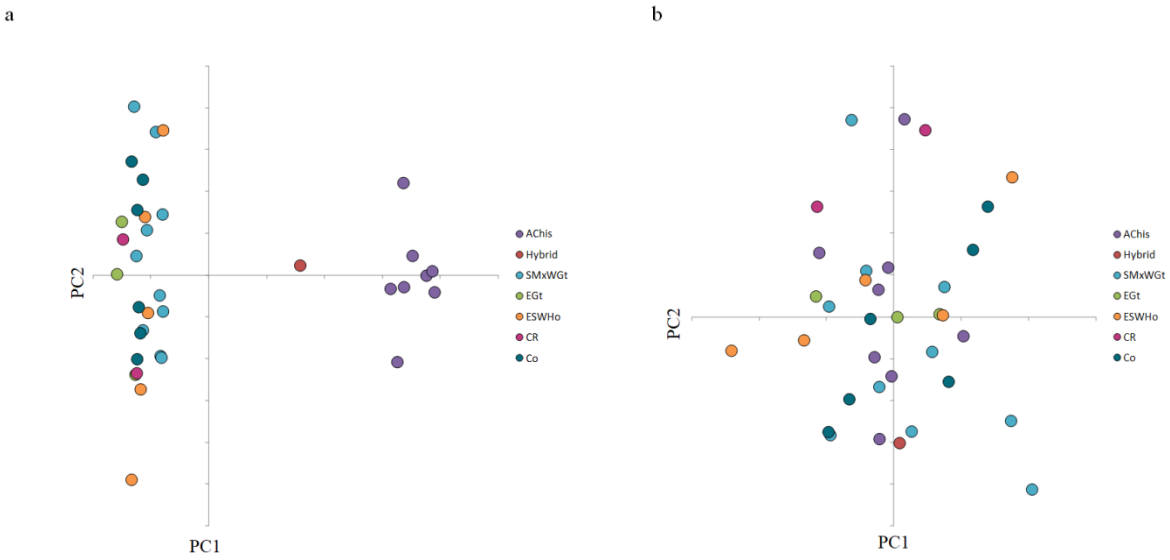


**Figure S5.** Principal Component Analyses on morphological data of *Atlapetes albinucha*. a) The extension of yellow color in the underparts dominates the variation in PC1. b) When excluding the extension of yellow color, there is no clustering based on morphological measurements.

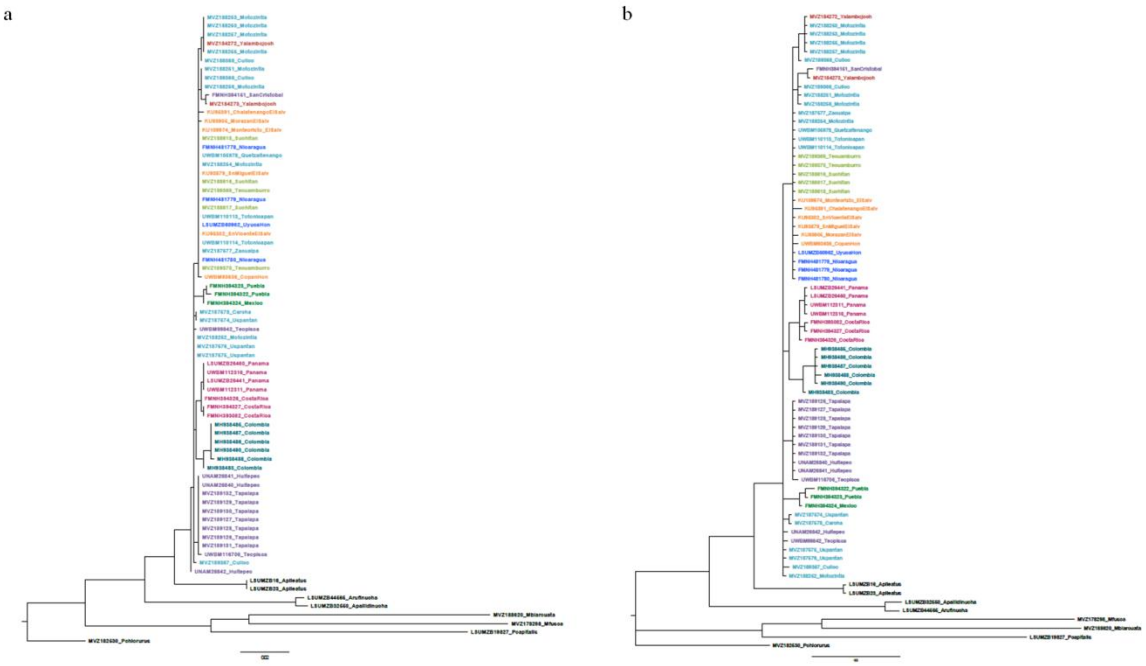


**Figure S6.** Mitochondrial ND2 phylogenetic trees of *Atlapetes albinucha*. a) Maximum Likelihood. b) Bayesian Inference.

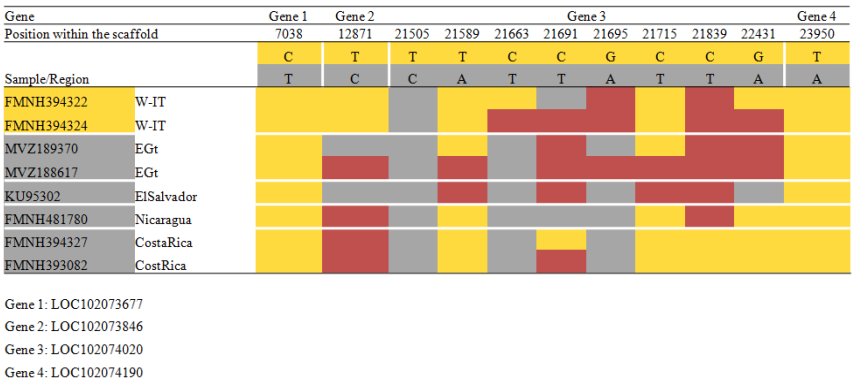


**Figure S7.** Genotypes for outlier SNPs within the four genes on scaffold NW_005082739.1. Yellow and gray colors were used to represent the homozygote positions and the samples collected in allopatry for either of both phenotypes. The brick red color represents the heterozygote positions, and the hybrid individuals. W-IT: West of the Isthmus of Tehuantepec; EGt: Eastern Guatemala.

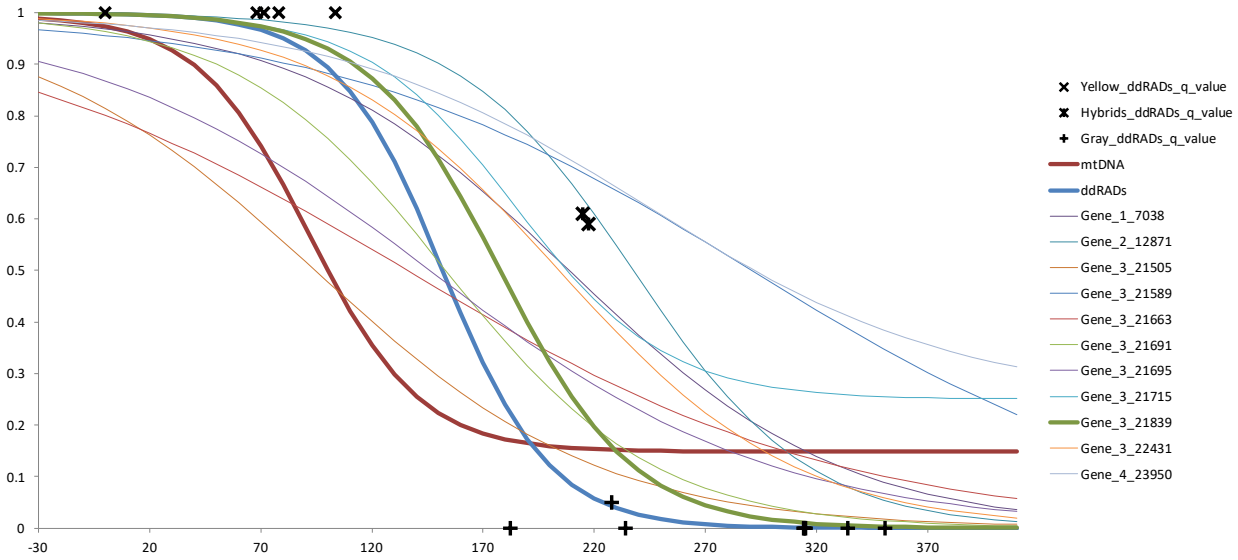


**Figure S8.** Geographic clines fitted for the mitochondrial DNA, ddRAD data, and SNPs within scaffold NW_005082739.1. The geographic distance used for this analysis was Euclidean distance. The "x" axis represents the distance in kilometers and the "y" axis represents allelic frequencies.

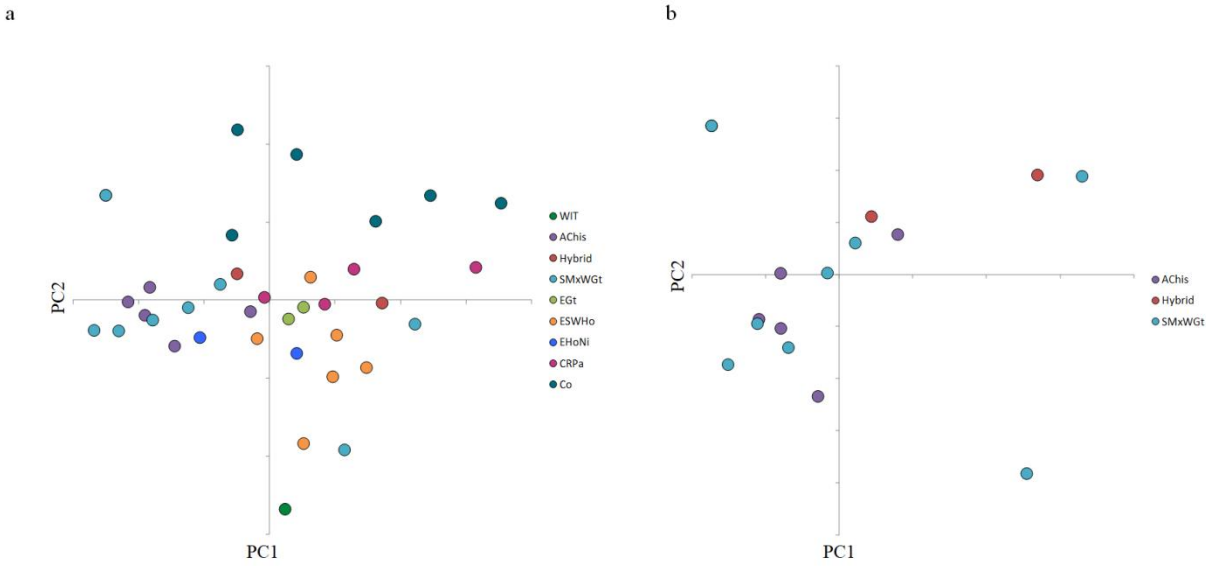


**Figure S9.** Principal Component Analyses on geographic and environmental data from the collecting sites of *Atlapetes albinucha*. a) Samples from the complete geographic range. b) Samples from the hybrid zone and parental populations.

# Chapter 3

## Shallow evolutionary divergence and mixed ancestry in *Saucerottia* hummingbirds sets the stage for studying the genetic basis of structural plumage coloration

### Introduction

Color can drive diversification through different selective processes (natural, sexual, and social selection) given the great variety of roles it plays in nature (e.g., camouflage, mate choice, individual and species recognition; Hill and McGraw 2006, Cuthill et al. 2017, Mason and Bowie 2020). Diversification in birds is linked to the rainbow of colors they display, and multiple closely related species differ primarily in plumage coloration (Winger and Bates 2015, Merwin et al. 2020, Beltrán et al. 2021). Bird plumage coloration is produced through the combination of light absorption by pigments and light scattering by nanostructures and feather microstructures (Stoddard and Prum 2011, Shawkey and D'Alba 2017, McCoy and Prum 2019). Thus, structural plumage coloration results from the physical structure of the feather and the genetics underlying that physical structure. Continued research on the physics of structural colors in birds finds new structures that birds use to produce different colors (Kulp et al. 2018, McCoy and Prum 2019). However, uncovering the genetic basis of structural plumage colors in birds remains elusive (Kardos et al. 2016, Price-Waldman and Stoddard 2021, Rubenstein et al. 2021).

Disentangling the genetic basis of structural plumage coloration requires finding a study system with variation in structural colors but at the same time, with similar genetic background to enable the detection of outlier loci. Therefore, identifying a study system requires understanding its evolutionary history and characterizing the physical basis of the structural colors of interest. Closely related avian species such as wood warblers (Toews et al. 2016) and recent rapid species radiations such as Capuchino finches (Campagna et al. 2017) have proven to represent ideal study systems with which to uncover the genetic basis of pigment-based plumage coloration. Additionally, recent advances in sequencing technologies (Funk and Taylor 2019) and the study of physical characteristics of avian feathers (Shawkey and D'Alba 2017, McCoy and Prum 2019) offer the opportunity to improve our understanding of avian structural coloration. However, establishing a biological non-model system with the knowledge of its evolutionary history and sufficient phenotypic variation to enable disentangling of the genetic basis for structural plumage coloration remains a challenge (Price-Waldman and Stoddard 2021, Rubenstein et al. 2021).

Hummingbirds represent an ideal system to study the genetic basis for structural plumage coloration. The hummingbird family Trochilidae is a highly diverse group of birds (McGuire et al. 2014) with structural plumage coloration present in most species (Greenewalt et al. 1960, Durrer 1977, Eliason et al. 2020). The rate of evolution of plumage coloration in hummingbirds has been associated with speciation rates, highlighting the importance of color in the diversification of hummingbirds (Beltrán et al. 2021). Additionally, studies on the physical structure of hummingbird feathers show that iridescence in this group is produced by melanosomes that are closely packed in mosaics of layers of 2 to 16 platelets (Greenewalt et al. 1960, Eliason et al. 2020). The nature of the iridescence varies according to the thickness of the melanosomes and the sizes of air spaces within them (Greenewalt et al. 1960, Eliason et al. 2020), together with cortex thickness, spacing between adjacent platelets, and the number of

layers of melanosomes (Eliason et al. 2020). Given that melanosomes are fundamental to the production of structural coloration, it is hypothesized that mutations that result in differential expression of genes involved in the melanin biosynthesis pathway underlie the genetic basis of the diverse array of hummingbird structural colors (Saranathan and Finet 2021). Melanin biosynthesis is highly conserved across vertebrates (Hubbard et al. 2010, Harris et al. 2020), and therefore mutations altering this pathway are likely to have important consequences for the biological machinery underpinning structural coloration in hummingbirds (Baxter et al. 2018) and, indeed, may be directly responsible for changes in hummingbird coloration.

Within hummingbirds, the genus *Saucerottia* is one of the most recently diversified clades (~ 3 Mya; McGuire et al. 2014, Ornelas et al. 2014), with high speciation rates (Beltrán et al. 2021), signatures of historical and contemporary genetic introgression (Rodríguez-Gómez et al. 2013, Jiménez and Ornelas 2016), and phenotypic variation mainly restricted to structural plumage coloration (Jiménez 2011, Jiménez and Ornelas 2016). The genus *Saucerottia* is a monophyletic group, part of the Emerald clade (McGuire et al. 2014), with ten described species that are differentiated by plumage coloration (Stiles et al. 2017). Most *Saucerottia* species have been included in published phylogenies, but their recent diversification and history of genetic introgression have hindered our understanding of the evolutionary relationships within the group. Increasing the geographic and individual sample representation of each species and the number of molecular markers would help to better understand the genetic and phenotypic variation of members of this genus across its geographic range and the evolutionary and biogeographic history driving *Saucerottia* diversification.

The species complex *S. beryllina – S. cyanura* shows evidence of historical and current introgression in Nuclear Central America, which is especially apparent in the variation in tail feather coloration (Jiménez 2011, Jiménez and Ornelas 2016). *Saucerottia beryllina* has a rufous-bronze colored tail, whereas *S. cyanura* has a metallic blue tail. There are also historic (Ridgway 1911; Dickey and Van Rosem 1938) and contemporary (Jiménez and Ornelas 2016) reports of individuals showing an array of intermediate tail colorations. The history of introgression in *S. beryllina – S. cyanura* suggests that the genetic background might be quite similar between the two different colorations, leaving tail coloration as one of the few phenotypic traits differentiating these species (Jiménez and Ornelas 2016). However, the physical structure responsible for the different tail colors has not been described.

The rufous-bronze/metallic blue tail coloration within the genus *Saucerottia* is not exclusive to the *S. beryllina – S. cyanura* complex; it is also present in two other species complexes. In Costa Rica and Panama, *S. edward* has a blue-black tail in the western part of the range and a rufous colored tail on the eastern side (Weller 2021). Only a single sample of *S. edward* has been included in previous phylogenies, and it is unknown whether the two tail color phenotypes represent sister groups. In South America, the closely related species *S. viridigaster* and *S. tobaci* have rufous and blue-black tails, respectively (Weller et al. 2021b, 2021c). The ranges of the species overlap in Venezuela, and it is unknown whether they represent reciprocally monophyletic groups.

Here, we assess the potential of *Saucerottia* hummingbirds as a system for studying the genetics of structural plumage colors. We integrated a biogeographic analysis of *Saucerottia* to place

studying the genomic and physical basis of tail structural coloration in geographical context. We followed a phylogeographic approach to understand the geographic distribution of genetic variation. Using mitochondrial sequences and ddRAD data, we uncovered the number of genetic groups within *Saucerottia*. We reconstructed the phylogeny of *Saucerottia* and examined tail color variation in an evolutionary context by tracing the history of the character states across the phylogeny. We identified candidate genomic regions underlying tail coloration in *S. beryllina* and *S. cyanura* and contrasted the candidate gene regions with the genomic data of *S. e. edward – S. e. niveoventer* and *S. viridigaster – S. tobaci*. We examined and described the physical structure of rufous, blue, and intermediately colored tail feathers. We discuss the role that shallow divergence and mixed ancestry play in *Saucerottia* evolution, and the importance for the design of studies on the genetic basis for structural plumage colors. Our conclusions focus on the implications of disentangling the genetic basis of structural coloration in birds and the evolution of complex traits to understand species diversification.

## Methods

### Sampling and field procedures

Our ingroup sampling comprised 113 individuals that included nine of the ten species recognized within the genus *Saucerottia*, and 15 additional individuals that comprise the outgroup sampling. This sampling includes a comprehensive geographic representation of the genus *Saucerottia*, covering the ranges of species from northern Mexico to Surinam, with more intensive sampling effort across the Nuclear Central American region, where historic and contemporary genetic introgression between *S. beryllina – S. cyanura – S. hoffmanni* has been reported in association with complex patterns of plumage coloration (**Figure 1**; Jiménez and Ornelas 2016). As part of the above sampling effort we collected a total of 64 individuals of *S. cyanocephala*, *S. beryllina*, and *S. cyanura* between 2009 and 2013 through joint expeditions of the Museum of Vertebrate Zoology (MVZ), University of California, Berkeley (UC Berkeley); Escuela de Biología (EB), Universidad de San Carlos de Guatemala (USAC); and the Museo de Zoología "Alfonso R. Herrera" (MZFC), Universidad Nacional Autónoma de México (UNAM). We sampled with permission granted by the Consejo Nacional de Áreas Protegidas in Guatemala through research and collecting permits provided to EB-USAC and with Mexico's Secretaría de Medio Ambiente y Recursos Naturales, Subsecretaría de Gestión para la Protección Ambiental, Dirección General de Vida Silvestre granted to UNAM. Ethical approval for all fieldwork procedures was provided by the UC Berkeley Institutional Animal Care and Use Committee (R317). We preserved the captured individuals as voucher specimens (study skins and tissue samples). We deposited the specimens in ornithological research collections at the EB-USAC, MVZ-UC Berkeley, and MZFC-UNAM (**Table S1**).

We supplemented our sampling with 56 individuals from tissue loans obtained from several museum collections: Burke Museum of Natural History and Culture – UWBM (30 individuals); Museum of Comparative Zoology, Harvard University – MCZ (10 individuals); Louisiana State University Museum of Natural Science – LSUMZ (7 individuals); American Museum of Natural History – AMNH (4 individuals); Kansas University, Natural History Museum – KU (2 individuals); Yale Peabody Museum of Natural History, Yale University – YPM (2 individuals); and Field Museum of Natural History – FMNH (1 individual). Eight individuals were added to

the mitochondrial dataset as sequences downloaded from GenBank (**Table S1**). We added fifteen individuals for our outgroup sampling, which represent thirteen species, all members of the Emerald clade of hummingbirds (McGuire et al. 2014). The outgroup sampling included the two hummingbird species in the genus *Leucolia*, that is sister to *Saucerottia*: *Leucolia violiceps* and *L. viridifrons*. The additional eleven species used as outgroup taxa were: *Cynanthus canivetii*, *Basilinna leucotis*, *Pampa rufa*, *Thalurania colombica*, *Eupherusa eximia*, *Trochilus polytmus*, *Amazilia rutila*, *A. yucatanensis*, *A. tzacatl*, *Polyerata decora*, and *Chlorestes candida*.

## Mitochondrial DNA sequencing

We extracted genomic DNA using the DNeasy blood and tissue extraction kit (Qiagen, Valencia, CA, USA), following the protocol recommended by the manufacturer. We PCR-amplified and sequenced 1041 base pairs (bp) of NADH nicotinamide dehydrogenase subunit 2 (ND2). The amplification of ND2 was performed with primers L5204 and H6312 (Cicero and Johnson 2001). Polymerase chain reaction conditions included an initial denaturation at 94 °C for 1 min; then 35 cycles at 94 °C for 30 s, 54 °C for 30 s, and 72 °C for 45 s; and a final extension at 72 °C for 10 min. The PCR products were cleaned with the ExoSAP-IT reagent following the protocol provided by the manufacturer protocol (Applied Biosystems, Foster City, CA, USA). We sequenced PCR products in both directions, forward and reverse, using BigDye terminator chemistry (Applied Biosystems, Foster City, CA, USA) on an ABI 3730 automated sequencer (Applied Biosystems, Foster City, CA, USA). We edited the sequences using Geneious v. 5.1.7 (http://www.geneious.com). We conducted our lab work in the Evolutionary Genetics Laboratory at the Museum of Vertebrate Zoology.

## ddRAD sequencing and SNP calling

We followed the protocol for double digest restriction site-associated DNA sequencing (ddRAD) described by Peterson et al. (2012). Briefly, 500 ng of genomic DNA, quantified with Qubit (Thermo Fisher Scientific), was digested over three hours using the restriction enzymes MluCI and SphI-HF (NEB). After digestion and bead clean-up, each sample was labeled with the ligation of one of 24 different adapters. Adapter ligation was followed by pooling sets of 24 samples (five pools of 24 samples) and two consecutive bead clean-ups. The cleaned product was PCR amplified and indexed with a second adaptor during 12 cycles using the Phusion DNA polymerase (NEB). After bead clean-up and qPCR, the five libraries were combined in an equimolar manner. The combined final library was subject to size selection through PippinPrep, targeting fragment sizes from 450 to 650 bp (300 to 500 bp without the adapters). The excised library was run on one lane of an Illumina NovaSeq S4 to generate 150 bp paired-end sequence reads. Given pooling issues in the sequencing facility, the recovered number of reads was lower than expected; therefore, our library was subsequently run again on one lane of an Illumina NovaSeq S4 to generate 150 bp paired-end sequence reads to supplement the previous set of reads. The sequencing was carried on at the QB3 Vincent J. Coates Genomic Sequencing Laboratory at UC Berkeley.

Raw sequence reads from both runs were demultiplexed and combined using the process_radtags program in Stacks (Catchen et al. 2013). Cleaned sequences from each individual were mapped to the annotated reference genome of *Calypte anna* available through NCBI (GenBank assembly

accession: GCF_003957555.1) using the software BWA (Li and Durbin 2009) and then converted to BAM files with SAMtools (Li et al. 2009). We used the gstacks program from Stacks to create loci and build a catalog using the BAM files as input. We then generated multiple datasets, including for all individuals and for subsets of the total sample. We used the following steps for building the different datasets, starting with (i) a dataset of 120 individuals that included the *Saucerottia* and outgroup species. We used the populations program from Stacks to assign 80% as the minimum percentage of individuals in the complete dataset (R = 0.8) required to process a locus and create a file in Variant Call Format (VCF). Then, we performed additional filtering steps in VCFtools (Danecek et al. 2011). We included only sites with a minor allele frequency greater than or equal to 0.01 (--maf 0.01) and with mean depth values greater than or equal to 3 (--min-meanDP 3) and less than or equal to 10 (--max-meanDP 10). We removed individuals with 30% or more missing data. We proceeded to prune sites with evidence of linkage disequilibrium by creating a BED file and estimating r2 in Plink v1.9 (Purcell et al. 2007) and used this to obtain a final VCF file that was used for downstream analyses. The additional datasets were: (ii) genus *Saucerottia* (105 individuals); (iii) *Saucerottia beryllina – S. cyanura* from Chiapas, Mexico to El Salvador (48 individuals); (iv) *Saucerottia beryllina – S. cyanura* from allopatric populations (17 individuals); (v) *Saucerottia edward edward – S. e. niveoventer* (4 individuals); and (vi) *Saucerottia viridigaster – S. tobaci* (10 individuals).

**Phylogeographic structure**

We analyzed the mitochondrial ND2 matrix and the ddRAD dataset to understand the geographic distribution of genetic variation. We started by generating an unrooted statistical parsimony haplotype network (Clement et al. 2000) of the ND2 matrix using POPART v.1.7 (Leigh and Bryant 2015). For the nuclear data we performed a Principal Component Analysis (PCA) that included the complete *Saucerottia* ddRAD data (dataset ii, 105 individuals). The PCA, as a clustering analysis, is a practical method with which to gain an understanding of the spatial distribution of the data and does not require meeting the assumptions of other genetic analyses (e.g., Hardy-Weinberg Equilibrium). We conducted the PCA as implemented in ADEgenet (Jombart 2008) and recorded the eigenvalues and eigenvectors for the first four principal components. We performed an additional PCA that included the *S. beryllina – S. cyanura* individuals (dataset iii, 48 individuals) to better understand fine spatial structure of these taxa since they clustered together as a single group in the PCA performed with dataset ii.

We estimated the number of ancestral populations (K) and individual admixture coefficients using the ddRAD datasets. We performed these analyses using sparse nonnegative matrix factorization algorithms (sNMF, Frichot et al. 2014) as implemented in the R package LEA (Frichot and François 2015). The sNMF approach is a time-efficient method with which to estimate individual ancestry coefficients using large genomic datasets (Frichot et al. 2014). To infer the number of populations, we assessed values from K=1 to K=10 with ten replicates for each value of K. We selected K based on the lowest cross-entropy value and subsequently plotted the Q matrix for the run of the selected K, which at the same time, showed the lowest cross-entropy value. We ran the analyses independently for both the complete *Saucerottia* dataset (dataset ii, 105 individuals) and the reduced *S. beryllina – S. cyanura* samples (dataset iii, 48 individuals).

We compared the genome-wide differentiation between *Saucerottia* species by estimating pairwise FST for the ddRAD dataset. Additionally, we estimated pairwise FST considering the different intraspecific sub-groups detected with the PCAs. We estimated the FSTs using the populations module from Stacks (--fstats --bootstrap-fst).

**Phylogenetic analysis and character evolution**

We reconstructed the phylogenetic relationships of the genus *Saucerottia* to understand the evolutionary history of the genus. We also aimed to compare our phylogeny, which was based on multiple representatives for most of the species and a large genomic set of SNPs (ddRAD data), with previously published phylogenies that included the genus but were not mainly focused on it or were based on a reduced number of molecular markers. We conducted a maximum likelihood analysis in RAxML v8.2 (Stamatakis 2014) using the complete dataset that included the outgroup taxa (dataset i, 120 individuals). We used the model of nucleotide substitutions GTRCAT for the complete SNP set. We obtained node support by running rapid bootstrapping with 100 iterations. The consensus tree was visualized in FIGTREE v1.2.3 (http://tree.bio.ed.ac.uk/software/figtree/).

To understand the evolution of tail plumage coloration, we traced the character history on the phylogenetic tree using the parsimony method in MESQUITE v3.70 (Maddison and Maddison 2021). We only analyzed tail coloration since that is the most variable trait within *Saucerottia*, and it is widely used in establishing specific and subspecific groups. The character state of tail coloration was assigned based on information in the literature (Howell and Webb 1995, Weller 2021, Weller et al. 2021a, b, c) and geographic origin of specimens, or by visual inspection of museum specimens. The character state was assigned to one of the following five categories: 1 – green, 2 – blue, 3 – rufous, 4 – mixed, 0 – outgroup (excluding the *Saucerottia* sister genus *Leucolia*, which was assigned the category "1 – green"). The category "4 – mixed" was used only for the specimens from the *S. beryllina – S. cyanura* sympatric/hybrid zone in Guatemala that did not have completely blue or rufous tails (**Figure 2**).

**Spectrophotometry and electron microscopy of tail feathers in *Saucerottia beryllina* and *S. cyanura***

We measured the reflectance of tail feathers to obtain objective estimates of the observed colors. We used a USB2000 spectrophotometer (Ocean Optics, Dunedin, FL, USA) to measure the reflectance of wavelengths between 300 and 700 nm. We also used a PX-2 pulsed xenon light source 224, and the spectrophotometer was held at an angle of 90° at a distance of 9 mm from each feather. After measuring the reflectance of a set of feathers, we selected the three individuals that showed evident variation in color. The three individual samples selected were: one *S. beryllina* from eastern Guatemala (red group in **Figure 1**, MVZ189204), one *S. cyanura* from southern Guatemala (light blue group in **Figure 1**, MVZ187120), and one *S. beryllina – S. cyanura* intermediate individual in tail color from southern Guatemala (lilac group in **Figure 1**, USAC967).

We used transmission electron microscopy (TEM) to study the structure of the barbules of tail feathers with different colors. From cross-sections of the barbs, we looked at the physical

arrangement of the barbules, and from cross-sections of the barbules, we looked at the physical arrangement of the melanosomes within the barbules. We examined with TEM the three individuals with evident variation in color as shown by reflectance data.

## Identification of candidate genes underlying tail coloration in *Saucerottia beryllina* and *S. cyanura*

We looked for outlier loci between *Saucerottia beryllina* and *S. cyanura* to disentangle the genetic basis of tail coloration. We selected samples from allopatric populations of both species for this analysis. *Saucerottia beryllina* was represented by ten samples from Chiapas, Mexico, and western Guatemala, where only the rufous tail phenotype is found. *Saucerottia cyanura* was represented by seven samples from southern Guatemala, a very localized area where only the blue tail phenotype occurs. The 17 samples correspond to the filtered "dataset iv." Additionally, as suggested by our previous analyses (PCA, admixture analysis, FSTs, and phylogenetic tree), the individuals that we selected are phylogenetically very closely related, which makes them an ideal sample with which to study the genetic basis of a particular trait, as the background divergence across the genome is likely to be small.

We used a method based on FST values computed from an ancestry matrix to identify outlier loci (Martins et al. 2016). This method is specifically designed to identify outlier loci when there is genetic admixture between populations. More specifically, it uses sNMF clusters and an associated Q matrix as input for testing for sites that have significant differentiation among clusters and under selection. We performed this analysis as implemented in the R package LEA (Frichot and François 2015), setting K=2. We recorded the *p*-values for all the different comparisons, one comparison per SNP in "dataset iv." We functionally annotated the sites with the lowest *p*-values ($p < 0.0001$) using the reference genome of *Calypte anna* (GenBank assembly accession: GCF_003957555.1). We looked for the outlier sites in the additional *S. beryllina* and *S. cyanura* individual samples from this study, including the samples with intermediate tail coloration.

## Comparing candidate tail color loci with other species in the genus *Saucerottia* that vary in tail color

We aimed to find potential genomic regions that differ between tail color phenotypes (rufous vs. blue) in *S. edward*, *S. viridigaster*, and *S. tobaci*. First, we looked for differentially fixed sites between the two *S. edward* subspecies, *S. e. edward* and *S. e. niveoventer* (dataset v). To do this, we filtered the dataset and kept only the sites that were fixed for the rufous tail (*S. e. edward*, two individuals) and blue tail (*S. e. niveoventer*, two individuals) phenotypes. We followed this procedure because our sample size for these two subspecies was too small to enable the use of alternate statistical frameworks.

We also filtered the data for sites that were differentially fixed between *Saucerottia viridigaster* and *S. tobaci* (dataset vi) using the same procedure as described above for *S. edward*. We selected the individuals to include in this analysis based on the phylogenetic tree estimated in this study. We filtered the dataset and kept the fixed sites for the rufous tail (*S. viridigaster*, four individuals) and blue tail (*S. tobaci*, four individuals, two from Trinidad and two from Tobago)

phenotypes. After obtaining the fixed sites, we added the genetic data from the two additional *S. tobaci* individuals from Venezuela.

We functionally annotated the fixed SNPs using the reference genome of *Calypte anna* (GenBank assembly accession: GCF_003957555.1). We report the candidate genes discovered from each comparison. Additionally, in order to check whether the identified outlier loci between *S. beryllina – S. cyanura* are also associated with tail coloration in *S. edward, S. viridigaster*, and *S. tobaci*, we looked for those sites in their genomic data (dataset ii).

**Results**

The mitochondrial and genomic datasets included nine of the ten species within the genus *Saucerottia* and our sampling spanned its distributional range (**Figure 1**). We compiled complete ND2 sequences (1041 bp) for 113 individuals, 105 which we sequenced, and eight additional sequences downloaded from GenBank (**Table S1**). We processed ddRAD genomic data from 105 *Saucerottia* individuals, in addition to 15 outgroup individuals. After building the catalog of loci with gstacks, the mean coverage was 15.8x (1.9x – 64.7x). The final number of individuals differed among the six ddRAD datasets (i to vi, **Table 1**); given that some individuals were excluded because they had more than 30% missing data (**Table S2**). The final number of variable sites also differed among the several datasets, ranging from 2,962 SNPs in *S. edward* – "dataset v" to 115,609 SNPs in *Saucerottia* and outgroup taxa – "dataset i" (**Table 1**).

**Phylogeographic structure**

The mitochondrial ND2 haplotype network showed correspondence with the expected geographic distribution of most species, although known species limits were not always reflected in the network (**Figure 3**). Individuals of *Saucerottia cyanocephala* formed a well-differentiated cluster consistent with an independent evolutionary trajectory from the other species within the genus. *Saucerottia beryllina*, *S. cyanura*, and *S. hoffmanni* were deeply interconnected, suggesting a more recent history of lineage divergence or recurrent gene flow. *Saucerottia edward* and *S. saucerottei* are two species that corresponded with well-differentiated mtDNA clusters, matching their geographic isolation (Panama and Colombia, respectively) and recognized species limits. A final haplotype cluster comprised *S. castaneiventris*, *S. viridigaster*, and *S. tobaci*; although the three different species did not share haplotypes, the differentiation among them was shallow. *Saucerottia viridigaster* and *S. tobaci* were separated by a single nucleotide difference, indicative of a recent divergence event.

The Principal Component Analysis of the complete *Saucerottia* genomic dataset (dataset ii, **Figure 4a**) revealed clusters associated with geography and recovered most species. PC1 corresponded with geographic distribution; on the left side of the plot were the species from Mexico and northern Central America (north of the Nicaraguan Depression), and on the right side were the species from southern Central America and South America (south of the Nicaraguan Depression). PC2 mainly separated *S. cyanocephala* from the other species within the genus. The genetic structure captured by the genomic data was higher than the structure suggested by the mitochondrial data, showing differentiation within species. For *S. beryllina*, two clusters corresponded with the western and eastern sides of the Isthmus of Tehuantepec.

Within *S. cyanura*, there were two clusters, matching the disjunct distributional range of the species (**Figure 4b)**. Interestingly, we discovered two clusters within *S. hoffmanni*, which corresponded with the two sampled populations, one from Nicaragua and one from Costa Rica, even though these two populations are located close to each other geographically, with no known barrier between them. East of the Isthmus of Panama, *Saucerottia viridigaster* and *S. tobaci* represented a single cluster, indicative of shallow divergence.

In the PCA of the complete *Saucerottia* genomic dataset (dataset ii, **Figure 4**), we recovered a single cluster comprising different species and phenotypes that included: *Saucerottia beryllina* from the eastern side of the Isthmus of Tehuantepec, *S. cyanura* from western Guatemala, as well as individuals with intermediate tail coloration. All three different phenotypes are sympatric in central Guatemala, specifically in the areas surrounding the Atitlan Volcano. To discern any additional structure within the cluster, we conducted a second PCA with a more narrow geographic focus (dataset iii**, Figure 5a**). The clustering pattern of *S. beryllina – S. cyanura* (Chiapas, Mexico to eastern Guatemala) showed shallow differentiation and suggested admixture between groups. PC1 mainly separated a cluster of allopatric *S. beryllina* from Chiapas and western Guatemala from the other analyzed individuals. Surprisingly, one individual (MVZ 187283) collected from the area of sympatry in central Guatemala was positioned close to this *S. beryllina* cluster, a genetic sample from a specimen with a rufous tail. This pattern suggests that the individual had a genetic background more similar to an external population than to the local population. PC2 separated allopatric *S. cyanura* from western Guatemala from the individuals with intermediate tail coloration sampled from the area of sympatry in central Guatemala. Four individuals with the *S. cyanura* phenotype were assigned as intermediate between the two clusters; with three of the four individuals sampled from the area of sympatry in central Guatemala. Finally, four individuals of *S. beryllina* from eastern Guatemala and five individuals from the area of sympatry in central Guatemala occupied the central portion of the PCA, suggesting that they are genetically intermediate between the differentiated clusters. The findings from the geographically restricted *S. beryllina – S. cyanura* PCA are consistent with the results from the admixture coefficient analysis (**Figure 5b**).

We discovered five ancestral population clusters in the complete *Saucerottia* genomic dataset (dataset ii, a dataset that included seven currently recognized species), in addition to samples representing multiple currently recognized species that show signs of admixture and suggest complex patterns of introgression (e.g., *S. beryllina*, *S. cyanura*, and *S. edward*; **Figures 6 and S2**). Two of the clusters corresponded with currently recognized species, *S. cyanocephala* and *S. hoffmanni*. A third group represented *S. beryllina* from the western side of the Isthmus of Tehuantepec. The fourth group was composed of *S. viridigaster* and *S. tobaci*, with weak divergence between these species indicated by both the mitochondrial haplotype network and the genomic PCA. The fifth group included a subset of the individuals with intermediate tail coloration from central Guatemala, where *S. cyanura* is sympatric with *S. beryllina*, together with allopatric *S. cyanura* from western Guatemala. Interestingly, the other subset of the individuals with intermediate tail coloration had coefficients similar to those of *S. beryllina* from the eastern side of the Isthmus of Tehuantepec; these coefficients suggested admixture mainly between the above mentioned as a fifth group and *S. beryllina* from the western side of the Isthmus of Tehuantepec. The eastern population of *S. cyanura* was admixed between the fifth group and *S. hoffmanni*. Surprisingly, *S. edward* was recognized as a species with a very

complex history of admixture, having ancestry coefficients from four of the five discovered clusters (all but *S. cyanocephala*).

The genome-wide differentiation (pairwise FST) between *Saucerottia* species was generally low (**Tables 2 and S3**). The lowest estimate of genome-wide differentiation was between *S. beryllina*, *S. beryllina – S. cyanura* sympatric/hybrid area, and *S. cyanura* (FSTs from 0.021 to 0.032). The highest genomic differentiation was between *S. cyanocephala* and the Central American species *S. edward* (FST 0.319), and between *S. cyanocephala* and the South American species *S. viridigaster* (FST 0.382) and *S. tobaci* (FST 0.294). Genomic differentiation between *S. viridigaster* and *S. tobaci* also was quite low (FST 0.100), consistent with recent (or perhaps incomplete) divergence.

**Phylogenetic analyses and character evolution**

Our phylogenetic estimate is consistent with monophyly of the genus *Saucerottia* (**Figure 7**), and furthermore indicates five major clades within the genus: (1) *S. cyanocephala*, (2) *S. beryllina – S. cyanura*, (3) *S. hoffmanni*, (4) *S. edward*, and (5) *S. viridigaster – S. tobaci*. Three of the five major phylogenetic clades correspond with three of the five ancestral population clusters detected with the ancestry analyses (**Figure 6**): *S. cyanocephala*, *S. hoffmanni*, and *S. viridigaster – S. tobaci*. The additional two major clades in the phylogeny, *S. beryllina – S cyanura* and *S. edward*, were not consistent with the ancestry analyses given to signs of admixture and complex patterns of introgression.

The phylogeny suggested a first divergence event that resulted in two clades, one represented by *S. cyanocephala* and the other by the remaining *Saucerottia* species. A second divergence event resulted in a clade that includes *S. beryllina* and *S. cyanura* and another that includes *S. hoffmanni*, *S. edward*, *S. viridigaster* and *S. tobaci*. Interestingly, *S. beryllina* and *S. cyanura* are not recovered as reciprocally monophyletic clades. *Saucerottia beryllina* from the western side of the Isthmus of Tehuantepec diverged earlier than the split between *S. beryllina* from the eastern side of the Isthmus and *S. cyanura*. Moreover, shallow divergence is evident in the clade that encompasses eastern *S. beryllina* and *S. cyanura* where there is a diversity of tail feather colorations. The mainly eastern *S. beryllina* group (rufous-tailed individuals from Chiapas and western Guatemala) includes one rufous-tailed specimen from the area of sympatry with *S. cyanura* in central Guatemala and one blue-tailed specimen from western Guatemala, which suggests gene flow among different populations. *Saucerottia cyanura* (*sensu stricto*) is within a clade with the highest variability of tail feather coloration, with individuals having blue, rufous, purple, and intermediate (blue, rufous, purple) tail feathers. The *S. cyanura* (*sensu lato*) clade ranges from western Guatemala to western Nicaragua and includes allopatric blue-tailed populations, allopatric rufous-tailed populations, and sympatric populations that have a diversity of tail colors (blue, rufous, purple, and intermediate).

Lineage divergences in the remaining members of genus follow a north to south pattern of divergence. First, *S. hoffmanni* split from the common ancestor of *S. edward*, *S. viridigaster*, and *S. tobaci*. Second, *S. edward* diverged from the common ancestor of the *S. viridigaster – S. tobaci* clade. Within *S. edward*, there are two clades, each corresponding to a different recognized subspecies with distinct tail feather coloration. *Saucerottia viridigaster* is found to be

nested within *S. tobaci*, with the phylogeographic structure corresponding more closely with geography than with described species limits. Similar to *S. cyanura* (*sensu lato*) and *S. edward*, the *S. viridigaster – S. tobaci* clade showed a variety of tail colorations within a single clade.

The analysis of character state evolution suggested tail coloration is a labile trait within *Saucerottia* hummingbird species (**Figure 8**). *Saucerottia cyanocephala* is the only species within the genus with a brownish-green tail. The reconstruction of tail coloration character states suggests a rufous ancestral state for the *S. beryllina – S. cyanura* clade and subsequent changes to blue or intermediately colored tails. The ancestral state suggested for the clade that includes *S. hoffmanni*, *S. edward*, *S. viridigaster – S. tobaci* is a blue tail with two subsequent changes to a rufous tail, one in *S. edward* and one in *S. viridigaster – S. tobaci*. Based on the additional analyses in this study, the multiple switches from rufous to blue and vice versa might not be independent and could result from shallow divergence and admixed ancestry.

## Spectrophotometry and electron microscopy of tail feathers in *Saucerottia beryllina* and *S. cyanura*

Our spectrophotometer and microscopy data showed that the blue feather was distinct from the rufous and purple feathers, whereas the differences between the rufous and purple feathers were more subtle (**Figure 9a**). Spectral data of the blue feather peaked between 400 and 500 nm, exactly where blue is found in the color spectrum. The rufous and purple feathers showed two peaks. One peak between 300 and 400 nm, right in the UV region of the color spectrum; both feathers had a peak of similar height. The second peak was around 700 nm, on the red side of the color spectrum; the peak of the rufous feather was higher than the peak of the purple feather.

Transmission electron microscopy revealed that the morphology of the blue feather sample was different from the other two feathers in barb shape and barbule length (**Figure 9c**). The morphology of the melanosomes was similar in the three feathers, and the three feathers had a layer of melanosomes around the edge of the barbules (**Figure 9d**). In addition to the melanosomes around the edge of the barbules, the blue feather also had melanosomes in the internal matrix of the barbules. Our microscopy data suggest that the differences in tail coloration arise from structural differences in the barbs, barbules, and melanosome organization rather than from pigment-based differences.

## Identification of candidate genes underlying tail coloration in *Saucerottia beryllina* and *S. cyanura*

We compared two allopatric parental populations of *S. beryllina* and *S. cyanura*, both from northern Central America, and discovered seven outlier loci ($p < 0.0001$) (**Table 3**). Two of the outlier loci were fixed for alternate alleles in *S. beryllina* and *S. cyanura*, and the remaining five outlier loci were nearly fixed (85% to 97%, **Figure 10a**). Three outlier loci were located in coding regions, one on chromosome 2 and two on chromosome Z. The gene on chromosome 2, DCLK3, codes for the protein Doublecortin Like Kinase 3, also known as Serine/Threonine-Protein Kinase DCLK3. The genes on chromosome Z, DAPK1 and FCHO2, code for Death-Associated Protein Kinase 1 and F-BAR Domain Only Protein 2, respectively. There were four outlier loci located in non-coding regions, two on chromosome 1 and two on chromosome 3.

After identifying the outlier loci in parental populations of *S. beryllina* and *S. cyanura* (**Figure 10a**), we examined those outlier loci across the complete sampling of *S. beryllina* and *S. cyanura* individuals from this study and discovered that only one SNP showed high correspondence with phenotype across populations (**Figure 10b**). This SNP was located on chromosome 3 (position 103,877,992) within a non-coding region. All the individuals assigned as *S. beryllina* (specimens with rufous tails) were homozygous GG. The western allopatric population of *S. cyanura* (specimens with blue tails) and blue-tailed hummingbirds in the area of sympatry with rufous-tailed birds were homozygous for the alternate AA or heterozygous for GA. Interestingly, the three different genotypes (GG, AA, and GA) were present in the sympatric population from central Guatemala, where *S. beryllina* and *S. cyanura* co-occur, and where all the different tail phenotypes cohabit. However, the eastern allopatric population of *S. cyanura* (specimens with blue tails) was also homozygous GG.

The other four SNPs for which we report data were only differentiated in *S. beryllina* from Chiapas, Mexico and western Guatemala. This suggests that the four SNPs may be more closely associated with the particular structure of that population rather than associated with tail feather coloration. We did not report the data of the SNPs on chromosome 1 for the additional *S. beryllina* and *S. cyanura* since we could not score these alleles for all individuals due to missing data.

**Candidate gene regions for other *Saucerottia* species that vary in tail color**

The outlier loci detected when comparing *S. beryllina* and *S. cyanura* were not associated with tail feather coloration in *S. edward*, *S. viridigaster*, or *S. tobaci* (**Figure 10c**), but were fixed in these species. However, we discovered 316 SNPs that were differentially fixed in the two *S. edward* subspecies, *S. e. edward* (rufous tail, two individuals) and *S. e. niveoventer* (blue tail, two individuals) (**Table S4**); and 50 SNPs differentially fixed in *S. viridigaster* (rufous tail, four individuals) and *S. tobaci* (blue tail, four individuals) (**Table S5**). One protein-coding gene was detected in both comparisons, *S. e. edward – S. e. niveoventer* and *S. viridigaster – S. tobaci*. The gene was PPP1R12B (chromosome 26) which codes for five isoforms of the protein phosphatase 1 regulatory subunit 12B that has a potential role in muscle cell proliferation (Montén et al. 2015). Interestingly, there was only one gene for which we discovered two fixed SNPs; the gene LRMDA was detected in the *S. edward* comparison, and it encodes for the protein "leucine-rich melanocyte differentiation-associated protein." The fixed SNPs in PPP1R12B and LRMDA were not detected as outliers in the *S. beryllina – S. cyanura* comparison.

Further analysis of the *S. viridigaster* – S. *tobaci* dataset showed that fourteen out of the 50 outlier SNPs were located in protein-coding regions (**Figure 11**). Nine of the fourteen proteins belong to gene families involved in the melanin biosynthesis pathway, or have been identified as candidate genes for plumage feather coloration (**Table S5).** Three of the nine genes code for serine/threonine protein kinases, ULK4, PRKD1, and MAP3K1; coincident with DCLK3, another serine/threonine protein kinase that was discovered when contrasting *S. beryllina* and *S. cyanura*. Finally, examination of the 50 fixed SNPs in *S. viridigaster – S. tobaci* enabled us to confirm genetic admixture in Venezuelan *S. tobaci* (**Figure 11**), as suggested by our phylogenetic reconstruction (**Figure 7**).

## Discussion

Our findings show that the evolutionary and biogeographic history of *Saucerottia* hummingbirds sets the biological stage for understanding the genetic basis of structural color variation in hummingbird plumage. Shallow sequence divergences and mixed ancestry in the recently diversified *Saucerottia* hummingbirds provide a similar genetic background between species that mainly differ in structural plumage coloration. Tail coloration, one of the most variable traits in *Saucerottia* species, was phylogenetically and geographically dispersed, suggesting that tail coloration is a labile trait within *Saucerottia* hummingbirds. FST outlier analyses between *S. beryllina* and *S. cyanura* allowed us to detect one SNP significantly and consistently associated with tail coloration, located in a non-coding region of chromosome 3. Additionally, when contrasting *S. viridigaster* with *S. tobaci*, we uncovered nine SNPs in protein-coding genes related to the melanin biosynthesis pathway. Our spectrophotometer and microscopy data confirmed that the different tail colors have a structural basis, and the blue feather was structurally distinct from the rufous and purple feathers. Our study highlights the importance of recently diverged lineages and highly admixed groups for disentangling the genetic basis of complex traits and understanding their role in species diversification.

Our genomic and mitochondrial DNA analyses provide evidence of shallow lineage divergence and mixed ancestry in the recently diversified *Saucerottia* hummingbirds. Consistent with previous research using microsatellites (Jiménez and Ornelas 2016), we detected genetic admixture between *S. beryllina* and *S. cyanura* in Central America. However, our genomic data set allowed us to restrict the genetic group to the populations from the Isthmus of Tehuantepec to eastern Guatemala, a smaller geographic range than the suggested by microsatellites (i.e., from the Isthmus of Tehuantepec to the Nicaraguan Depression; Jiménez and Ornelas 2016). Moreover, we uncovered shallow divergence within the region from the Isthmus of Tehuantepec to eastern Guatemala consistent with the geographic distribution of tail color variants. Interestingly, the sympatric population where *S. beryllina* and *S. cyanura* co-occur in central Guatemala showed the lowest genetic differentiation from surrounding populations (FST from 0.023 to 0.028) along with high genetic admixture, supporting previous suggestions of hybridization in the area (Ridgway 1911, Jiménez 2011, Jiménez and Ornelas 2016). Hybridization might also be enhanced by the possibility of interspecific mixed courtship displays (Wagner 1954).

We confirmed, through phylogenetic analyses, the presence of three species/subspecies pairs within *Saucerottia* that differ primarily in tail coloration. First, the species complex *S. beryllina* – *S. cyanura*, which has low genetic differentiation between the two species, and in addition to rufous and blue tails, displays intermediate tail coloration in areas of sympatry (Jiménez and Ornelas 2016). Second, the two subspecies of *S. edward*: *S. e. niveoventer* (blue-black tail) is reciprocally monophyletic relative to *S. e. edward* (rufous tail). Third, the species complex *S. viridigaster* (rufous tail) – *S. tobaci* (blue-black tail), where genomic data suggests that these two species are also genetically admixed. A similar genetic background and different species pairs exhibiting phenotypic changes mainly in tail color highlight *Saucerottia* as an excellent system to disentangle the genetic basis for structural plumage coloration.

The reconstruction of character states suggested that tail coloration is a labile trait within *Saucerottia* hummingbirds. However, the geographic distribution of tail coloration suggests that some selective force may be acting to maintain differentially colored populations despite genetic admixture. Given that differences in gorget color in *Lampornis amethystinus* evolved about one million years ago, it has been hypothesized that structural colors are more labile and easily switched relative to pigment-based coloration (Ornelas et al. 2016). In contrast, pigment based color divergence in geographically isolated populations typically develops over approximately two million years in various neotropical bird species (Winger et al. 2015). In *Coeligena* hummingbirds, switches in plumage coloration have also been reported in recently diverged clades with shallow sequence divergence (Palacios et al. 2019).

Through spectrophotometry and microscopy, we confirmed that the blue feathers of *Saucerottia* hummingbirds are structurally distinct from rufous and purple feathers. The main difference between differently-colored feathers was in the arrangement of melanosomes in the feather matrix. Notably, *Saucerottia* tail feathers are not iridescent as are many gorgets and crowns in hummingbird species. Future research should also focus on finding study systems to investigate the genetic basis for iridescent plumage coloration. Structural colors in birds have complex and varied physical nanostructures and microstructures (Stoddard and Prum 2011, Shawkey and D'Alba 2017, McCoy and Prum 2019); therefore, understanding the genetic basis of structural plumage colors will require the study of multiple biological systems. The physical properties of feather coloration provide another layer of evidence for the shallow divergences and admixed ancestry of *Saucerottia* hummingbirds and confirm the relevance of the system for understanding the genomic basis of structural plumage coloration in birds.

Structural plumage coloration occurs as a consequence of feather structure and melanosome arrangement within the barbules. Therefore, we hypothesized that genes involved in the melanin biosynthesis pathway might underlie the genetic basis of structural colors. *Saucerottia* hummingbirds offered us the possibility of multiple comparisons to look for candidate genes underlying differences in structural colors. Furthermore, given that the genetic background between phenotypically different species/subspecies pairs was very similar, several genes involved in the melanin pathway stood out as outliers, some with fixed alleles between alternate colored tails. We were surprised by the recurrence of serine/threonine protein kinases as candidate genes as are proteins that regulate cellular processes through phosphorylation. For example, DCLK is a classical microtubule-associated protein (Reiner et al. 2006) and DAPK1 is thought to be involved in programmed cell death (NCBI).

Additional protein kinases were also detected, including the mitogen-activated protein kinase "MAP3K1", which has been reported to be involved in melatonin-induced melanosome aggregation in *Xenopus* (Andersson et al. 2003) and has been suggested as a candidate gene for iridescent structural color in chickens (Fogelholm 2020) and *Coeligena* hummingbirds (Palacios 2020). Genetic and biochemical complexity could allow for quick tuning-up and frequent and labile switches in structural feather coloration (Saranathan and Finet 2021). However, our candidate genes were recovered from ddRAD data, which do not represent the best approach to study the landscape of divergence (Szarmach et al. 2021) and consequently disentangle the genetic basis of traits. We look forward to the results of our ongoing *Saucerottia* projects using exon capture data and whole-genome resequencing approaches.

Our study has taxonomic implications since the species currently recognized as *S. beryllina* and *S. cyanura* are not reciprocally monophyletic. Genomic data support the differentiation between *S. beryllina* on the western side of the Isthmus of Tehuantepec from *S. beryllina – S. cyanura* of the eastern side of the Isthmus. However, shallow sequence divergence and genetic admixture play an important role in the evolutionary history of this species complex (Jiménez and Ornelas 2016), and establishing species limits is not straightforward. Additionally, *S. cyanura* is recognized as a different species from *S. beryllina* based on the deep blue color in its tail. As we show in this study, tail coloration is labile in *Saucerottia* hummingbirds and, therefore, not the best character with which to differentiate these species. We recommend either synonymizing the two species and referring them *S. beryllina* (this name has taxonomic priority), or splitting the species into S. *beryllina*, including the populations from the western side of the Isthmus of Tehuantepec, and *S. cyanura*, including the populations from the eastern side of the Isthmus. *Saucerottia viridigaster* and *S. tobaci* could also warrant taxonomic revision, although exhaustive geographic sampling is encouraged to better understand hybridization and genetic introgression in this species complex.

## Conclusions

Structural plumage coloration is of importance to furthering our understanding of avian diversification. However, disentangling the genetic basis of structural plumage colors remains elusive, partly due to the difficulty in identifying biological tractable study systems. Here, we showed how *Saucerottia* hummingbirds represent an excellent study system for investigating the genetic basis of structural colors. Shallow divergence and mixed ancestry in *Saucerottia* provide similar genetic backgrounds across species. Evolutionary labile tail coloration and its physical structural basis offer multiple species pairs differing mainly in structural coloration. Additionally, we identified various candidate genes in the melanin biosynthesis pathway that may underlie variation in structural coloration, suggesting that structural plumage coloration is a complex trait similar to melanin pigmentation across vertebrates (Harris et al. 2020). Understanding the genetic basis of structural plumage coloration and the regulatory processes involved will advance the study of species diversification in highly diverse groups that rely on a structural coloration for their gamut of plumage coloration.

## Tables and figures

**Table 1.** Genomic datasets (ddRAD) generated to explore different evolutionary and biogeographic questions regarding the hummingbird genus *Saucerottia*.

| No. | Dataset | Initial number of individuals | Number of individuals after filtering | Number of variant sites after filtering |
|---|---|---|---|---|
| I | *Saucerottia* + outgroup | 120 | 107 | 115,609 |
| Ii | *Saucerottia* | 105 | 96 | 78,839 |
| Iii | *Saucerottia beryllina – S. cyanura* | 48 | 42 | 52,691 |
| Iv | Allopatric *Saucerottia beryllina – S. cyanura* | 17 | 17 | 14,611 |
| v | *Saucerottia edward edward – S. e. niveoventer* | 4 | 4 | 2,962 |
| vi | *Saucerottia viridigaster – S. tobaci* | 10 | 10 | 7,458 |

**Table 2.** Genomic-wide differentiation (pairwise FST) between species of *Saucerottia* hummingbirds based on ddRAD data.

| | ***S. beryllina*** | ***S. beryllina – S. cyanura*** | ***S. cyanura*** | ***S. hoffmanni*** | ***S. edward*** | ***S. viridigaster*** | ***S. tobaci*** |
|---|---|---|---|---|---|---|---|
| ***S. cyanocephala*** | 0.086 | 0.085 | 0.092 | 0.097 | 0.319 | 0.382 | 0.294 |
| ***S. beryllina*** | ----- | 0.031 | 0.032 | 0.042 | 0.053 | 0.076 | 0.071 |
| ***S. beryllina – S. cyanura*** | | ----- | 0.021 | 0.044 | 0.051 | 0.072 | 0.070 |
| ***S. cyanura*** | | | ----- | 0.044 | 0.055 | 0.077 | 0.074 |
| ***S. hoffmanni*** | | | | ----- | 0.045 | 0.070 | 0.067 |
| ***S. edward*** | | | | | ----- | 0.230 | 0.162 |
| ***S. viridigaster*** | | | | | | ----- | 0.100 |
| ***S. tobaci*** | | | | | | | ----- |

*S. beryllina – S. cyanura*: sympatric/hybrid area.

**Table 3.** Outlier loci ($p < 0.0001$) between *Saucerottia beryllina* and *Saucerottia cyanura*.

| No. | Chromosome | SNP position | Gene | Gene position | Protein name | Function | *p* value |
|---|---|---|---|---|---|---|---|
| 1 | 2 | 51,198,092 | DCLK3 | 51,185,489 – 51,208,673 | serine/threonine-protein kinase DCLK3 | "Gene Ontology (GO) annotations related to this gene include transferase activity, transferring phosphorus-containing groups and protein tyrosine kinase activity." (GeneCards). "DCLK (doublecortin-like kinase) are classical microtubule (MT) associated proteins (MAPs), and contain two evolutionary conserved tubulin binding repeat sequences." (Reiner et al. 2006). | 3.426E-07 |
| 2 | 3 | 103,877,992 | Non-coding | | | | 5.927E-07 |
| 3 | 1 | 4,746,424 | Non-coding | | | | 1.448E-05 |
| 4 | 3 | 69,498,592 | Non-coding | | | | 6.980E-05 |
| 5 | Z | 33,673,458 | DAPK1 | 33,657,957 – 33,741,675 | death-associated protein kinase 1 isoform X1 | "Positive mediator of gamma-interferon induced programmed cell death." (NCBI). | 8.054E-05 |
| 6 | Z | 47,554,136 | FCHO2 | 47,489,682 – 47,580,727 | F-BAR domain only protein 2 | "Functions in an early step of clathrin-mediated endocytosis. Has both a membrane binding/bending activity and the ability to recruit proteins essential to the formation of functional clathrin-coated pits." (UNIPROT). | 9.122E-05 |
| 7 | 1 | 27,497,071 | Non-coding | | | | 9.230E-05 |

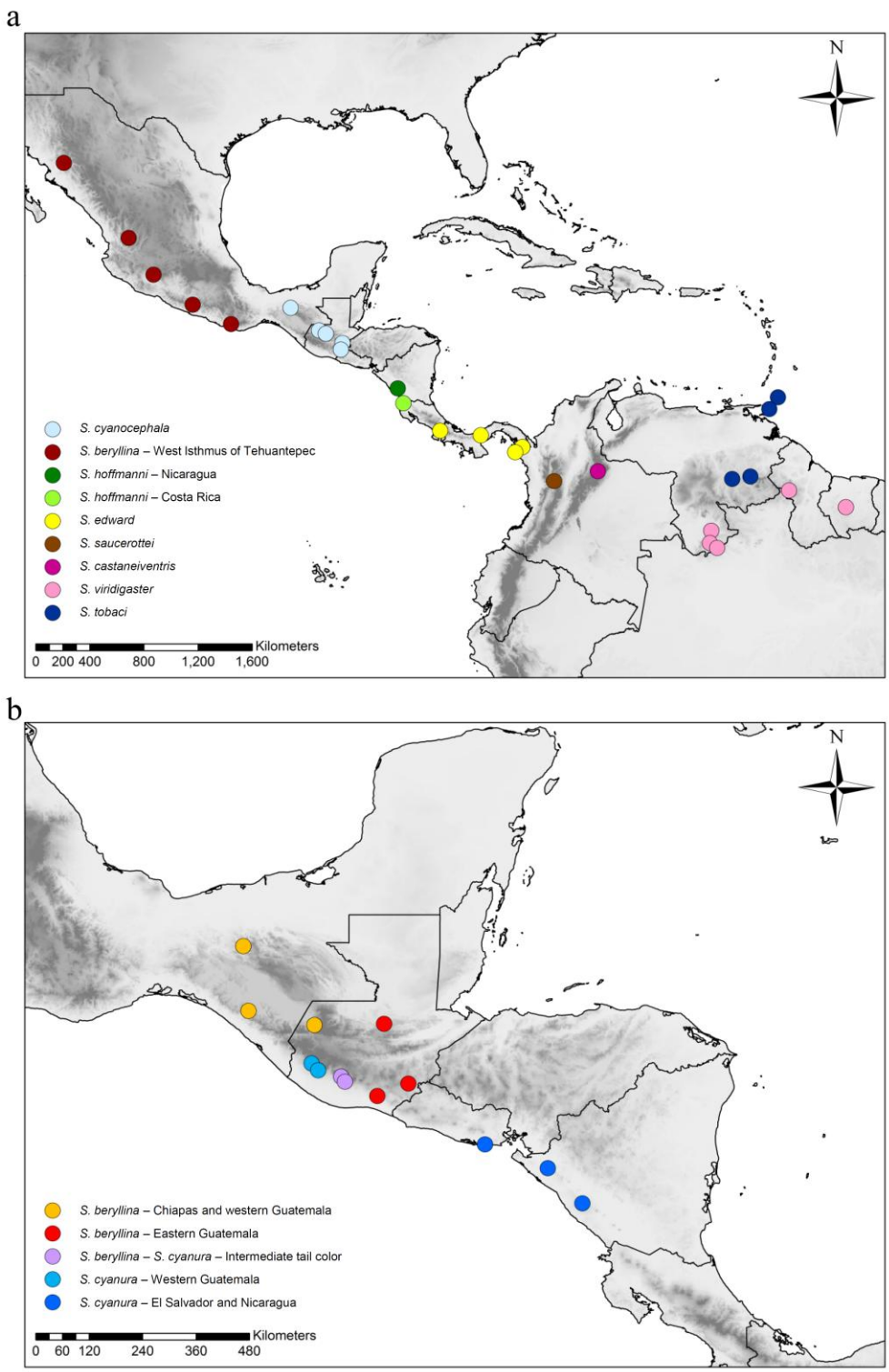


**Figure 1.** Geographic locations where *Saucerottia* samples were collected. a) Map depicts sampling from northern Mexico to Surinam, excluding geographically overlapping species. b) Map depicts sampling emphasizing northern Central America, showing species which ranges overlap with *S. cyanocephala* or *S. hoffmanni*.

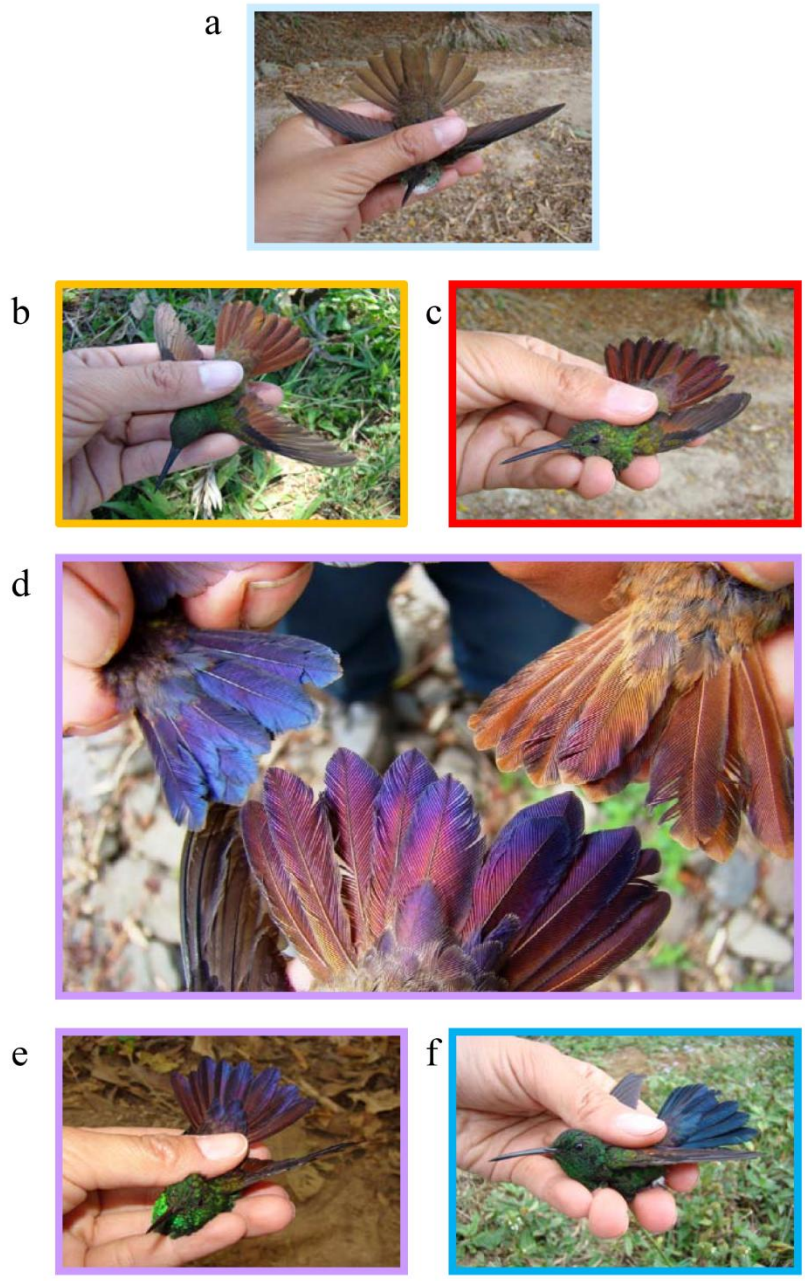


**Figure 2.** Different tail colorations in *Saucerottia* hummingbirds. a) Green tail in *S. cyanocephala* from Guatemala. b) Rufous tail in allopatric *S. beryllina* from western Guatemala. c) Rufous tail in allopatric *S. beryllina* from eastern Guatemala. d) Blue (upper left), rufous (upper right), and intermediate (lower center) tails from the sympatric population in central Guatemala, Suchitepéquez. e) Intermediate tail from the sympatric population in central Guatemala, Chimaltenango. f) Blue tail in allopatric *S. cyanura* from western Guatemala.

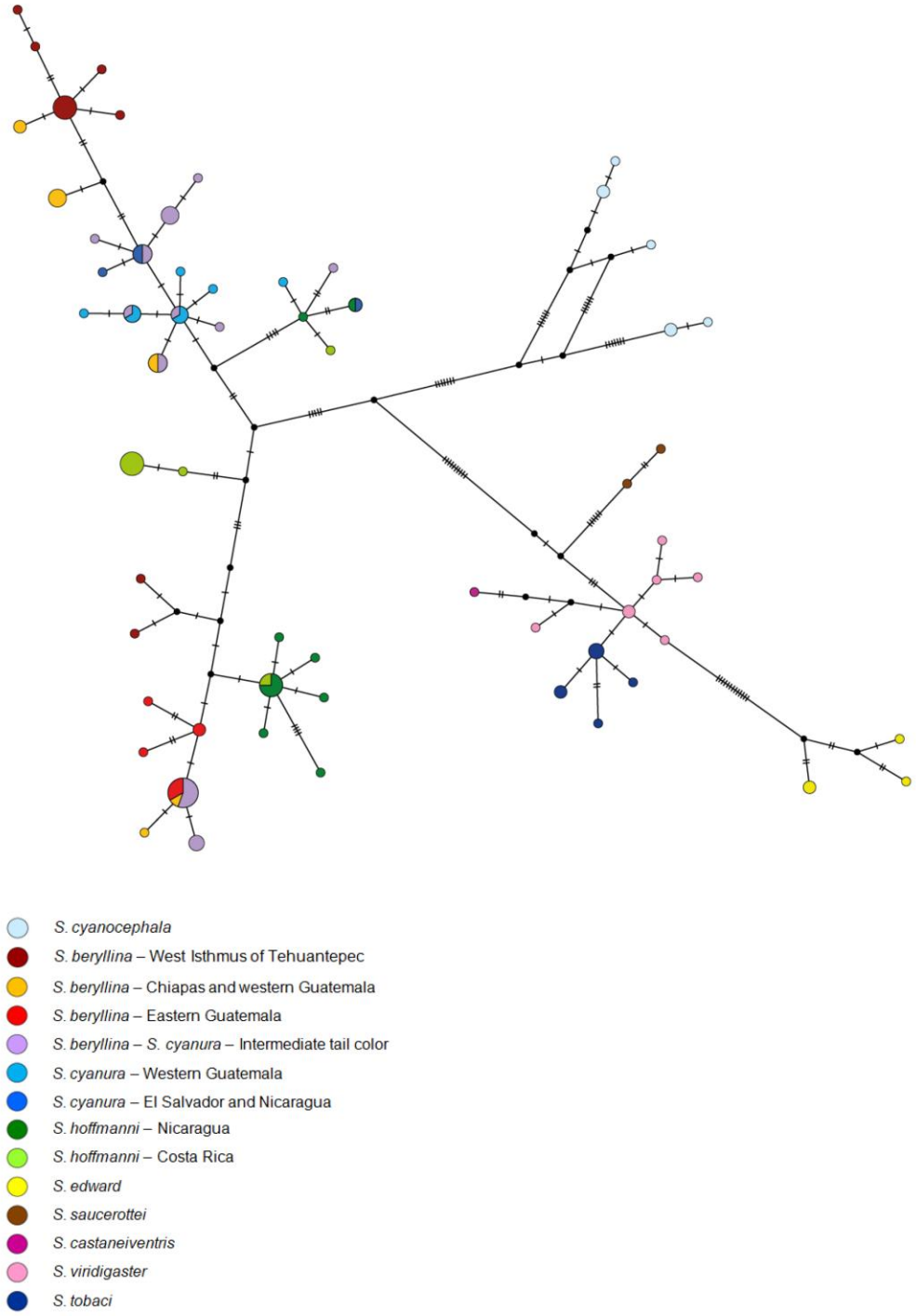


**Figure 3.** Haplotype network of mitochondrial ND2. Colors represent the species and geographic location of origin of the individual. The size of the circles on the network corresponds with the number of individuals with the same haplotype. Crossed dashes over lines connecting haplotypes represent nucleotide changes.

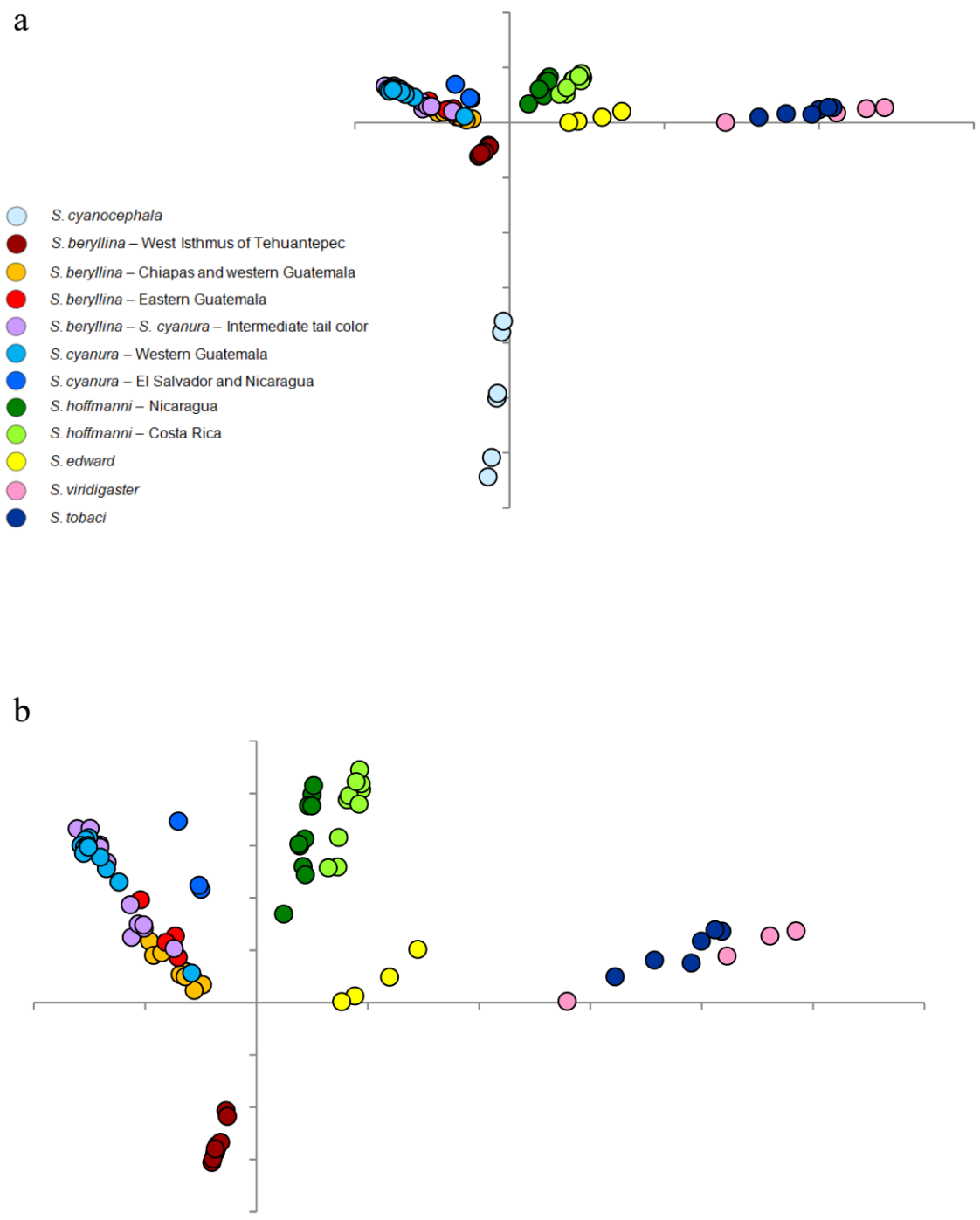


**Figure 4.** Principal Component Analysis (PCA) on ddRAD data of members of the genus *Saucerottia*. a) PCA of components 1 and 2. Variation explained by PC1 – 7.9% and by PC2 – 5.9%. b) Close-up of the PCA of components 1 and 2, with *S. cyanocephala* excluded.

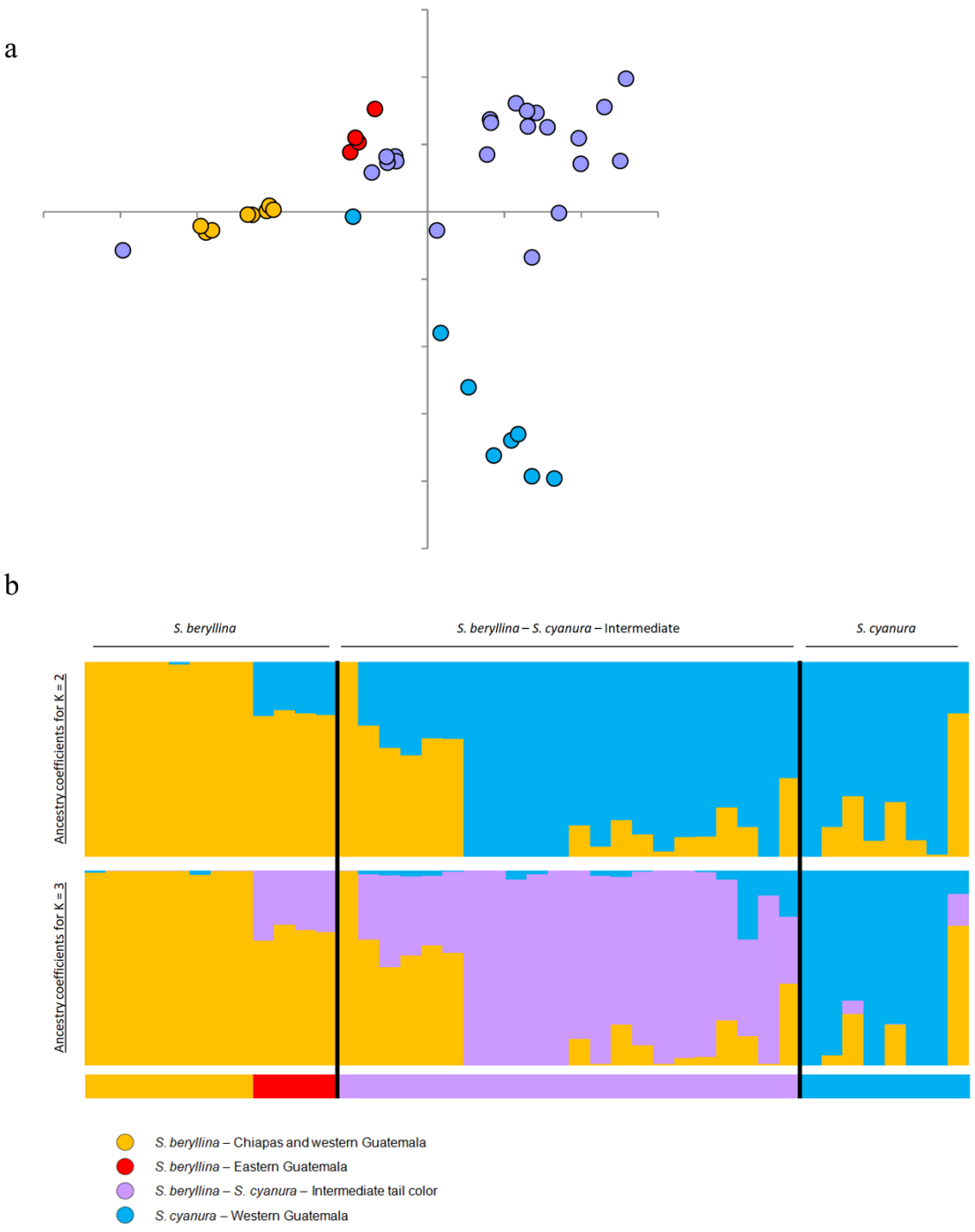


**Figure 5.** Population genetic structure of the northern Central America species complex *Saucerottia beryllina – S. cyanura* based on ddRAD data. A) Principal Component Analysis of components 1 and 2. Variation explained by PC1 – 4.0% and by PC2 – 3.6%. b) Ancestry analysis showing the admixture coefficients (Q-matrix) for K = 2 and K = 3. The bar below represents the geographic location of each lineage following the color legend in Figure 1.

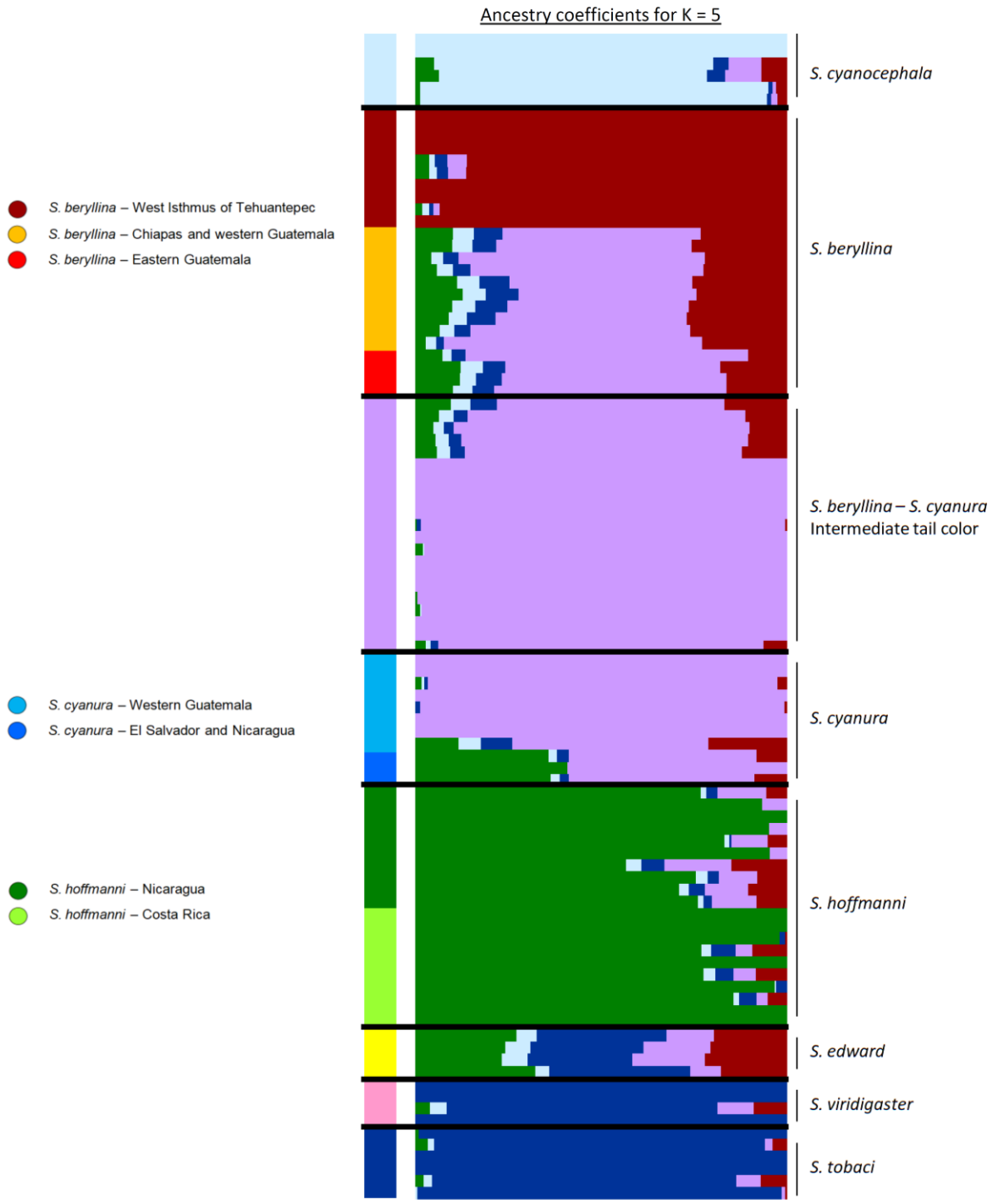


**Figure 6.** Ancestry analysis of the genus *Saucerottia* based on ddRAD data. The first column represents the geographic location of each lineage following the color legend in Figure 1. Detail on geographic location is provided for species with different intraspecific groups as detected with Principal Component Analysis. The second column shows the admixture coefficients (Q-matrix) for K = 5.

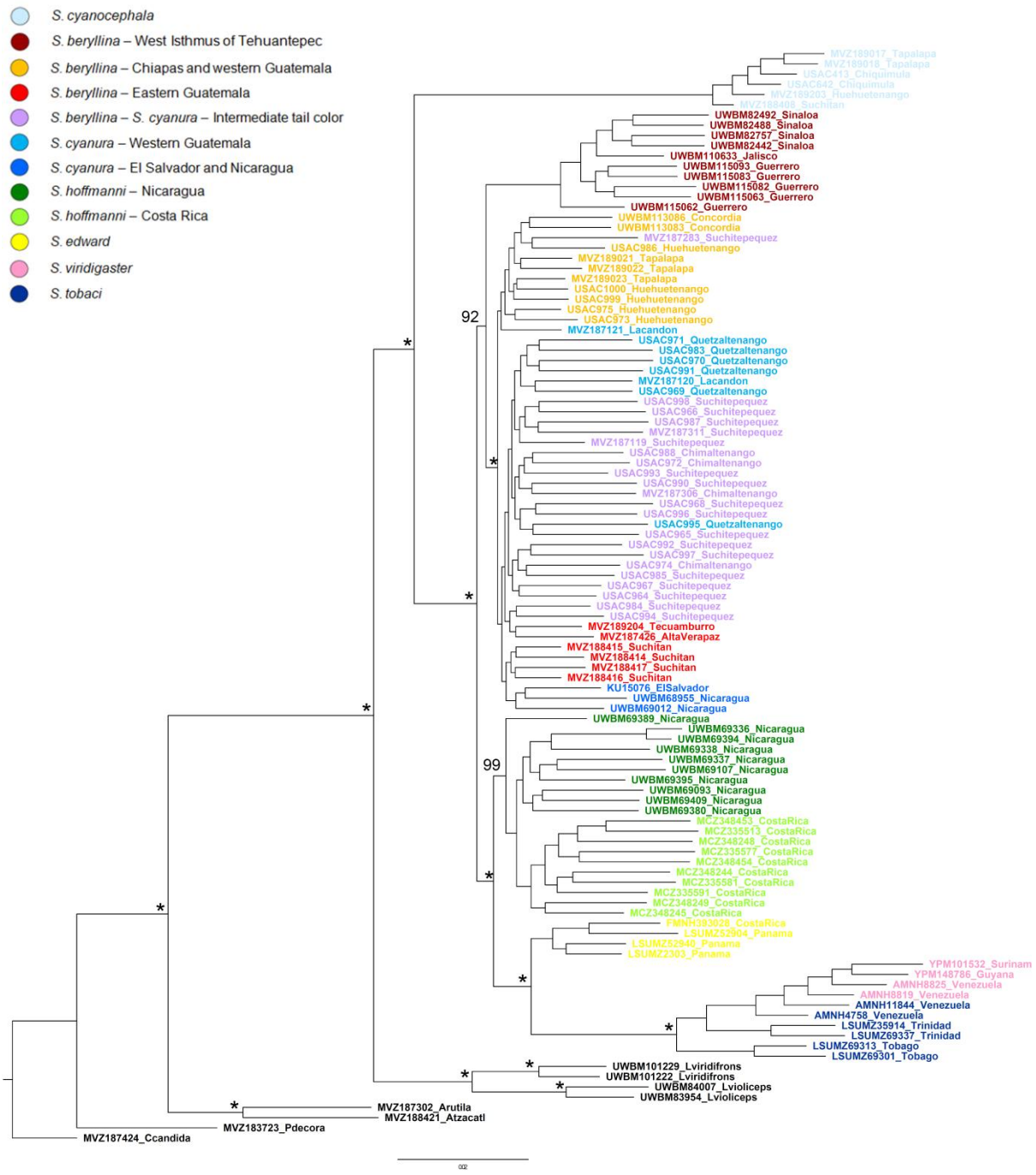


**Figure 7.** Maximum likelihood phylogeny of the genus *Saucerottia* based on ddRAD data. Node support was estimated with 100 iterations of rapid bootstrapping. Node support is provided when values are higher than 80, asterisks at nodes represent a support value of 100.

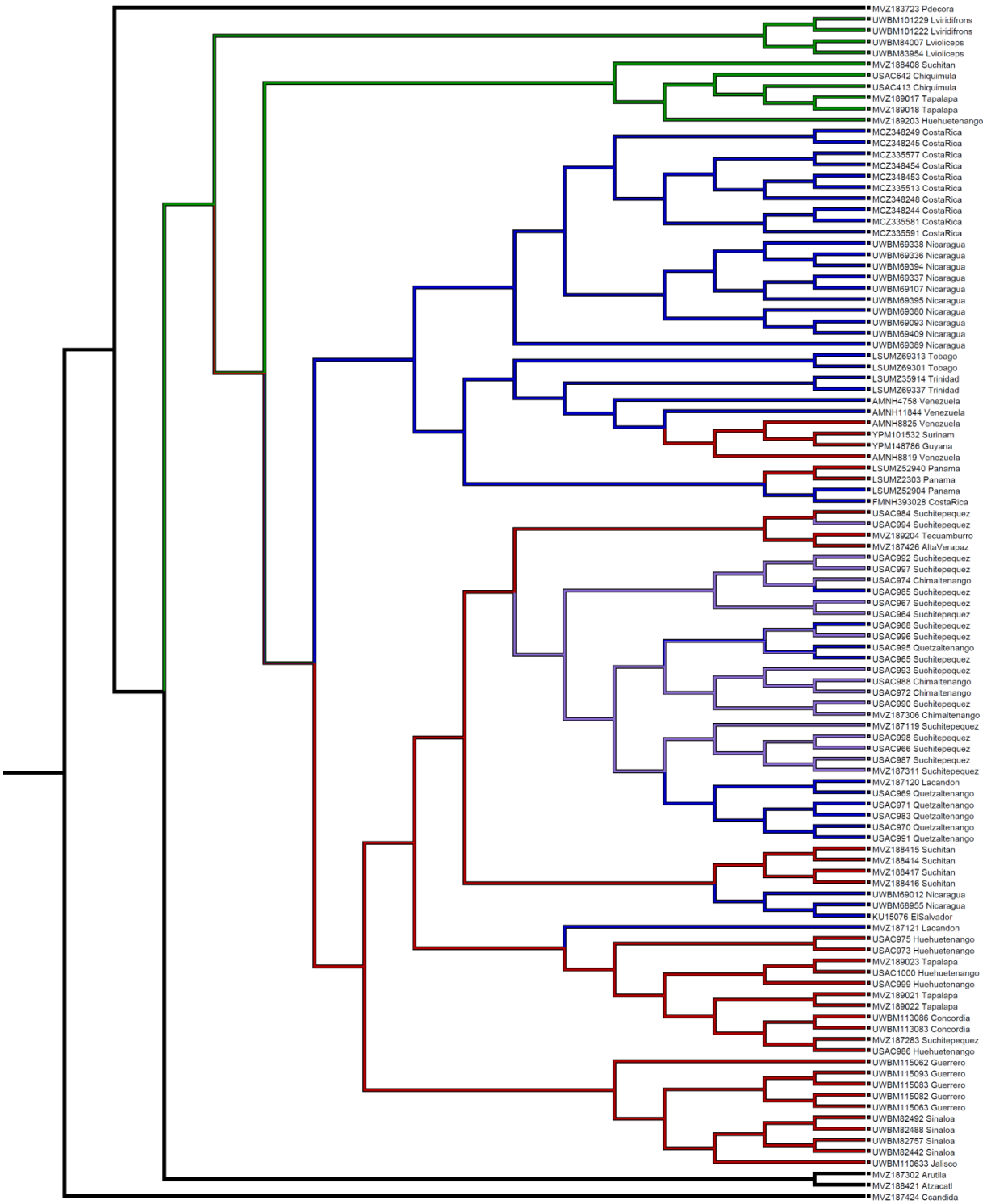


**Figure 8.** Character state reconstruction of tail coloration in *Saucerottia* hummingbirds. The ancestral state is shown as black in the phylogeny. Green, blue, and rufous tails correspond with green, blue, and red in the phylogeny, respectively. Intermediate tail color corresponds with lilac in the phylogeny.

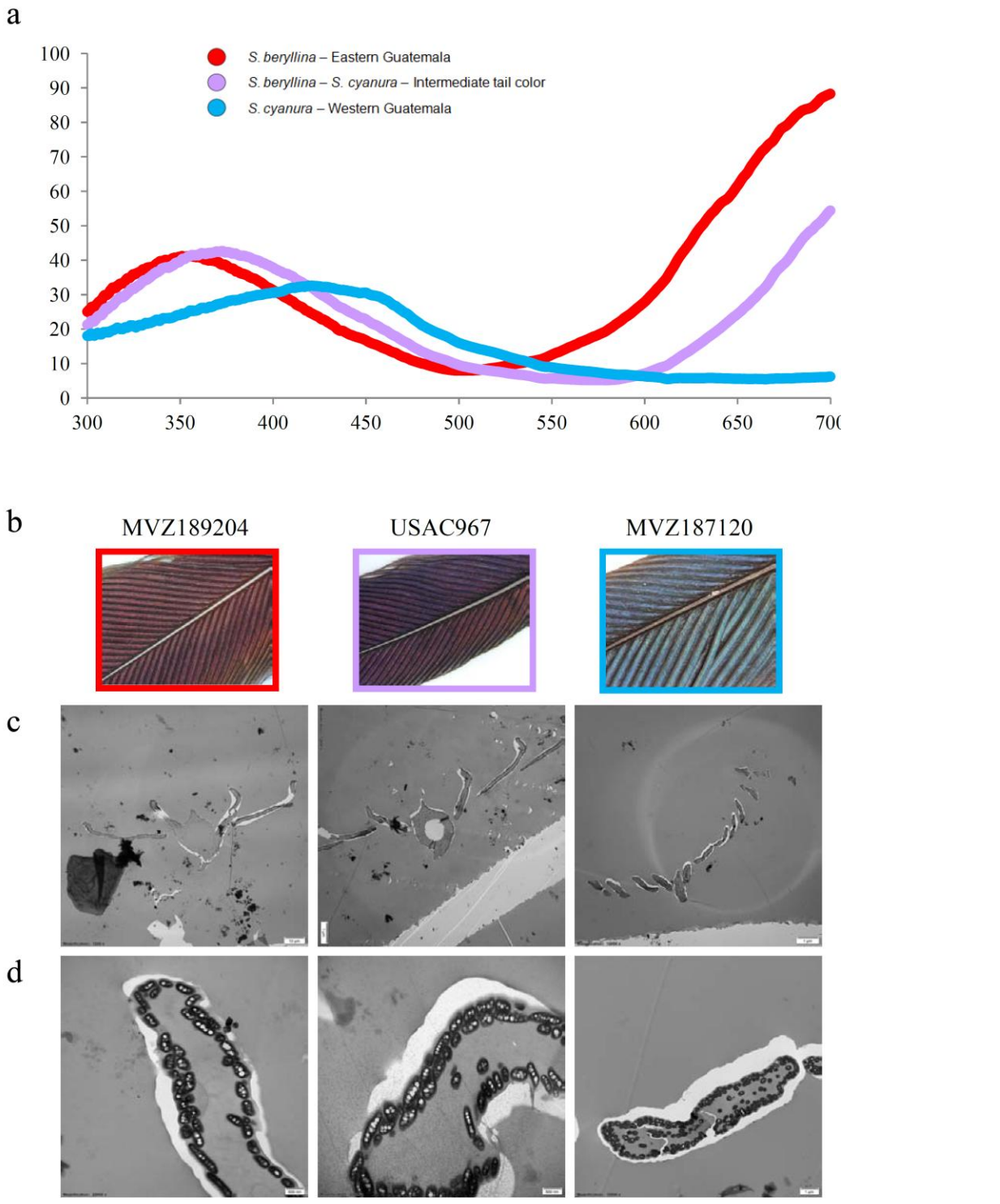


**Figure 9.** Spectrophotometry and microscopy of *Saucerottia beryllina – S. cyanura* tail feathers. a) Spectrophotometry of one tail feather from three individuals, which show contrasting reflectance patterns, x-axis – light spectrum in nanometers, y-axis – reflectance. b) Photos of the examined tail feathers. c) Microscopy showing barb shape and barbules length. d) Microscopy showing the morphology of melanosomes and their physical arrangement within the barbule.

| **Chromosome** | 1 | 1 | 2 | 3 | 3 | Z | Z |
|---|---|---|---|---|---|---|---|
| **Position** | 4,746,424 | 27,497,071 | 51,198,092 | 69,498,592 | 103,877,992 | 33,673,458 | 47,554,136 |
| **Gene** | Non-coding | Non-coding | DCLK3 | Non-coding | Non-coding | DAPK1 | FCHO2 |
| ***p* value** | 1.44871E-05 | 9.23042E-05 | 3.42645E-07 | 6.98073E-05 | 5.92721E-07 | 8.0545E-05 | 9.12293E-05 |
| | C | C | G | C | G | T | G |
| **Samples / genotypes** | T | T | A | T | A | C | A |
| MVZ189021_Tapalapa | | | | | | | |
| MVZ189022_Tapalapa | | | | | | | |
| MVZ189023_Tapalapa | | | | | | | |
| UWBM113083_Concordia | | | | | | | |
| UWBM113086_Concordia | | | | | | | |
| USAC1000_Huehuetenango | | | | | | | |
| USAC975_Huehuetenango | | | | | | | |
| USAC999_Huehuetenango | | | | | | | |
| USAC973_Huehuetenango | | | | | | | |
| USAC986_Huehuetenango | | | | | | | |
| USAC995_Quetzaltenango | | | | | | | |
| USAC970_Quetzaltenango | | | | | | | |
| USAC971_Quetzaltenango | | | | | | | |
| USAC969_Quetzaltenango | | | | | | | |
| USAC991_Quetzaltenango | | | | | | | |
| USAC983_Quetzaltenango | | | | | | | |
| MVZ187120_Lacandon | | | | | | | |

**Figure 10a.** Outlier analysis of *Saucerottia beryllina* – *Saucerottia cyanura*. Orange and blue colors represent the two homozygote states, lilac represents the heterozygote state, and white represents missing data.

| Chromosome | 2 | 3 | 3 | Z | Z |
|---|---|---|---|---|---|
| Position | 51,198,092 | 69,498,592 | 103,877,992 | 33,673,458 | 47,554,136 |
| Gene | DCLK3 | Non-coding | Non-coding | DAPK1 | FCHO2 |
| *p* value | 3.42645E-07 | 6.98073E-05 | 5.92721E-07 | 8.0545E-05 | 9.12293E-05 |
| | G | C | G | T | G |
| Samples / genotypes | A | T | A | C | A |
| UWBM82492_Sinaloa | | | | | |
| UWBM82757_Sinaloa | | | | | |
| UWBM82442_Sinaloa | | | | | |
| UWBM82488_Sinaloa | | | | | |
| UWBM110633_Jalisco | | | | | |
| UWBM115062_Guerrero | | | | | |
| UWBM115063_Guerrero | | | | | |
| UWBM115082_Guerrero | | | | | |
| UWBM115083_Guerrero | | | | | |
| UWBM115093_Guerrero | | | | | |
| MVZ187426_AltaVerapaz | | | | | |
| MVZ189204_Tecuamburro | | | | | |
| MVZ188414_Suchitan | | | | | |
| MVZ188417_Suchitan | | | | | |
| MVZ187283_Suchitepequez | | | | | |
| MVZ187119_Suchitepequez | | | | | |
| USAC964_Suchitepequez | | | | | |
| USAC993_Suchitepequez | | | | | |
| USAC967_Suchitepequez | | | | | |
| USAC984_Suchitepequez | | | | | |
| USAC987_Suchitepequez | | | | | |
| USAC966_Suchitepequez | | | | | |
| USAC992_Suchitepequez | | | | | |
| USAC997_Suchitepequez | | | | | |
| USAC998_Suchitepequez | | | | | |
| USAC994_Suchitepequez | | | | | |
| MVZ187311_Suchitepequez | | | | | |
| USAC996_Suchitepequez | | | | | |
| USAC990_Suchitepequez | | | | | |
| USAC974_Chimaltenango | | | | | |
| USAC972_Chimaltenango | | | | | |
| MVZ187306_Chimaltenango | | | | | |
| USAC988_Chimaltenango | | | | | |
| USAC968_Suchitepequez | | | | | |
| USAC965_Suchitepequez | | | | | |
| USAC985_Suchitepequez | | | | | |
| MVZ187121_Lacandon | | | | | |
| KU15076_ElSalvador | | | | | |
| UWBM68955_Nicaragua | | | | | |
| UWBM69012_Nicaragua | | | | | |

**Figure 10b.** Genotypes of *Saucerottia beryllina – S. cyanura* individuals for the outlier SNPs detected when contrasting differentiated groups from Central America. Orange and blue colors represent the two homozygote states, lilac represents the heterozygote state, and white represents missing data. The two SNPs on chromosome 1 were excluded due to missing data.

| **Chromosome** | 2 | 3 | 3 | Z | Z |
|---|---|---|---|---|---|
| **Position** | 51,198,092 | 69,498,592 | 103,877,992 | 33,673,458 | 47,554,136 |
| **Gene** | DCLK3 | Non-coding | Non-coding | DAPK1 | FCHO2 |
| ***p* value** | 3.42645E-07 | 6.98073E-05 | 5.92721E-07 | 8.0545E-05 | 9.12293E-05 |
| | G | C | G | T | G |
| **Samples / genotypes** | A | T | A | C | A |
| FMNH393028_CostaRica | | | | | |
| LSUMZ52940_Panama | | | | | |
| LSUMZ2303_Panama | | | | | |
| LSUMZ52904_Panama | | | | | |
| YPM101532_Surinam | | | | | |
| YPM148786_Guyana | | | | | |
| AMNH8819_Venezuela | | | | | |
| AMNH8825_Venezuela | | | | | |
| LSUMZ69301_Tobago | | | | | |
| LSUMZ69313_Tobago | | | | | |
| LSUMZ35914_Trinidad | | | | | |
| LSUMZ69337_Trinidad | | | | | |
| AMNH4758_Venezuela | | | | | |
| AMNH11844_Venezuela | | | | | |

**Figure 10c.** Genotypes of *Saucerottia edward*, *S. viridigaster*, and *S. tobaci* individuals for the outlier SNPs detected when contrasting differentiated *S. beryllina* and *S. cyanura* from Central America. Orange and blue colors represent the two homozygote states, lilac represents the heterozygote state, and white represents missing data. The two SNPs on chromosome 1 were excluded due to missing data.

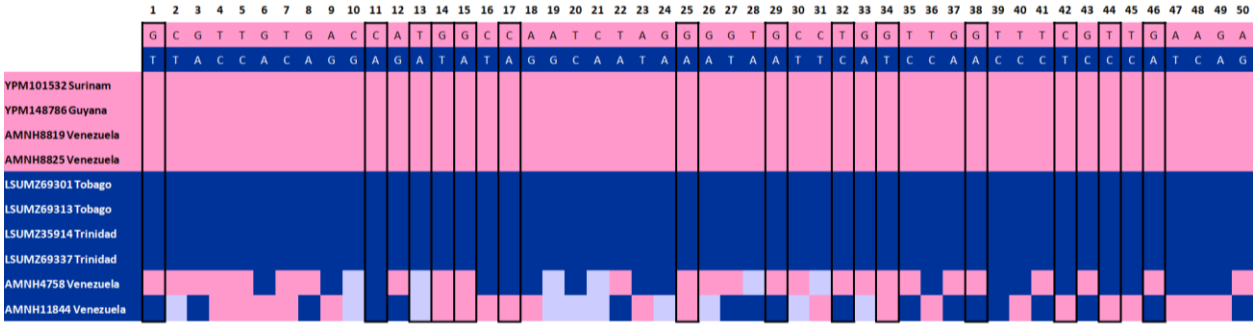


**Figure 11.** Differentially fixed SNPs between *Saucerottia viridigaster* and *S. tobaci* from Trinidad and Tobago. *Saucerottia tobaci* from Venezuela are genetically intermixed between *S. viridigaster* and allopatric *S. tobaci*. Highlighted SNPs with black boxes represent SNPs in protein-coding regions. Pink and dark blue colors represent the homozygote states, and light purple represents the heterozygote state.

**References**


Andersson, T. P., Svensson, S. P., & Karlsson, A. M. (2003). Regulation of melanosome movement by MAP kinase. Pigment Cell Research, 16(3), 215-221.

Baxter, L. L., Watkins-Chow, D. E., Pavan, W. J., & Loftus, S. K. (2019). A curated gene list for expanding the horizons of pigmentation biology. Pigment Cell & Melanoma Research, 32(3), 348-358.

Beltrán, D. F., Shultz, A. J., & Parra, J. L. (2021). Speciation rates are positively correlated with the rate of plumage color evolution in hummingbirds. Evolution.

Campagna, L., Repenning, M., Silveira, L. F., Fontana, C. S., Tubaro, P. L., & Lovette, I. J. (2017). Repeated divergent selection on pigmentation genes in a rapid finch radiation. Science Advances, 3(5), e1602404.

Catchen, J., Hohenlohe, P. A., Bassham, S., Amores, A., & Cresko, W. A. (2013). Stacks: an analysis tool set for population genomics. Molecular Ecology, 22(11), 3124-3140.

Cicero, C., & Johnson, N. K. (2001). Higher-level phylogeny of New World vireos (Aves: Vireonidae) based on sequences of multiple mitochondrial DNA genes. Molecular Phylogenetics and Evolution, 20(1), 27-40.

Clement, M., Posada, D., & Crandall, K. A. (2000). TCS: a computer program to estimate gene genealogies. Molecular Ecology, 9(10):1657-1659.

Cuthill, I. C., Allen, W. L., Arbuckle, K., Caspers, B., Chaplin, G., Hauber, M. E., ... & Caro, T. (2017). The biology of color. Science, 357(6350).

Danecek, P., Auton, A., Abecasis, G., Albers, C. A., Banks, E., DePristo, M. A., ... & 1000 Genomes Project Analysis Group. (2011). The variant call format and VCFtools. Bioinformatics, 27(15), 2156-2158.

Dickey, D. R., & Van, R. A. J. (1938). The birds of El Salvador. Chicago: Field Museum of Natural History.

Durrer, H. (1977). Schillerfarben der Vogelfeder als Evolutionsproblem: elektronenmikroskopische Untersuchung der Schillerstrukturen, ihrer Morphogenese und Analyse von Selektionsmechanismen (speziell dargelegt am Beispiel der Hühnervögel). Fretz.

Eliason, C. M., Maia, R., Parra, J. L., & Shawkey, M. D. (2020). Signal evolution and morphological complexity in hummingbirds (Aves: Trochilidae). Evolution, 74(2), 447-458.

Fogelholm, J. (2020). Genomics and Transcriptomics of Behaviour and Plumage Colouration (Vol. 2073). Linköping University Electronic Press.

Frichot, E., & François, O. (2015). LEA: An R package for landscape and ecological association studies. Methods in Ecology and Evolution, 6(8), 925-929.

Frichot, E., Mathieu, F., Trouillon, T., Bouchard, G., & François, O. (2014). Fast and efficient estimation of individual ancestry coefficients. Genetics, 196(4), 973-983.

Funk, E. R., & Taylor, S. A. (2019). High-throughput sequencing is revealing genetic associations with avian plumage color. The Auk, 136(4), ukz048.

Greenewalt, C. H., Brandt, W., & Friel, D. D. (1960). Iridescent colors of hummingbird feathers. JOSA, 50(10), 1005-1013.

Harris, R. B., Irwin, K., Jones, M. R., Laurent, S., Barrett, R. D., Nachman, M. W., ... & Pfeifer, S. P. (2020). The population genetics of crypsis in vertebrates: recent insights from mice, hares, and lizards. Heredity, 124(1), 1-14.

Hill, G. E., & McGraw. (2006). Bird coloration: mechanisms and measurements (Vol. 1). Harvard University Press.
Howell, S. N., & Webb, S. (1995). A guide to the birds of Mexico and northern Central America. Oxford University Press.
Hubbard, J. K., Uy, J. A. C., Hauber, M. E., Hoekstra, H. E., & Safran, R. J. (2010). Vertebrate pigmentation: from underlying genes to adaptive function. Trends in Genetics, 26(5), 231-239.
Jiménez, R. A. (2011). Diversidad morfológica y genética del Colibrí de Berilo (*Amazilia beryllina*) y el Colibrí Coliazul (*Amazilia cyanura*) en Guatemala: ¿hibridación o variaciones intraespecíficas? Tesis de Licenciatura, Universidad de San Carlos de Guatemala.
Jiménez, R. A., & Ornelas, J. F. (2016). Historical and current introgression in a Mesoamerican hummingbird species complex: a biogeographic perspective. PeerJ, 4, e1556.
Jombart, T. (2008). adegenet: a R package for the multivariate analysis of genetic markers. Bioinformatics, 24(11), 1403-1405.
Kardos, M., Husby, A., McFarlane, S. E., Qvarnström, A., & Ellegren, H. (2016). Whole-genome resequencing of extreme phenotypes in collared flycatchers highlights the difficulty of detecting quantitative trait loci in natural populations. Molecular Ecology Resources, 16(3), 727-741.
Kulp, F. B., D'Alba, L., Shawkey, M. D., & Clarke, J. A. (2018). Keratin nanofiber distribution and feather microstructure in penguins. The Auk: Ornithological Advances, 135(3), 777-787.
Leigh, J. W., & Bryant, D. (2015). popart: full-feature software for haplotype network construction. Methods in Ecology and Evolution, 6(9), 1110-1116.
Li, H., & Durbin, R. (2009). Fast and accurate short read alignment with Burrows–Wheeler transform. Bioinformatics, 25(14), 1754-1760.
Li, H., Handsaker, B., Wysoker, A., Fennell, T., Ruan, J., Homer, N., ... & Durbin, R. (2009). The sequence alignment/map format and SAMtools. Bioinformatics, 25(16), 2078-2079.
Maddison, W. P. and D.R. Maddison. 2021. Mesquite: a modular system for evolutionary analysis. Version 3.70 http://www.mesquiteproject.org
Mason, N. A., & Bowie, R. C. (2020). Plumage patterns: Ecological functions, evolutionary origins, and advances in quantification. The Auk, 137(4), ukaa060.
Martins, H., Caye, K., Luu, K., Blum, M. G., & François, O. (2016). Identifying outlier loci in admixed and in continuous populations using ancestral population differentiation statistics. Molecular Ecology, 25(20), 5029-5042.
McCoy, D. E., & Prum, R. O. (2019). Convergent evolution of super black plumage near bright color in 15 bird families. Journal of Experimental Biology, 222(18), jeb208140.
McGuire, J. A., Witt, C. C., Remsen Jr, J. V., Corl, A., Rabosky, D. L., Altshuler, D. L., & Dudley, R. (2014). Molecular phylogenetics and the diversification of hummingbirds. Current Biology, 24(8), 910-916.
Merwin, J. T., Seeholzer, G. F., & Smith, B. T. (2020). Macroevolutionary bursts and constraints generate a rainbow in a clade of tropical birds. BMC Evolutionary Biology, 20(1), 1-19.
Ornelas, J. F., González, C., de los Monteros, A. E., Rodríguez-Gómez, F., & García-Feria, L. M. (2014). In and out of Mesoamerica: temporal divergence of *Amazilia* hummingbirds pre-dates the orthodox account of the completion of the Isthmus of Panama. Journal of Biogeography, 41(1), 168-181.

Ornelas, J. F., González, C., Hernández-Baños, B. E., & García-Moreno, J. (2016). Molecular and iridescent feather reflectance data reveal recent genetic diversification and phenotypic differentiation in a cloud forest hummingbird. Ecology and Evolution, 6(4), 1104-1127.
Palacios, D. C. (2020). Evolution, speciation, and genomics of the andean hummingbirds: *Coeligena bonapartei* and *Coeligena helianthea* (Doctoral dissertation, Uniandes).
Palacios, C., García-R, S., Parra, J. L., Cuervo, A. M., Stiles, F. G., McCormack, J. E., & Cadena, C. D. (2019). Shallow genetic divergence and distinct phenotypic differences between two Andean hummingbirds: Speciation with gene flow? The Auk, 136(4), ukz046.
Peterson, B. K., Weber, J. N., Kay, E. H., Fisher, H. S., & Hoekstra, H. E. (2012). Double digest RADseq: an inexpensive method for de novo SNP discovery and genotyping in model and non-model species. PloS one, 7(5), e37135.
Price-Waldman, R., & Stoddard, M. C. (2021). Avian Coloration Genetics: Recent Advances and Emerging Questions. Journal of Heredity.
Purcell, S., Neale, B., Todd-Brown, K., Thomas, L., Ferreira, M. A., Bender, D., ... & Sham, P. C. (2007). PLINK: a tool set for whole-genome association and population-based linkage analyses. The American Journal of Human Genetics, 81(3), 559-575.
Reiner, O., Coquelle, F. M., Peter, B., Levy, T., Kaplan, A., Sapir, T., ... & Bergmann, S. (2006). The evolving doublecortin (DCX) superfamily. BMC Genomics, 7(1), 1-16.
Ridgway, R. (1911). The birds of North and Middle America. Bulletin of the United States National Museum, 50(5), 1-964.
Rodríguez-Gómez, F., Gutiérrez-Rodríguez, C., & Ornelas, J. F. (2013). Genetic, phenotypic and ecological divergence with gene flow at the Isthmus of Tehuantepec: the case of the azure-crowned hummingbird (*Amazilia cyanocephala*). Journal of Biogeography, 40(7), 1360-1373.
Rubenstein, D. R., Corvelo, A., MacManes, M. D., Maia, R., Narzisi, G., Rousaki, A., ... & Solomon, J. (2021). Feather Gene Expression Elucidates the Developmental Basis of Plumage Iridescence in African Starlings. Journal of Heredity.
Saranathan, V., & Finet, C. (2021). Cellular and developmental basis of avian structural coloration. Current Opinion in Genetics & Development, 69, 56-64.
Shawkey, M. D., & D'Alba, L. (2017). Interactions between colour-producing mechanisms and their effects on the integumentary colour palette. Philosophical Transactions of the Royal Society B: Biological Sciences, 372(1724), 20160536.
Stamatakis, A. (2014). RAxML version 8: a tool for phylogenetic analysis and post-analysis of large phylogenies. Bioinformatics, 30(9), 1312-1313.
Stiles, F. G., Remsen, J. J., & McGuire, J. A. (2017). The generic classification of the Trochilini (Aves: Trochilidae): reconciling taxonomy with phylogeny. Zootaxa, 4353(3), 401-424.
Stoddard, M. C., & Prum, R. O. (2011). How colorful are birds? Evolution of the avian plumage color gamut. Behavioral Ecology, 22(5), 1042-1052.
Szarmach, S. J., Brelsford, A., Witt, C. C., & Toews, D. P. (2021). Comparing divergence landscapes from reduced-representation and whole genome resequencing in the yellow-rumped warbler (Setophaga coronata) species complex. Molecular Ecology.
Toews, D. P., Taylor, S. A., Vallender, R., Brelsford, A., Butcher, B. G., Messer, P. W., & Lovette, I. J. (2016). Plumage genes and little else distinguish the genomes of hybridizing warblers. Current Biology, 26(17), 2313-2318.
Wagner, H. O. (1954). Versuch einer Analyse der Kolibribalz. Zeitschrift für Tierpsychologie, 11(2), 182-212.

Weller, A.A. (2021). Snowy-bellied Hummingbird (*Saucerottia edward*), version 1.1. In Birds of the World (J. del Hoyo, A. Elliott, J. Sargatal, D. A. Christie, and E. de Juana, Editors). Cornell Lab of Ornithology, Ithaca, NY, USA.
Weller, A.A., P. F. D. Boesman, and H. F. Greeney (2021a). Blue-vented Hummingbird (*Saucerottia hoffmanni*), version 1.1. In Birds of the World (S. M. Billerman, B. K. Keeney, P. G. Rodewald, and T. S. Schulenberg, Editors). Cornell Lab of Ornithology, Ithaca, NY, USA.
Weller, A.A., P. F. D. Boesman, and H. F. Greeney (2021b). Green-bellied Hummingbird (*Saucerottia viridigaster*), version 1.1. In Birds of the World (H. F. Greeney, Editor). Cornell Lab of Ornithology, Ithaca, NY, USA.
Weller, A.A., P. F. D. Boesman, and G. M. Kirwan (2021c). Copper-rumped Hummingbird (*Saucerottia tobaci*), version 1.1. In Birds of the World (J. del Hoyo, A. Elliott, J. Sargatal, D. A. Christie, and E. de Juana, Editors). Cornell Lab of Ornithology, Ithaca, NY, USA.
Winger, B. M., & Bates, J. M. (2015). The tempo of trait divergence in geographic isolation: Avian speciation across the Marañón Valley of Peru. Evolution, 69(3), 772-787.

**Supplementary tables and figures**

**Table S1.** Species names, voucher information, and localities of origin of the specimens examined genetically in this study. Museum abbreviations used in voucher numbers: MVZ = Museum of Vertebrate Zoology, University of California, Berkeley; USAC = Escuela de Biología, Universidad de San Carlos de Guatemala; AMNH = American Museum of Natural History; FMNH = Field Museum of Natural History; KU = Kansas University, Natural History Museum; UWBM = Burke Museum of Natural History and Culture; LSUMZ = Louisiana State University Museum of Natural Science; MCZ = Museum of Comparative Zoology, Harvard University; YPM = Yale Peabody Museum, Yale University. MX = México, GT = Guatemala, ES = El Salvador, NI = Nicaragua, CR = Costa Rica, PA = Panamá, CO = Colombia, VE = Venezuela, GU = Guyana, SU = Surinam, TT = Trinidad and Tobago, JA = Jamaica, USA = United States of America.

| Species | Museum | Voucher number | Locality | Latitude | Longitude |
|---|---|---|---|---|---|
| *Saucerottia cyanocephala cyanocephala* | LSUMZ | 19260 | MX: GenBank KJ602167 | | |
| *Saucerottia cyanocephala cyanocephala* | MVZ | 189017 | MX: Chiapas, Tapalapa | 17.187556° | -93.123174° |
| *Saucerottia cyanocephala cyanocephala* | MVZ | 189018 | MX: Chiapas, Tapalapa | 17.187556° | -93.123174° |
| *Saucerottia cyanocephala cyanocephala* | MVZ | 189203 | GT: Huehuetenango, Soloma | 15.68203° | -91.22838° |
| *Saucerottia cyanocephala cyanocephala* | MVZ | 187420 | GT: Quiché, Uspantán | 15.46773° | -90.777083° |
| *Saucerottia cyanocephala cyanocephala* | MVZ | 188408 | GT: Jutiapa, Volcán Suchitán | 14.40648° | -89.780126° |
| *Saucerottia cyanocephala cyanocephala* | MVZ | 188410 | GT: Jutiapa, Volcán Suchitán | 14.40648° | -89.780126° |
| *Saucerottia cyanocephala guatemalensis* | USAC | 413 | GT: Chiquimula, Bosque El Gigante | 14.843528° | -89.669561° |
| *Saucerottia cyanocephala guatemalensis* | USAC | 642 | GT: Chiquimula, Bosque El Gigante | 14.843528° | -89.669561° |
| *Saucerottia hoffmanni* | UWBM | 69093 | NI: Granada, Mombacho | 11.834167° | -85.995° |
| *Saucerottia hoffmanni* | UWBM | 69107 | NI: Granada, Mombacho | 11.834167° | -85.995° |
| *Saucerottia hoffmanni* | UWBM | 69336 | NI: Granada, Mombacho | 11.834167° | -85.995° |
| *Saucerottia hoffmanni* | UWBM | 69337 | NI: Granada, Mombacho | 11.834167° | -85.995° |
| *Saucerottia hoffmanni* | UWBM | 69338 | NI: Granada, Mombacho | 11.834167° | -85.995° |
| *Saucerottia hoffmanni* | UWBM | 69380 | NI: Granada, Mombacho | 11.834167° | -85.995° |
| *Saucerottia hoffmanni* | UWBM | 69389 | NI: Granada, Mombacho | 11.834167° | -85.995° |
| *Saucerottia hoffmanni* | UWBM | 69394 | NI: Granada, Mombacho | 11.834167° | -85.995° |
| *Saucerottia hoffmanni* | UWBM | 69395 | NI: Granada, Mombacho | 11.834167° | -85.995° |
| *Saucerottia hoffmanni* | UWBM | 69409 | NI: Granada, Mombacho | 11.834167° | -85.995° |
| *Saucerottia hoffmanni* | MCZ | 335513 | CR: Guanacaste, Área de Conservación | 10.839444° | -85.618056° |
| *Saucerottia hoffmanni* | MCZ | 335577 | CR: Guanacaste, Área de Conservación | 10.839444° | -85.618056° |
| *Saucerottia hoffmanni* | MCZ | 335581 | CR: Guanacaste, Área de Conservación | 10.839444° | -85.618056° |
| *Saucerottia hoffmanni* | MCZ | 335591 | CR: Guanacaste, Área de Conservación | 10.839444° | -85.618056° |
| *Saucerottia hoffmanni* | MCZ | 348244 | CR: Guanacaste, Área de Conservación | 10.839444° | -85.618056° |
| *Saucerottia hoffmanni* | MCZ | 348245 | CR: Guanacaste, Área de Conservación | 10.839444° | -85.618056° |
| *Saucerottia hoffmanni* | MCZ | 348248 | CR: Guanacaste, Área de Conservación | 10.839444° | -85.618056° |
| *Saucerottia hoffmanni* | MCZ | 348249 | CR: Guanacaste, Área de Conservación | 10.839444° | -85.618056° |
| *Saucerottia hoffmanni* | MCZ | 348453 | CR: Guanacaste, Área de Conservación | 10.839444° | -85.618056° |
| *Saucerottia hoffmanni* | MCZ | 348454 | CR: Guanacaste, Área de Conservación | 10.839444° | -85.618056° |

| | | | | | |
|---|---|---|---|---|---|
| *Saucerottia beryllina viola* | UWBM | 82442 | MX: Sinaloa, Choix | 26.820000° | -108.2° |
| *Saucerottia beryllina viola* | UWBM | 82488 | MX: Sinaloa, Choix | 26.820000° | -108.2° |
| *Saucerottia beryllina viola* | UWBM | 82492 | MX: Sinaloa, Choix | 26.820000° | -108.2° |
| *Saucerottia beryllina viola* | UWBM | 82751 | MX: Sinaloa, Choix | 26.820000° | -108.2° |
| *Saucerottia beryllina viola* | UWBM | 82757 | MX: Sinaloa, Choix | 26.820000° | -108.2° |
| *Saucerottia beryllina viola* | UWBM | 110633 | MX: Jalisco | 21.828333° | -103.89° |
| *Saucerottia beryllina viola* | UWBM | 115119 | MX: Michoacán, Nuevo Parangaricutiro | 19.385333° | -102.24217° |
| *Saucerottia beryllina beryllina* | UWBM | 115062 | MX: Guerrero, Chilpancingo de los Bravos | 17.395500° | -99.633667° |
| *Saucerottia beryllina beryllina* | UWBM | 115063 | MX: Guerrero, Chilpancingo de los Bravos | 17.395500° | -99.633667° |
| *Saucerottia beryllina beryllina* | UWBM | 115082 | MX: Guerrero, Chilpancingo de los Bravos | 17.395500° | -99.633667° |
| *Saucerottia beryllina beryllina* | UWBM | 115083 | MX: Guerrero, Chilpancingo de los Bravos | 17.395500° | -99.633667° |
| *Saucerottia beryllina beryllina* | UWBM | 115093 | MX: Guerrero, Chilpancingo de los Bravos | 17.395500° | -99.633667° |
| *Saucerottia beryllina beryllina* | FMNH | 394217 | MX: Oaxaca – GenBank KJ602161 | 16.104167° | -97.083056° |
| *Saucerottia beryllina lichtensteini* | MVZ | 189021 | MX: Chiapas, Tapalapa | 17.187556° | -93.123174° |
| *Saucerottia beryllina lichtensteini* | MVZ | 189022 | MX: Chiapas, Tapalapa | 17.187556° | -93.123174° |
| *Saucerottia beryllina lichtensteini* | MVZ | 189023 | MX: Chiapas, Tapalapa | 17.187556° | -93.123174° |
| *Saucerottia beryllina sumichrasti* | UWBM | 113083 | MX: Chiapas, Concordia | 15.8772° | -93.0193° |
| *Saucerottia beryllina sumichrasti* | UWBM | 113086 | MX: Chiapas, Concordia | 15.8772° | -93.0193° |
| *Saucerottia beryllina devillei* | USAC | 1000 | GT: Huehuetenango, Todos Santos Cuchumatán | 15.59093° | -91.68322° |
| *Saucerottia beryllina devillei* | USAC | 975 | GT: Huehuetenango, Todos Santos Cuchumatán | 15.59093° | -91.68322° |
| *Saucerottia beryllina devillei* | USAC | 999 | GT: Huehuetenango, Todos Santos Cuchumatán | 15.59093° | -91.68322° |
| *Saucerottia beryllina devillei* | USAC | 973 | GT: Huehuetenango, Todos Santos Cuchumatán | 15.59093° | -91.68322° |
| *Saucerottia beryllina devillei* | USAC | 986 | GT: Huehuetenango, Todos Santos Cuchumatán | 15.59093° | -91.68322° |
| *Saucerottia beryllina devillei* | MVZ | 187283 | GT: Suchitepéquez, Patulul | 14.546089° | -91.147359° |
| *Saucerottia beryllina devillei* | MVZ | 187426 | GT: Alta Verapaz, San Pedro Carchá | 15.613624° | -90.273532° |
| *Saucerottia beryllina devillei* | MVZ | 189204 | GT: Santa Rosa, Volcán Tecuamburro | 14.15393° | -90.41051° |
| *Saucerottia beryllina devillei* | MVZ | 188414 | GT: Jutiapa, Volcán Suchitán | 14.40648° | -89.780126° |
| *Saucerottia beryllina devillei* | MVZ | 188415 | GT: Jutiapa, Volcán Suchitán | 14.40648° | -89.780126° |
| *Saucerottia beryllina devillei* | MVZ | 188416 | GT: Jutiapa, Volcán Suchitán | 14.40648° | -89.780126° |
| *Saucerottia beryllina devillei* | MVZ | 188417 | GT: Jutiapa, Volcán Suchitán | 14.40648° | -89.780126° |
| *Saucerottia beryllina devillei* | MVZ | 188418 | GT: Jutiapa, Volcán Suchitán | 14.40648° | -89.780126° |
| *S. b. devillei* x *S. c. guatemalae* | MVZ | 187119 | GT: Suchitepéquez, Patulul | 14.55668° | -91.16538° |
| *S. b. devillei* x *S. c. guatemalae* | USAC | 964 | GT: Suchitepéquez, Patulul | 14.54408° | -91.1422° |
| *S. b. devillei* x *S. c. guatemalae* | USAC | 993 | GT: Suchitepéquez, Patulul | 14.54408° | -91.1422° |
| *S. b. devillei* x *S. c. guatemalae* | USAC | 967 | GT: Suchitepéquez, Patulul | 14.54408° | -91.1422° |
| *S. b. devillei* x *S. c. guatemalae* | USAC | 984 | GT: Suchitepéquez, Patulul | 14.54408° | -91.1422° |
| *S. b. devillei* x *S. c. guatemalae* | USAC | 987 | GT: Suchitepéquez, Patulul | 14.54408° | -91.1422° |
| *S. b. devillei* x *S. c. guatemalae* | USAC | 966 | GT: Suchitepéquez, Patulul | 14.54408° | -91.1422° |
| *S. b. devillei* x *S. c. guatemalae* | USAC | 992 | GT: Suchitepéquez, Patulul | 14.54408° | -91.1422° |
| *S. b. devillei* x *S. c. guatemalae* | USAC | 997 | GT: Suchitepéquez, Patulul | 14.54408° | -91.1422° |
| *S. b. devillei* x *S. c. guatemalae* | USAC | 998 | GT: Suchitepéquez, Patulul | 14.54408° | -91.1422° |
| *S. b. devillei* x *S. c. guatemalae* | USAC | 994 | GT: Suchitepéquez, Patulul | 14.54408° | -91.1422° |
| *S. b. devillei* x *S. c. guatemalae* | MVZ | 187311 | GT: Suchitepéquez, Patulul | 14.54408° | -91.1422° |

| | | | | | |
|---|---|---|---|---|---|
| *S. b. devillei* x *S. c. guatemalae* | USAC | 996 | GT: Suchitepéquez, Patulul | 14.54408° | -91.1422° |
| *S. b. devillei* x *S. c. guatemalae* | USAC | 990 | GT: Suchitepéquez, Patulul | 14.54408° | -91.1422° |
| *S. b. devillei* x *S. c. guatemalae* | USAC | 974 | GT: Chimaltenango, San Pedro Yepocapa | 14.443315° | -91.064975° |
| *S. b. devillei* x *S. c. guatemalae* | USAC | 972 | GT: Chimaltenango, San Pedro Yepocapa | 14.443315° | -91.064975° |
| *S. b. devillei* x *S. c. guatemalae* | MVZ | 187306 | GT: Chimaltenango, San Pedro Yepocapa | 14.443315° | -91.064975° |
| *S. b. devillei* x *S. c. guatemalae* | USAC | 988 | GT: Chimaltenango, San Pedro Yepocapa | 14.443315° | -91.064975° |
| *S. b. devillei* x *S. c. cyanura* | KU | 14987 | ES: Usulután | 13.17595° | -88.23085° |
| *Saucerottia cyanura guatemalae* | USAC | 968 | GT: Suchitepéquez, Patulul | 14.54408° | -91.1422° |
| *Saucerottia cyanura guatemalae* | USAC | 965 | GT: Suchitepéquez, Patulul | 14.54408° | -91.1422° |
| *Saucerottia cyanura guatemalae* | USAC | 985 | GT: Suchitepéquez, Patulul | 14.54408° | -91.1422° |
| *Saucerottia cyanura guatemalae* | USAC | 995 | GT: Quetzaltenango, El Palmar | 14.67244° | -91.60835° |
| *Saucerottia cyanura guatemalae* | USAC | 970 | GT: Quetzaltenango, El Palmar | 14.67244° | -91.60835° |
| *Saucerottia cyanura guatemalae* | USAC | 971 | GT: Quetzaltenango, El Palmar | 14.67244° | -91.60835° |
| *Saucerottia cyanura guatemalae* | USAC | 969 | GT: Quetzaltenango, El Palmar | 14.67244° | -91.60835° |
| *Saucerottia cyanura guatemalae* | USAC | 991 | GT: Quetzaltenango, El Palmar | 14.67244° | -91.60835° |
| *Saucerottia cyanura guatemalae* | USAC | 983 | GT: Quetzaltenango, El Palmar | 14.67244° | -91.60835° |
| *Saucerottia cyanura guatemalae* | MVZ | 187120 | GT: Quetzaltenango, Volcán Lacandón | 14.81263° | -91.7424° |
| *Saucerottia cyanura guatemalae* | MVZ | 187121 | GT: Quetzaltenango, Volcán Lacandón | 14.81263° | -91.7424° |
| *Saucerottia cyanura cyanura* | KU | 15076 | ES: Usulután | 13.17595° | -88.23085° |
| *Saucerottia cyanura cyanura* | UWBM | 68955 | NI: Managua | 11.983333° | -86.26° |
| *Saucerottia cyanura cyanura* | UWBM | 69012 | NI: Chinandega, Volcán Casita | 12.693333° | -86.958333° |
| *Saucerottia edward niveoventer* | FMNH | 393028 | CR: Puntarenas, Potrero Grande | 9.014722° | -83.176111° |
| *Saucerottia edward niveoventer* | LSUMZ | 52904 | PA: Coclé, Cascajal | 8.716944° | -80.4675° |
| *Saucerottia edward edward* | LSUMZ | 2303 | PA: Darién, Cerro Pirré | 7.933333° | -77.702222° |
| *Saucerottia edward edward* | LSUMZ | 52940 | PA: Darién, Puerto Piña | 7.593611° | -78.1775° |
| *Saucerottia saucerottei* | | | CO: GenBank GU167205 | | |
| *Saucerottia saucerottei* | | | CO: GenBank KJ602171 | | |
| *Saucerottia castaneiventris* | | | CO: GenBank KJ602165 | | |
| *Saucerottia viridigaster cupreicauda* | YPM | 101532 | SU: Tafelberg, Augustus Creek Waterfall | 3.9300° | -56.1883° |
| *Saucerottia viridigaster cupreicauda* | YPM | 148786 | GU: Potaro-Siparuni, Kaibarupai | 5.049° | -59.969° |
| *Saucerottia viridigaster laireti* | AMNH | DOT-8819 | VE: Amazonas | 1.225° | -64.7482° |
| *Saucerottia viridigaster laireti* | AMNH | DOT-8825 | VE: Amazonas | 1.55° | -65.23° |
| *Saucerottia viridigaster laireti* | LSUMZ | 7587 | VE: Amazonas – GenBank GU167207 | 2.374167° | -65.137222° |
| *Saucerottia viridigaster laireti* | LSUMZ | 7490 | VE: Amazonas – GenBank EU42526 | 2.374167° | -65.137222° |
| *Saucerottia tobaci tobaci* | LSUMZ | 69301 | TT: Tobago | 11.2361° | -60.6989° |
| *Saucerottia tobaci tobaci* | LSUMZ | 69313 | TT: Tobago | 11.2361° | -60.6989° |
| *Saucerottia tobaci erythronotos* | LSUMZ | 35914 | TT: Trinidad | 10.4556° | -61.2761° |
| *Saucerottia tobaci erythronotos* | LSUMZ | 69337 | TT: Trinidad | 10.4556° | -61.2761° |
| *Saucerottia tobaci erythronotos* | LSUMZ | 35895 | TT: GenBank KJ602173 | 10.4556° | -61.2761° |
| *Saucerottia tobaci caurensis* | AMNH | DOT-4758 | VE: Bolívar | 5.9697° | -62.5394° |
| *Saucerottia tobaci caurensis* | AMNH | DOT-11844 | VE: Bolívar | 5.8094° | -63.7458° |
| *Cynanthus canivetii* | MVZ | 187264 | GT: Chiquimula | | |
| *Basilinna leucotis* | MVZ | 187313 | GT: Chiquimula | | |

| | | | | | |
|---|---|---|---|---|---|
| *Pampa rufa* | MVZ | 187269 | GT: Suchitepéquez | | |
| *Thalurania colombica* | MVZ | 188378 | GT: Izabal | | |
| *Eupherusa eximia* | MVZ | 187637 | GT: Huehuetenango | | |
| *Trochilus polytmus* | MVZ | 183598 | JA: Portland Parish | | |
| *Leucolia violiceps* | UWBM | 83954 | MX: Sinaloa | | |
| *Leucolia violiceps* | UWBM | 84007 | MX: Sinaloa | | |
| *Leucolia viridifrons* | UWBM | 101222 | MX: Chiapas | | |
| *Leucolia viridifrons* | UWBM | 101229 | MX: Chiapas | | |
| *Amazilia rutila* | MVZ | 187302 | GT: Suchitepéquez | | |
| *Amazilia yucatanensis* | MVZ | 176503 | USA: Texas | | |
| *Amazilia tzacatl* | MVZ | 188421 | GT: Izabal | | |
| *Polyerata decora* | MVZ | 183723 | CR: Heredia | | |
| *Chlorestes candida* | MVZ | 187424 | GT: Alta Verapaz | | |

**Table S2.** Samples with more than 30% missing data that were excluded from the different datasets and downstream analyses.

| Dataset | Sample |
|---|---|
| (i) *Saucerottia* + outgroup | MVZ187420_Quiche |
| | MVZ188410_Suchitan |
| | UWBM82751_Sinaloa |
| | UWBM115119_Michoacan |
| | MVZ188418_Suchitan |
| | KU14987_ElSalvador |
| | MVZ187264_Ccanivetii |
| | MVZ187313_Bleucotis |
| | MVZ187269_Prufa |
| | MVZ188378_Tcolombica |
| | MVZ187637_Eeximia |
| | MVZ183598_Tpolytmus |
| | MVZ176503_Ayucatanesis |
| (ii) *Saucerottia* | MVZ187420_Quiche |
| | MVZ188410_Suchitan |
| | UWBM82751_Sinaloa |
| | UWBM115119_Michoacan |
| | MVZ189023_Tapalapa |
| | MVZ188415_Suchitan |
| | MVZ188416_Suchitan |
| | MVZ188418_Suchitan |
| | KU14987_ElSalvador |
| (iii) *Saucerottia beryllina – S. cyanura* | MVZ189023_Tapalapa |
| | USAC975_Huehuetenango |
| | MVZ188415_Suchitan |
| | MVZ188416_Suchitan |
| | MVZ188418_Suchitan |
| | KU14987_ElSalvador |
| (iv) *Allopatric Saucerottia beryllina – S. cyanura* | None |
| (v) *Saucerottia edward edward – S. e. niveoventer* | None |
| (vi) *Saucerottia viridigaster – S. tobaci* | None |

**Table S3.** Genetic differentiation (pairwise FST) between species and populations of *Saucerottia* hummingbirds based on ddRAD data.

| | ***S. beryllina* 1** | ***S. beryllina* 2** | ***S. beryllina* 3** | ***S. beryllina* - *S. cyanura*** | ***S. cyanura* 1** | ***S. cyanura* 2** | ***S. hoffmanni* 1** | ***S. hoffmanni* 2** | ***S. edward* 1** | ***S. edward* 2** | ***S. viridigaster*** | ***S. tobaci* 1** | ***S. tobaci* 2** |
|---|---|---|---|---|---|---|---|---|---|---|---|---|---|
| ***S .cyanocephala*** | 0.227 | 0.173 | 0.241 | 0.082 | 0.112 | 0.255 | 0.141 | 0.147 | 0.390 | 0.393 | 0.382 | 0.340 | 0.419 |
| ***S. beryllina* 1** | ----- | 0.092 | 0.120 | 0.054 | 0.073 | 0.137 | 0.090 | 0.096 | 0.158 | 0.166 | 0.201 | 0.184 | 0.191 |
| ***S. beryllina* 2** | | ----- | 0.074 | 0.028 | 0.041 | 0.092 | 0.064 | 0.070 | 0.107 | 0.115 | 0.147 | 0.136 | 0.135 |
| ***S. beryllina* 3** | | | ----- | 0.025 | 0.043 | 0.110 | 0.068 | 0.075 | 0.166 | 0.173 | 0.204 | 0.181 | 0.200 |
| ***S. beryllina* - *S. cyanura*** | | | | ----- | 0.023 | 0.036 | 0.045 | 0.051 | 0.043 | 0.047 | 0.070 | 0.067 | 0.056 |
| ***S. cyanura* 1** | | | | | ----- | 0.054 | 0.056 | 0.062 | 0.062 | 0.066 | 0.095 | 0.090 | 0.079 |
| ***S. cyanura* 2** | | | | | | ----- | 0.068 | 0.075 | 0.172 | 0.177 | 0.213 | 0.188 | 0.205 |
| ***S. hoffmanni* 1** | | | | | | | ----- | 0.041 | 0.069 | 0.073 | 0.108 | 0.100 | 0.090 |
| ***S. hoffmanni* 2** | | | | | | | | ----- | 0.068 | 0.072 | 0.109 | 0.101 | 0.091 |
| ***S. edward* 1** | | | | | | | | | ----- | 0.250 | 0.281 | 0.224 | 0.335 |
| ***S. edward* 2** | | | | | | | | | | ----- | 0.287 | 0.231 | 0.339 |
| ***S. viridigaster*** | | | | | | | | | | | ----- | 0.148 | 0.149 |
| ***S. tobaci* 1** | | | | | | | | | | | | ----- | 0.154 |
| ***S. tobaci* 2** | | | | | | | | | | | | | ----- |

*S. beryllina* 1 – West of the Isthmus of Tehuantepec; *S. beryllina* 2 – Chiapas, Mexico and western Guatemala; *S. beryllina* 3 – eastern Guatemala; *S. beryllina* – *S. cyanura* – sympatric/hybrid area; *S. cyanura* 1 – western Guatemala; *S. cyanura* 2 – El Salvador and Nicaragua; *S. hoffmanni* 1 – Nicaragua; *S. hoffmanni* 2 – Costa Rica; *S. edward* 1 – Costa Rica and western Panama; *S. edward* 2 – eastern Panama; *S. tobaci* 1 – Trinidad and Tobago; *S. tobaci* 2 – Venezuela.

**Table S4.** Differentially fixed SNPs in two *Saucerottia edward* subspecies, *S. e. edward* (rufous tail, two samples) and *S. e. niveoventer* (blue tail, two samples).

| No. | Chromosome | SNP position | Gene | Start | Stop | Protein name |
|---|---|---|---|---|---|---|
| 1 | 1 | 2,331,789 | PLXNA4 | 2,305,435 | 2,784,648 | plexin-A4 |
| 2 | 1 | 3,316,946 | MKLN1 | 3,217,197 | 3,320,413 | muskelin |
| 3 | 1 | 6,657,630 | CAMK1D | 6,514,692 | 6,734,920 | calcium/calmodulin-dependent protein kinase type 1D |
| 4 | 1 | 7,334,591 | non-coding | | | |
| 5 | 1 | 9,467,558 | non-coding | | | |
| 6 | 1 | 18,313,734 | non-coding | | | |
| 7 | 1 | 21,927,834 | ATP6AP1 | 21,914,938 | 21,966,007 | V-type proton ATPase subunit S1 |
| 8 | 1 | 34,489,364 | non-coding | | | |
| 9 | 1 | 36,248,273 | ANO2 | 36,126,153 | 36,281,077 | anoctamin-2 |
| 10 | 1 | 36,552,123 | non-coding | | | |
| 11 | 1 | 40,944,149 | SULT4A1 | 40,937,624 | 40,964,037 | sulfotransferase 4A1 |
| 12 | 1 | 41,111,522 | MPPED1 | 41,100,101 | 41,148,048 | metallophosphoesterase domain-containing protein 1 |
| 13 | 1 | 42,419,057 | SSPN | 42,400,318 | 42,419,813 | sarcospan |
| 14 | 1 | 46,830,412 | SLC15A5 | 46,815,935 | 46,852,271 | solute carrier family 15 member 5 |
| 15 | 1 | 53,885,805 | non-coding | | | |
| 16 | 1 | 56,393,746 | STAB2 | 56,315,181 | 56,401,145 | stabilin-2 |
| 17 | 1 | 57,055,150 | DRAM1 | 57,050,913 | 57,067,061 | DNA damage-regulated autophagy modulator protein 1 |
| 18 | 1 | 59,897,971 | non-coding | | | |
| 19 | 1 | 64,850,126 | non-coding | | | |
| 20 | 1 | 65,976,566 | non-coding | | | |
| 21 | 1 | 68,352,857 | OTOGL | 68,261,637 | 68,357,770 | otogelin-like protein |
| 22 | 1 | 70,528,632 | non-coding | | | |
| 23 | 1 | 73,238,433 | ARL13B | 73,230,803 | 73,273,253 | ADP-ribosylation factor-like protein 13B |
| 24 | 1 | 78,063,004 | POLQ | 78,032,841 | 78,080,623 | DNA polymerase theta |
| 25 | 1 | 78,821,831 | non-coding | | | |
| 26 | 1 | 80,038,114 | non-coding | | | |
| 27 | 1 | 80,927,438 | LSAMP | 80,886,956 | 81,069,314 | limbic system-associated membrane protein |
| 28 | 1 | 82,776,914 | DPT | 82,776,559 | 82,801,700 | dermatopontin |
| 29 | 1 | 93,655,614 | non-coding | | | |
| 30 | 1 | 94,839,071 | non-coding | | | |
| 31 | 1 | 100,786,132 | non-coding | | | |
| 32 | 1 | 102,762,607 | non-coding | | | |
| 33 | 1 | 103,747,714 | non-coding | | | |
| 34 | 1 | 106,400,561 | non-coding | | | |
| 35 | 1 | 108,272,779 | VPS26C | 108,260,423 | 108,278,603 | vacuolar protein sorting-associated protein 26C |
| 36 | 1 | 108,958,928 | non-coding | | | |
| 37 | 1 | 111,868,011 | non-coding | | | |
| 38 | 1 | 113,432,202 | DDX3X | 113,420,027 | 113,435,757 | ATP-dependent RNA helicase DDX3X |

| | | | | | | |
|---|---|---|---|---|---|---|
| 39 | 1 | 115,653,015 | non-coding | | | |
| 40 | 1 | 117,138,558 | GK | 117,102,981 | 117,141,323 | glycerol kinase |
| 41 | 1 | 120,865,879 | non-coding | | | |
| 42 | 1 | 121,893,804 | non-coding | | | |
| 43 | 1 | 132,046,012 | HERC2 | 131,973,141 | 132,082,270 | E3 ubiquitin-protein ligase HERC2 |
| 44 | 1 | 133,296,305 | non-coding | | | |
| 45 | 1 | 133,788,365 | non-coding | | | |
| 46 | 1 | 136,558,147 | non-coding | | | |
| 47 | 1 | 137,755,460 | non-coding | | | |
| 48 | 1 | 138,063,696 | non-coding | | | |
| 49 | 1 | 138,505,494 | SH3RF3 | 138,308,043 | 138,560,700 | E3 ubiquitin-protein ligase SH3RF3 |
| 50 | 1 | 139,794,352 | ATP11A | 139,694,791 | 139,813,183 | probable phospholipid-transporting ATPase IH |
| 51 | 1 | 140,948,675 | COL4A2 | 140,899,373 | 141,043,453 | collagen alpha-2(IV) chain |
| 52 | 1 | 147,312,197 | non-coding | | | |
| 53 | 1 | 152,815,829 | non-coding | | | |
| 54 | 1 | 157,246,494 | non-coding | | | |
| 55 | 1 | 168,445,775 | non-coding | | | |
| 56 | 1 | 168,850,503 | non-coding | | | |
| 57 | 1 | 171,717,961 | ATP7B | 171,693,925 | 171,724,056 | copper-transporting ATPase 2 |
| 58 | 1 | 172,082,375 | non-coding | | | |
| 59 | 1 | 176,955,344 | non-coding | | | |
| 60 | 1 | 179,045,830 | non-coding | | | |
| 61 | 1 | 180,208,139 | ZDHHC20 | 180,203,696 | 180,246,566 | palmitoyltransferase ZDHHC20 |
| 62 | 1 | 182,132,114 | RAB39A | 182,125,728 | 182,134,777 | ras-related protein Rab-39A |
| 63 | 1 | 190,618,225 | non-coding | | | |
| 64 | 1 | 193,201,596 | non-coding | | | |
| 65 | 2 | 1,981,434 | non-coding | | | |
| 66 | 2 | 5,356,450 | PLCD1 | 5,335,619 | 5,385,196 | 1-phosphatidylinositol 4,5-bisphosphate phosphodiesterase delta-1 |
| 67 | 2 | 6,452,175 | non-coding | | | |
| 68 | 2 | 20,950,790 | non-coding | | | |
| 69 | 2 | 23,876,223 | FAM133B | 23,872,175 | 23,885,303 | protein FAM133B |
| 70 | 2 | 24,696,406 | non-coding | | | |
| 71 | 2 | 25,189,449 | DYNC1I1 | 25,142,954 | 25,316,283 | cytoplasmic dynein 1 intermediate chain 1 |
| 72 | 2 | 28,368,704 | non-coding | | | |
| 73 | 2 | 30,303,706 | non-coding | | | |
| 74 | 2 | 34,170,332 | non-coding | | | |
| 75 | 2 | 34,532,141 | JAZF1 | 34,400,596 | 34,590,354 | juxtaposed with another zinc finger protein 1 |
| 76 | 2 | 35,245,916 | non-coding | | | |
| 77 | 2 | 35,833,472 | non-coding | | | |
| 78 | 2 | 38,039,884 | non-coding | | | |
| 79 | 2 | 48,525,495 | PDE1C | 48,503,068 | 48,797,705 | calcium/calmodulin-dependent 3\',5\'-cyclic nucleotide phosphodiesterase 1C |
| 80 | 2 | 53,465,464 | non-coding | | | |
| 81 | 2 | 60,604,177 | ADCY1 | 60,507,448 | 60,646,686 | adenylate cyclase type 1 |

| | | | | | | |
|---|---|---|---|---|---|---|
| 82 | 2 | 62,572,255 | JARID2 | 62,357,359 | 62,579,837 | protein Jumonji |
| 83 | 2 | 63,614,485 | non-coding | | | |
| 84 | 2 | 65,282,638 | non-coding | | | |
| 85 | 2 | 68,980,529 | GMDS | 68,598,281 | 69,018,417 | GDP-mannose 4,6 dehydratase |
| 86 | 2 | 72,308,614 | non-coding | | | |
| 87 | 2 | 76,895,636 | non-coding | | | |
| 88 | 2 | 78,729,943 | CTNND2 | 78,407,020 | 78,929,832 | catenin delta-2 |
| 89 | 2 | 84,171,103 | FHOD3 | 84,021,046 | 84,405,767 | FH1/FH2 domain-containing protein 3 |
| 90 | 2 | 85,793,588 | non-coding | | | |
| 91 | 2 | 90,272,552 | INVS | 90,257,444 | 90,337,926 | inversin |
| 92 | 2 | 92,423,449 | non-coding | | | |
| 93 | 2 | 98,227,674 | PRELID3A | 98,225,868 | 98,236,472 | PRELI domain containing protein 3A |
| 94 | 2 | 102,049,298 | non-coding | | | |
| 95 | 2 | 109,690,278 | non-coding | | | |
| 96 | 2 | 110,278,572 | non-coding | | | |
| 97 | 2 | 113,436,348 | non-coding | | | |
| 98 | 2 | 115,702,822 | non-coding | | | |
| 99 | 2 | 116,929,382 | PPP1R42 | 116,898,236 | 116,923,112 | protein phosphatase 1 regulatory subunit 42 |
| 100 | 2 | 119,342,645 | TERF1 | 119,331,907 | 119,349,788 | telomeric repeat-binding factor 1 |
| 101 | 2 | 124,916,696 | non-coding | | | |
| 102 | 2 | 125,550,399 | non-coding | | | |
| 103 | 2 | 131,115,219 | non-coding | | | |
| 104 | 2 | 134,493,266 | non-coding | | | |
| 105 | 2 | 137,096,012 | non-coding | | | |
| 106 | 2 | 137,574,998 | non-coding | | | |
| 107 | 2 | 139,959,232 | non-coding | | | |
| 108 | 2 | 143,722,200 | non-coding | | | |
| 109 | 2 | 145,389,160 | non-coding | | | |
| 110 | 2 | 149,282,441 | ADGRB1 | 149,148,975 | 149,372,238 | adhesion G protein-coupled receptor B1 |
| 111 | 3 | 3,381,838 | non-coding | | | |
| 112 | 3 | 10,506,539 | SPAST | 10,502,897 | 10,535,486 | spastin |
| 113 | 3 | 17,287,856 | TTC7A | 17,281,125 | 17,446,966 | tetratricopeptide repeat protein 7A |
| 114 | 3 | 18,450,216 | non-coding | | | |
| 115 | 3 | 19,712,821 | non-coding | | | |
| 116 | 3 | 24,730,125 | non-coding | | | |
| 117 | 3 | 28,702,501 | non-coding | | | |
| 118 | 3 | 31,691,314 | UST | 31,555,026 | 31,706,654 | uronyl 2-sulfotransferase |
| 119 | 3 | 32,161,217 | non-coding | | | |
| 120 | 3 | 34,984,017 | PRKN | 34,484,247 | 35,193,532 | E3 ubiquitin-protein ligase parkin |
| 121 | 3 | 39,647,492 | VPS54 | 39,642,148 | 39,681,001 | vacuolar protein sorting-associated protein 54 |
| 122 | 3 | 39,739,820 | non-coding | | | |
| 123 | 3 | 44,135,522 | SLX4IP | 44,348,748 | 44,420,850 | protein SLX4IP |
| 124 | 3 | 54,433,094 | LBR | 54,427,395 | 54,440,373 | delta(14)-sterol reductase LBR |

| | | | | | | |
|---|---|---|---|---|---|---|
| 125 | 3 | 61,186,332 | ARHGAP18 | 61,141,730 | 61,201,654 | rho GTPase-activating protein 18 |
| 126 | 3 | 65,507,806 | non-coding | | | |
| 127 | 3 | 66,012,428 | non-coding | | | |
| 128 | 3 | 68,435,466 | non-coding | | | |
| 129 | 3 | 74,092,215 | non-coding | | | |
| 130 | 3 | 74,871,826 | non-coding | | | |
| 131 | 3 | 75,961,759 | non-coding | | | |
| 132 | 3 | 79,084,429 | non-coding | | | |
| 133 | 3 | 79,794,042 | non-coding | | | |
| 134 | 3 | 99,887,272 | CPSF3 | 99,883,008 | 99,902,351 | cleavage and polyadenylation specificity factor subunit 3 |
| 135 | 3 | 101,374,809 | non-coding | | | rho-associated protein kinase 2 isoform X5 |
| 136 | 3 | 102,792,516 | DDX1 | 102,776,017 | 102,796,126 | ATP-dependent RNA helicase DDX1 |
| 137 | 3 | 104,414,776 | non-coding | | | |
| 138 | 3 | 105,967,519 | non-coding | | | |
| 139 | 3 | 106,689,129 | non-coding | | | |
| 140 | 3 | 108,499,579 | non-coding | | | |
| 141 | 3 | 111,861,635 | MCM3 | 111,856,583 | 111,867,101 | DNA replication licensing factor MCM3 |
| 142 | 3 | 113,513,553 | non-coding | | | |
| 143 | 3 | 114,524,398 | non-coding | | | |
| 144 | 4 | 657,113 | non-coding | | | |
| 145 | 4 | 1,307,900 | GPR50 | 1,281,475 | 1,325,749 | melatonin-related receptor |
| 146 | 4 | 2,333,290 | non-coding | | | |
| 147 | 4 | 3,721,792 | GCNA | 3,719,891 | 3,722,755 | acidic repeat-containing protein |
| 148 | 4 | 8,171,158 | non-coding | | | |
| 149 | 4 | 12,966,453 | non-coding | | | |
| 150 | 4 | 17,870,126 | non-coding | | | |
| 151 | 4 | 18,455,151 | non-coding | | | |
| 152 | 4A | 826,358 | non-coding | | | |
| 153 | 4A | 7,110,643 | non-coding | | | |
| 154 | 4A | 8,562,689 | non-coding | | | |
| 155 | 4A | 14,542,772 | LIMCH1 | 14,521,389 | 14,693,667 | LIM and calponin homology domains-containing protein 1 |
| 156 | 4A | 15,039,984 | ATP8A1 | 14,952,952 | 15,047,686 | phospholipid-transporting ATPase IA |
| 157 | 4A | 17,203,724 | non-coding | | | |
| 158 | 4A | 18,041,623 | non-coding | | | |
| 159 | 4A | 26,887,289 | non-coding | | | |
| 160 | 4A | 28,363,612 | non-coding | | | |
| 161 | 4A | 34,584,664 | non-coding | | | |
| 162 | 4A | 40,840,933 | non-coding | | | |
| 163 | 4A | 42,141,283 | TBCK | 42,136,754 | 42,191,279 | TBC domain-containing protein kinase-like protein |
| 164 | 4A | 44,318,420 | non-coding | | | |
| 165 | 4B | 3,645,942 | non-coding | | | |
| 166 | 4B | 12,708,833 | non-coding | | | |
| 167 | 4B | 13,618,718 | ABLIM2 | 13,545,121 | 13,642,185 | actin-binding LIM protein 2 |

| | | | | | | |
|---|---|---|---|---|---|---|
| 168 | 4B | 14,008,305 | non-coding | | | |
| 169 | 4B | 15,857,254 | non-coding | | | |
| 170 | 4B | 16,877,164 | non-coding | | | |
| 171 | 4B | 19,102,224 | non-coding | | | |
| 172 | 5 | 5,294,051 | non-coding | | | |
| 173 | 5 | 6,340,905 | PAX6 | 6,339,357 | 6,357,810 | paired box protein Pax-6 |
| 174 | 5 | 13,675,891 | LSP1 | 13,650,987 | 13,685,350 | lymphocyte-specific protein 1 |
| 175 | 5 | 14,029,409 | BRSK2 | 13,967,022 | 14,264,468 | serine/threonine-protein kinase BRSK2 |
| 176 | 5A | 1,374,149 | RGS6 | 1,171,103 | 1,384,626 | regulator of G-protein signaling 6 |
| 177 | 5A | 4,582,962 | LOC103534463 | 4,427,441 | 4,640,158 | transmembrane protein 263 |
| 178 | 5A | 9,918,392 | RAD51B | 9,730,049 | 10,118,750 | DNA repair protein RAD51 homolog 2 |
| 179 | 5A | 12,198,865 | non-coding | | | |
| 180 | 5A | 13,652,755 | DPH6 | 13,620,018 | 13,803,720 | diphthine--ammonia ligase |
| 181 | 5A | 17,182,161 | NPAS3 | 17,025,140 | 17,606,470 | neuronal PAS domain-containing protein 3 |
| 182 | 5A | 19,029,351 | non-coding | | | |
| 183 | 5A | 39,760,962 | non-coding | | | |
| 184 | 5A | 43,138,708 | non-coding | | | |
| 185 | 6 | 689,840 | NOLC1 | 687,492 | 694,379 | nucleolar and coiled-body phosphoprotein 1 |
| 186 | 6 | 2,658,941 | LRMDA | 2,566,865 | 3,116,802 | leucine-rich melanocyte differentiation-associated protein |
| 187 | 6 | 2,944,906 | LRMDA | 2,566,865 | 3,116,802 | leucine-rich melanocyte differentiation-associated protein |
| 188 | 6 | 4,723,492 | ZCCHC24 | 4,704,169 | 4,796,568 | zinc finger CCHC domain-containing protein 24 |
| 189 | 6 | 6,390,116 | NRG3 | 6,189,227 | 6,537,193 | pro-neuregulin-3, membrane-bound isoform |
| 190 | 6 | 8,906,340 | non-coding | | | |
| 191 | 6 | 9,843,035 | RHOBTB1 | 9,823,902 | 9,846,856 | rho-related BTB domain-containing protein 1 |
| 192 | 6 | 17,003,742 | non-coding | | | |
| 193 | 6 | 27,281,539 | CCDC186 | 27,264,382 | 27,282,269 | coiled-coil domain-containing protein 186 |
| 194 | 6 | 29,607,038 | non-coding | | | |
| 195 | 6 | 30,571,053 | non-coding | | | |
| 196 | 7 | 2,774,814 | non-coding | | | |
| 197 | 7 | 16,633,581 | SLC4A3 | 16,618,516 | 16,646,350 | anion exchange protein 3 |
| 198 | 7 | 23,751,386 | TTN | 23,711,885 | 23,954,089 | titin |
| 199 | 7 | 26,115,744 | HDAC4 | 26,029,456 | 26,287,396 | histone deacetylase 4 |
| 200 | 7 | 27,933,565 | LRRFIP1 | 27,930,713 | 28,030,408 | leucine-rich repeat flightless-interacting protein 1 |
| 201 | 7 | 28,218,076 | non-coding | | | |
| 202 | 7 | 36,788,085 | non-coding | | | |
| 203 | 8 | 3,348,479 | non-coding | | | |
| 204 | 8 | 26,071,028 | non-coding | | | |
| 205 | 8 | 26,660,741 | non-coding | | | |
| 206 | 8 | 28,857,345 | non-coding | | | |
| 207 | 9 | 2,551,034 | non-coding | | | |
| 208 | 9 | 16,449,568 | non-coding | | | |
| 209 | 9 | 18,112,491 | non-coding | | | |
| 210 | 9 | 18,998,618 | non-coding | | | |

| | | | | | | |
|---|---|---|---|---|---|---|
| 211 | 9 | 19,447,243 | NAALADL2 | 19,439,508 | 19,629,043 | inactive N-acetylated-alpha-linked acidic dipeptidase-like protein 2 |
| 212 | 9 | 21,607,011 | non-coding | | | |
| 213 | 9 | 21,946,642 | non-coding | | | |
| 214 | 9 | 24,658,261 | non-coding | | | |
| 215 | 9 | 25,559,550 | non-coding | | | |
| 216 | 10 | 15,061,730 | AKAP13 | 14,927,824 | 15,070,769 | A-kinase anchor protein 13 |
| 217 | 10 | 16,932,550 | non-coding | | | |
| 218 | 10 | 18,817,190 | CHSY1 | 18,753,108 | 18,825,771 | chondroitin sulfate synthase 1 |
| 219 | 10 | 19,599,124 | MEGF11 | 19,458,168 | 19,644,794 | multiple epidermal growth factor-like domains protein 11 |
| 220 | 11 | 1,150,096 | HYDIN | 1,127,614 | 1,279,930 | hydrocephalus-inducing protein homolog |
| 221 | 11 | 4,443,308 | non-coding | | | |
| 222 | 11 | 10,257,032 | non-coding | | | |
| 223 | 11 | 16,794,555 | ATP2C2 | 16,780,777 | 16,803,818 | calcium-transporting ATPase type 2C member 2 |
| 224 | 11 | 19,846,715 | non-coding | | | |
| 225 | 12 | 3,789,637 | non-coding | | | |
| 226 | 12 | 7,291,225 | non-coding | | | |
| 227 | 12 | 8,220,755 | non-coding | | | |
| 228 | 12 | 9,437,515 | non-coding | | | |
| 229 | 12 | 13,987,341 | non-coding | | | |
| 230 | 12 | 15,280,346 | MAGI1 | 15,040,261 | 15,369,672 | membrane-associated guanylate kinase, WW and PDZ domain-containing protein 1 |
| 231 | 12 | 18,167,773 | non-coding | | | |
| 232 | 13 | 5,863,595 | non-coding | | | |
| 233 | 13 | 8,006,241 | SH3PXD2B | 7,956,223 | 8,020,930 | SH3 and PX domain-containing protein 2B |
| 234 | 13 | 11,516,546 | non-coding | | | |
| 235 | 13 | 12,928,962 | non-coding | | | |
| 236 | 13 | 15,242,399 | non-coding | | | |
| 237 | 13 | 15,462,371 | TCF7 | 15,424,025 | 15,487,769 | transcription factor 7 |
| 238 | 13 | 16,189,324 | non-coding | | | |
| 239 | 13 | 16,836,250 | ARHGAP26 | 16,796,813 | 16,893,482 | rho GTPase-activating protein 26 |
| 240 | 14 | 1,922,341 | CHTF18 | 1,914,062 | 1,926,488 | chromosome transmission fidelity protein 18 homolog |
| 241 | 14 | 3,888,491 | non-coding | | | |
| 242 | 14 | 7,771,673 | non-coding | | | |
| 243 | 14 | 9,728,475 | ABCC1 | 9,703,971 | 9,752,266 | multidrug resistance-associated protein 1 |
| 244 | 14 | 10,491,563 | non-coding | | | |
| 245 | 14 | 11,112,302 | MOSMO | 11,095,915 | 11,119,725 | modulator of smoothened protein |
| 246 | 14 | 12,557,237 | LOC103536849 | 12,537,746 | 12,571,913 | syntaxin-binding protein 4 |
| 247 | 14 | 15,106,489 | SBK1 | 15,101,606 | 15,114,489 | serine/threonine-protein kinase SBK1 |
| 248 | 15 | 361,685 | MN1 | 332,011 | 362,677 | transcriptional activator MN1 |
| 249 | 15 | 4,660,494 | TMEM132D | 4,542,817 | 4,751,909 | transmembrane protein 132D |
| 250 | 15 | 8,625,609 | RIMBP2 | 8,598,503 | 8,714,852 | RIMS-binding protein 2 |
| 251 | 15 | 9,780,269 | EIF4ENIF1 | 9,768,763 | 9,788,483 | eukaryotic translation initiation factor 4E transporter |
| 252 | 15 | 10,728,455 | LOC103535438 | 10,725,346 | 10,734,269 | P2X purinoceptor 6 |
| 253 | 15 | 11,692,099 | MTMR3 | 11,654,467 | 11,695,291 | myotubularin-related protein 3 |

| | | | | | | |
|---|---|---|---|---|---|---|
| 254 | 17 | 2,700,844 | non-coding | | | |
| 255 | 17 | 3,687,789 | non-coding | | | |
| 256 | 17 | 4,087,877 | COL27A1 | 4,034,958 | 4,176,094 | collagen alpha-1(XXVII) chain |
| 257 | 17 | 8,737,009 | SURF4 | 8,732,653 | 8,743,353 | surfeit locus protein 4 |
| 258 | 17 | 9,038,317 | VAV2 | 8,940,332 | 9,071,945 | guanine nucleotide exchange factor VAV2 |
| 259 | 17 | 9,789,394 | AGPAT2 | 9,783,465 | 9,789,765 | 1-acyl-sn-glycerol-3-phosphate acyltransferase beta |
| 260 | 18 | 336,614 | TMC6 | 329,960 | 335,629 | transmembrane channel-like protein 6 |
| 261 | 19 | 4,547,570 | GUSB | 4,539,355 | 4,550,405 | beta-glucuronidase |
| 262 | 19 | 7,268,029 | non-coding | | | |
| 263 | 19 | 10,492,674 | non-coding | | | |
| 264 | 20 | 806,140 | AHCY | 781,966 | 808,635 | adenosylhomocysteinase |
| 265 | 20 | 2,195,859 | non-coding | | | |
| 266 | 20 | 11,935,910 | non-coding | | | |
| 267 | 20 | 14,328,980 | KIF3B | 14,325,564 | 14,329,651 | kinesin-like protein KIF3B |
| 268 | 21 | 902,392 | DVL1 | 859,866 | 925,356 | segment polarity protein dishevelled homolog DVL-1 |
| 269 | 21 | 2,803,050 | non-coding | | | |
| 270 | 21 | 3,043,325 | non-coding | | | |
| 271 | 22 | 558,465 | non-coding | | | |
| 272 | 22 | 3,053,949 | DOCK5 | 3,009,704 | 3,080,689 | dedicator of cytokinesis protein 5 |
| 273 | 24 | 572,994 | non-coding | | | |
| 274 | 24 | 2,574,890 | LOC103526084 | 2,359,545 | 2,620,950 | opioid-binding protein/cell adhesion molecule homolog |
| 275 | 24 | 5,706,394 | SIK3 | 5,701,605 | 5,730,332 | serine/threonine-protein kinase SIK3 |
| 276 | 26 | 3,979,856 | PPP1R12B | 3,948,101 | 4,045,247 | protein phosphatase 1 regulatory subunit 12B |
| 277 | 26 | 4,604,215 | non-coding | | | |
| 278 | 26 | 4,827,166 | ETNK2 | 4,819,572 | 4,827,696 | ethanolamine kinase 2 |
| 279 | 26 | 5,377,800 | non-coding | | | |
| 280 | 27 | 2,292,330 | non-coding | | | |
| 281 | 28 | 405,573 | non-coding | | | |
| 282 | 28 | 1,670,600 | non-coding | | | |
| 283 | 28 | 3,538,534 | non-coding | | | |
| 284 | 28 | 4,579,408 | non-coding | | | |
| 285 | 28 | 5,138,135 | non-coding | | | |
| 286 | Z | 7,051,973 | non-coding | | | |
| 287 | Z | 9,044,626 | non-coding | | | |
| 288 | Z | 9,577,293 | UBAP2 | 9,502,329 | 9,596,436 | ubiquitin-associated protein 2 |
| 289 | Z | 10,803,741 | UNC13B | 10,759,106 | 10,970,859 | protein unc-13 homolog B |
| 290 | Z | 11,128,371 | RUSC2 | 11,121,513 | 11,138,942 | iporin |
| 291 | Z | 11,589,299 | non-coding | | | |
| 292 | Z | 12,751,501 | RAI14 | 12,701,007 | 12,775,303 | ankycorbin |
| 293 | Z | 14,287,100 | OSMR | 14,270,151 | 14,292,786 | oncostatin-M-specific receptor subunit beta |
| 294 | Z | 15,374,731 | FBXO4 | 15,372,777 | 15,379,628 | F-box only protein 4 |
| 295 | Z | 21,414,198 | non-coding | | | |
| 296 | Z | 24,152,284 | non-coding | | | |

| | | | | | | |
|---|---|---|---|---|---|---|
| 297 | Z | 35,601,980 | non-coding | | | |
| 298 | Z | 40,411,886 | non-coding | | | |
| 299 | Z | 41,790,996 | non-coding | | | |
| 300 | Z | 43,162,051 | non-coding | | | |
| 301 | Z | 48,779,068 | non-coding | | | |
| 302 | Z | 50,822,270 | AP3B1 | 50,723,573 | 50,881,047 | AP-3 complex subunit beta-1 |
| 303 | Z | 52,587,462 | non-coding | | | |
| 304 | Z | 54,093,718 | non-coding | | | |
| 305 | Z | 56,609,558 | PRDM6 | 56,594,398 | 56,666,467 | putative histone-lysine N-methyltransferase PRDM6 |
| 306 | Z | 57,880,043 | non-coding | | | |
| 307 | Z | 60,227,135 | B4GALT1 | 60,223,000 | 60,246,006 | beta-1,4-galactosyltransferase 1 |
| 308 | Z | 60,469,955 | non-coding | | | |
| 309 | Z | 63,297,050 | non-coding | | | |
| 310 | Z | 64,869,644 | KIAA1958 | 64,862,625 | 64,884,324 | uncharacterized protein KIAA1958 homolog |
| 311 | Z | 65,344,682 | non-coding | | | |
| 312 | Z | 67,441,906 | ATG10 | 67,379,475 | 67,461,168 | ubiquitin-like-conjugating enzyme ATG10 |
| 313 | Z | 73,482,682 | CAST | 73,473,056 | 73,529,351 | calpastatin |
| 314 | W | 211,498 | non-coding | | | |
| 315 | Un | 16,939 | non-coding | | | |
| 316 | Un | 164,414 | non-coding | | | |

**Table S5.** Differentially fixed SNPs in *Saucerottia viridigaster* (rufous tail, four samples) and *S. tobaci* (blue tail, four samples).

| No. | Chromosome | SNP position | Gene | Start | Stop | Protein name | Function |
|---|---|---|---|---|---|---|---|
| 1 | 1 | 12,826,830 | RELN | 12,706,577 | 12,976,462 | reelin | "This gene encodes a large secreted extracellular matrix protein thought to control cell-cell interactions critical for cell positioning and neuronal migration during brain development." (NCBI). |
| 2 | 1 | 50,165,539 | non-coding | | | | |
| 3 | 1 | 53,889,687 | non-coding | | | | |
| 4 | 1 | 69,677,384 | non-coding | | | | |
| 5 | 1 | 71,815,505 | non-coding | | | | |
| 6 | 1 | 73,203,348 | non-coding | | | | |
| 7 | 1 | 81,774,084 | non-coding | | | | |
| 8 | 1 | 157,238,717 | non-coding | | | | |
| 9 | 2 | 34,183,302 | non-coding | | | | |
| 10 | 2 | 35,996,786 | non-coding | | | | |
| 11 | 2 | 53,642,476 | ULK4 | 53,469,655 | 53,671,859 | serine/threonine-protein kinase ULK4 | "A member of the unc-51-like serine/threonine kinase (STK) family. Members of this protein family play a role in neuronal growth and endocytosis." (NCBI).<br>Microtubule-associated protein, regulates acetylation of α-tubulin, regulates the Sonic Hedgehog (SHH, a morphogenesis regulator) at the primary cilium (Mecklenburg et al. 2021).<br>"ULK1 and mTOR are potential genetic mediators of melanosome degradation." (Kim et al. 2020). |
| 12 | 2 | 68,518,837 | non-coding | | | | |
| 13 | 2 | 109,206,295 | SPIDR | 109,092,248 | 109,293,358 | DNA repair-scaffolding protein | Contributes to maintain genomic integrity (UNIPROT). |
| 14 | 3 | 14,784,825 | BTBD9 | 14,695,203 | 14,801,188 | BTB/POZ domain-containing protein 9 | "It is known to be involved in protein-protein interactions." (NCBI). |
| 15 | 4A | 36,924,352 | GRID2 | 36,812,554 | 37,518,211 | glutamate receptor ionotropic, delta-2 isoform X1 | "The encoded protein is a multi-pass membrane protein that is expressed selectively in cerebellar Purkinje cells." (NCBI).<br>It was one of the two identified genes in a GWAS studying spotted phenotype in ducks, although the authors discuss that this gene has not been found to affect pigment deposition (Xi et al. 2021). |
| 16 | 5 | 5,681,416 | non-coding | | | | |

| | | | | | | | |
|---|---|---|---|---|---|---|---|
| 17 | 5A | 15,808,990 | PRKD1 | 15,704,448 | 15,828,729 | serine/threonine-protein kinase D1 | "Involved in many cellular processes, including Golgi body membrane integrity and transport, cell migration and differentiation, MAPK8/JNK1 and Ras pathway signaling, MAPK1/3 (ERK1/2) pathway signaling, cell survival, and regulation of cell shape and adhesion." (NCBI).<br>"PAR1 and PAR2 can activate PKD1 in malignant melanoma cells, thereby enhancing cell proliferation and motility." (Kempkes et al. 2012).<br>"PKD1 is expressed in a wide range of cells and tissues like fibroblasts, endothelial cells and dendritic cells and participates in a number of intracellular signaling pathways to regulate essential processes including cell survival, proliferation, cell motility, membrane trafficking, and immune response" (Hollenback et al. 2013). |
| 18 | 5A | 19,393,591 | non-coding | | | | |
| 19 | 7 | 24,332,943 | non-coding | | | | |
| 20 | 7 | 36,301,146 | non-coding | | | | |
| 21 | 8 | 9,844,708 | non-coding | | | | |
| 22 | 8 | 12,080,201 | non-coding | | | | |
| 23 | 8 | 17,226,526 | non-coding | | | | |
| 24 | 9 | 109,708 | non-coding | | | | |
| 25 | 9 | 6,164,966 | HS6ST1 | 6,088,845 | 6,251,439 | heparan-sulfate 6-O-sulfotransferase 1 | "This enzyme is a type II integral membrane protein and is responsible for 6-O-sulfation of heparan sulfate." (NCBI). |
| 26 | 9 | 12,412,630 | non-coding | | | | |
| 27 | 11 | 5,518,008 | non-coding | | | | |
| 28 | 11 | 8,344,372 | non-coding | | | | |
| 29 | 15 | 6,542,177 | ZDHHC8 | 6,499,256 | 6,597,379 | probable palmitoyltransferase ZDHHC8 isoform X1 | Transmembrane protein that may function as a palmitoyltransferase (NCBI).<br>"MC1R palmitoylation, primarily mediated by the protein-acyl transferase ZDHHC13, is essential for activating MC1R signalling, which triggers increased pigmentation." (Chen et al. 2017). |
| | | | ZDHHC8 | 6,553,228 | 6,597,379 | probable palmitoyltransferase ZDHHC8 isoform X3 | |
| | | | ZDHHC8 | 6,569,147 | 6,597,379 | probable palmitoyltransferase ZDHHC8 isoform X2 | |
| 30 | 15 | 11,094,877 | non-coding | | | | |
| 31 | 17 | 6,291,079 | non-coding | | | | |
| 32 | 22 | 696,781 | TACC1 | 682,563 | 697,418 | transforming acidic coiled-coil-containing protein 1 | "Involved in transcription regulation induced by nuclear receptors. Might promote the nuclear localization of the receptors. Likely involved in the |

| | | | | | | | |
|---|---|---|---|---|---|---|---|
| | | | | | | | processes that promote cell division prior to the formation of differentiated tissues." (UNIPROT). Related to microtubules (Hertel and Mocarski 2004). It is one of the genes significantly mutated in melanoma, a malignant tumour originating from melanocytes (Papadodima et al. 2019). |
| 33 | 24 | 1,558,663 | non-coding | | | | |
| 34 | 26 | 3,956,793 | PPP1R12B | 3,948,101 | 4,045,247 | protein phosphatase 1 regulatory subunit 12B isoform X2 | "Myosin phosphatase is a protein complex comprised of three subunits: a catalytic subunit (PP1c-delta, protein phosphatase 1, catalytic subunit delta), a large regulatory subunit (MYPT, myosin phosphatase target) and small regulatory subunit (sm-M20)." (NCBI). It has a potential role in muscle cell proliferation (Montén et al. 2015). |
| | | | PPP1R12B | 3,948,101 | 4,045,167 | protein phosphatase 1 regulatory subunit 12B isoform X3 | |
| | | | PPP1R12B | 3,948,101 | 4,042,037 | protein phosphatase 1 regulatory subunit 12B isoform X1 | |
| | | | PPP1R12B | 3,948,101 | 4,042,037 | protein phosphatase 1 regulatory subunit 12B isoform X4 | |
| | | | PPP1R12B | 3,948,101 | 4,042,037 | protein phosphatase 1 regulatory subunit 12B isoform X5 | |
| 35 | Z | 6,777,679 | non-coding | | | | |
| 36 | Z | 11,163,861 | non-coding | | | | |
| 37 | Z | 17,169,173 | non-coding | | | | |
| 38 | Z | 19,424,490 | MAP3K1 | 19,401,445 | 19,451,444 | mitogen-activated protein kinase kinase kinase 1 isoform X1 | "It is part of some signal transduction cascades, including the ERK and JNK kinase pathways as well as the NF-kappa-B pathway." (NCBI). "Activation of MAPK by tyrosine/threonine phosphorylation are involved in melatonin-induced melanosome aggregation in *Xenopus* melanophores." (Andersson et al. 2003). It is one of the three main candidate genes for iridescent structural color in chickens (Fogelholm 2020). |
| | | | MAP3K1 | 19,402,097 | 19,451,444 | mitogen-activated protein kinase kinase kinase 1 isoform X3 | |
| | | | MAP3K1 | 19,433,030 | 19,451,444 | mitogen-activated protein kinase kinase kinase 1 isoform X2 | |
| 39 | Z | 22,268,769 | non-coding | | | | |
| 40 | Z | 22,924,132 | non-coding | | | | |
| 41 | Z | 25,275,506 | non-coding | | | | |
| 42 | Z | 37,200,135 | VPS13A | 37,145,940 | 37,239,444 | vacuolar protein sorting-associated protein 13A isoform X2 | "May control steps in the cycling of proteins through the trans-Golgi network to endosomes, lysosomes and the plasma membrane." (NCBI). "vps zebrafish mutants have skin and eye hypopigmentation phenotypes due to defects in the production of melanin producing organelles, melanosomes." (Cooper 2017). |
| | | | VPS13A | 37,145,940 | 37,239,444 | vacuolar protein sorting-associated protein 13A isoform X1 | |
| 43 | Z | 38,893,760 | non-coding | | | | |

| | | | | | | | |
|---|---|---|---|---|---|---|---|
| 44 | Z | 42,999,266 | NFIB | 42,869,841 | 43,033,198 | nuclear factor 1 B-type isoform X6 | "Transcriptional activator of GFAP, essential for proper brain development." (UNIPROT).<br>In mammals, "NFIB is a governor of epithelial–melanocyte stem cell behavior" (Chang et al. 2013). |
| | | | NFIB | 42,869,908 | 43,033,198 | nuclear factor 1 B-type isoform X1 | |
| | | | NFIB | 42,869,908 | 43,033,198 | nuclear factor 1 B-type isoform X2 | |
| | | | NFIB | 42,869,908 | 43,033,198 | nuclear factor 1 B-type isoform X4 | |
| | | | NFIB | 42,869,908 | 43,033,086 | nuclear factor 1 B-type isoform X3 | |
| | | | NFIB | 42,869,908 | 43,033,086 | nuclear factor 1 B-type isoform X5 | |
| | | | NFIB | 42,979,808 | 43,033,198 | nuclear factor 1 B-type isoform X7 | |
| 45 | Z | 44,108,283 | non-coding | | | | |
| 46 | Z | 51,208,966 | DMGDH | 51,181,461 | 51,221,047 | dimethylglycine dehydrogenase, mitocondrial | "Enzyme involved in the catabolism of choline, catalyzing the oxidative demethylation of dimethylglycine to form sarcosine. The enzyme is found as a monomer in the mitochondrial matrix, and uses flavin adenine dinucleotide and folate as cofactors." (NCBI).<br>"Choline may have a pigment-dispersing effect in fish melanophores" (Oshima et al. 1992).<br>In the lizard and the toad, choline is implicated in permitting melanosome dispersion (Hadley and Castrucci 1988). |
| 47 | Z | 58,544,847 | non-coding | | | | |
| 48 | Z | 60,708,750 | non-coding | | | | |
| 49 | Z | 66,305,927 | non-coding | | | | |
| 50 | Z | 70,194,664 | non-coding | | | | |

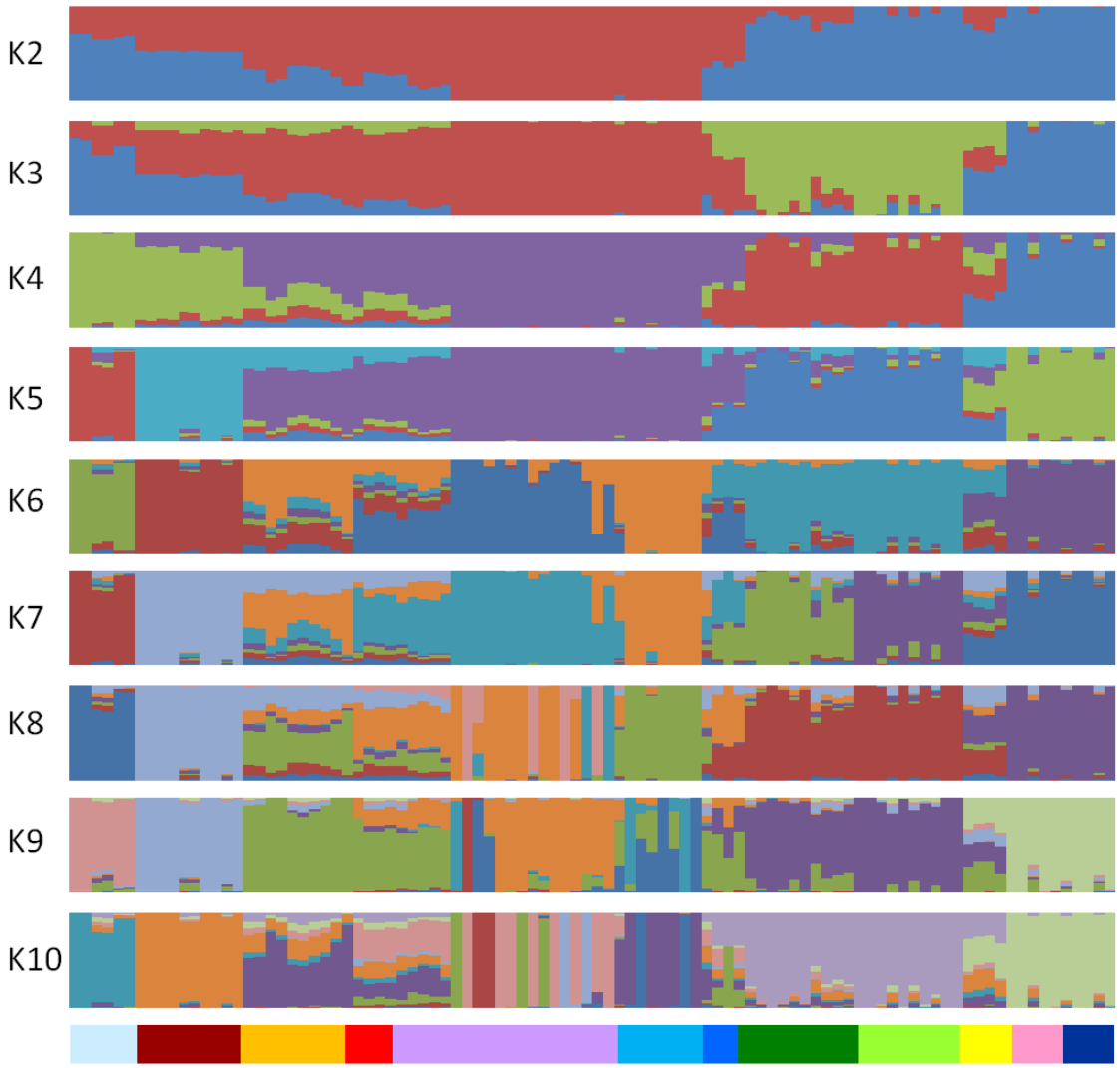


**Figure S1.** Ancestry analysis results from K = 2 to K = 10. The bar below K = 10 represents the geographic origin of the individuals, as depicted in Figure 1.

**Supplementary references**


Andersson, T. P., Svensson, S. P., & Karlsson, A. M. (2003). Regulation of melanosome movement by MAP kinase. Pigment Cell Research, 16(3), 215-221.

Chang, C. Y., Pasolli, H. A., Giannopoulou, E. G., Guasch, G., Gronostajski, R. M., Elemento, O., & Fuchs, E. (2013). NFIB is a governor of epithelial–melanocyte stem cell behaviour in a shared niche. Nature, 495(7439), 98-102.

Chen, S., Zhu, B., Yin, C., Liu, W., Han, C., Chen, B., ... & Cui, R. (2017). Palmitoylation-dependent activation of MC1R prevents melanomagenesis. Nature, 549(7672), 399-403.

Cooper, C. D. (2017). Insights from zebrafish on human pigment cell disease and treatment. Developmental Dynamics, 246(11), 889-896.

Fogelholm, J. (2020). Genomics and Transcriptomics of Behaviour and Plumage Colouration (Vol. 2073). Linköping University Electronic Press.

Hadley, M. E., & Castrucci, A. M. D. L. (1988). Melanotropin mechanisms of action: melanosome movements. In The Melanotropic Peptides (pp. 15-26). CRC Press.

Hertel, L., & Mocarski, E. S. (2004). Global analysis of host cell gene expression late during cytomegalovirus infection reveals extensive dysregulation of cell cycle gene expression and induction of Pseudomitosis independent of US28 function. Journal of Virology, 78(21), 11988-12011.

Hollenbach, M., Stoll, S. J., Jörgens, K., Seufferlein, T., & Kroll, J. (2013). Different regulation of physiological and tumor angiogenesis in zebrafish by protein kinase D1 (PKD1). PloS one, 8(7), e68033.

Kempkes, C., Rattenholl, A., Buddenkotte, J., Strozyk, E., Eberle, J., Hausser, A., ... & Steinhoff, M. (2012). Proteinase-activated receptors 1 and 2 regulate invasive behavior of human melanoma cells via activation of protein kinase D1. Journal of Investigative Dermatology, 132(2), 375-384.

Kim, J. Y., Kim, J., Ahn, Y., Lee, E. J., Hwang, S., Almurayshid, A., ... & Oh, S. H. (2020). Autophagy induction can regulate skin pigmentation by causing melanosome degradation in keratinocytes and melanocytes. Pigment Cell & Melanoma Research, 33(3), 403-415.

Mecklenburg, N., Kowalczyk, I., Witte, F., Görne, J., Laier, A., Mamo, T. M., ... & Hammes, A. (2021). Identification of disease-relevant modulators of the SHH pathway in the developing brain. Development, 148(17), dev199307.

Montén, C., Gudjonsdottir, A. H., Browaldh, L., Arnell, H., Nilsson, S., Agardh, D., & Naluai, Å. T. (2015). Genes involved in muscle contractility and nutrient signaling pathways within celiac disease risk loci show differential mRNA expression. BMC Medical Genetics, 16(1), 1-9.

Oshima, N., Sugimoto, M., & Fujii, R. (1992). Effects of choline chloride on the pigment translocation within fish melanophores. Comparative Biochemistry and Physiology Part C: Comparative Pharmacology, 102(1), 11-15.

Papadodima, O., Kontogianni, G., Piroti, G., Maglogiannis, I., & Chatziioannou, A. (2019). Genomics of cutaneous melanoma: focus on next-generation sequencing approaches and bioinformatics. Journal of Translational Genetics and Genomics, 3.

Xi, Y., Xu, Q., Huang, Q., Ma, S., Wang, Y., Han, C., ... & Li, L. (2021). Genome-wide association analysis reveals that EDNRB2 causes a dose-dependent loss of pigmentation in ducks. BMC Genomics, 22(1), 1-11.

# Chapter 4

## Comparative phylogeography of montane birds across Nuclear Central America

## Introduction

Comparative phylogeography provides the conceptual framework with which to understand historical and spatial processes influencing species diversity in current assemblages (Bermingham and Moritz 1998). Species assemblages change through time (Hewitt and Nichols 2005); while common geographic features and historic events might impact different species in apparent concordance, species respond to change independently of one another (Hannah et al. 2005). What appear to be cohesive species assemblages today suggesting a common underlying diversification process may instead represent a combination of distinct independent processes that have nevertheless resulted in syntopy. Niche conservatism could play a role, given that different populations of a species will exhibit similar environmental tolerances (Wiens and Graham 2005). It is important to investigate in detail the diversification processes for each species or species complex comprising a focal community that is being investigated from a comparative biogeographical standpoint. Whereas general biogeographical trends have been proposed for Central America, inadequate attention has been focused on elucidating the evolutionary patterns and processes behind regional and local species assemblages in Central America.

Uncovering the processes driving the origin and maintenance of species assemblages is essential for formulating and implementing effective conservation policy, particularly in a high biodiversity and geographically complex region such as Central America. Central America has connected North and South America for approximately three million years (O'Dea et al. 2016). However, it has been an intermittent bridge during the past 70 million years due to the collision of the North American and Caribbean plates and their subsequent movements (Iturralde-Vinent 2006). Central America lies in the transition zone between the Nearctic and Neotropical regions, acting as a corridor, filter, or barrier to the dispersal of northern and southern biotas (Lomolino et al. 2010). As a result, Central America is an area rich in biological diversity as its biota has biogeographical affinities with both of the older continental landmasses, North and South America.

Research on the Central American fauna and flora has primarily focused on discovering the origin and directionality of movement of different taxa (north to south or vice versa), and whether the movement preceded the final closure of the Central American bridge. For example, for terrestrial mammals (Simpson 1950) and freshwater fishes (Miller 1966), the predominant pattern has been one of North American taxa having passed through Central America to colonize South America. In contrast, for the majority clades that originated in South America and dispersed northward, dispersal either terminated in Central America before reaching North America or they reached North America but subsequently went extinct there. The bird families Furnariidae and Thraupidae are exceptions in that both families originated in South America and successfully penetrated into North America (Weir et al. 2009). For the family Icteridae and for several montane clades (e.g., *Lampornis, Chlorospingus, Arremon*), a northern origin is inferred from phylogenies (Weir et al. 2008, 2009). On the timing of movement, recent research show

that migration across the Isthmus of Panama occurred in waves at 20 and 6 million years ago, likely reflecting the intermittent presence of emergent land bridges (Bacon et al. 2015). These patterns are based on studies at the species level or above. However, the analysis of assemblages at a finer spatial scale and at a more recent temporal frame, from the Pleistocene to the present, might reveal that more complex scenarios of faunal exchange between the continental landmasses have occurred.

Central America encompasses two regions delimited by geographic features: Nuclear Central America (Schuchert 1935) and the younger land bridge of Lower Central America (i.e., mainly Costa Rica and Panama; Bagley and Johnson 2014). Nuclear Central America (NCA) lies between the Isthmus of Tehuantepec in southern Mexico and the Nicaraguan Depression in southern Nicaragua (Schuchert 1935) (**Figure 1**). The Isthmus of Tehuantepec (IT) is a continental strait with a width of 200 km, with 2000 m mountain ranges both its western and eastern margins (the Trans-Mexican Volcanic Belt to the west and the Chiapas highlands to the east). The current structure of the IT is the result of three tectonic episodes that started in the Late Miocene (ca. 6 Ma) and continue today with subsidence in the south and extension in the north (Barrier et al. 1998). The Nicaraguan Depression (ND) also represents an area of lowland habitat that separates mountains of up to 2000 m asl in central Nicaragua and 1770 m asl in the south. The ND has the two largest Central American lakes, Xolotlán and Cocibolca (commonly known as Managua and Nicaragua, respectively). The ND emerged from the sea at the beginning of the Pleistocene (Schuchert 1935).

The Isthmus of Tehuantepec and the Nicaraguan Depression play an essential role in Nuclear Central American biological diversity. Both geographic features represent isolating barriers to mountain species (Daza et al. 2010, Ornelas et al. 2013, Jiménez and Ornelas 2016). Populations geographically isolated by these natural barriers diverge independently, increasing the levels of endemicity in the region. Endemic species add to the high biological richness in NCA that results from the transition between the Nearctic and Neotropical regions. In birds, twenty-two species have geographic ranges restricted to the mountain forests in NCA (Howell and Webb 1995). Hitherto, comprehensive biogeographic studies at the intraspecific level of NCA mountain birds are still lacking. It is unknown whether the populations restricted between the IT and ND represent monophyletic groups.

The geological history of NCA and its location encompasing three tectonic plates creates a complex topography with mountain ranges that have different origins and ages. The western side of NCA has rocks from the early Paleozoic, covered by ice during the Quaternary glacial cycles. The middle region has uplifted volcanic rocks that date to the Carboniferous. The Pacific Volcanic Chain and eastern mountains emerged during the Tertiary and Quaternary, with five volcanoes that are still active (Schuchert 1935, Iturralde-Vinent 2006, Bergoeing 2015). Additionally, the dynamic climate history, mainly during the Pleistocene glacial cycles, have set the stage for *in situ* diversification, both above the species level (Cano et al. 2018, beetles) and at the intraspecific level (Rodríguez-Gómez and Ornelas 2014, birds; Pérez Consuegra and Vázquez-Domínguez 2015, mammals).

The Motagua-Polochic-Jocotán Fault System (MPJFS) and the Honduras Depression (HD) are important biogeographic barriers within NCA (Daza et al. 2010, snakes; Pérez Consuegra and

Vázquez-Domínguez 2015, mammals; Rovito and Parra-Olea 2016, amphibians; Hofmann and Townsend 2017, lizards). The MPJFS is part of the suture zone between the North American and Caribbean plates (Ortega-Gutiérrez et al. 2007), and the HD extends north to south from the Caribbean Sea to the Gulf of Fonseca (Schuchert 1935). The MPJFS and the HD are dry lowland valleys that serve as barriers to the movement of montane species. Additionally, the glacial cycles of the Pleistocene are drivers of population divergence, both for genotypes and phenotypes, on either side of the MPJFS (Daza et al. 2010, Rodríguez-Gómez and Ornelas 2014). However, recent studies have discovered additional geographic breaks within NCA (Pérez Consuegra and Vázquez-Domínguez 2015, Firneno et al. 2020), and have also suggested that the MPJFS is a semi-permeable barrier with ongoing gene flow (Rodríguez-Gómez and Ornelas 2014).

Phylogeographic studies based on mtDNA of neotropical bird species suggest that: (i) montane bird populations in NCA are phylogenetically related to either northern or southern clades, but relationships can be more complex; (ii) for some species, NCA populations do not group as a single monophyletic group; and (iii) geographic barriers within NCA might enhance *in situ* diversification (*Henicorhina leucophrys*, Cadena et al. 2019; *Myioborus miniatus*, Pérez-Emán et al. 2010; *Chlorospingus flavopectus*, Bonaccorso et al. 2008, Weir et al. 2008; *Arremon brunneinucha*, Cadena et al. 2007, Navarro et al. 2008). However, such patterns have been overlooked and have not been explicitly stated and discussed. Additionally, avian phylogeographic studies that connect the Americas are scarce, have low geographic representation across the region, and mainly use organelle DNA and few nuclear loci.

Here, through a comparative phylogeographic approach, we aim to understand the role of common biogeographic history and species idiosyncratic evolutionary pathways in shaping the current NCA montane bird assemblage. More specifically, we pose the following questions: a) what are the phylogenetic relationships of the montane NCA avifauna? b) Do the populations from NCA represent monophyletic groups? c) What processes have promoted *in situ* diversification in NCA birds? To answer these questions, we assemble mitochondrial and genomic data for seven avian species that compose the typical montane avifauna of NCA. We analyze the phylogenetic divergence events leading to the current assemblage of montane birds in NCA, describe patterns of monophyly within NCA, unravel common phylogeographic breaks within NCA, and investigate NCA *in situ* diversification.

## Methods

### Sampling and field procedures

We conducted exhaustive geographic sampling within Nuclear Central America, visiting 16 localities between 2008 and 2017. For this comparative study, we analyzed 676 individuals from seven avian species: *Lampornis viridipallens* (157 individuals), *Lampornis sybillae* (13 individuals), *Henicorhina leucophrys* (83 individuals), *Basileuterus belli* (89 individuals), *Myioborus miniatus* (86 individuals), *Chlorospingus flavopectus* (152 individuals), and *Arremon brunneinucha* (96 individuals) (**Table S1**). The seven species represent ideal systems for studying the montane biogeography of NCA because they all inhabit Neotropical mountains, and the different species have different biogeographic origins, with some having their sister species

in North America and others having their sister lineages in Lower Central America or South America. Previous research, mainly from Mexico or South America, has shown that each of these taxa exhibit intraspecific genetic and phenotypic geographic structure, with differentiated subgroupings inhabiting different mountain ranges. Additionally, they all are common species inhabiting the forest understory. Finally, we selected the outgroup taxa following published phylogenies (Lovette et al. 2010; Klicka et al. 2014; McGuire et al. 2014; Cadena et al. 2019).

We conducted scientific collection of specimens in joint expeditions of the Museum of Vertebrate Zoology (MVZ), University of California, Berkeley (UC Berkeley); Escuela de Biología (EB), Universidad de San Carlos de Guatemala (USAC); and Museo de Zoología "Alfonso R. Herrera" (MZFC), Universidad Nacional Autónoma de México (UNAM). We sampled with the permission granted by the Consejo Nacional de Áreas Protegidas in Guatemala through research and collecting permits provided to EB-USAC, the Mexico's Secretaría de Medio Ambiente y Recursos Naturales, Subsecretaría de Gestión para la Protección Ambiental, Dirección General de Vida Silvestre granted to UNAM, and ethical approval R317 granted by the UC Berkeley Institutional Animal Care and Use Committee. We preserved the captured individuals as voucher specimens (study skins and tissue samples) and deposited them in ornithological research collections at MVZ-UC Berkeley, EB-USAC, and MZFC-UNAM.

We supplemented our sampling with tissue loans from various museum collections: American Museum of Natural History – AMNH; Burke Museum of Natural History and Culture – UWBM; Cornell University Museum of Vertebrates – CUMV; Field Museum of Natural History – FMNH; Instituto de Biología, Universidad Nacional Autónoma de México – IBUNAM; Kansas University, Natural History Museum – KU; Louisiana State University Museum of Natural Science – LSUMZ; Museum of Southern Biology – MSB; University of Alaska Museum – UAM; and Yale Peabody Museum of Natural History, Yale University – YPM.

## Mitochondrial DNA sequencing

We extracted genomic DNA using the DNeasy blood and tissue extraction kit (Qiagen, Valencia, CA, USA), following the protocol recommended by the manufacturer. We PCR-amplified and sequenced 1041 base pairs (bp) of NADH nicotinamide dehydrogenase subunit 2 (ND2). We used the primers L5204 and H6312 for ND2 amplification (Cicero and Johnson 2001). Polymerase chain reaction conditions included an initial denaturation at 94 °C for 1 min; then 35 cycles at 94 °C for 30 s, 54 °C for 30 s, and 72 °C for 45 s; and a final extension at 72 °C for 10 min. We sequenced PCR products in both directions, forward and reverse, using BigDye terminator chemistry (Applied Biosystems, Foster City, CA, USA) on an ABI 3730 automated sequencer (Applied Biosystems, Foster City, CA, USA). We edited the sequences using Geneious v. 5.1.7 (http://www.geneious.com). We conducted our lab work in the Evolutionary Genetics Laboratory at the Museum of Vertebrate Zoology.

## ddRAD sequencing and SNP calling

We followed the protocol for double digest restriction site-associated DNA sequencing (ddRAD) described by Peterson et al. (2012). The different genera were processed independently, and the six final libraries were as follow: (1) *Lampornis viridipallens* and *L. sybillae*, (2) *Henicorhina*

*leucophrys*, (3) *Basileuterus belli*, (4) *Myioborus miniatus*, (5) *Chlorospingus flavopectus*, and (6) *Arremon brunneinucha*. Briefly, 500 ng of genomic DNA, quantified with Qubit (Thermo Fisher Scientific), were digested for three hours using the restriction enzymes EcoRI and SphI-HF (NEB). After digestion and bead clean-up, we labeled each individual with the ligation of one of 24 different adapters. Adapter ligation was followed by pooling sets of up to 24 individuals and two consecutive bead clean-ups. The cleaned products were PCR-amplified and indexed during 12 cycles using the Phusion DNA polymerase (NEB). After bead clean-up and qPCR, we combined libraries of 24 individuals in an equimolar manner. The combined final library per genus was subjected to size selection through PippinPrep.

Two of the final libraries (*Lampornis* and *Basileuterus*) were excised as expected and yielded concentrations suitable for sequencing. However, the other four libraries (*Henicorhina*, *Myioborus*, *Chlorospingus*, and *Arremon*) yielded too low concentrations for sequencing. We proceeded to amplify the four libraries for three cycles using the Phusion DNA polymerase. Unfortunately, we recovered a high peak of shorter fragments in addition to the desired peak that was previously excised. Fortunately, we had duplicate backup libraries to be submitted for excision. Once again, the excised libraries yielded low concentrations, and through a test of amplifying 0.5 µL of the libraries, we discovered that the shorter fragments were also present in this batch. We proceeded with two consecutive bead clean-ups with low-ratio beads (0.55X) to exclude the shorter fragments in the excised libraries as much as possible. Subsequently, we amplified the libraries during three (*Myioborus*) or four cycles (*Henicorhina*, *Chlorospingus*, *Arremon*) using the KAPA HiFi HotStart DNA Polymerase in the 2X ReadyMix (Roche). We did a single bead clean-up with regular beads (1.2X) and submitted for excision one more time. The newly excised libraries yielded concentrations and fragment size distributions suitable for sequencing.

The final libraries were run on one lane of an Illumina NovaSeq S4 to generate 150 bp paired-end sequence reads. Given pooling issues in the sequencing facility, we recovered an uneven number of reads for our different libraries. Therefore, the libraries were subsequently run again on one lane of an Illumina NovaSeq S4 to generate 150 bp paired-end sequence reads to supplement the previous set of reads. The sequencing was carried on at the QB3 Vincent J. Coates Genomic Sequencing Laboratory at UC Berkeley.

Raw sequence reads from both runs were demultiplexed and combined using the process_radtags program in Stacks (Catchen et al. 2013). Then, for the *Lampornis* dataset, we built the loci catalog mapping clean sequences from each individual to the reference annotated genome of *Calypte anna* available through NCBI (GenBank assembly accession: GCF_003957555.1). The sequence reads were mapped to the genome using the software BWA (Li and Durbin 2009) and then converted to BAM files with SAMtools (Li et al. 2009). We used the gstacks program from Stacks to create loci and build a catalog using the BAM files as input. After that, we went through the subsequent steps twice, once for the dataset that included the ingroup and outgroup and once for the dataset with only the ingroup. We used the populations program from Stacks to assign 80% as the minimum percentage of individuals in the complete dataset (R = 0.8) required to process a locus and create a file in Variant Call Format (VCF). Then, we performed additional filtering steps in VCFtools (Danecek et al. 2011). We included only sites with a minor allele frequency of 0.01 (--maf 0.01), with mean depth values greater than or equal to 3 (--min-

meanDP 3) and less than or equal to 10 (--max-meanDP 10). We removed the individuals with 30% or more missing data. We proceeded to prune sites with evidence of linkage disequilibrium creating a BED file and estimating r2 in Plink v1.9 (Purcell et al. 2007). We obtained a final VCF file for phylogenetic analysis (ingroup and outgroup) and another VCF file to study population structure (ingroup only).

We used the denovo_map.pl program from Stacks for the non-hummingbird datasets: *Henicorhina*, *Basileuterus*, *Myioborus*, *Chlorospingus*, and *Arremon*. We used the default Stacks parameters (*m* 3, *M* 2, and *n* 1) to build a *de novo* alignment. We set the populations program to assign 80% as the minimum percentage of individuals in the complete dataset (R = 0.8) required to process a locus. We only used one variant site per locus (--write-single-snp) to prevent linked sites in the final dataset. We got two final VCF files per genus for downstream analyses, one for phylogenetic analysis and one for population structure analyses.

**Phylogenetic relationships of montane birds from Nuclear Central America**

We reconstructed phylogenies to uncover the relationships between NCA and surrounding areas, west of the Isthmus of Tehuantepec and south of the Nicaraguan Depression. We also used the phylogenies to understand the colonization of NCA populations and test their monophyly. We analyzed the ddRAD nuclear dataset, specifically, unliked SNPs (i.e., one variant site per locus), and followed the same procedure for each of the six different genera. First, we converted the VCF file with the ingroup and outgroup to a fasta file using the Python script vcf2phylip.py (Ortiz 2019). Then, we conducted a maximum likelihood analysis in RAxML v8.2 (Stamatakis 2014) using the GTRCAT model for the complete SNP set. We obtained node support by running rapid bootstrapping with 100 iterations. Finally, the consensus tree was visualized and edited in FIGTREE v1.2.3 (http://tree.bio.ed.ac.uk/software/figtree/).

**Genetic structure and geographic barriers within Nuclear Central America**

We analyzed the mitochondrial ND2 matrix and the ddRAD dataset to understand the geographic distribution of genetic variation and uncover processes that have promoted *in situ* diversification. We started by generating an unrooted statistical parsimony haplotype network (Clement et al. 2000) of the ND2 matrixes, using the software POPART v.1.7 (Leigh and Bryant 2015). We also performed a Principal Component Analysis (PCA) of the ddRAD datasets. The PCA, a clustering analysis, is a useful method with which to understand the spatial distribution of the data and does not require meeting the assumptions of other genetic analyses (e.g., Hardy-Weinberg Equilibrium). We conducted the PCA as implemented in ADEgenet (Jombart 2008) and recorded the eigenvalues and eigenvectors for the first four principal components.

We estimated the number of ancestral populations (K) and individual admixture coefficients using the ddRAD datasets. We performed the admixture analyses with sparse nonnegative matrix factorization algorithms (sNMF, Frichot et al. 2014) as implemented in the R package LEA (Frichot and François 2015). The sNMF is an effective and time-efficient method to estimate individual ancestry coefficients in large genomic datasets (Frichot et al. 2014). To infer the number of populations, we assessed K1 to K10 with ten replicates for each value of K. We

selected K based on the lowest cross-entropy value and plotted the Q matrix for the run of the selected K, which showed the lowest cross-entropy value within the ten replicates.

To understand the isolating strength of the geographic barriers within NCA, we estimated pairwise FST using the ddRAD dataset. We calculated pairwise FST between the five most consistent population groups across the six genomic datasets: (1) Altos de Chiapas, (2) highlands north of the MPJFS, (3) Pacific Volcanic Chain in southern Mexico and Guatemala, (4) highlands east of the MPJFS and west of the Honduras Depression, and (5) highlands east of the HD and north of the Nicaraguan Depression. We estimated the FST in the populations module from Stacks (--fstats --bootstrap-fst).

**Results**

We sequenced complete ND2 sequences (1041 bp) for 674 individual samples (**Table S1**). We obtained ddRAD genomic data from 665 individual samples, including the ingroup and outgroup taxa of the studied avian species. After filtering and excluding the samples with a low number of reads (less than 1,000,000 reads), we ended up with 630 individuals distributed as follows: 139 *Lampornis viridipallens – L. sybillae*, 81 *Henicorhina leucophrys*, 89 *Basileuterus belli*, 82 *Myioborus miniatus*, 151 *Chlorospingus flavopectus*, and 88 *Arremon brunneinucha*. The mean effective per-sample coverage of the six different genera ranged from 50.3x to 106.0x, with a minimum individual sample coverage of 15.6x (**Table S2**). The total number of unlinked SNPs was variable among datasets and ranged from 9,364 to 18,395 variable sites (**Table S3**).

**Phylogenetic relationships of montane birds from Nuclear Central America**

Nuclear Central American populations of *Basileuterus belli* (**Figure 2c**), *Myioborus miniatrus* (**Figure 2d**), and *Chlorospingus flavopectus* (**Figure 2e**) are closely related to populations west of the Isthmus of Tehuantepec. NCA populations of *B. belli* and *M. miniatus* represent monophyletic groups. NCA *B. belli*, together with the populations west of the Isthmus of Tehuantepec, comprise a monophyletic species sister to *B. melanogenys* from Lower Central America (Costa Rica and Panama). NCA *M. miniatus* is sister to the samples from the Tuxtlas region, which together are related to a clade comprising both Lower Central American and South American populations. Finally, all of these clades together are sister to *M. miniatus* from west of the IT (excluding the Tuxtlas region). In contrast, NCA populations of *C. flavopectus* (**Figure 2e**) do not represent a monophyletic group. Populations of *C. flavopectus* geographically close to the limits of NCA, IT and ND, are more closely related to populations from west of the IT or south of the ND than to NCA populations. The individuals from Tapalapa, within the Altos de Chiapas region, are related to individuals from the Sierra Madre Oriental in Mexico, west of the IT. In contrast, the individuals from Tila, also from Altos de Chiapas, are related to individuals from the mountains north of the MPJFS. Similarly, individuals from Uyuca, north of the Nicaraguan Depression, are related to individuals from west of the Honduras Depression; and individuals from Estelí, north of the ND, are related to individuals from Lower Central America.

On the other hand, NCA populations of *Henicorhina leucophrys* (**Figure 2b**) and *Arremon brunneinucha* (**Figure 2f**) are more closely related to populations south of the Nicaraguan Depression. NCA populations of *H. leucophrys* represent a monophyletic group. *Henicorhina*

*leucoprhys* from NCA are closely related to a clade of populations from Lower Central America and South America; then, all of them are related to populations west of the IT. In contrast, NCA populations of *A. brunneinucha* are not monophyletic. The first bifurcation in the phylogeny of the species results in a clade that includes the samples from Altos de Chiapas and the samples from west of the IT, and the second clade includes all the other samples from NCA and the samples from Lower Central America and South America. Interestingly, the two individuals of *A. virenticeps* are nested within *A. brunneinucha* from west of the IT.

Within NCA, we found recurrent divergence in the following regions across species: (1) Altos de Chiapas, (2) highlands north of the MPJFS, (3) Pacific Volcanic Chain in southern Mexico and Guatemala, (4) highlands east of the MPJFS and west of the Honduras Depression, and (5) highlands east of the HD and north of the Nicaraguan Depression (**Figure 2**). However, the phylogenetic relationships among the populations from the five regions were not consistent across all species, although general patterns exist. For instance, the divergences across eastern MPJFS and the Honduras and Nicaraguan Depressions are usually older than the divergences across western MPJFS, the geographic barrier between the highlands north of the MPJFS and the Pacific Volcanic Chain. Interestingly, the individuals from the locality of Zacualpa in Guatemala, geographically located between the highlands north of the MPJFS and the Pacific Volcanic Chain, were more closely related to populations from the Pacific Volcanic Chain in most species (*Lampornis, Henicorhina, Basileuterus*) but more closely related to the populations from the highlands north of the MPJFS in *Chlorospingus*. Finally, *Myioborus miniatus* populations from NCA showed very shallow divergence and no internal phylogenetic structure.

**Genetic structure and geographic barriers within Nuclear Central America**

Mitochondrial haplotype networks, genomic PCAs, and genomic admixture analyses recover considerable genetic structure for birds within Nuclear Central America (**Figures 3 to 8**). Consistent with phylogenetic results, general patterns emerged and the same five regions listed above were differentiated across species. Therefore, significant barriers for isolating bird populations within the mountains of NCA are: (1) the break between Altos de Chiapas and the highlands north of the MPJFS, (2) the western area of the MPJFS, (3) the eastern area of the MPJFS, and (4) the Honduras Depression. However, gene flow across the barriers is suggested by genetic admixture analyses, particularly across the break between Altos de Chiapas and the highlands north of the MPJFS, and the western area of the MPJFS. *Chlorospingus flavopectus* is the only species in which the four geographic barriers are highly effective.

Notably, the isolating effect of the Motagua-Polochic-Jocotán Fault System is not homogenous along its extent. The isolation imposed by the eastern area of the MPJFS is stronger than the isolation imposed by the western area of the MPJFS. The six species that live in the MPJFS area showed higher pairwise FST values (**Table 1**) between the highlands north of the MPJFS and the highlands east of the MPJFS and west of the Honduras Depression (eastern area of the MPJFS) than the values between the highlands north of the MPJFS and the Pacific Volcanic Chain (western area of the MPJFS). Moreover, genetic differentiation between the Pacific Volcanic Chain and the highlands east of the MPJFS was even higher. Additionally, gene flow across the western area of the MPJFS was suggested by the admixture ancestry analysis in *Basileturus belli*.

Species idiosyncrasy was evident in the different examined members of the montane bird assemblage in NCA. *Lampornis viridipallens* and *L. sybillae* are species endemic to NCA, both species are highly genetically differentiated, and the Honduras Depression separates the two species. *Henicorhina leucophrys* and *Basileuterus belli*, while similar in being rare to absent in the highlands east of the HD and north of the Nicaraguan Depression, showed different levels of genetic differentiation within NCA, which were higher in *H. leucophrys* than in *B. belli*, both in mitochondrial DNA and in genomic DNA. Genetic differentiation among populations of *Myiborus miniatus* within NCA was shallow, and a common ND2 haplotype was found from northwestern Guatemala to Panama. As mentioned previously, NCA populations of *Chlorospingus flavopectus* and *Arremon brunneinucha* are not monophyletic groups and, therefore, represent multiple independent lineages coming together in the NCA region.

**Discussion**

We showed how common biogeographic history and species idiosyncratic evolutionary paths shape the current NCA montane bird assemblage. Phylogenetic relationships supported the role of Nuclear Central America as a gateway between North and South America. NCA populations of *Basileuterus belli*, *Myioborus miniatus*, and *Chlorospingus flavopectus* are closely related to populations west of the Isthmus of Tehuantepec. In contrast, NCA populations of *Henicorhina leucophrys* and *Arremon brunneinucha* are more closely related to populations south of the Nicaraguan Depression. For some taxa, NCA populations do not represent monophyletic groups (e.g., *C. flavopectus* and *A. brunneinucha*). However, for others, it is clear that NCA represents its own area of endemism and biogeographical unit. For example, the NCA populations are each monophyletic for *L. viridipallens – L. sybillae*, *H. leucophrys*, *B. belli*, and *M. miniatus*. Furthermore, we recovered high levels of population genetic structure between different mountain ranges within NCA for each of these groups, suggest that NCA is characterized by substantial *in situ* diversification. Significant geographic barriers isolating bird populations within the mountains of NCA include: (1) the break between Altos de Chiapas and the highlands north of the MPJFS, (2) the western area of the MPJFS, (3) the eastern area of the MPJFS, and (4) the Honduras Depression. Interestingly, the isolating effect of the Motagua-Polochic-Jocotán Fault System is not homogenous along its extent. Phylogenies suggested relatively older divergence events in the eastern area of the MPJFS. In contrast, we uncovered genetic admixture across the western area of the MPJS. Recurrent species assemblages in different mountain ranges suggest niche conservatism. Understanding historical processes shaping current species assemblages is fundamental for designing effective conservation strategies.

The montane birds of Central America exemplify the role of the region in connecting the biota of North and South America. Consistent with previously published phylogenies based on mitochondrial DNA (Cadena et al. 2007, Bonaccorso et al. 2008, Navarro et al. 2008, Weir et al. 2008, Pérez-Emán et al. 2010, Cadena et al. 2019), our genomic data recover mixed ancestry of Nuclear Central American montane birds, with some lineages more related to those in either North or South America. However, our geographic and genomic sampling allowed us to uncover and confirm additional complexity. NCA *H. leucophrys* are closely related to populations distributed across Lower Central America and South America. However, we could not include *H. negreti* from South America in our dataset, which has been suggested as the sister clade to NCA populations (Cadena et al. 2019). NCA *M. miniatus* are all closely related to populations of the

species from the Tuxtlas region on the western side of the Isthmus of Tehuantepec; Lower Central American populations are not part of the NCA clade, contrary to what mitochondrial data suggests (Pérez-Emán et al. 2010). *Chlorospingus flavopectus* highlights the phylogenetic complexity within Nuclear Central America. NCA populations of *C. flavopectus* are closely related to either those from the Sierra Madre Oriental on the western side of the IT (Altos de Chiapas), to the clade including the Altos de Chiapas and all of the populations west of the IT (most of NCA populations), or to Lower Central America populations (Estelí, Nicaragua; Bonaccorso et al. 2008, Weir et al. 2008). Finally, NCA *A. brunneinucha* are closely related to either all of the populations west of the IT (Altos de Chiapas) or to Lower Central America and South America (most of NCA populations) (Cadena et al. 2007, Navarro et al. 2008). Our genomic data also confirmed that *A. brunneinucha* is paraphyletic because it includes *A. virenticeps*; a detailed study on *A. virenticeps* is necessary to describe the genetic variation across its geographic range and to understand its phylogenetic relationships with *A. brunneinucha*.

To our knowledge, ours are the first published phylogenies of *Lampornis viridipallens – L. sybillae* and *Basileuterus belli*. *Lampornis viridipallens – L. sybillae* and *B. belli* show contrasting patterns in phylogenetic relationships between NCA populations and populations from contiguous regions. The sister species *L. viridipallens – L. sybillae* are endemic to NCA, and previous phylogenies on the genus *Lampornis* suggest that they are closely related to species from Lower Central America (García-Moreno et al. 2006, McGuire et al. 2014). For *Basileuterus belli*, although included in previous comparative phylogeographic studies, only estimates of genetic differentiation and time since divergence have been previously reported (Barber and Klicka 2010, Ornelas et al. 2013). In *B. belli*, we discovered reciprocal monophyly across the Isthmus of Tehuantepec (west of IT vs. NCA), with the time since divergence having been estimated at 1.5 (1.71 – 0.67) Mya (Ornelas et al. 2013).

Phylogenetic analyses support Nuclear Central America as a biogeographic unit. Monophyly in NCA populations of *L. viridipallens – L. sybillae*, *H. leucophrys*, *B. belli* and *M. miniatus* is enhanced by the strong isolating effect of the Isthmus of Tehuantepec and the Nicaraguan Depression. Intraspecific monophyly in NCA populations of montane birds adds to the region's high levels of endemism, and with further work some of these lineages may warrant species rank. However, it is important to note that we recovered paraphyly in NCA populations of *C. flavopectus* and *A. brunneinucha*. We advise that intraspecific monophyly of NCA populations should not be assumed; monophyly of geographically circumscribed lineages should be tested with appropriate geographic sampling and subsequent phylogenetic reconstructions.

The complex topography within NCA enhances *in situ* diversification. Consistent with previous studies on vertebrates, the Motagua-Polochic-Jocotán Fault System and the Honduras Depression are important biogeographic barriers within NCA (Daza et al. 2010, Pérez Consuegra and Vázquez-Domínguez 2015, Rovito and Parra-Olea 2016, Hofmann and Townsed 2017). The Honduras Depression is a significant barrier separating *Lampornis viridipallens* from *L. sybillae*. It also plays a role in limiting dispersal in populations from *Myioborus miniatus*, *Chlorospingus flavopectus*, and *Arremon brunneinucha*. Presumably, the HD might also limit the geographic range of *Henicorhina leucophrys* and *Basileuterus belli*, both species absent or rare east of the HD. However, other evolutionary and ecological processes should not be ruled out.

Our analyses show that the isolating effect of the Motagua-Polochic-Jocotán Fault System is not homogenous along its extent. The MPJFS is considered one of the most important biogeographic breaks within NCA, given that it is the suture zone between the North American and the Caribbean Plates. Unfortunately, generalization on the importance of the MPJFS sometimes leads researchers to conclude that it is the barrier with major effects in their study system, even when their geographic sampling is sparse. Here, we show the importance of dense geographic sampling to advance the understanding of NCA biogeography, particularly around the MPJFS area. The most substantial isolating effect on the eastern area of the MPJFS and the relatively older divergence events contrast with the shallower divergence and genetic admixture observed in the western area. A possible explanation for these patterns is that within the eastern area of the MPJFS, the three faults, Motagua, Polochic, and Jocotán, co-occur. In contrast, only the Polochic fault reaches the western area. Additionally, mountains located between the highlands north of the Polochic fault and the Pacific Volcanic Chain, such as Zacualpa that we sampled, might interconnect both regions.

We uncovered an important barrier between Altos de Chiapas and the highlands north of the MPJFS. Previous literature already states that the Central Depression in Chiapas separates the region Altos de Chiapas from the Pacific mountains (Gutiérrez-García and Vázquez-Domínguez 2013, Ornelas et al. 2013), which coincides with the genetic differentiation we found between Altos de Chiapas and the Pacific Volcanic Chain. However, we add that the region Altos de Chiapas is also separated from the highlands north of the MPJFS by a recently characterized geographic break (see Chapter 2 of this dissertation). This break is particularly strong in *Chlorospingus flavopectus* and *Arremon brunneinucha*, although more permeable for the other four studied species. We encourage researchers to test the role of this biogeographic barrier with other study systems to advance the understanding of its role in different groups of organisms.

Repeated species assemblages of birds in different mountain ranges of NCA arose through idiosyncratic evolutionary histories. Species assemblages are transitory by nature, ecosystems disassemble, and species reassemble into new ecosystems (Hewitt and Nichols 2005). Here, we provide evidence that a group of bird species might be present simultaneously in multiple mountain ranges and be part of a "common mountain bird assemblage" but have assembled in the different mountain ranges through species-specific historical and spatial processes. The study of assembly processes is usually performed at the species rank; however, we think incorporating intraspecific patterns and processes might help understand species assemblages. Here, we propose that a plausible explanation for the "common assemblage" pattern is niche conservatism because different populations of a species will exhibit similar environmental tolerances given their recently shared evolutionary history (Wiens and Graham 2005). Testing the hypothesis of niche conservatism is our following step.

**Conclusions**

In summary, our work reveals that the current montane bird assemblage in Nuclear Central America results from common biogeographic history and species idiosyncratic evolutionary paths. Nuclear Central America is a region with high levels of biodiversity given the region's role in connecting the biota from North and South America. Additionally, we uncovered high *in situ* diversification promoted by divergence in allopatry in different mountain ranges within

NCA. We found phylogenetic support for considering NCA as a biogeographic unit. However, we recommend that monophyly be tested and not assumed since not all the species we studied are intraspecifically monophyletic within the region. We show that the isolating effect of the Motagua-Polochic-Jocotán Fault System is not homogenous along its extent; detailed and exhaustive geographic sampling in NCA should be considered before assuming that MPJFS is the primary and homogeneous barrier within the region. For example, the biogeographic barrier between Altos de Chiapas and the highlands north of the MPJFS, an important barrier to montane birds, might have been previously overlooked given sparse geographic sampling. We hypothesize that recurrent species assemblages of birds in different mountain ranges, which arise through idiosyncratic evolutionary histories, might be explained by niche conservatism given the recently shared evolutionary history among intraspecific populations. We suggest that accounting for intraspecific patterns and processes could improve our comprehension of species assemblages. Understanding the processes shaping current species assemblages and their constant change is fundamental for designing effective conservation and management strategies, particularly in the highly biodiverse Nuclear Central America.

## Table and figures

**Table 1.** Pairwise FST between the five most consistently recovered population groups across six genomic datasets of montane birds from Nuclear Central America.

| | Altos de Chiapas | North MPJFS | West MPJFS | East MPJFS | North ND |
|---|---|---|---|---|---|
| ***Lampornis viridipallens*** | | | | | |
| Altos de Chiapas | ----- | 0.0198 | 0.0244 | 0.0519 | 0.0817 |
| North MPJFS | | ----- | 0.0200 | 0.0295 | 0.0446 |
| West MPJFS | | | ----- | 0.0337 | 0.0457 |
| East MPJFS | | | | ----- | 0.0926 |
| North ND | | | | | ----- |
| ***Henicorhina leucophrys*** | | | | | |
| Altos de Chiapas | ----- | 0.0233 | 0.1199 | 0.1905 | NA |
| North MPJFS | | ----- | 0.0390 | 0.0847 | NA |
| West MPJFS | | | ----- | 0.1881 | NA |
| East MPJFS | | | | ----- | NA |
| North ND | | | | | NA |
| ***Basileuterus belli*** | | | | | |
| Altos de Chiapas | ----- | 0.0297 | 0.0464 | 0.0954 | NA |
| North MPJFS | | ----- | 0.0226 | 0.0371 | NA |
| West MPJFS | | | ----- | 0.0546 | NA |
| East MPJFS | | | | ----- | NA |
| North ND | | | | | NA |
| ***Myioborus miniatus*** | | | | | |
| Altos de Chiapas | ----- | 0.0204 | 0.0359 | 0.0954 | 0.1194 |
| North MPJFS | | ----- | 0.0189 | 0.0253 | 0.0332 |
| West MPJFS | | | ----- | 0.0416 | 0.0528 |
| East MPJFS | | | | ----- | 0.2241 |
| North ND | | | | | ----- |
| ***Chlorospingus flavopectus*** | | | | | |
| Altos de Chiapas | ----- | 0.0407 | 0.0697 | 0.0967 | 0.1103 |
| North MPJFS | | ----- | 0.0303 | 0.0423 | 0.0461 |
| West MPJFS | | | ----- | 0.0731 | 0.0808 |
| East MPJFS | | | | ----- | 0.0704 |
| North ND | | | | | ----- |
| ***Arremon brunneinucha*** | | | | | |
| Altos de Chiapas | ----- | 0.0707 | 0.0920 | 0.2114 | 0.2477 |
| North MPJFS | | ----- | 0.0232 | 0.0794 | 0.0814 |
| West MPJFS | | | ----- | 0.0984 | 0.1034 |
| East MPJFS | | | | ----- | 0.0951 |
| North ND | | | | | ----- |

MPJFS – Motagua-Polochic-Jocotán Fault System; ND – Nicaraguan Depression.

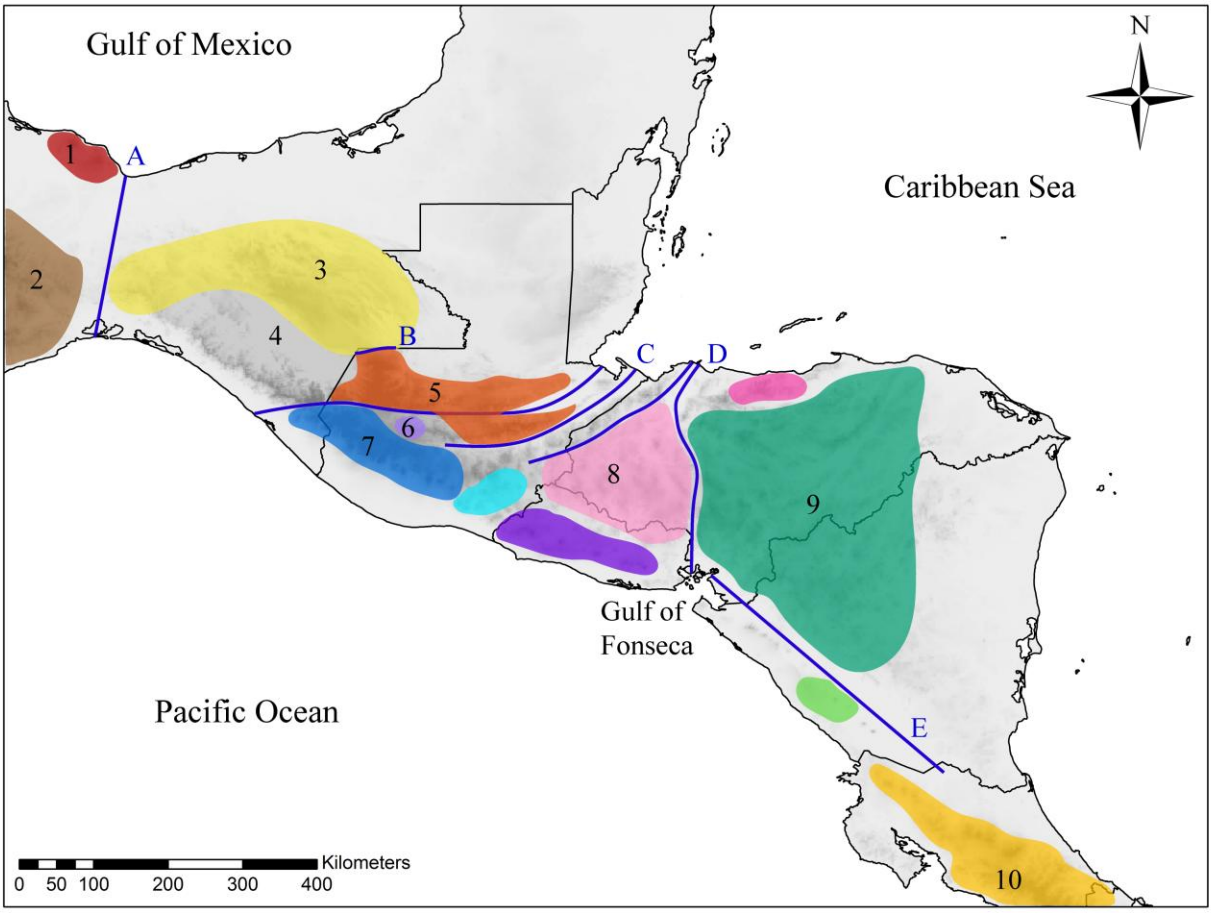


**Figure 1.** Geographic location of Nuclear Central America, which is delimited to the north by the Isthmus of Tehuantepec (A) and to the south by the Nicaraguan Depression (E). Biogeographic barriers within Nuclear Central America are the break between Altos de Chiapas and the highlands north of the Motagua-Polochic-Jocotán Fault System – MPJFS (B), the MPJFS (C), and the Honduras Depression (D). The identification of geographic areas mentioned in the text is as follows: (1) Tuxtlas, (2) west of the Isthmus of Tehuantepec, (3) Altos de Chiapas, (4) Chiapas Central Depression, (5) highlands north of the MPJFS, (6) Zacualpa, (7) Pacific Volcanic Chain in southern Mexico and Guatemala, (8) highlands east of the MPJFS and west of the Honduras Depression, (9) highlands east of the Honduras Depression and north of the Nicaraguan Depression, (10) Lower Central America. Grayscale used on the map represents elevation with darker tones assigned to higher elevations. All the colored areas show different mountain ranges sampled in our study.

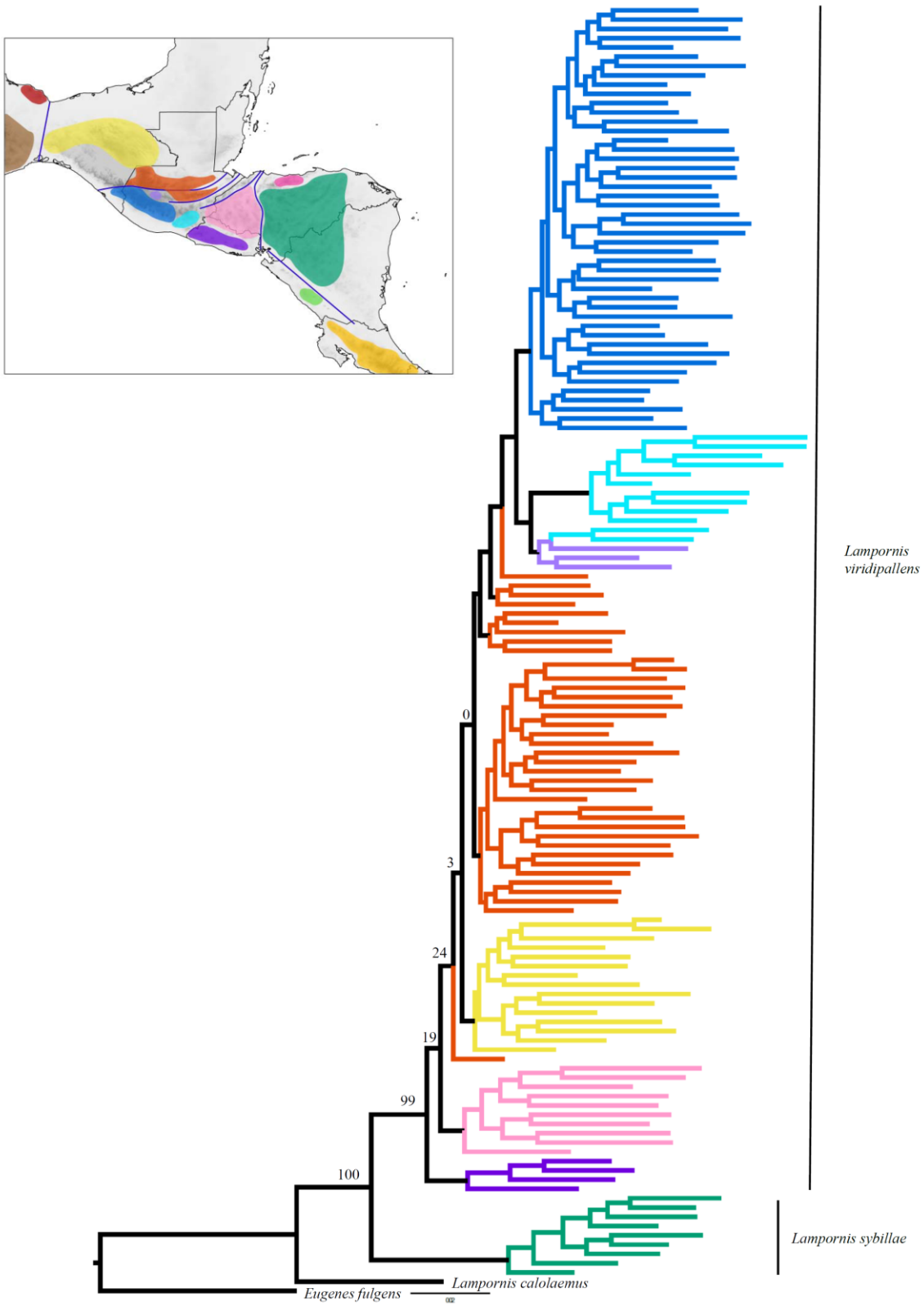


**Figure 2a.** Maximum likelihood phylogeny of *Lampornis viridipallens – L. sybillae* based on ddRAD data (10,617 SNPs). Node support was estimated with 100 iterations of rapid bootstrapping. Map inserted for geographic reference.

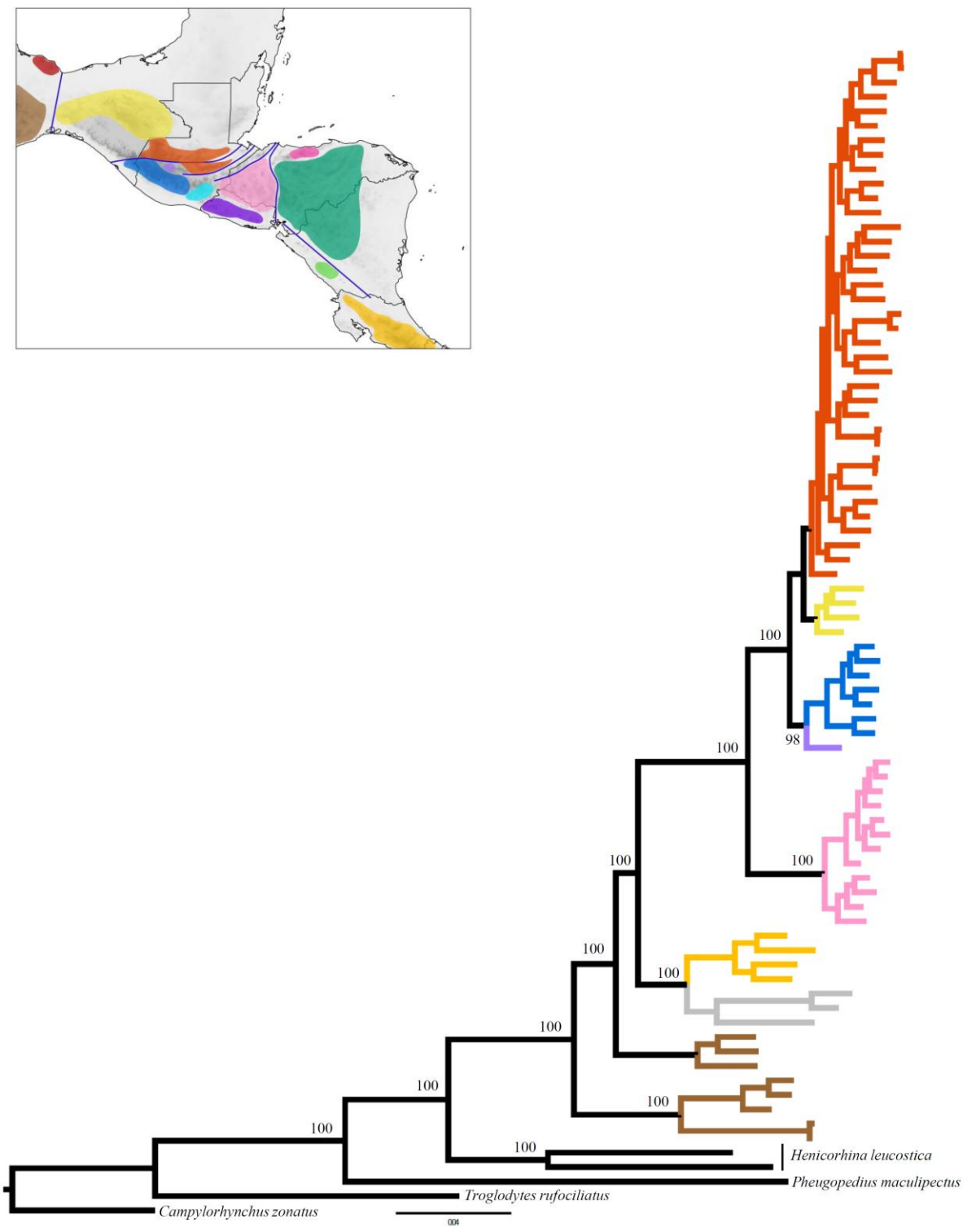


**Figure 2b.** Maximum likelihood phylogeny of *Henicorhina leucophrys* based on ddRAD data (12,102 SNPs). Node support was estimated with 100 iterations of rapid bootstrapping. Map inserted for geographic reference; branches in gray correspond to South America.

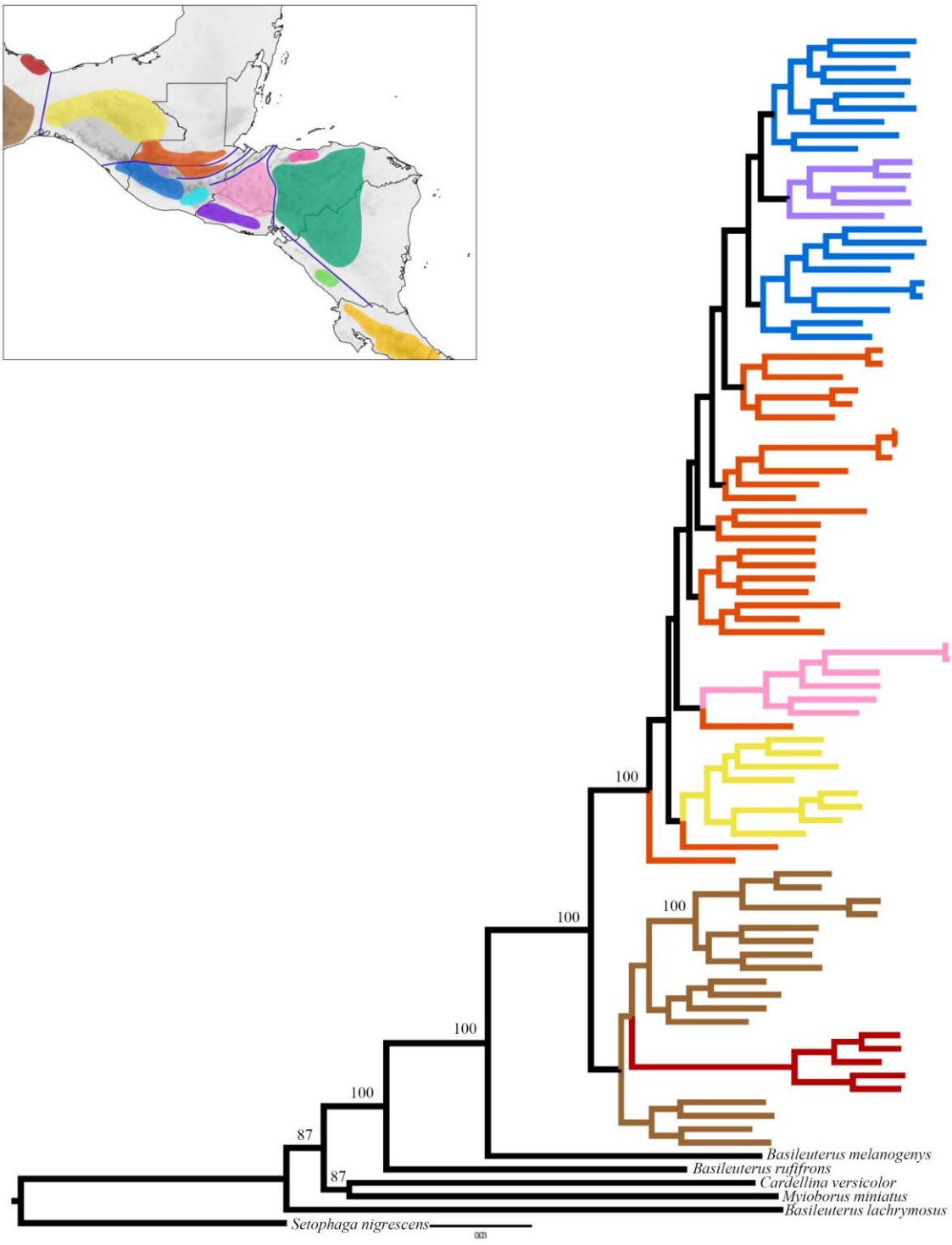


**Figure 2c.** Maximum likelihood phylogeny of *Basileuterus belli* based on ddRAD data (14,309 SNPs). Node support was estimated with 100 iterations of rapid bootstrapping. Map inserted for geographic reference.

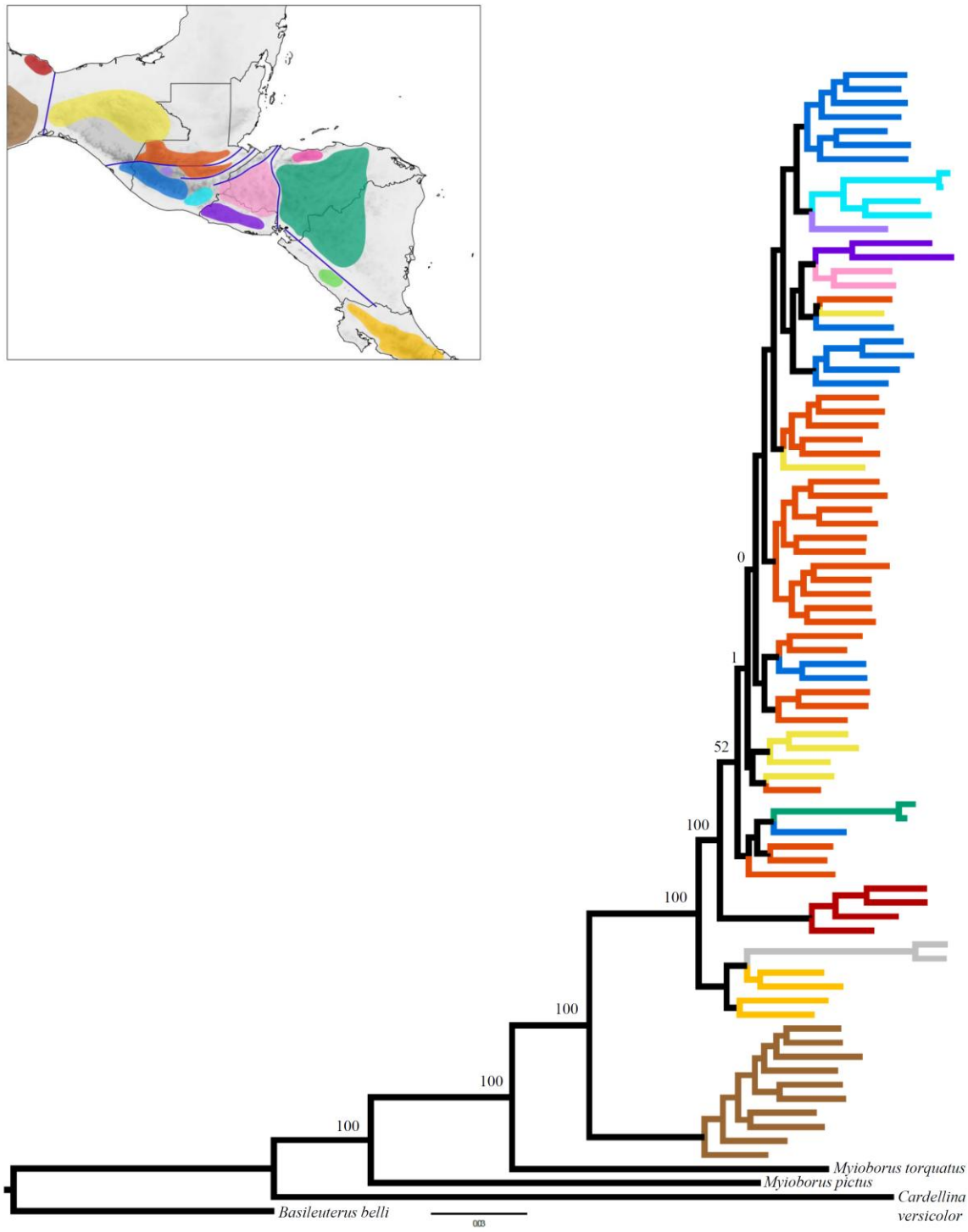


**Figure 2d.** Maximum likelihood phylogeny of *Myioborus miniatus* based on ddRAD data (17,849 SNPs). Node support was estimated with 100 iterations of rapid bootstrapping. Map inserted for geographic reference; branches in gray correspond to South America.

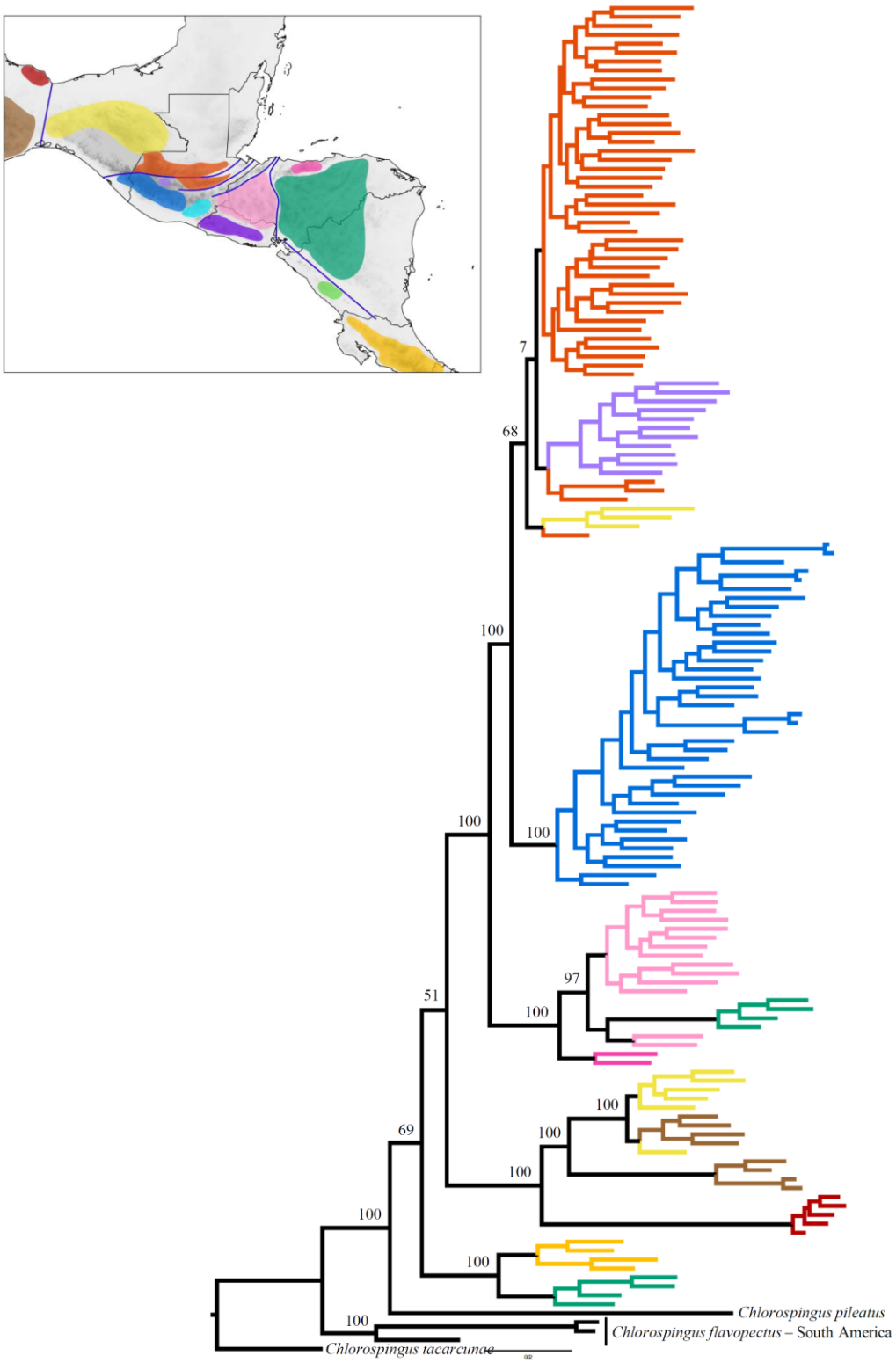


**Figure 2e.** Maximum likelihood phylogeny of *Chlorospingus flavopectus* based on ddRAD data (14,635 SNPs). Node support was estimated with 100 iterations of rapid bootstrapping. Map inserted for geographic reference.

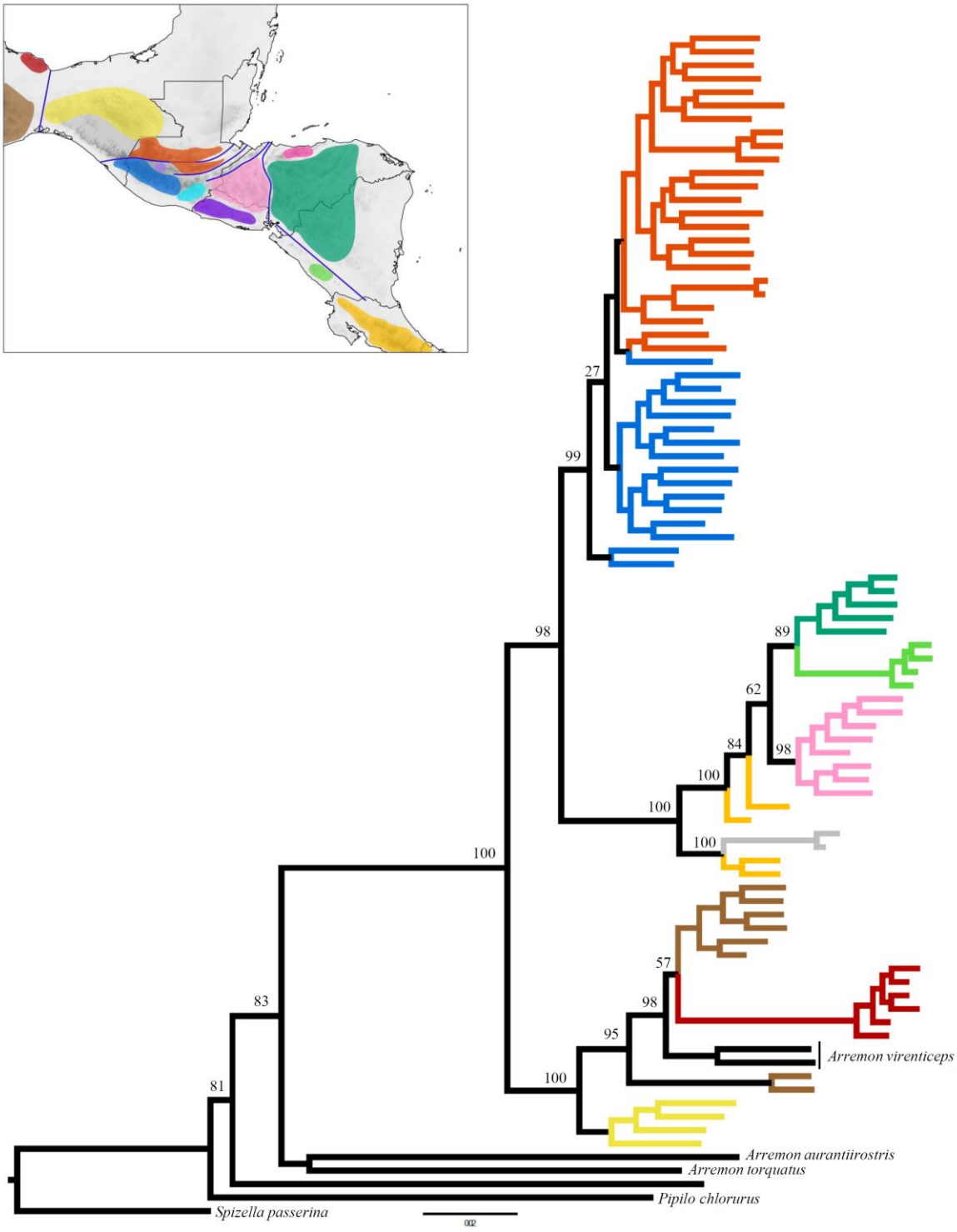


**Figure 2f.** Maximum likelihood phylogeny of *Arremon brunneinucha* based on ddRAD data (9,364 SNPs). Node support was estimated with 100 iterations of rapid bootstrapping. Map inserted for geographic reference; branches in gray correspond to South America.

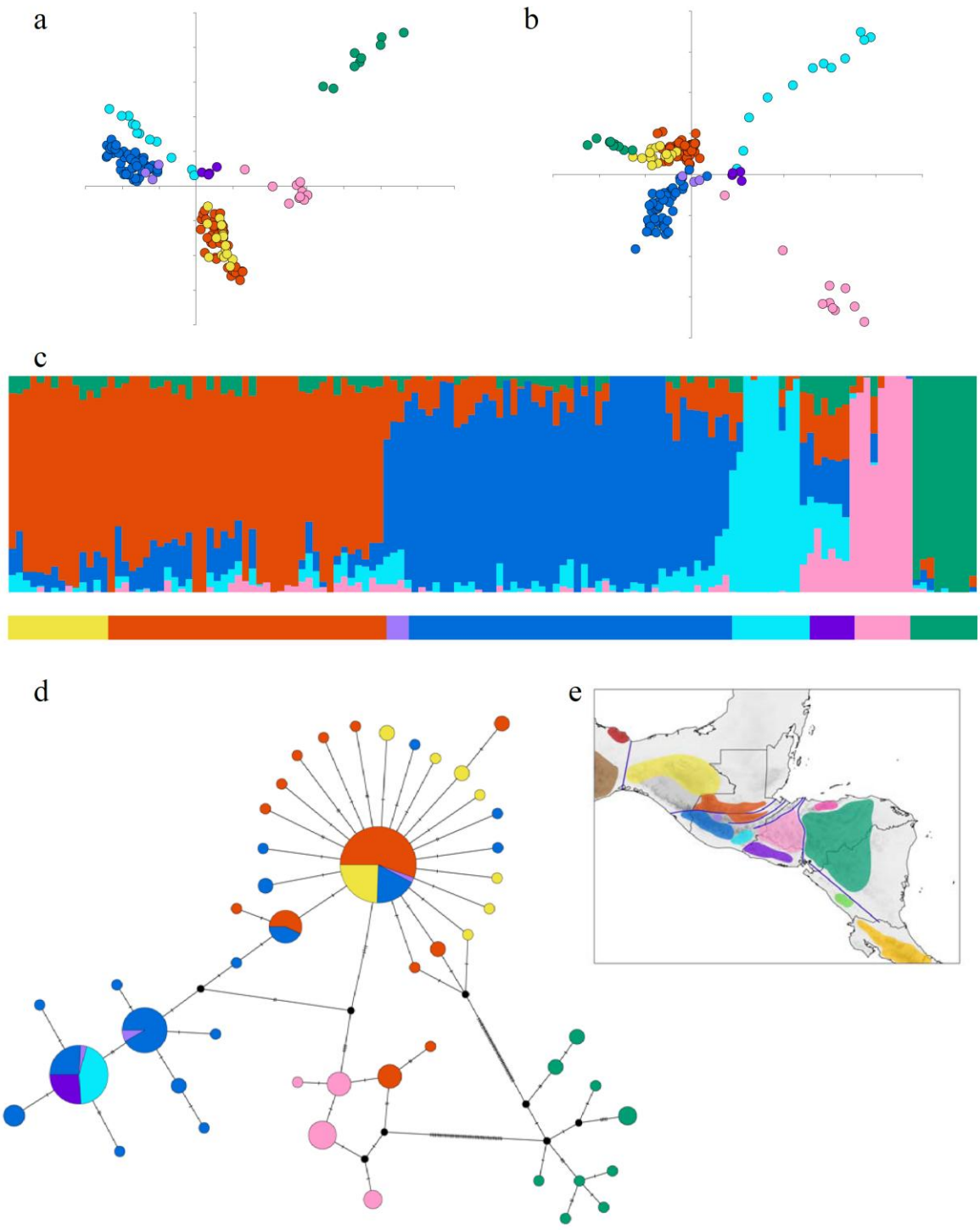


**Figure 3.** Population genetic structure of *Lampornis viridipallens* and *L. sybillae* in Nuclear Central America. a) Principal Component Analysis on ddRAD data, PC1 (4.2%) and PC2 (3.0%). b) Principal Component Analysis on ddRAD data, PC3 (2.2%) and PC4 (2.0%). c) Ancestry analysis based on ddRAD data, K=5; colors on the bar below represent the geographic location. d) Haplotype network based on the complete ND2 mitochondrial gene. e) Map for geographic reference.

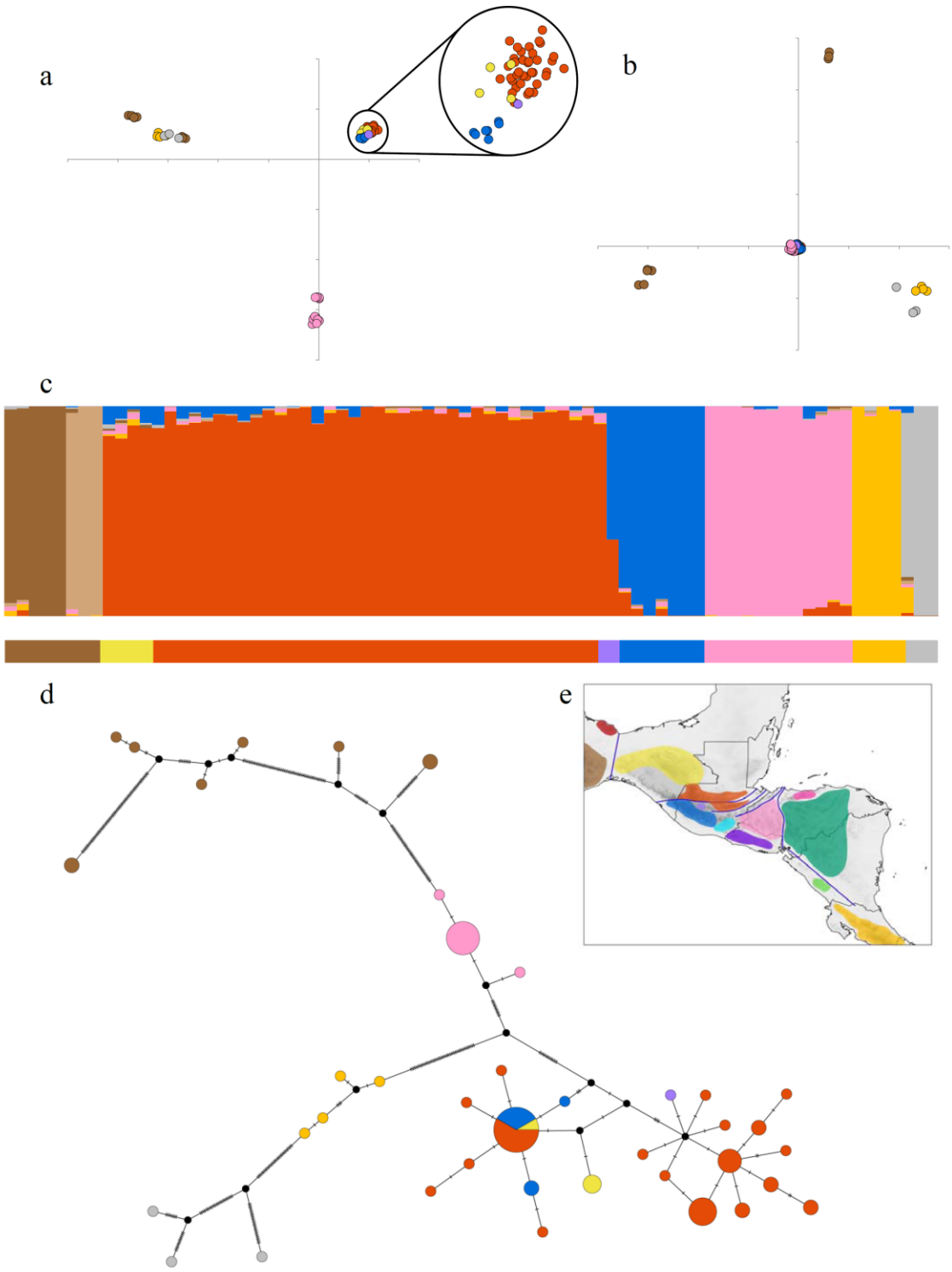


**Figure 4.** Population genetic structure of *Henicorhina leucophrys* in Nuclear Central America. a) Principal Component Analysis on ddRAD data, PC1 (17.9%) and PC2 (11.6%). b) Principal Component Analysis on ddRAD data, PC3 (7.5%) and PC4 (4.2%). c) Ancestry analysis based on ddRAD data, K=7; colors on the bar below represent the geographic location. d) Haplotype network based on the complete ND2 mitochondrial gene. e) Map for geographic reference (gray color in figures, not shown in the map, correspond to South America).

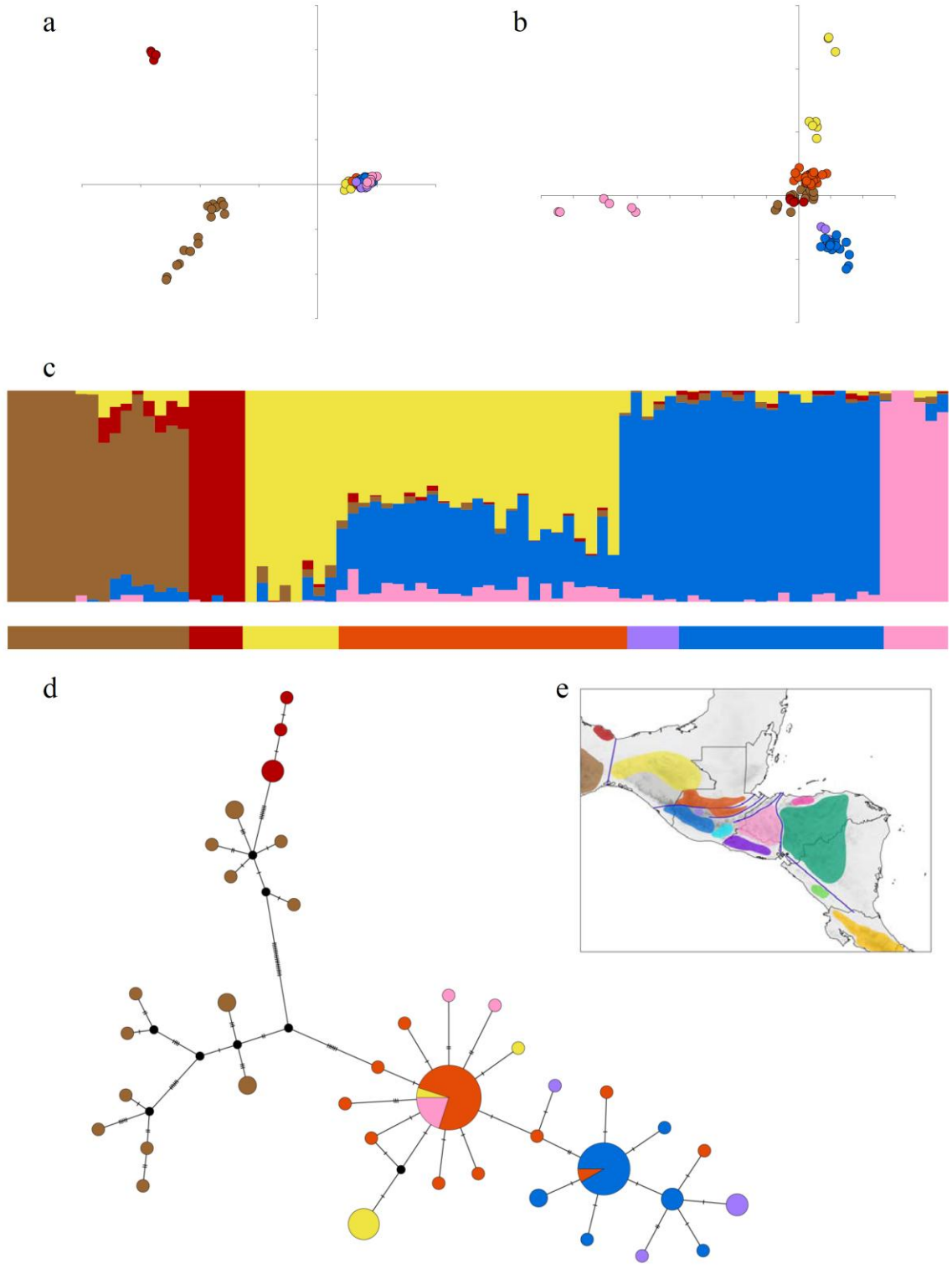


**Figure 5.** Population genetic structure of *Basileuterus belli* in Nuclear Central America. a) Principal Component Analysis on ddRAD data, PC1 (9.7%) and PC2 (4.6%). b) Principal Component Analysis on ddRAD data, PC3 (3.0%) and PC4 (2.8%). c) Ancestry analysis based on ddRAD data, K=5; colors on the bar below represent the geographic location. d) Haplotype network based on the complete ND2 mitochondrial gene. e) Map for geographic reference.

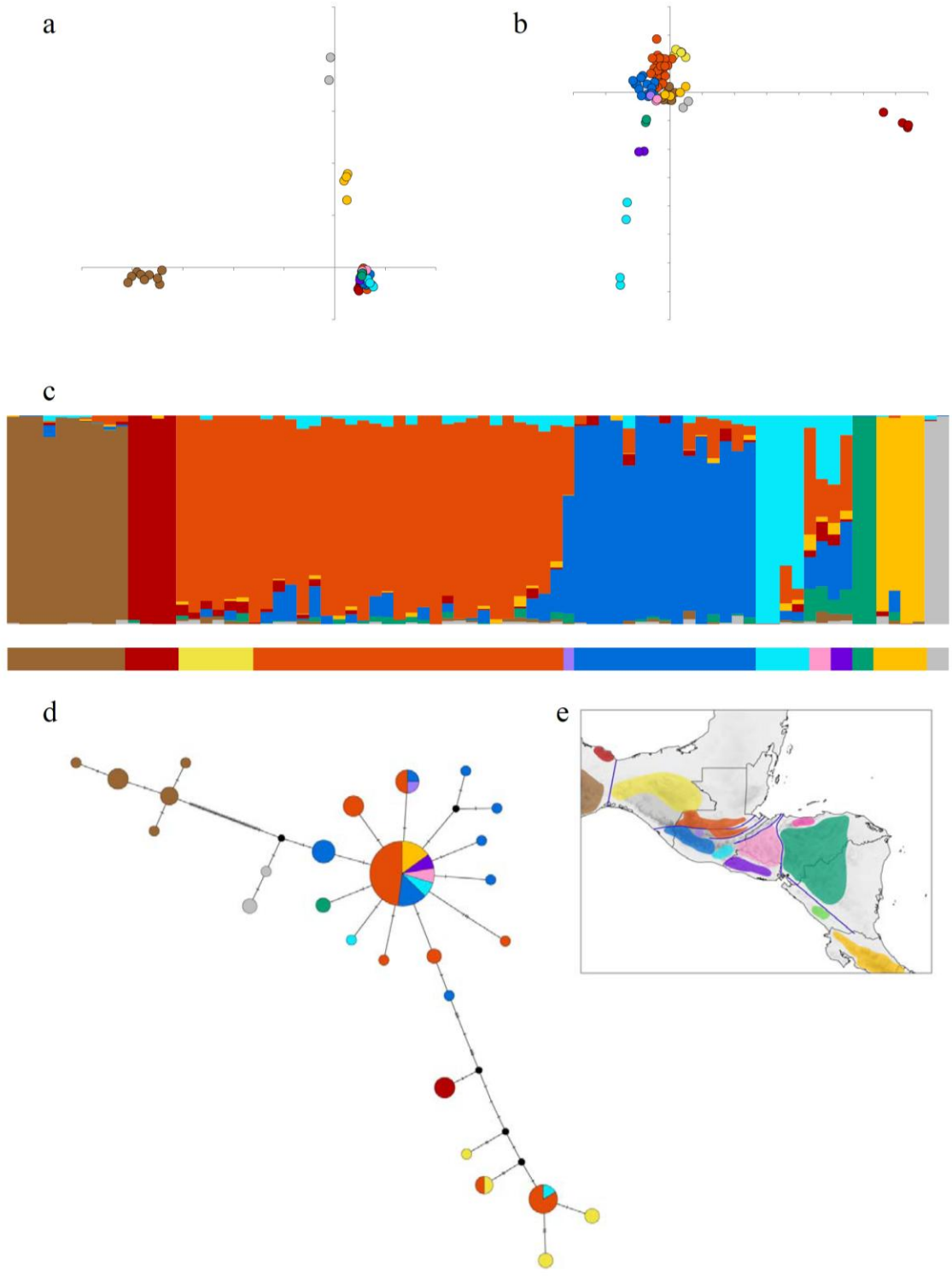


**Figure 6.** Population genetic structure of *Myioborus miniatus* in Nuclear Central America. a) Principal Component Analysis on ddRAD data, PC1 (12.3%) and PC2 (3.3%). b) Principal Component Analysis on ddRAD data, PC3 (2.8%) and PC4 (2.1%). c) Ancestry analysis based on ddRAD data, K=8; colors on the bar below represent the geographic location. d) Haplotype network based on the complete ND2 mitochondrial gene. e) Map for geographic reference (gray color in figures, not shown in the map, correspond to South America).

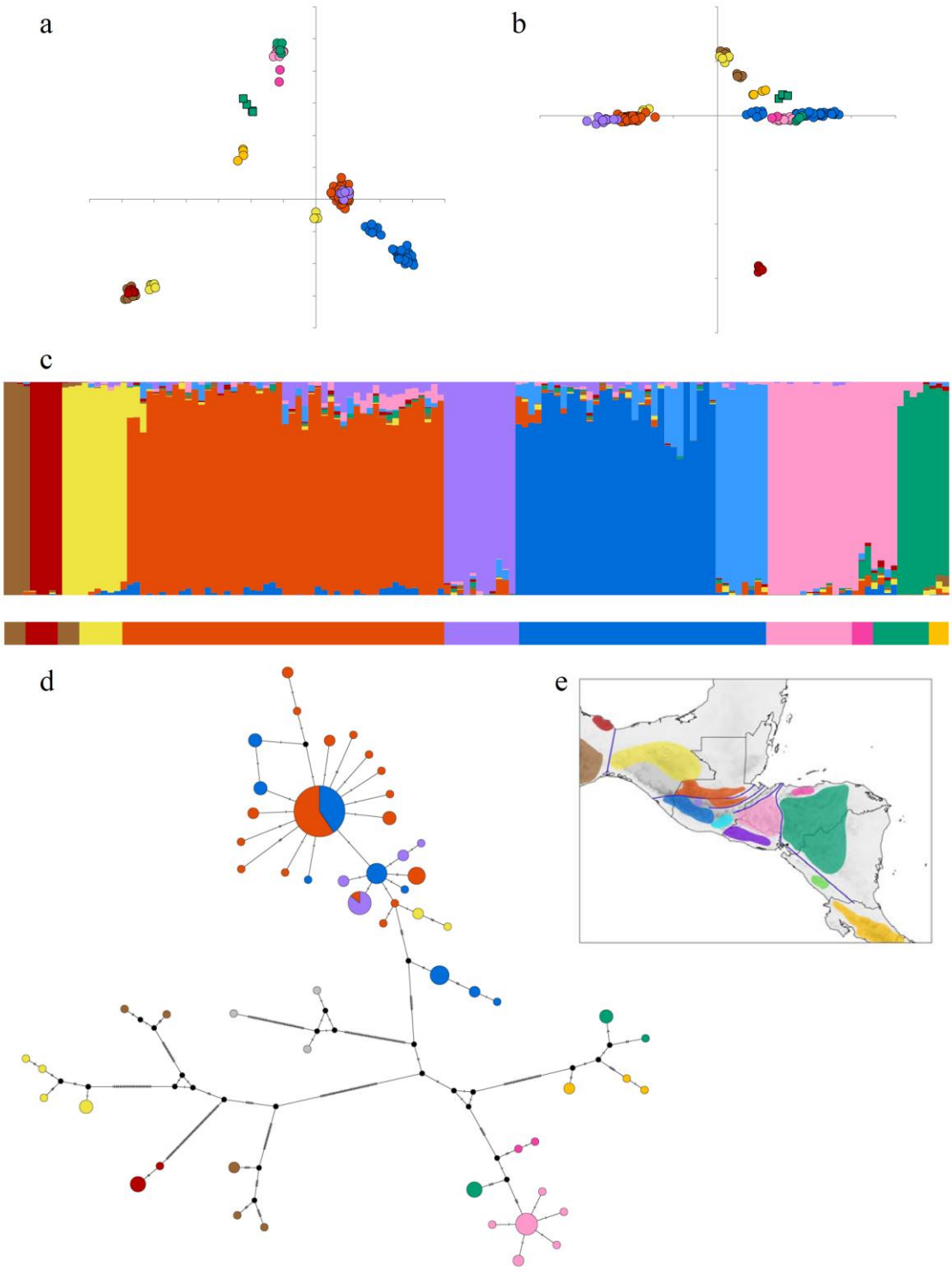


**Figure 7.** Population genetic structure of *Chlorospingus flavopectus* in Nuclear Central America. a) Principal Component Analysis on ddRAD data, PC1 (9.8%) and PC2 (7.5%). b) Principal Component Analysis on ddRAD data, PC3 (5.1%) and PC4 (3.6%). c) Ancestry analysis based on ddRAD data, K=9; colors on the bar below represent the geographic location. d) Haplotype network based on the complete ND2 mitochondrial gene. e) Map for geographic reference (gray color in figures, not shown in the map, correspond to South America).

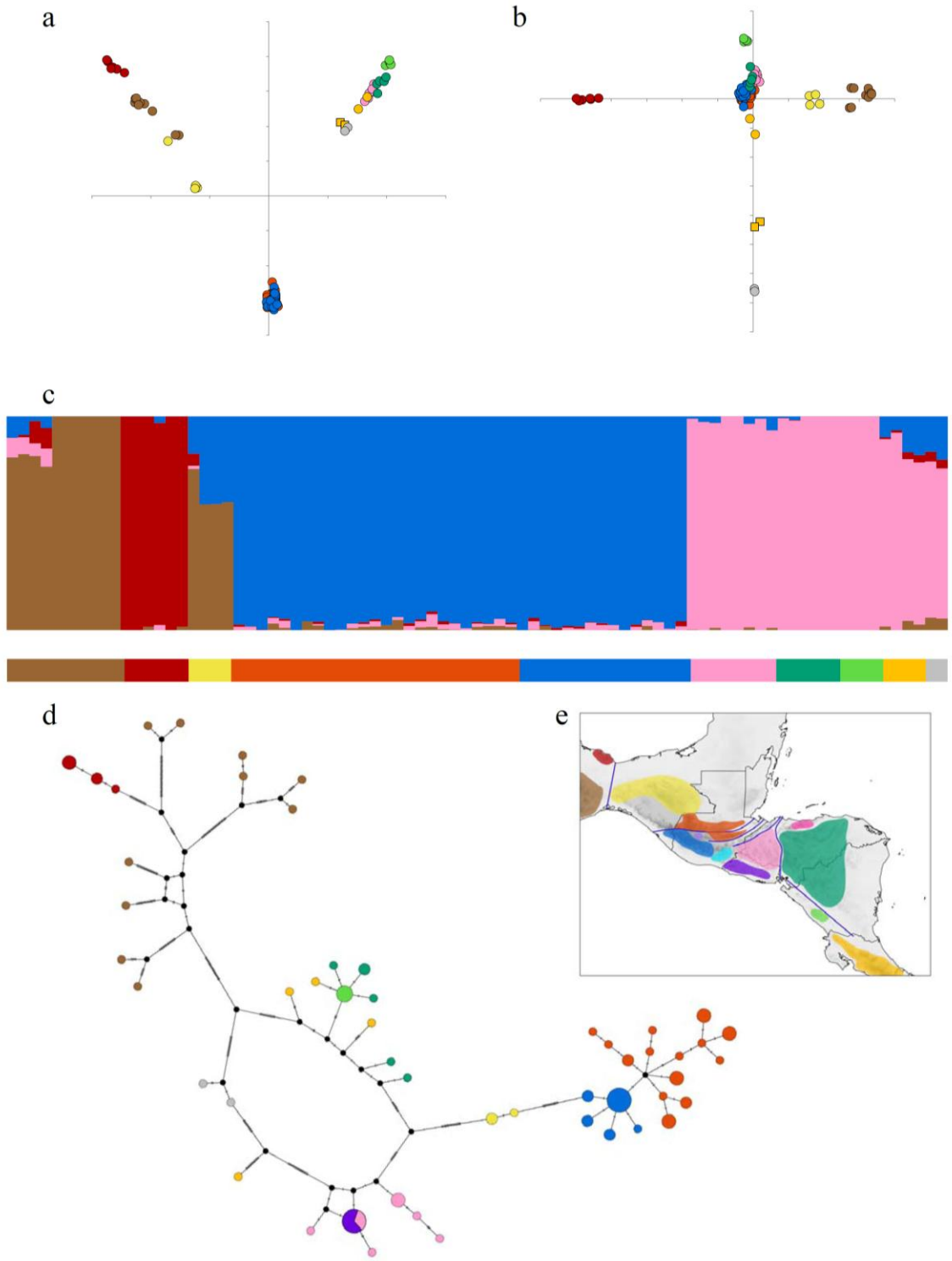


**Figure 8.** Population genetic structure of *Arremon brunneinucha* in Nuclear Central America. a) Principal Component Analysis on ddRAD data, PC1 (17.9%) and PC2 (12.5%). b) Principal Component Analysis on ddRAD data, PC3 (4.3%) and PC4 (2.7%). c) Ancestry analysis based on ddRAD data, K=4; colors on the bar below represent the geographic location. d) Haplotype network based on the complete ND2 mitochondrial gene. e) Map for geographic reference (gray color in figures, not shown in the map, correspond to South America).

## References


Bacon, C. D., Silvestro, D., Jaramillo, C., Smith, B. T., Chakrabarty, P., & Antonelli, A. (2015). Biological evidence supports an early and complex emergence of the Isthmus of Panama. Proceedings of the National Academy of Sciences, 112(19), 6110-6115.

Bagley, J. C., & Johnson, J. B. (2014). Phylogeography and biogeography of the lower Central American Neotropics: diversification between two continents and between two seas. Biological Reviews, 89(4), 767-790.

Barber, B. R., & Klicka, J. (2010). Two pulses of diversification across the Isthmus of Tehuantepec in a montane Mexican bird fauna. Proceedings of the Royal Society B: Biological Sciences, 277(1694), 2675-2681.

Barrier, E., Velasquillo, L., Chavez, M., & Gaulon, R. (1998). Neotectonic evolution of the Isthmus of Tehuantepec (southeastern Mexico). Tectonophysics, 287(1-4), 77-96.

Bergoeing, J. P. (2015). Geomorphology of Central America: A Syngenetic Perspective. Elsevier.

Bermingham, E., & Moritz, C. (1998). Comparative phylogeography: concepts and applications. Molecular Ecology, 7(4), 367-369.

Bonaccorso, E., Navarro-Sigüenza, A. G., Sánchez-González, L. A., Townsend Peterson, A., & García-Moreno, J. (2008). Genetic differentiation of the *Chlorospingus ophthalmicus* complex in Mexico and Central America. Journal of Avian Biology, 39(3), 311-321.

Cadena, C. D., Klicka, J., & Ricklefs, R. E. (2007). Evolutionary differentiation in the Neotropical montane region: Molecular phylogenetics and phylogeography of *Buarremon* brush-finches (Aves, Emberizidae). Molecular phylogenetics and evolution, 44(3), 993-1016.

Cadena, C. D., Pérez-Emán, J. L., Cuervo, A. M., Céspedes, L. N., Epperly, K. L., & Klicka, J. T. (2019). Extreme genetic structure and dynamic range evolution in a montane passerine bird: implications for tropical diversification. Biological Journal of the Linnean Society, 126(3), 487-506.

Cano, E. B., Schuster, J. C., & Morrone, J. J. (2018). Phylogenetics of *Ogyges kaup* and the biogeography of Nuclear Central America (Coleoptera, Passalidae). ZooKeys, (737), 81.

Catchen, J., Hohenlohe, P. A., Bassham, S., Amores, A., & Cresko, W. A. (2013). Stacks: an analysis tool set for population genomics. Molecular Ecology, 22(11), 3124-3140.

Cicero, C., & Johnson, N. K. (2001). Higher-level phylogeny of New World vireos (Aves: Vireonidae) based on sequences of multiple mitochondrial DNA genes. Molecular Phylogenetics and Evolution, 20(1), 27-40.

Clement, M., Posada, D., & Crandall, K. A. (2000). TCS: a computer program to estimate gene genealogies. Molecular Ecology, 9(10):1657-1659.

Danecek, P., Auton, A., Abecasis, G., Albers, C. A., Banks, E., DePristo, M. A., ... & 1000 Genomes Project Analysis Group. (2011). The variant call format and VCFtools. Bioinformatics, 27(15), 2156-2158.

Daza, J. M., Castoe, T. A., & Parkinson, C. L. (2010). Using regional comparative phylogeographic data from snake lineages to infer historical processes in Middle America. Ecography, 33(2), 343-354.

Firneno Jr, T. J., O'Neill, J. R., Portik, D. M., Emery, A. H., Townsend, J. H., & Fujita, M. K. (2020). Finding complexity in complexes: Assessing the causes of mitonuclear discordance

in a problematic species complex of Mesoamerican toads. Molecular Ecology, 29(18), 3543-3559.
Frichot, E., & François, O. (2015). LEA: An R package for landscape and ecological association studies. Methods in Ecology and Evolution, 6(8), 925-929.
Frichot, E., Mathieu, F., Trouillon, T., Bouchard, G., & François, O. (2014). Fast and efficient estimation of individual ancestry coefficients. Genetics, 196(4), 973-983.
García-Moreno, J., Cortés, N., García-Deras, G. M., & Hernández-Baños, B. E. (2006). Local origin and diversification among *Lampornis* hummingbirds: a Mesoamerican taxon. Molecular Phylogenetics and Evolution, 38(2), 488-498.
Gutiérrez-García, T. A., & Vázquez-Domínguez, E. (2013). Consensus between genes and stones in the biogeographic and evolutionary history of Central America. Quaternary Research, 79(3), 311-324.
Hannah, L., Lovejoy, T. E., & Schneider, S. H. (2005). Biodiversity and Climate Change in Context. In: T. E. Lovejoy & L. Hannah (Eds.) Climate Change and Biodiversity (pp 3-14). Yale University Press.
Hewitt, G. M., & Nichols, R. A. (2005). Genetic and Evolutionary Impacts of Climate Change. In: T. E. Lovejoy & L. Hannah (Eds.) Climate Change and Biodiversity (pp 176-192). Yale University Press.
Hofmann, E. P., & Townsend, J. H. (2017). Origins and biogeography of the Anolis crassulus subgroup (Squamata: Dactyloidae) in the highlands of Nuclear Central America. BMC Evolutionary Biology, 17(1), 1-14.
Howell, S. N., & Webb, S. (1995). A guide to the birds of Mexico and northern Central America. Oxford University Press.
Iturralde-Vinent, M. A. (2006). El origen paleogeográfico de la biota de Guatemala. In: E. B. Cano (Ed.) Biodiversidad de Guatemala (pp 1-6).
Jiménez, R. A., & Ornelas, J. F. (2016). Historical and current introgression in a Mesoamerican hummingbird species complex: a biogeographic perspective. PeerJ, 4, e1556.
Jombart, T. (2008). adegenet: a R package for the multivariate analysis of genetic markers. Bioinformatics, 24(11), 1403-1405.
Klicka, J., Barker, F. K., Burns, K. J., Lanyon, S. M., Lovette, I. J., Chaves, J. A., & Bryson Jr, R. W. (2014). A comprehensive multilocus assessment of sparrow (Aves: Passerellidae) relationships. Molecular Phylogenetics and Evolution, 77, 177-182.
Leigh, J. W., & Bryant, D. (2015). popart: full-feature software for haplotype network construction. Methods in Ecology and Evolution, 6(9), 1110-1116.
Li, H., & Durbin, R. (2009). Fast and accurate short read alignment with Burrows–Wheeler transform. bioinformatics, 25(14), 1754-1760.
Li, H., Handsaker, B., Wysoker, A., Fennell, T., Ruan, J., Homer, N., ... & Durbin, R. (2009). The sequence alignment/map format and SAMtools. Bioinformatics, 25(16), 2078-2079.
Lomolino, M. V., Riddle, B. R., Whittaker, R. J., & Brown, J. H. (2010). Biogeography (Sinauer, Sunderland, MA).
Lovette, I. J., Pérez-Emán, J. L., Sullivan, J. P., Banks, R. C., Fiorentino, I., Córdoba-Córdoba, S., ... & Bermingham, E. (2010). A comprehensive multilocus phylogeny for the wood-warblers and a revised classification of the Parulidae (Aves). Molecular Phylogenetics and Evolution, 57(2), 753-770.

McGuire, J. A., Witt, C. C., Remsen Jr, J. V., Corl, A., Rabosky, D. L., Altshuler, D. L., & Dudley, R. (2014). Molecular phylogenetics and the diversification of hummingbirds. Current Biology, 24(8), 910-916.
Miller, R. R. (1966). Geographical distribution of Central American freshwater fishes. Copeia, 773-802.
Navarro-Sigüenza, A. G., Peterson, A. T., Nyari, A., García-Deras, G. M., & García-Moreno, J. (2008). Phylogeography of the *Buarremon* brush-finch complex (Aves, Emberizidae) in Mesoamerica. Molecular Phylogenetics and Evolution, 47(1), 21-35.
O'Dea, A., Lessios, H. A., Coates, A. G., Eytan, R. I., Restrepo-Moreno, S. A., Cione, A. L., ... & Jackson, J. B. (2016). Formation of the Isthmus of Panama. Science Advances, 2(8), e1600883.
Ornelas, J. F., Sosa, V., Soltis, D. E., Daza, J. M., González, C., Soltis, P. S., ... & Ruiz-Sanchez, E. (2013). Comparative phylogeographic analyses illustrate the complex evolutionary history of threatened cloud forests of northern Mesoamerica. PloS one, 8(2), e56283.
Ortega-Gutiérrez, F., Solari, L. A., Ortega-Obregon, C., Elias-Herrera, M., Martens, U., Moran-Ical, S., ... & Schaaf, P. (2007). The Maya-Chortís boundary: a tectonostratigraphic approach. International Geology Review, 49(11), 996-1024.
Ortiz, E. M. (2019). vcf2phylip v2.0: convert a VCF matrix into several matrix formats for phylogenetic analysis. https://doi.org/10.5281/zenodo.2540861
Pérez Consuegra, S. G., & Vázquez-Domínguez, E. (2015). Mitochondrial diversification of the *Peromyscus mexicanus* species group in Nuclear Central America: biogeographic and taxonomic implications. Journal of Zoological Systematics and Evolutionary Research, 53(4), 300-311.
Pérez-Emán, J. L., Mumme, R. L., & Jabłoński, P. G. (2010). Chapter 8: Phylogeography and Adaptive Plumage Evolution in Central American Subspecies of the Slate-Throated Redstart (*Myioborus miniatus*). Ornithological Monographs, 67(1), 90-102.
Peterson, B. K., Weber, J. N., Kay, E. H., Fisher, H. S., & Hoekstra, H. E. (2012). Double digest RADseq: an inexpensive method for de novo SNP discovery and genotyping in model and non-model species. PloS one, 7(5), e37135.
Purcell, S., Neale, B., Todd-Brown, K., Thomas, L., Ferreira, M. A., Bender, D., ... & Sham, P. C. (2007). PLINK: a tool set for whole-genome association and population-based linkage analyses. The American journal of human genetics, 81(3), 559-575.
Rodríguez-Gómez, F., & Ornelas, J. F. (2014). Genetic divergence of the Mesoamerican Azure-crowned Hummingbird (*Amazilia cyanocephala*, Trochilidae) across the Motagua-Polochic-Jocotán fault system. Journal of Zoological Systematics and Evolutionary Research, 52(2), 142-153.
Rovito, S. M., & Parra-Olea, G. (2016). Neotropical plethodontid biogeography: insights from molecular phylogenetics. Copeia, 104(1), 222-232.
Schuchert C. (1935). Historical geology of the Antillean-Caribbean region (John Wiley and Sons, New York).
Simpson, G. G. (1950). History of the fauna of Latin America. American Scientist, 38(3), 361-389.
Stamatakis, A. (2014). RAxML version 8: a tool for phylogenetic analysis and post-analysis of large phylogenies. Bioinformatics, 30(9), 1312-1313.
Weir, J. T., Bermingham, E., Miller, M. J., Klicka, J., & González, M. A. (2008). Phylogeography of a morphologically diverse Neotropical montane species, the Common

Bush-Tanager (*Chlorospingus ophthalmicus*). Molecular Phylogenetics and Evolution, 47(2), 650-664.
Weir, J. T., Bermingham, E., & Schluter, D. (2009). The great American biotic interchange in birds. Proceedings of the National Academy of Sciences, 106(51), 21737-21742.
Wiens, J. J., & Graham, C. H. (2005). Niche conservatism: integrating evolution, ecology, and conservation biology. Annu. Rev. Ecol. Evol. Syst., 36, 519-539.

## Supplementary tables

**Table S1.** Species names, voucher information, and localities of origin for the specimens examined genetically in this study. Museum abbreviations used in voucher numbers: MVZ = Museum of Vertebrate Zoology, University of California, Berkeley; USAC = Escuela de Biología, Universidad de San Carlos de Guatemala; AMNH = American Museum of Natural History; UWBM = Burke Museum of Natural History and Culture; CUMV = Cornell University Museum of Vertebrates; FMNH = Field Museum of Natural History; IBUNAM = Instituto de Biología, Universidad Nacional Autónoma de México; KU = Kansas University, Natural History Museum; LSUMZ = Louisiana State University Museum of Natural Science; MSB = Museum of Southern Biology; UAM = University of Alaska Museum; and YPM = Yale Peabody Museum of Natural History, Yale University. MX = Mexico, GT = Guatemala, ES = El Salvador, HO = Honduras, NI = Nicaragua.

| No. | Species | Museum | Voucher number | Locality | ND2 / ddRADs |
|---|---|---|---|---|---|
| 1 | *Lampornis viridipallens* | LSUMZ | B-19268 | MX: Oaxaca, San Miguel Chimalapa | X / X |
| 2 | *Lampornis viridipallens* | LSUMZ | B-19269 | MX: Oaxaca, San Miguel Chimalapa | X / X |
| 3 | *Lampornis viridipallens* | LSUMZ | B-19270 | MX: Oaxaca, San Miguel Chimalapa | X / X |
| 4 | *Lampornis viridipallens* | MVZ | 188991 | MX: Oaxaca, Cintalapa de Figueroa | X / X |
| 5 | *Lampornis viridipallens* | MVZ | 188992 | MX: Oaxaca, Cintalapa de Figueroa | X / X |
| 6 | *Lampornis viridipallens* | MVZ | 188993 | MX: Oaxaca, Cintalapa de Figueroa | X / X |
| 7 | *Lampornis viridipallens* | MVZ | 188994 | MX: Oaxaca, Cintalapa de Figueroa | X / X |
| 8 | *Lampornis viridipallens* | MVZ | 188995 | MX: Oaxaca, Cintalapa de Figueroa | X / X |
| 9 | *Lampornis viridipallens* | MVZ | 188996 | MX: Oaxaca, Cintalapa de Figueroa | X / - |
| 10 | *Lampornis viridipallens* | MVZ | 188997 | MX: Chiapas, Tapalapa | X / X |
| 11 | *Lampornis viridipallens* | MVZ | 188998 | MX: Chiapas, Tapalapa | X / X |
| 12 | *Lampornis viridipallens* | MVZ | 188999 | MX: Chiapas, Tapalapa | X / - |
| 13 | *Lampornis viridipallens* | MVZ | 189000 | MX: Chiapas, Tapalapa | X / X |
| 14 | *Lampornis viridipallens* | MVZ | 189001 | MX: Chiapas, Tapalapa | X / X |
| 15 | *Lampornis viridipallens* | MVZ | 189002 | MX: Chiapas, Tapalapa | X / X |
| 16 | *Lampornis viridipallens* | MVZ | 189003 | MX: Chiapas, Tapalapa | X / X |
| 17 | *Lampornis viridipallens* | MVZ | 189004 | MX: Chiapas, Tapalapa | X / X |
| 18 | *Lampornis viridipallens* | MVZ | 189005 | MX: Chiapas, Tapalapa | X / X |
| 19 | *Lampornis viridipallens* | MVZ | 189006 | MX: Chiapas, Tapalapa | X / X |
| 20 | *Lampornis viridipallens* | MVZ | 189007 | MX: Chiapas, Tapalapa | X / X |
| 21 | *Lampornis viridipallens* | MVZ | 184218 | GT: Huehuetenango, Yalambojoch | X / X |
| 22 | *Lampornis viridipallens* | MVZ | 184219 | GT: Huehuetenango, Yalambojoch | X / X |
| 23 | *Lampornis viridipallens* | MVZ | 184220 | GT: Huehuetenango, Yalambojoch | X / X |
| 24 | *Lampornis viridipallens* | MVZ | 184221 | GT: Huehuetenango, Yalambojoch | X / X |
| 25 | *Lampornis viridipallens* | MVZ | 184222 | GT: Huehuetenango, Yalambojoch | X / X |
| 26 | *Lampornis viridipallens* | MVZ | 184223 | GT: Huehuetenango, Yalambojoch | X / X |
| 27 | *Lampornis viridipallens* | MVZ | 184224 | GT: Huehuetenango, Yalambojoch | X / X |
| 28 | *Lampornis viridipallens* | MVZ | 184225 | GT: Huehuetenango, Yalambojoch | X / X |
| 29 | *Lampornis viridipallens* | MVZ | 189153 | GT: Huehuetenango, Soloma | X / X |

| | | | | | |
|---|---|---|---|---|---|
| 30 | *Lampornis viridipallens* | MVZ | 189154 | GT: Huehuetenango, Soloma | X / X |
| 31 | *Lampornis viridipallens* | MVZ | 189155 | GT: Huehuetenango, Soloma | X / X |
| 32 | *Lampornis viridipallens* | MVZ | 189156 | GT: Huehuetenango, Soloma | X / X |
| 33 | *Lampornis viridipallens* | MVZ | 189157 | GT: Huehuetenango, Soloma | X / X |
| 34 | *Lampornis viridipallens* | MVZ | 189158 | GT: Huehuetenango, Soloma | X / X |
| 35 | *Lampornis viridipallens* | MVZ | 189160 | GT: Huehuetenango, Soloma | X / X |
| 36 | *Lampornis viridipallens* | MVZ | 189161 | GT: Huehuetenango, Soloma | X / X |
| 37 | *Lampornis viridipallens* | MVZ | 189162 | GT: Huehuetenango, Soloma | X / X |
| 38 | *Lampornis viridipallens* | MVZ | 189163 | GT: Huehuetenango, Soloma | X / X |
| 39 | *Lampornis viridipallens* | MVZ | 189164 | GT: Huehuetenango, Soloma | X / X |
| 40 | *Lampornis viridipallens* | MVZ | 189165 | GT: Huehuetenango, Soloma | X / X |
| 41 | *Lampornis viridipallens* | MVZ | 189166 | GT: Huehuetenango, Soloma | X / X |
| 42 | *Lampornis viridipallens* | MVZ | 189167 | GT: Huehuetenango, Soloma | X / X |
| 43 | *Lampornis viridipallens* | MVZ | 187366 | GT: Quiché, Uspantán | X / X |
| 44 | *Lampornis viridipallens* | MVZ | 187367 | GT: Quiché, Uspantán | X / X |
| 45 | *Lampornis viridipallens* | MVZ | 187351 | GT: Alta Verapaz, San Pedro Carchá | X / X |
| 46 | *Lampornis viridipallens* | MVZ | 187352 | GT: Alta Verapaz, San Pedro Carchá | X / X |
| 47 | *Lampornis viridipallens* | MVZ | 187353 | GT: Alta Verapaz, San Pedro Carchá | X / - |
| 48 | *Lampornis viridipallens* | MVZ | 187354 | GT: Alta Verapaz, San Pedro Carchá | X / X |
| 49 | *Lampornis viridipallens* | MVZ | 187355 | GT: Alta Verapaz, San Pedro Carchá | X / X |
| 50 | *Lampornis viridipallens* | MVZ | 187356 | GT: Alta Verapaz, San Pedro Carchá | X / X |
| 51 | *Lampornis viridipallens* | MVZ | 187357 | GT: Alta Verapaz, San Pedro Carchá | X / X |
| 52 | *Lampornis viridipallens* | MVZ | 187358 | GT: Alta Verapaz, San Pedro Carchá | X / X |
| 53 | *Lampornis viridipallens* | MVZ | 187359 | GT: Alta Verapaz, San Pedro Carchá | X / X |
| 54 | *Lampornis viridipallens* | MVZ | 187360 | GT: Alta Verapaz, San Pedro Carchá | X / X |
| 55 | *Lampornis viridipallens* | MVZ | 187361 | GT: Alta Verapaz, San Pedro Carchá | X / X |
| 56 | *Lampornis viridipallens* | MVZ | 187362 | GT: Alta Verapaz, San Pedro Carchá | X / X |
| 57 | *Lampornis viridipallens* | MVZ | 187363 | GT: Alta Verapaz, San Pedro Carchá | X / X |
| 58 | *Lampornis viridipallens* | MVZ | 187364 | GT: Alta Verapaz, San Pedro Carchá | X / X |
| 59 | *Lampornis viridipallens* | MVZ | 187365 | GT: Alta Verapaz, San Pedro Carchá | X / X |
| 60 | *Lampornis viridipallens* | USAC | RAJ219 | GT: Baja Verapaz, Purulhá | X / X |
| 61 | *Lampornis viridipallens* | USAC | RAJ221 | GT: Baja Verapaz, Purulhá | X / X |
| 62 | *Lampornis viridipallens* | USAC | RAJ224 | GT: Baja Verapaz, Purulhá | X / X |
| 63 | *Lampornis viridipallens* | USAC | RAJ237 | GT: Baja Verapaz, Purulhá | X / X |
| 64 | *Lampornis viridipallens* | USAC | SH7 | GT: Baja Verapaz, Purulhá | X / X |
| 65 | *Lampornis viridipallens* | USAC | SH12 | GT: Baja Verapaz, Purulhá | X / X |
| 66 | *Lampornis viridipallens* | USAC | ALAR21 | GT: Baja Verapaz, Purulhá | X / X |
| 67 | *Lampornis viridipallens* | MVZ | 187369 | GT: Quiché, Zacualpa | X / X |
| 68 | *Lampornis viridipallens* | MVZ | 187371 | GT: Quiché, Zacualpa | X / X |
| 69 | *Lampornis viridipallens* | MVZ | 187373 | GT: Quiché, Zacualpa | X / X |
| 70 | *Lampornis viridipallens* | MVZ | 188056 | MX: Chiapas, Motozintla | X / X |
| 71 | *Lampornis viridipallens* | MVZ | 188057 | MX: Chiapas, Motozintla | X / X |
| 72 | *Lampornis viridipallens* | MVZ | 188058 | MX: Chiapas, Motozintla | X / X |
| 73 | *Lampornis viridipallens* | MVZ | 188059 | MX: Chiapas, Motozintla | X / X |
| 74 | *Lampornis viridipallens* | MVZ | 188060 | MX: Chiapas, Motozintla | X / X |
| 75 | *Lampornis viridipallens* | MVZ | 188061 | MX: Chiapas, Motozintla | X / X |
| 76 | *Lampornis viridipallens* | MVZ | 188062 | MX: Chiapas, Motozintla | X / X |

| | | | | | |
|---|---|---|---|---|---|
| 77 | *Lampornis viridipallens* | MVZ | 188063 | MX: Chiapas, Motozintla | X / X |
| 78 | *Lampornis viridipallens* | MVZ | 188064 | MX: Chiapas, Motozintla | X / - |
| 79 | *Lampornis viridipallens* | MVZ | 188065 | MX: Chiapas, Motozintla | X / X |
| 80 | *Lampornis viridipallens* | MVZ | 188066 | MX: Chiapas, Motozintla | X / X |
| 81 | *Lampornis viridipallens* | MVZ | 188067 | MX: Chiapas, Motozintla | X / X |
| 82 | *Lampornis viridipallens* | MVZ | 188068 | MX: Chiapas, Motozintla | X / X |
| 83 | *Lampornis viridipallens* | MVZ | 188070 | MX: Chiapas, Motozintla | X / X |
| 84 | *Lampornis viridipallens* | MVZ | 187070 | GT: Quetzaltenango, Volcán Lacandón | X / X |
| 85 | *Lampornis viridipallens* | MVZ | 187071 | GT: Quetzaltenango, Volcán Lacandón | X / X |
| 86 | *Lampornis viridipallens* | MVZ | 187072 | GT: Quetzaltenango, Volcán Lacandón | X / X |
| 87 | *Lampornis viridipallens* | MVZ | 187073 | GT: Quetzaltenango, Volcán Lacandón | X / X |
| 88 | *Lampornis viridipallens* | MVZ | 187074 | GT: Quetzaltenango, Volcán Lacandón | X / X |
| 89 | *Lampornis viridipallens* | MVZ | 187075 | GT: Quetzaltenango, Volcán Lacandón | X / X |
| 90 | *Lampornis viridipallens* | MVZ | 187076 | GT: Quetzaltenango, Volcán Lacandón | X / X |
| 91 | *Lampornis viridipallens* | MVZ | 187077 | GT: Quetzaltenango, Volcán Lacandón | X / X |
| 92 | *Lampornis viridipallens* | MVZ | 187078 | GT: Quetzaltenango, Volcán Lacandón | X / X |
| 93 | *Lampornis viridipallens* | MVZ | 187079 | GT: Quetzaltenango, Volcán Lacandón | X / X |
| 94 | *Lampornis viridipallens* | MVZ | 187080 | GT: Quetzaltenango, Volcán Lacandón | X / X |
| 95 | *Lampornis viridipallens* | MVZ | 187081 | GT: Quetzaltenango, Volcán Lacandón | X / X |
| 96 | *Lampornis viridipallens* | MVZ | 187082 | GT: Quetzaltenango, Volcán Lacandón | X / X |
| 97 | *Lampornis viridipallens* | MVZ | 187083 | GT: Quetzaltenango, Volcán Lacandón | X / X |
| 98 | *Lampornis viridipallens* | MVZ | 187084 | GT: Quetzaltenango, Volcán Lacandón | X / X |
| 99 | *Lampornis viridipallens* | MVZ | 187085 | GT: Quetzaltenango, Volcán Lacandón | X / X |
| 100 | *Lampornis viridipallens* | MVZ | 187607 | GT: Quetzaltenango, Volcán Zunil | X / X |
| 101 | *Lampornis viridipallens* | MVZ | 187608 | GT: Quetzaltenango, Volcán Zunil | X / X |
| 102 | *Lampornis viridipallens* | MVZ | 187609 | GT: Quetzaltenango, Volcán Zunil | X / X |
| 103 | *Lampornis viridipallens* | MVZ | 187611 | GT: Quetzaltenango, Volcán Zunil | X / X |
| 104 | *Lampornis viridipallens* | MVZ | 187612 | GT: Quetzaltenango, Volcán Zunil | X / X |
| 105 | *Lampornis viridipallens* | MVZ | 187613 | GT: Quetzaltenango, Volcán Zunil | X / X |
| 106 | *Lampornis viridipallens* | MVZ | 187614 | GT: Quetzaltenango, Volcán Zunil | X / X |
| 107 | *Lampornis viridipallens* | MVZ | 187615 | GT: Quetzaltenango, Volcán Zunil | X / X |
| 108 | *Lampornis viridipallens* | MVZ | 187086 | GT: Suchitepéquez, Volcán Atitlán | X / X |
| 109 | *Lampornis viridipallens* | MVZ | 187087 | GT: Suchitepéquez, Volcán Atitlán | X / X |
| 110 | *Lampornis viridipallens* | MVZ | 187088 | GT: Suchitepéquez, Volcán Atitlán | X / X |
| 111 | *Lampornis viridipallens* | MVZ | 187089 | GT: Suchitepéquez, Volcán Atitlán | X / X |
| 112 | *Lampornis viridipallens* | MVZ | 187090 | GT: Suchitepéquez, Volcán Atitlán | X / X |
| 113 | *Lampornis viridipallens* | MVZ | 187259 | GT: Suchitepéquez, Volcán Atitlán | X / X |
| 114 | *Lampornis viridipallens* | MVZ | 187260 | GT: Suchitepéquez, Volcán Atitlán | X / X |
| 115 | *Lampornis viridipallens* | MVZ | 187261 | GT: Suchitepéquez, Volcán Atitlán | X / X |
| 116 | *Lampornis viridipallens* | MVZ | MFAR84 | GT: Sacatepéquez, San Cristóbal El Alto | X / X |
| 117 | *Lampornis viridipallens* | MVZ | 189168 | GT: Santa Rosa, Volcán Tecuamburro | X / X |
| 118 | *Lampornis viridipallens* | MVZ | 189169 | GT: Santa Rosa, Volcán Tecuamburro | X / X |
| 119 | *Lampornis viridipallens* | MVZ | 189170 | GT: Santa Rosa, Volcán Tecuamburro | X / X |
| 120 | *Lampornis viridipallens* | MVZ | 189171 | GT: Santa Rosa, Volcán Tecuamburro | X / X |
| 121 | *Lampornis viridipallens* | MVZ | 189172 | GT: Santa Rosa, Volcán Tecuamburro | X / X |
| 122 | *Lampornis viridipallens* | MVZ | 189173 | GT: Santa Rosa, Volcán Tecuamburro | X / X |
| 123 | *Lampornis viridipallens* | MVZ | 189174 | GT: Santa Rosa, Volcán Tecuamburro | X / X |

| | | | | | |
|---|---|---|---|---|---|
| 124 | *Lampornis viridipallens* | MVZ | 189175 | GT: Santa Rosa, Volcán Tecuamburro | X / X |
| 125 | *Lampornis viridipallens* | MVZ | 189176 | GT: Santa Rosa, Volcán Tecuamburro | X / X |
| 126 | *Lampornis viridipallens* | MVZ | 189191 | GT: Santa Rosa, Volcán Tecuamburro | X / X |
| 127 | *Lampornis viridipallens* | MVZ | 188343 | GT: Jutiapa, Volcán Suchitán | X / X |
| 128 | *Lampornis viridipallens* | MVZ | 188344 | GT: Jutiapa, Volcán Suchitán | X / X |
| 129 | *Lampornis viridipallens* | KU | 9526 | ES: Santa Ana, Volcán Santa Ana | X / X |
| 130 | *Lampornis viridipallens* | KU | 25034 | ES: Santa Ana, Volcán Santa Ana | X / X |
| 131 | *Lampornis viridipallens* | KU | 6457 | ES: San Vicente, Volcán San Vicente | X / X |
| 132 | *Lampornis viridipallens* | KU | 7683 | ES: San Vicente, Volcán San Vicente | X / X |
| 133 | *Lampornis viridipallens* | KU | 7737 | ES: San Vicente, Volcán San Vicente | X / X |
| 134 | *Lampornis viridipallens* | KU | 7763 | ES: San Vicente, Volcán San Vicente | X / X |
| 135 | *Lampornis viridipallens* | KU | 7767 | ES: San Vicente, Volcán San Vicente | X / X |
| 136 | *Lampornis viridipallens* | MVZ | 187262 | GT: Chiquimula, Cerro El Gigante | X / X |
| 137 | *Lampornis viridipallens* | MVZ | 187263 | GT: Chiquimula, Cerro El Gigante | X / X |
| 138 | *Lampornis viridipallens* | MVZ | 187616 | GT: Zacapa, La Unión | X / X |
| 139 | *Lampornis viridipallens* | MVZ | 187617 | GT: Zacapa, La Unión | X / X |
| 140 | *Lampornis viridipallens* | MVZ | 187618 | GT: Zacapa, La Unión | X / X |
| 141 | *Lampornis viridipallens* | MVZ | 187619 | GT: Zacapa, La Unión | X / X |
| 142 | *Lampornis viridipallens* | MVZ | 187620 | GT: Zacapa, La Unión | X / X |
| 143 | *Lampornis viridipallens* | MVZ | 187621 | GT: Zacapa, La Unión | X / X |
| 144 | *Lampornis viridipallens* | MVZ | 187622 | GT: Zacapa, La Unión | X / X |
| 145 | *Lampornis viridipallens* | MVZ | 187623 | GT: Zacapa, La Unión | X / X |
| 146 | *Lampornis viridipallens* | MVZ | 187624 | GT: Zacapa, La Unión | X / X |
| 147 | *Lampornis viridipallens* | MVZ | 187625 | GT: Zacapa, La Unión | X / X |
| 148 | *Lampornis viridipallens* | MVZ | 187626 | GT: Zacapa, La Unión | X / X |
| 149 | *Lampornis viridipallens* | MVZ | 187627 | GT: Zacapa, La Unión | X / X |
| 150 | *Lampornis viridipallens* | MVZ | 187628 | GT: Zacapa, La Unión | X / X |
| 151 | *Lampornis viridipallens* | KU | 9408 | ES: Santa Ana, Cerro Montecristo | X / X |
| 152 | *Lampornis viridipallens* | KU | 9459 | ES: Santa Ana, Cerro Montecristo | X / X |
| 153 | *Lampornis viridipallens* | KU | 5064 | ES: Chalatenango, Cerro El Pital | X / - |
| 154 | *Lampornis sybillae* | FMNH | 481715 | NI: Estelí | X / X |
| 155 | *Lampornis sybillae* | FMNH | 481716 | NI: Estelí | X / X |
| 156 | *Lampornis sybillae* | FMNH | 481717 | NI: Estelí | X / X |
| 157 | *Lampornis sybillae* | FMNH | 481718 | NI: Estelí | X / X |
| 158 | *Lampornis sybillae* | FMNH | 481719 | NI: Estelí | X / X |
| 159 | *Lampornis sybillae* | UWBM | 56113 | NI: Matagalpa | X / X |
| 160 | *Lampornis sybillae* | UWBM | 56118 | NI: Matagalpa | X / X |
| 161 | *Lampornis sybillae* | UWBM | 56121 | NI: Matagalpa | X / X |
| 162 | *Lampornis sybillae* | UWBM | 56159 | NI: Matagalpa | X / X |
| 163 | *Lampornis sybillae* | UWBM | 56160 | NI: Matagalpa | X / X |
| 164 | *Lampornis sybillae* | UWBM | 56178 | NI: Matagalpa | X / X |
| 165 | *Lampornis sybillae* | UWBM | 70086 | NI: Matagalpa | X / X |
| 166 | *Lampornis sybillae* | UWBM | 70112 | NI: Matagalpa | X / X |
| 167 | *Lampornis calolaemus* | MVZ | 183727 | Outgroup | X / X |
| 168 | *Lampornis amethystinus* | MVZ | 184737 | Outgroup | X / X |
| 169 | *Lamprolaima rhami* | MVZ | 184738 | Outgroup | X / X |
| 170 | *Eugenes fulgens* | MVZ | 187256 | Outgroup | X / X |

| | | | | | |
|---|---|---|---|---|---|
| 171 | *Henicorhina leucophrys* | AMNH | DOT-15694 | MX: Hidalgo | X / X |
| 172 | *Henicorhina leucophrys* | FMNH | 393788 | MX: Oaxaca, Totontepec | X / X |
| 173 | *Henicorhina leucophrys* | FMNH | 393789 | MX: Oaxaca, Totontepec | X / X |
| 174 | *Henicorhina leucophrys* | FMNH | 393980 | MX: Jalisco | X / X |
| 175 | *Henicorhina leucophrys* | FMNH | 393981 | MX: Jalisco | X / X |
| 176 | *Henicorhina leucophrys* | UWBM | 118480 | MX: Guerrero | X / X |
| 177 | *Henicorhina leucophrys* | UWBM | 118479 | MX: Guerrero | X / X |
| 178 | *Henicorhina leucophrys* | UWBM | 112981 | MX: Oaxaca, Pochutla | X / X |
| 179 | *Henicorhina leucophrys* | UWBM | 118955 | MX: Oaxaca, Pochutla | X / X |
| 180 | *Henicorhina leucophrys* | MVZ | 189072 | MX: Chiapas, Tapalapa | X / X |
| 181 | *Henicorhina leucophrys* | MVZ | 189073 | MX: Chiapas, Tapalapa | X / X |
| 182 | *Henicorhina leucophrys* | MVZ | 189074 | MX: Chiapas, Tapalapa | X / X |
| 183 | *Henicorhina leucophrys* | MVZ | 189075 | MX: Chiapas, Tapalapa | X / X |
| 184 | *Henicorhina leucophrys* | MVZ | 184244 | GT: Huehuetenango, Yalambojoch | X / X |
| 185 | *Henicorhina leucophrys* | MVZ | 184245 | GT: Huehuetenango, Yalambojoch | X / X |
| 186 | *Henicorhina leucophrys* | MVZ | 184246 | GT: Huehuetenango, Yalambojoch | X / X |
| 187 | *Henicorhina leucophrys* | MVZ | 184247 | GT: Huehuetenango, Yalambojoch | X / X |
| 188 | *Henicorhina leucophrys* | MVZ | 184248 | GT: Huehuetenango, Yalambojoch | X / X |
| 189 | *Henicorhina leucophrys* | MVZ | 184249 | GT: Huehuetenango, Yalambojoch | X / X |
| 190 | *Henicorhina leucophrys* | MVZ | 184250 | GT: Huehuetenango, Yalambojoch | X / X |
| 191 | *Henicorhina leucophrys* | MVZ | 189276 | GT: Huehuetenango, Soloma | X / X |
| 192 | *Henicorhina leucophrys* | MVZ | 189277 | GT: Huehuetenango, Soloma | X / X |
| 193 | *Henicorhina leucophrys* | MVZ | 189279 | GT: Huehuetenango, Soloma | X / X |
| 194 | *Henicorhina leucophrys* | MVZ | 189280 | GT: Huehuetenango, Soloma | X / X |
| 195 | *Henicorhina leucophrys* | MVZ | 189281 | GT: Huehuetenango, Soloma | X / X |
| 196 | *Henicorhina leucophrys* | MVZ | 187478 | GT: Quiché, Uspantán | X / X |
| 197 | *Henicorhina leucophrys* | MVZ | 187479 | GT: Quiché, Uspantán | X / X |
| 198 | *Henicorhina leucophrys* | MVZ | 187480 | GT: Quiché, Uspantán | X / X |
| 199 | *Henicorhina leucophrys* | MVZ | 187481 | GT: Quiché, Uspantán | X / X |
| 200 | *Henicorhina leucophrys* | MVZ | 187482 | GT: Quiché, Uspantán | X / X |
| 201 | *Henicorhina leucophrys* | MVZ | 187483 | GT: Quiché, Uspantán | X / X |
| 202 | *Henicorhina leucophrys* | MVZ | 187484 | GT: Quiché, Uspantán | X / X |
| 203 | *Henicorhina leucophrys* | MVZ | 187485 | GT: Quiché, Uspantán | X / X |
| 204 | *Henicorhina leucophrys* | MVZ | 187486 | GT: Quiché, Uspantán | X / X |
| 205 | *Henicorhina leucophrys* | MVZ | 187487 | GT: Quiché, Uspantán | X / X |
| 206 | *Henicorhina leucophrys* | MVZ | 187489 | GT: Alta Verapaz, San Pedro Carchá | X / X |
| 207 | *Henicorhina leucophrys* | MVZ | 187490 | GT: Alta Verapaz, San Pedro Carchá | X / X |
| 208 | *Henicorhina leucophrys* | MVZ | 187491 | GT: Alta Verapaz, San Pedro Carchá | X / X |
| 209 | *Henicorhina leucophrys* | MVZ | 187492 | GT: Alta Verapaz, San Pedro Carchá | X / X |
| 210 | *Henicorhina leucophrys* | MVZ | 187493 | GT: Alta Verapaz, San Pedro Carchá | X / X |
| 211 | *Henicorhina leucophrys* | MVZ | 187494 | GT: Alta Verapaz, San Pedro Carchá | X / X |
| 212 | *Henicorhina leucophrys* | MVZ | 187495 | GT: Alta Verapaz, San Pedro Carchá | X / X |
| 213 | *Henicorhina leucophrys* | MVZ | 187496 | GT: Alta Verapaz, San Pedro Carchá | X / X |
| 214 | *Henicorhina leucophrys* | MVZ | 187497 | GT: Alta Verapaz, San Pedro Carchá | X / X |
| 215 | *Henicorhina leucophrys* | MVZ | 184746 | GT: Reserva de la Biosfera Sierra de las Minas | X / X |
| 216 | *Henicorhina leucophrys* | MVZ | 184747 | GT: Reserva de la Biosfera Sierra de las Minas | X / X |
| 217 | *Henicorhina leucophrys* | MVZ | 184748 | GT: Reserva de la Biosfera Sierra de las Minas | X / X |

| | | | | | |
|---|---|---|---|---|---|
| 218 | *Henicorhina leucophrys* | MVZ | 184749 | GT: Reserva de la Biosfera Sierra de las Minas | X / X |
| 219 | *Henicorhina leucophrys* | USAC | RAJ251 | GT: Baja Verapaz, Purulhá | X / X |
| 220 | *Henicorhina leucophrys* | USAC | ALAR17 | GT: Baja Verapaz, Purulhá | X / X |
| 221 | *Henicorhina leucophrys* | USAC | SH11 | GT: Baja Verapaz, Purulhá | X / X |
| 222 | *Henicorhina leucophrys* | MVZ | 187488 | GT: Quiché, Zacualpa | X / X |
| 223 | *Henicorhina leucophrys* | MVZ | 188157 | MX: Chiapas, Motozintla | X / X |
| 224 | *Henicorhina leucophrys* | MVZ | 188158 | MX: Chiapas, Motozintla | X / X |
| 225 | *Henicorhina leucophrys* | MVZ | 187140 | GT: Quetzaltenango, Volcán Lacandón | X / X |
| 226 | *Henicorhina leucophrys* | MVZ | 187141 | GT: Quetzaltenango, Volcán Lacandón | X / X |
| 227 | *Henicorhina leucophrys* | MVZ | 187675 | GT: Quetzaltenango, Volcán Zunil | X / X |
| 228 | *Henicorhina leucophrys* | MVZ | 187676 | GT: Quetzaltenango, Volcán Zunil | X / X |
| 229 | *Henicorhina leucophrys* | MVZ | 187677 | GT: Quetzaltenango, Volcán Zunil | X / X |
| 230 | *Henicorhina leucophrys* | MVZ | 187678 | GT: Zacapa, La Unión | X / X |
| 231 | *Henicorhina leucophrys* | MVZ | 187679 | GT: Zacapa, La Unión | X / X |
| 232 | *Henicorhina leucophrys* | MVZ | 187680 | GT: Zacapa, La Unión | X / X |
| 233 | *Henicorhina leucophrys* | MVZ | 187681 | GT: Zacapa, La Unión | X / X |
| 234 | *Henicorhina leucophrys* | MVZ | 187682 | GT: Zacapa, La Unión | X / X |
| 235 | *Henicorhina leucophrys* | MVZ | 187683 | GT: Zacapa, La Unión | X / X |
| 236 | *Henicorhina leucophrys* | MVZ | 187684 | GT: Zacapa, La Unión | X / X |
| 237 | *Henicorhina leucophrys* | MVZ | 187685 | GT: Zacapa, La Unión | X / X |
| 238 | *Henicorhina leucophrys* | YPM | 100350 | ES: Chalatenango | X / X |
| 239 | *Henicorhina leucophrys* | YPM | 100401 | ES: Chalatenango | X / X |
| 240 | *Henicorhina leucophrys* | YPM | 100351 | ES: Chalatenango | X / X |
| 241 | *Henicorhina leucophrys* | YPM | 100477 | ES: Chalatenango | X / X |
| 242 | *Henicorhina leucophrys* | LSUMZ | 19885 | Costa Rica | X / X |
| 243 | *Henicorhina leucophrys* | LSUMZ | 27303 | Costa Rica | X / X |
| 244 | *Henicorhina leucophrys* | LSUMZ | 28157 | Panamá | X / X |
| 245 | *Henicorhina leucophrys* | LSUMZ | 28163 | Panamá | X / X |
| 246 | *Henicorhina leucophrys* | LSUMZ | 12151 | Ecuador | X / X |
| 247 | *Henicorhina leucophrys* | MSB | 32231 | Perú | X / X |
| 248 | *Henicorhina leucophrys* | MSB | 34591 | Perú | X / X |
| 249 | *Henicorhina leucosticta* | MVZ | 188575 | Outgroup | X / X |
| 250 | *Henicorhina leucosticta* | LSUMZ | 30012 | Outgroup | X / X |
| 251 | *Troglodytes rufociliatus* | MVZ | 187672 | Outgroup | X / X |
| 252 | *Pheugopedius maculipectus* | MVZ | 189272 | Outgroup | X / X |
| 253 | *Campylorhynchus zonatus* | MVZ | 187476 | Outgroup | X / X |
| 254 | *Basileuterus belli* | UWBM | 82651 | MX: Sinaloa | X / X |
| 255 | *Basileuterus belli* | UWBM | 82662 | MX: Sinaloa | X / X |
| 256 | *Basileuterus belli* | FMNH | 343399 | MX: Jalisco | X / X |
| 257 | *Basileuterus belli* | FMNH | 343398 | MX: Jalisco | X / X |
| 258 | *Basileuterus belli* | UWBM | 115150 | MX: Michoacán | X / X |
| 259 | *Basileuterus belli* | UWBM | 115162 | MX: Michoacán | X / X |
| 260 | *Basileuterus belli* | UWBM | 113606 | MX: Morelos | X / X |
| 261 | *Basileuterus belli* | UWBM | 113619 | MX: Morelos | X / X |
| 262 | *Basileuterus belli* | AMNH | DOT-15693 | MX: Hidalgo | X / X |
| 263 | *Basileuterus belli* | AMNH | DOT-15719 | MX: Hidalgo | X / X |

| | | | | | |
|---|---|---|---|---|---|
| 264 | *Basileuterus belli* | FMNH | 393830 | MX: Oaxaca, Totontepec | X / X |
| 265 | *Basileuterus belli* | FMNH | 393826 | MX: Oaxaca, Totontepec | X / X |
| 266 | *Basileuterus belli* | FMNH | 393821 | MX: Guerrero | X / X |
| 267 | *Basileuterus belli* | FMNH | 394156 | MX: Guerrero | X / X |
| 268 | *Basileuterus belli* | UWBM | 112987 | MX: Oaxaca, Pochutla | X / X |
| 269 | *Basileuterus belli* | UWBM | 113052 | MX: Oaxaca, Pochutla | X / X |
| 270 | *Basileuterus belli* | FMNH | 393944 | MX: Veracruz, Los Tuxtlas | X / X |
| 271 | *Basileuterus belli* | IBUNAM | PEP2653 | MX: Veracruz, Los Tuxtlas | X / X |
| 272 | *Basileuterus belli* | IBUNAM | PEP2700 | MX: Veracruz, Los Tuxtlas | X / X |
| 273 | *Basileuterus belli* | IBUNAM | PEP2445 | MX: Veracruz, Los Tuxtlas | X / X |
| 274 | *Basileuterus belli* | IBUNAM | PEP2491 | MX: Veracruz, Los Tuxtlas | X / X |
| 275 | *Basileuterus belli* | MVZ | 189092 | MX: Chiapas, Tapalapa | X / X |
| 276 | *Basileuterus belli* | MVZ | 189093 | MX: Chiapas, Tapalapa | X / X |
| 277 | *Basileuterus belli* | MVZ | 189094 | MX: Chiapas, Tapalapa | X / X |
| 278 | *Basileuterus belli* | MVZ | 189095 | MX: Chiapas, Tapalapa | X / X |
| 279 | *Basileuterus belli* | MVZ | 189096 | MX: Chiapas, Tapalapa | X / X |
| 280 | *Basileuterus belli* | MVZ | 189097 | MX: Chiapas, Tapalapa | X / X |
| 281 | *Basileuterus belli* | MVZ | 189098 | MX: Chiapas, Tapalapa | X / X |
| 282 | *Basileuterus belli* | MVZ | 189099 | MX: Chiapas, Tapalapa | X / X |
| 283 | *Basileuterus belli* | MVZ | 184290 | GT: Huehuetenango, Yalambojoch | X / X |
| 284 | *Basileuterus belli* | MVZ | 184291 | GT: Huehuetenango, Yalambojoch | X / X |
| 285 | *Basileuterus belli* | MVZ | 184292 | GT: Huehuetenango, Yalambojoch | X / X |
| 286 | *Basileuterus belli* | MVZ | 184293 | GT: Huehuetenango, Yalambojoch | X / X |
| 287 | *Basileuterus belli* | MVZ | 184294 | GT: Huehuetenango, Yalambojoch | X / X |
| 288 | *Basileuterus belli* | MVZ | 184295 | GT: Huehuetenango, Yalambojoch | X / X |
| 289 | *Basileuterus belli* | MVZ | 184296 | GT: Huehuetenango, Yalambojoch | X / X |
| 290 | *Basileuterus belli* | MVZ | 184297 | GT: Huehuetenango, Yalambojoch | X / X |
| 291 | *Basileuterus belli* | MVZ | 184298 | GT: Huehuetenango, Yalambojoch | X / X |
| 292 | *Basileuterus belli* | MVZ | 184299 | GT: Huehuetenango, Yalambojoch | X / X |
| 293 | *Basileuterus belli* | MVZ | 189337 | GT: Huehuetenango, Soloma | X / X |
| 294 | *Basileuterus belli* | MVZ | 187544 | GT: Quiché, Uspantán | X / X |
| 295 | *Basileuterus belli* | MVZ | 187545 | GT: Quiché, Uspantán | X / X |
| 296 | *Basileuterus belli* | MVZ | 187546 | GT: Quiché, Uspantán | X / X |
| 297 | *Basileuterus belli* | MVZ | 187547 | GT: Quiché, Uspantán | X / X |
| 298 | *Basileuterus belli* | MVZ | 187548 | GT: Quiché, Uspantán | X / X |
| 299 | *Basileuterus belli* | MVZ | 187554 | GT: Alta Verapaz, San Pedro Carchá | X / X |
| 300 | *Basileuterus belli* | MVZ | 184768 | GT: Reserva de la Biosfera Sierra de las Minas | X / X |
| 301 | *Basileuterus belli* | MVZ | 184769 | GT: Reserva de la Biosfera Sierra de las Minas | X / X |
| 302 | *Basileuterus belli* | MVZ | 184770 | GT: Reserva de la Biosfera Sierra de las Minas | X / X |
| 303 | *Basileuterus belli* | MVZ | 184771 | GT: Reserva de la Biosfera Sierra de las Minas | X / X |
| 304 | *Basileuterus belli* | USAC | RAJ222 | GT: Baja Verapaz, Purulhá | X / X |
| 305 | *Basileuterus belli* | USAC | RAJ232 | GT: Baja Verapaz, Purulhá | X / X |
| 306 | *Basileuterus belli* | USAC | SH4 | GT: Baja Verapaz, Purulhá | X / X |
| 307 | *Basileuterus belli* | USAC | SH17 | GT: Baja Verapaz, Purulhá | X / X |
| 308 | *Basileuterus belli* | MVZ | 187549 | GT: Quiché, Zacualpa | X / X |
| 309 | *Basileuterus belli* | MVZ | 187550 | GT: Quiché, Zacualpa | X / X |
| 310 | *Basileuterus belli* | MVZ | 187551 | GT: Quiché, Zacualpa | X / X |

| | | | | | |
|---|---|---|---|---|---|
| 311 | *Basileuterus belli* | MVZ | 187552 | GT: Quiché, Zacualpa | X / X |
| 312 | *Basileuterus belli* | MVZ | 187553 | GT: Quiché, Zacualpa | X / X |
| 313 | *Basileuterus belli* | MVZ | 188209 | MX: Chiapas, Motozintla | X / X |
| 314 | *Basileuterus belli* | MVZ | 188210 | MX: Chiapas, Motozintla | X / X |
| 315 | *Basileuterus belli* | MVZ | 188211 | MX: Chiapas, Motozintla | X / X |
| 316 | *Basileuterus belli* | MVZ | 188212 | MX: Chiapas, Motozintla | X / X |
| 317 | *Basileuterus belli* | MVZ | 188213 | MX: Chiapas, Motozintla | X / X |
| 318 | *Basileuterus belli* | MVZ | 188214 | MX: Chiapas, Motozintla | X / X |
| 319 | *Basileuterus belli* | MVZ | 188215 | MX: Chiapas, Motozintla | X / X |
| 320 | *Basileuterus belli* | MVZ | 187717 | GT: Quetzaltenango, Volcán Zunil | X / X |
| 321 | *Basileuterus belli* | MVZ | 187718 | GT: Quetzaltenango, Volcán Zunil | X / X |
| 322 | *Basileuterus belli* | MVZ | 187719 | GT: Quetzaltenango, Volcán Zunil | X / X |
| 323 | *Basileuterus belli* | MVZ | 187720 | GT: Quetzaltenango, Volcán Zunil | X / X |
| 324 | *Basileuterus belli* | MVZ | 187721 | GT: Quetzaltenango, Volcán Zunil | X / X |
| 325 | *Basileuterus belli* | MVZ | 187722 | GT: Quetzaltenango, Volcán Zunil | X / X |
| 326 | *Basileuterus belli* | MVZ | 187723 | GT: Quetzaltenango, Volcán Zunil | X / X |
| 327 | *Basileuterus belli* | MVZ | 187724 | GT: Quetzaltenango, Volcán Zunil | X / X |
| 328 | *Basileuterus belli* | MVZ | 187212 | GT: Suchitepéquez, Volcán Atitlán | X / X |
| 329 | *Basileuterus belli* | MVZ | 187213 | GT: Suchitepéquez, Volcán Atitlán | X / X |
| 330 | *Basileuterus belli* | MVZ | 187214 | GT: Suchitepéquez, Volcán Atitlán | X / X |
| 331 | *Basileuterus belli* | KU | 109437 | ES: Santa Ana, Cerro Montecristo | X / X |
| 332 | *Basileuterus belli* | KU | 109447 | ES: Santa Ana, Cerro Montecristo | X / X |
| 333 | *Basileuterus belli* | KU | 109429 | ES: Santa Ana, Cerro Montecristo | X / X |
| 334 | *Basileuterus belli* | KU | 109435 | ES: Santa Ana, Cerro Montecristo | X / X |
| 335 | *Basileuterus belli* | YPM | 100403 | ES: Chalatenango | X / X |
| 336 | *Basileuterus belli* | YPM | 100492 | ES: Chalatenango | X / X |
| 337 | *Basileuterus melanogenys* | LSUMZ | 72166 | Outgroup | X / X |
| 338 | *Basileuterus rufifrons* | MVZ | 189336 | Outgroup | X / X |
| 339 | *Basileuterus lachrymosus* | MVZ | 187209 | Outgroup | X / X |
| 340 | *Setophaga nigrescens* | MVZ | 191379 | Outgroup | X / X |
| 341 | *Myioborus miniatus* | MVZ | 189351 | Outgroup | X / X |
| 342 | *Cardellina versicolor* | MVZ | 189342 | Outgroup | X / X |
| 343 | *Myioborus miniatus* | UWBM | 114400 | MX: Chihuahua | X / X |
| 344 | *Myioborus miniatus* | UWBM | 114290 | MX: Chihuahua | X / X |
| 345 | *Myioborus miniatus* | UWBM | 112405 | MX: Michoacán | X / X |
| 346 | *Myioborus miniatus* | UWBM | 115219 | MX: Michoacán | X / X |
| 347 | *Myioborus miniatus* | UWBM | 111875 | MX: Morelos | X / X |
| 348 | *Myioborus miniatus* | UWBM | 106878 | MX: Morelos | X / X |
| 349 | *Myioborus miniatus* | UWBM | 114574 | MX: Guerrero | X / X |
| 350 | *Myioborus miniatus* | UWBM | 114581 | MX: Guerrero | X / X |
| 351 | *Myioborus miniatus* | AMNH | DOT-16473 | MX: Oaxaca | X / X |
| 352 | *Myioborus miniatus* | AMNH | DOT-16519 | MX: Oaxaca | X / X |
| 353 | *Myioborus miniatus* | IBUNAM | PEP2919 | MX: Veracruz, Los Tuxtlas | X / X |
| 354 | *Myioborus miniatus* | IBUNAM | PEP2927 | MX: Veracruz, Los Tuxtlas | X / X |
| 355 | *Myioborus miniatus* | IBUNAM | PEP2308 | MX: Veracruz, Los Tuxtlas | X / X |
| 356 | *Myioborus miniatus* | IBUNAM | PEP2488 | MX: Veracruz, Los Tuxtlas | X / X |
| 357 | *Myioborus miniatus* | MVZ | 189102 | MX: Chiapas, Tapalapa | X / X |

| | | | | | |
|---|---|---|---|---|---|
| 358 | *Myioborus miniatus* | MVZ | 188222 | MX: Chiapas, Tila | X / X |
| 359 | *Myioborus miniatus* | AMNH | DOT-15686 | MX: Chiapas, Teopisca | X / X |
| 360 | *Myioborus miniatus* | AMNH | DOT-15709 | MX: Chiapas, Teopisca | X / X |
| 361 | *Myioborus miniatus* | AMNH | DOT-16297 | MX: Chiapas, Teopisca | X / X |
| 362 | *Myioborus miniatus* | AMNH | DOT-16427 | MX: Chiapas, Teopisca | X / X |
| 363 | *Myioborus miniatus* | MVZ | 184287 | GT: Huehuetenango, Yalambojoch | X / X |
| 364 | *Myioborus miniatus* | MVZ | 184288 | GT: Huehuetenango, Yalambojoch | X / X |
| 365 | *Myioborus miniatus* | MVZ | 184289 | GT: Huehuetenango, Yalambojoch | X / X |
| 366 | *Myioborus miniatus* | MVZ | 189345 | GT: Huehuetenango, Soloma | X / X |
| 367 | *Myioborus miniatus* | MVZ | 189346 | GT: Huehuetenango, Soloma | X / X |
| 368 | *Myioborus miniatus* | MVZ | 189347 | GT: Huehuetenango, Soloma | X / X |
| 369 | *Myioborus miniatus* | MVZ | 189348 | GT: Huehuetenango, Soloma | X / X |
| 370 | *Myioborus miniatus* | MVZ | 189349 | GT: Huehuetenango, Soloma | X / X |
| 371 | *Myioborus miniatus* | MVZ | 189350 | GT: Huehuetenango, Soloma | X / X |
| 372 | *Myioborus miniatus* | MVZ | 187537 | GT: Quiché, Uspantán | X / X |
| 373 | *Myioborus miniatus* | MVZ | 187538 | GT: Quiché, Uspantán | X / X |
| 374 | *Myioborus miniatus* | MVZ | 187539 | GT: Quiché, Uspantán | X / X |
| 375 | *Myioborus miniatus* | MVZ | 187540 | GT: Quiché, Uspantán | X / X |
| 376 | *Myioborus miniatus* | MVZ | 187528 | GT: Alta Verapaz, San Pedro Carchá | X / X |
| 377 | *Myioborus miniatus* | MVZ | 187529 | GT: Alta Verapaz, San Pedro Carchá | X / X |
| 378 | *Myioborus miniatus* | MVZ | 187530 | GT: Alta Verapaz, San Pedro Carchá | X / X |
| 379 | *Myioborus miniatus* | MVZ | 187531 | GT: Alta Verapaz, San Pedro Carchá | X / X |
| 380 | *Myioborus miniatus* | MVZ | 187532 | GT: Alta Verapaz, San Pedro Carchá | X / X |
| 381 | *Myioborus miniatus* | MVZ | 187533 | GT: Alta Verapaz, San Pedro Carchá | X / X |
| 382 | *Myioborus miniatus* | MVZ | 187534 | GT: Alta Verapaz, San Pedro Carchá | X / X |
| 383 | *Myioborus miniatus* | MVZ | 187535 | GT: Alta Verapaz, San Pedro Carchá | X / X |
| 384 | *Myioborus miniatus* | MVZ | 187536 | GT: Alta Verapaz, San Pedro Carchá | X / X |
| 385 | *Myioborus miniatus* | MVZ | 184766 | GT: Reserva de la Biosfera Sierra de las Minas | X / X |
| 386 | *Myioborus miniatus* | MVZ | 184767 | GT: Reserva de la Biosfera Sierra de las Minas | X / X |
| 387 | *Myioborus miniatus* | USAC | RAJ226 | GT: Baja Verapaz, Purulhá | X / X |
| 388 | *Myioborus miniatus* | USAC | RAJ254 | GT: Baja Verapaz, Purulhá | X / X |
| 389 | *Myioborus miniatus* | USAC | RAJ255 | GT: Baja Verapaz, Purulhá | X / X |
| 390 | *Myioborus miniatus* | USAC | ALAR15 | GT: Baja Verapaz, Purulhá | X / X |
| 391 | *Myioborus miniatus* | USAC | SH6 | GT: Baja Verapaz, Purulhá | X / X |
| 392 | *Myioborus miniatus* | MVZ | 187541 | GT: Quiché, Zacualpa | X / X |
| 393 | *Myioborus miniatus* | MVZ | 188223 | MX: Chiapas, Motozintla | X / X |
| 394 | *Myioborus miniatus* | MVZ | 188224 | MX: Chiapas, Motozintla | X / X |
| 395 | *Myioborus miniatus* | MVZ | 188225 | MX: Chiapas, Motozintla | X / X |
| 396 | *Myioborus miniatus* | MVZ | 188226 | MX: Chiapas, Motozintla | X / X |
| 397 | *Myioborus miniatus* | MVZ | 188227 | MX: Chiapas, Motozintla | X / X |
| 398 | *Myioborus miniatus* | MVZ | 188228 | MX: Chiapas, Motozintla | X / X |
| 399 | *Myioborus miniatus* | MVZ | 188229 | MX: Chiapas, Motozintla | X / X |
| 400 | *Myioborus miniatus* | MVZ | 188230 | MX: Chiapas, Motozintla | X / X |
| 401 | *Myioborus miniatus* | MVZ | 188231 | MX: Chiapas, Motozintla | X / X |
| 402 | *Myioborus miniatus* | MVZ | 187228 | GT: Quetzaltenango, Volcán Lacandón | X / X |
| 403 | *Myioborus miniatus* | MVZ | 187229 | GT: Quetzaltenango, Volcán Lacandón | X / X |
| 404 | *Myioborus miniatus* | MVZ | 187230 | GT: Quetzaltenango, Volcán Lacandón | X / X |

| | | | | | |
|---|---|---|---|---|---|
| 405 | *Myioborus miniatus* | MVZ | 187231 | GT: Quetzaltenango, Volcán Lacandón | X / X |
| 406 | *Myioborus miniatus* | MVZ | 187232 | GT: Quetzaltenango, Volcán Lacandón | X / X |
| 407 | *Myioborus miniatus* | MVZ | 187732 | GT: Quetzaltenango, Volcán Zunil | X / X |
| 408 | *Myioborus miniatus* | MVZ | 189351 | GT: Santa Rosa, Volcán Tecuamburro | X / X |
| 409 | *Myioborus miniatus* | MVZ | 189352 | GT: Santa Rosa, Volcán Tecuamburro | X / X |
| 410 | *Myioborus miniatus* | MVZ | 189353 | GT: Santa Rosa, Volcán Tecuamburro | X / X |
| 411 | *Myioborus miniatus* | MVZ | 189354 | GT: Santa Rosa, Volcán Tecuamburro | X / X |
| 412 | *Myioborus miniatus* | MVZ | 187731 | GT: Zacapa, La Unión | X / X |
| 413 | *Myioborus miniatus* | KU | 109425 | ES: Santa Ana, Cerro Montecristo | X / X |
| 414 | *Myioborus miniatus* | KU | 109440 | ES: Santa Ana, Cerro Montecristo | X / X |
| 415 | *Myioborus miniatus* | FMNH | 434204 | ES: Ahuachapán | X / X |
| 416 | *Myioborus miniatus* | FMNH | 434205 | ES: Ahuachapán | X / X |
| 417 | *Myioborus miniatus* | LSUMZ | 60982 | HO: Francisco Morazán | X / X |
| 418 | *Myioborus miniatus* | LSUMZ | 60955 | HO: Francisco Morazán | X / X |
| 419 | *Myioborus miniatus* | LSUMZ | 27304 | Costa Rica | X / X |
| 420 | *Myioborus torquatus* | LSUMZ | 19945 | Costa Rica | X / X |
| 421 | *Myioborus miniatus* | LSUMZ | 28175 | Panamá | X / X |
| 422 | *Myioborus miniatus* | LSUMZ | 29046 | Panamá | X / X |
| 423 | *Myioborus miniatus* | LSUMZ | 26421 | Panamá | X / X |
| 424 | *Myioborus miniatus* | MVZ | 169694 | Perú | X / X |
| 425 | *Myioborus miniatus* | FMNH | 474614 | Perú | X / X |
| 426 | *Myioborus pictus* | MSB | 41158 | Outgroup | X / X |
| 427 | *Cardellina versicolor* | MVZ | 189342 | Outgroup | X / X |
| 428 | *Basileuterus belli* | MVZ | 184770 | Outgroup | X / X |
| 429 | *Chlorospingus flavopectus* | UWBM | 82870 | MX: Hidalgo | - / X |
| 430 | *Chlorospingus flavopectus* | UWBM | 82906 | MX: Hidalgo | - / X |
| 431 | *Chlorospingus flavopectus* | FMNH | 346816 | MX: Oaxaca, Totontepec | X / X |
| 432 | *Chlorospingus flavopectus* | FMNH | 346815 | MX: Oaxaca, Totontepec | X / X |
| 433 | *Chlorospingus flavopectus* | UWBM | 118488 | MX: Guerrero | X / X |
| 434 | *Chlorospingus flavopectus* | UWBM | 118489 | MX: Guerrero | X / X |
| 435 | *Chlorospingus flavopectus* | UWBM | 112984 | MX: Oaxaca, Pochutla | X / X |
| 436 | *Chlorospingus flavopectus* | UWBM | 112985 | MX: Oaxaca, Pochutla | X / X |
| 437 | *Chlorospingus flavopectus* | UAM | 20758 | MX: Veracruz, Los Tuxtlas | X / X |
| 438 | *Chlorospingus flavopectus* | IBUNAM | PEP2273 | MX: Veracruz, Los Tuxtlas | X / X |
| 439 | *Chlorospingus flavopectus* | IBUNAM | PEP2473 | MX: Veracruz, Los Tuxtlas | X / X |
| 440 | *Chlorospingus flavopectus* | IBUNAM | PEP2631 | MX: Veracruz, Los Tuxtlas | X / X |
| 441 | *Chlorospingus flavopectus* | IBUNAM | PEP2680 | MX: Veracruz, Los Tuxtlas | X / X |
| 442 | *Chlorospingus flavopectus* | MVZ | 189113 | MX: Chiapas, Tapalapa | X / X |
| 443 | *Chlorospingus flavopectus* | MVZ | 189114 | MX: Chiapas, Tapalapa | X / X |
| 444 | *Chlorospingus flavopectus* | MVZ | 189115 | MX: Chiapas, Tapalapa | X / X |
| 445 | *Chlorospingus flavopectus* | MVZ | 189116 | MX: Chiapas, Tapalapa | X / X |
| 446 | *Chlorospingus flavopectus* | MVZ | 189117 | MX: Chiapas, Tapalapa | X / X |
| 447 | *Chlorospingus flavopectus* | MVZ | 189118 | MX: Chiapas, Tapalapa | X / X |
| 448 | *Chlorospingus flavopectus* | MVZ | 188271 | MX: Chiapas, Tila | X / X |
| 449 | *Chlorospingus flavopectus* | MVZ | 188272 | MX: Chiapas, Tila | X / X |
| 450 | *Chlorospingus flavopectus* | MVZ | 188273 | MX: Chiapas, Tila | X / X |
| 451 | *Chlorospingus flavopectus* | MVZ | 184275 | GT: Huehuetenango, Yalambojoch | X / X |

| | | | | | |
|---|---|---|---|---|---|
| 452 | *Chlorospingus flavopectus* | MVZ | 184276 | GT: Huehuetenango, Yalambojoch | X / X |
| 453 | *Chlorospingus flavopectus* | MVZ | 184277 | GT: Huehuetenango, Yalambojoch | X / X |
| 454 | *Chlorospingus flavopectus* | MVZ | 184278 | GT: Huehuetenango, Yalambojoch | X / X |
| 455 | *Chlorospingus flavopectus* | MVZ | 184279 | GT: Huehuetenango, Yalambojoch | X / X |
| 456 | *Chlorospingus flavopectus* | MVZ | 184280 | GT: Huehuetenango, Yalambojoch | X / X |
| 457 | *Chlorospingus flavopectus* | MVZ | 184281 | GT: Huehuetenango, Yalambojoch | X / X |
| 458 | *Chlorospingus flavopectus* | MVZ | 184282 | GT: Huehuetenango, Yalambojoch | X / X |
| 459 | *Chlorospingus flavopectus* | MVZ | 189391 | GT: Huehuetenango, Soloma | X / X |
| 460 | *Chlorospingus flavopectus* | MVZ | 189392 | GT: Huehuetenango, Soloma | X / X |
| 461 | *Chlorospingus flavopectus* | MVZ | 189393 | GT: Huehuetenango, Soloma | X / X |
| 462 | *Chlorospingus flavopectus* | MVZ | 189394 | GT: Huehuetenango, Soloma | X / X |
| 463 | *Chlorospingus flavopectus* | MVZ | 189395 | GT: Huehuetenango, Soloma | X / X |
| 464 | *Chlorospingus flavopectus* | MVZ | 189396 | GT: Huehuetenango, Soloma | X / X |
| 465 | *Chlorospingus flavopectus* | MVZ | 189397 | GT: Huehuetenango, Soloma | X / X |
| 466 | *Chlorospingus flavopectus* | MVZ | 189398 | GT: Huehuetenango, Soloma | X / X |
| 467 | *Chlorospingus flavopectus* | MVZ | 189399 | GT: Huehuetenango, Soloma | X / X |
| 468 | *Chlorospingus flavopectus* | MVZ | 189400 | GT: Huehuetenango, Soloma | X / X |
| 469 | *Chlorospingus flavopectus* | MVZ | 189401 | GT: Huehuetenango, Soloma | X / X |
| 470 | *Chlorospingus flavopectus* | MVZ | 189402 | GT: Huehuetenango, Soloma | X / X |
| 471 | *Chlorospingus flavopectus* | MVZ | 187579 | GT: Quiché, Uspantán | X / X |
| 472 | *Chlorospingus flavopectus* | MVZ | 187580 | GT: Quiché, Uspantán | X / X |
| 473 | *Chlorospingus flavopectus* | MVZ | 187581 | GT: Quiché, Uspantán | X / X |
| 474 | *Chlorospingus flavopectus* | MVZ | 187582 | GT: Quiché, Uspantán | X / X |
| 475 | *Chlorospingus flavopectus* | MVZ | 187583 | GT: Quiché, Uspantán | X / X |
| 476 | *Chlorospingus flavopectus* | MVZ | 187584 | GT: Quiché, Uspantán | X / X |
| 477 | *Chlorospingus flavopectus* | MVZ | 187585 | GT: Quiché, Uspantán | X / X |
| 478 | *Chlorospingus flavopectus* | MVZ | 187586 | GT: Quiché, Uspantán | X / X |
| 479 | *Chlorospingus flavopectus* | MVZ | 187587 | GT: Quiché, Uspantán | X / X |
| 480 | *Chlorospingus flavopectus* | MVZ | 187599 | GT: Alta Verapaz, San Pedro Carchá | X / X |
| 481 | *Chlorospingus flavopectus* | MVZ | 187600 | GT: Alta Verapaz, San Pedro Carchá | X / X |
| 482 | *Chlorospingus flavopectus* | MVZ | 187601 | GT: Alta Verapaz, San Pedro Carchá | X / X |
| 483 | *Chlorospingus flavopectus* | MVZ | 187602 | GT: Alta Verapaz, San Pedro Carchá | X / X |
| 484 | *Chlorospingus flavopectus* | MVZ | 184776 | GT: Reserva de la Biosfera Sierra de las Minas | X / X |
| 485 | *Chlorospingus flavopectus* | MVZ | 184777 | GT: Reserva de la Biosfera Sierra de las Minas | X / X |
| 486 | *Chlorospingus flavopectus* | USAC | RAJ220 | GT: Baja Verapaz, Purulhá | X / X |
| 487 | *Chlorospingus flavopectus* | USAC | RAJ229 | GT: Baja Verapaz, Purulhá | X / X |
| 488 | *Chlorospingus flavopectus* | USAC | RAJ231 | GT: Baja Verapaz, Purulhá | X / X |
| 489 | *Chlorospingus flavopectus* | USAC | RAJ256 | GT: Baja Verapaz, Purulhá | X / X |
| 490 | *Chlorospingus flavopectus* | USAC | RAJ257 | GT: Baja Verapaz, Purulhá | X / X |
| 491 | *Chlorospingus flavopectus* | USAC | AJRC2 | GT: Baja Verapaz, Purulhá | X / X |
| 492 | *Chlorospingus flavopectus* | USAC | ALAR20 | GT: Baja Verapaz, Purulhá | X / X |
| 493 | *Chlorospingus flavopectus* | USAC | SH5 | GT: Baja Verapaz, Purulhá | X / X |
| 494 | *Chlorospingus flavopectus* | USAC | SH9 | GT: Baja Verapaz, Purulhá | X / X |
| 495 | *Chlorospingus flavopectus* | USAC | SH13 | GT: Baja Verapaz, Purulhá | X / X |
| 496 | *Chlorospingus flavopectus* | USAC | SH14 | GT: Baja Verapaz, Purulhá | X / X |
| 497 | *Chlorospingus flavopectus* | USAC | SH23 | GT: Baja Verapaz, Purulhá | X / X |
| 498 | *Chlorospingus flavopectus* | MVZ | 187588 | GT: Quiché, Zacualpa | X / X |

| | | | | | |
|---|---|---|---|---|---|
| 499 | *Chlorospingus flavopectus* | MVZ | 187589 | GT: Quiché, Zacualpa | X / X |
| 500 | *Chlorospingus flavopectus* | MVZ | 187590 | GT: Quiché, Zacualpa | X / X |
| 501 | *Chlorospingus flavopectus* | MVZ | 187591 | GT: Quiché, Zacualpa | X / X |
| 502 | *Chlorospingus flavopectus* | MVZ | 187592 | GT: Quiché, Zacualpa | X / X |
| 503 | *Chlorospingus flavopectus* | MVZ | 187593 | GT: Quiché, Zacualpa | X / X |
| 504 | *Chlorospingus flavopectus* | MVZ | 187594 | GT: Quiché, Zacualpa | X / X |
| 505 | *Chlorospingus flavopectus* | MVZ | 187595 | GT: Quiché, Zacualpa | X / X |
| 506 | *Chlorospingus flavopectus* | MVZ | 187596 | GT: Quiché, Zacualpa | X / X |
| 507 | *Chlorospingus flavopectus* | MVZ | 187597 | GT: Quiché, Zacualpa | X / X |
| 508 | *Chlorospingus flavopectus* | MVZ | 187598 | GT: Quiché, Zacualpa | X / X |
| 509 | *Chlorospingus flavopectus* | MVZ | 188274 | MX: Chiapas, Motozintla | X / X |
| 510 | *Chlorospingus flavopectus* | MVZ | 188275 | MX: Chiapas, Motozintla | X / X |
| 511 | *Chlorospingus flavopectus* | MVZ | 188276 | MX: Chiapas, Motozintla | X / X |
| 512 | *Chlorospingus flavopectus* | MVZ | 188277 | MX: Chiapas, Motozintla | X / X |
| 513 | *Chlorospingus flavopectus* | MVZ | 188278 | MX: Chiapas, Motozintla | X / X |
| 514 | *Chlorospingus flavopectus* | MVZ | 188279 | MX: Chiapas, Motozintla | X / X |
| 515 | *Chlorospingus flavopectus* | MVZ | 188280 | MX: Chiapas, Motozintla | X / X |
| 516 | *Chlorospingus flavopectus* | MVZ | 188281 | MX: Chiapas, Motozintla | X / X |
| 517 | *Chlorospingus flavopectus* | MVZ | 188282 | MX: Chiapas, Motozintla | X / X |
| 518 | *Chlorospingus flavopectus* | MVZ | 188283 | MX: Chiapas, Motozintla | X / X |
| 519 | *Chlorospingus flavopectus* | MVZ | 188284 | MX: Chiapas, Motozintla | X / X |
| 520 | *Chlorospingus flavopectus* | MVZ | 188285 | MX: Chiapas, Motozintla | X / X |
| 521 | *Chlorospingus flavopectus* | MVZ | 188286 | MX: Chiapas, Motozintla | X / X |
| 522 | *Chlorospingus flavopectus* | MVZ | 188287 | MX: Chiapas, Motozintla | X / X |
| 523 | *Chlorospingus flavopectus* | MVZ | 188288 | MX: Chiapas, Motozintla | X / X |
| 524 | *Chlorospingus flavopectus* | MVZ | 188289 | MX: Chiapas, Motozintla | X / X |
| 525 | *Chlorospingus flavopectus* | MVZ | 188290 | MX: Chiapas, Motozintla | X / X |
| 526 | *Chlorospingus flavopectus* | MVZ | 188291 | MX: Chiapas, Motozintla | X / X |
| 527 | *Chlorospingus flavopectus* | MVZ | 187238 | GT: Quetzaltenango, Volcán Lacandón | X / X |
| 528 | *Chlorospingus flavopectus* | MVZ | 187239 | GT: Quetzaltenango, Volcán Lacandón | X / X |
| 529 | *Chlorospingus flavopectus* | MVZ | 187240 | GT: Quetzaltenango, Volcán Lacandón | X / X |
| 530 | *Chlorospingus flavopectus* | MVZ | 187241 | GT: Quetzaltenango, Volcán Lacandón | X / X |
| 531 | *Chlorospingus flavopectus* | MVZ | 187242 | GT: Quetzaltenango, Volcán Lacandón | X / X |
| 532 | *Chlorospingus flavopectus* | MVZ | 187243 | GT: Quetzaltenango, Volcán Lacandón | X / X |
| 533 | *Chlorospingus flavopectus* | MVZ | 187244 | GT: Quetzaltenango, Volcán Lacandón | X / X |
| 534 | *Chlorospingus flavopectus* | MVZ | 187245 | GT: Quetzaltenango, Volcán Lacandón | X / X |
| 535 | *Chlorospingus flavopectus* | MVZ | 187246 | GT: Quetzaltenango, Volcán Lacandón | X / X |
| 536 | *Chlorospingus flavopectus* | MVZ | 187247 | GT: Quetzaltenango, Volcán Lacandón | X / X |
| 537 | *Chlorospingus flavopectus* | MVZ | 187248 | GT: Quetzaltenango, Volcán Lacandón | X / X |
| 538 | *Chlorospingus flavopectus* | MVZ | 187249 | GT: Quetzaltenango, Volcán Lacandón | X / X |
| 539 | *Chlorospingus flavopectus* | MVZ | 187250 | GT: Quetzaltenango, Volcán Lacandón | X / X |
| 540 | *Chlorospingus flavopectus* | MVZ | 187745 | GT: Quetzaltenango, Volcán Zunil | X / X |
| 541 | *Chlorospingus flavopectus* | MVZ | 187746 | GT: Quetzaltenango, Volcán Zunil | X / X |
| 542 | *Chlorospingus flavopectus* | MVZ | 187747 | GT: Quetzaltenango, Volcán Zunil | X / X |
| 543 | *Chlorospingus flavopectus* | MVZ | 187748 | GT: Quetzaltenango, Volcán Zunil | X / X |
| 544 | *Chlorospingus flavopectus* | MVZ | 187749 | GT: Quetzaltenango, Volcán Zunil | X / X |
| 545 | *Chlorospingus flavopectus* | MVZ | 187750 | GT: Quetzaltenango, Volcán Zunil | X / X |

| | | | | | |
|---|---|---|---|---|---|
| 546 | *Chlorospingus flavopectus* | MVZ | 187751 | GT: Quetzaltenango, Volcán Zunil | X / X |
| 547 | *Chlorospingus flavopectus* | MVZ | 187752 | GT: Quetzaltenango, Volcán Zunil | X / X |
| 548 | *Chlorospingus flavopectus* | MVZ | 187753 | GT: Zacapa, La Unión | X / X |
| 549 | *Chlorospingus flavopectus* | MVZ | 187754 | GT: Zacapa, La Unión | X / X |
| 550 | *Chlorospingus flavopectus* | MVZ | 187755 | GT: Zacapa, La Unión | X / X |
| 551 | *Chlorospingus flavopectus* | MVZ | 187756 | GT: Zacapa, La Unión | X / X |
| 552 | *Chlorospingus flavopectus* | MVZ | 187757 | GT: Zacapa, La Unión | X / X |
| 553 | *Chlorospingus flavopectus* | MVZ | 187758 | GT: Zacapa, La Unión | X / X |
| 554 | *Chlorospingus flavopectus* | MVZ | 187759 | GT: Zacapa, La Unión | X / X |
| 555 | *Chlorospingus flavopectus* | MVZ | 187760 | GT: Zacapa, La Unión | X / X |
| 556 | *Chlorospingus flavopectus* | KU | 109456 | ES: Santa Ana, Cerro Montecristo | X / X |
| 557 | *Chlorospingus flavopectus* | KU | 109457 | ES: Santa Ana, Cerro Montecristo | X / X |
| 558 | *Chlorospingus flavopectus* | KU | 93858 | ES: Chalatenango | X / X |
| 559 | *Chlorospingus flavopectus* | KU | 93868 | ES: Chalatenango | X / X |
| 560 | *Chlorospingus flavopectus* | UWBM | 105630 | HO: Copán | X / X |
| 561 | *Chlorospingus flavopectus* | UWBM | 114696 | HO: Copán | X / X |
| 562 | *Chlorospingus flavopectus* | UWBM | 102048 | HO: Atlántida | X / X |
| 563 | *Chlorospingus flavopectus* | UWBM | 109590 | HO: Atlántida | X / X |
| 564 | *Chlorospingus flavopectus* | LSUMZ | 60958 | HO: Cerro Uyuca | X / X |
| 565 | *Chlorospingus flavopectus* | LSUMZ | 60960 | HO: Cerro Uyuca | X / X |
| 566 | *Chlorospingus flavopectus* | LSUMZ | 60964 | HO: Cerro Uyuca | X / X |
| 567 | *Chlorospingus flavopectus* | LSUMZ | 60972 | HO: Cerro Uyuca | X / X |
| 568 | *Chlorospingus flavopectus* | FMNH | 481664 | NI: Estelí | X / X |
| 569 | *Chlorospingus flavopectus* | FMNH | 481662 | NI: Estelí | X / X |
| 570 | *Chlorospingus flavopectus* | FMNH | 481663 | NI: Estelí | X / X |
| 571 | *Chlorospingus flavopectus* | FMNH | 481665 | NI: Estelí | X / X |
| 572 | *Chlorospingus flavopectus* | LSUMZ | 81947 | Costa Rica | X / X |
| 573 | *Chlorospingus flavopectus* | LSUMZ | 81954 | Costa Rica | X / X |
| 574 | *Chlorospingus flavopectus* | LSUMZ | 28158 | Panamá | X / X |
| 575 | *Chlorospingus flavopectus* | LSUMZ | 28177 | Panamá | X / X |
| 576 | *Chlorospingus flavopectus* | FMNH | 474466 | Perú | X / X |
| 577 | *Chlorospingus flavopectus* | AMNH | DOT-2818 | Bolivia | X / X |
| 578 | *Chlorospingus flavopectus* | AMNH | DOT-2803 | Bolivia | X / X |
| 579 | *Chlorospingus tacarcuna* | AMNH | DOT-17050 | Outgroup | X / X |
| 580 | *Chlorospingus pileatus* | CUMV | 50566 | Outgroup | X / X |
| 581 | *Arremon brunneinucha* | UWBM | 82863 | MX: Hidalgo, Tlanchinol | X / X |
| 582 | *Arremon brunneinucha* | UWBM | 82877 | MX: Hidalgo, Tlanchinol | X / X |
| 583 | *Arremon virenticeps* | UWBM | 113665 | MX: Morelos | X / X |
| 584 | *Arremon virenticeps* | UWBM | 115156 | MX: Michoacán | X / X |
| 585 | *Arremon brunneinucha* | FMNH | 394026 | MX: Guerrero, El Iris | X / X |
| 586 | *Arremon brunneinucha* | FMNH | 394152 | MX: Guerrero, El Iris | X / X |
| 587 | *Arremon brunneinucha* | FMNH | 393773 | MX: Oaxaca, Totontepec | X / X |
| 588 | *Arremon brunneinucha* | FMNH | 393766 | MX: Oaxaca, Totontepec | X / X |
| 589 | *Arremon brunneinucha* | UWBM | 113012 | MX: Oaxaca, Pochutla | X / X |
| 590 | *Arremon brunneinucha* | UWBM | 118947 | MX: Oaxaca, Pochutla | X / X |
| 591 | *Arremon brunneinucha* | FMNH | 393870 | MX: Veracruz, Los Tuxtlas | X / X |
| 592 | *Arremon brunneinucha* | FMNH | 393763 | MX: Veracruz, Los Tuxtlas | X / X |

| | | | | | |
|---|---|---|---|---|---|
| 593 | *Arremon brunneinucha* | IBUNAM | PEP2442 | MX: Veracruz, Los Tuxtlas | X / X |
| 594 | *Arremon brunneinucha* | IBUNAM | PEP2866 | MX: Veracruz, Los Tuxtlas | X / X |
| 595 | *Arremon brunneinucha* | IBUNAM | PRZ10-6 | MX: Veracruz, Los Tuxtlas | X / X |
| 596 | *Arremon brunneinucha* | IBUNAM | PRZ10-34 | MX: Veracruz, Los Tuxtlas | X / X |
| 597 | *Arremon brunneinucha* | MVZ | 189119 | MX: Oaxaca, Cintalapa de Figueroa | X / X |
| 598 | *Arremon brunneinucha* | MVZ | 189120 | MX: Chiapas, Tapalapa | X / X |
| 599 | *Arremon brunneinucha* | MVZ | 189121 | MX: Chiapas, Tapalapa | X / X |
| 600 | *Arremon brunneinucha* | MVZ | 189122 | MX: Chiapas, Tapalapa | X / X |
| 601 | *Arremon brunneinucha* | MVZ | 184267 | GT: Huehuetenango, Yalambojoch | X / X |
| 602 | *Arremon brunneinucha* | MVZ | 184268 | GT: Huehuetenango, Yalambojoch | X / X |
| 603 | *Arremon brunneinucha* | MVZ | 184269 | GT: Huehuetenango, Yalambojoch | X / X |
| 604 | *Arremon brunneinucha* | MVZ | 184270 | GT: Huehuetenango, Yalambojoch | X / X |
| 605 | *Arremon brunneinucha* | MVZ | 184271 | GT: Huehuetenango, Yalambojoch | X / X |
| 606 | *Arremon brunneinucha* | MVZ | 189360 | GT: Huehuetenango, Soloma | X / X |
| 607 | *Arremon brunneinucha* | MVZ | 189361 | GT: Huehuetenango, Soloma | X / X |
| 608 | *Arremon brunneinucha* | MVZ | 189362 | GT: Huehuetenango, Soloma | X / X |
| 609 | *Arremon brunneinucha* | MVZ | 189363 | GT: Huehuetenango, Soloma | X / X |
| 610 | *Arremon brunneinucha* | MVZ | 189364 | GT: Huehuetenango, Soloma | X / X |
| 611 | *Arremon brunneinucha* | MVZ | 189365 | GT: Huehuetenango, Soloma | X / X |
| 612 | *Arremon brunneinucha* | MVZ | 187570 | GT: Quiché, Uspantán | X / X |
| 613 | *Arremon brunneinucha* | MVZ | 187571 | GT: Quiché, Uspantán | X / X |
| 614 | *Arremon brunneinucha* | MVZ | 187572 | GT: Quiché, Uspantán | X / X |
| 615 | *Arremon brunneinucha* | MVZ | 187573 | GT: Alta Verapaz, San Pedro Carchá | X / X |
| 616 | *Arremon brunneinucha* | MVZ | 184772 | GT: Reserva de la Biósfera Sierra de las Minas | X / X |
| 617 | *Arremon brunneinucha* | MVZ | 184773 | GT: Reserva de la Biósfera Sierra de las Minas | X / X |
| 618 | *Arremon brunneinucha* | MVZ | 184774 | GT: Reserva de la Biósfera Sierra de las Minas | X / X |
| 619 | *Arremon brunneinucha* | MVZ | 184775 | GT: Reserva de la Biósfera Sierra de las Minas | X / X |
| 620 | *Arremon brunneinucha* | USAC | RAJ228 | GT: Baja Verapaz, Purulhá | X / X |
| 621 | *Arremon brunneinucha* | USAC | RAJ249 | GT: Baja Verapaz, Purulhá | X / X |
| 622 | *Arremon brunneinucha* | USAC | RAJ250 | GT: Baja Verapaz, Purulhá | X / X |
| 623 | *Arremon brunneinucha* | USAC | RAJ252 | GT: Baja Verapaz, Purulhá | X / X |
| 624 | *Arremon brunneinucha* | USAC | RAJ259 | GT: Baja Verapaz, Purulhá | X / - |
| 625 | *Arremon brunneinucha* | USAC | ALAR19 | GT: Baja Verapaz, Purulhá | X / X |
| 626 | *Arremon brunneinucha* | USAC | AJRC4 | GT: Baja Verapaz, Purulhá | X / X |
| 627 | *Arremon brunneinucha* | MVZ | 188243 | MX: Chiapas, Motozintla | X / X |
| 628 | *Arremon brunneinucha* | MVZ | 188244 | MX: Chiapas, Motozintla | X / X |
| 629 | *Arremon brunneinucha* | MVZ | 188245 | MX: Chiapas, Motozintla | X / X |
| 630 | *Arremon brunneinucha* | MVZ | 188246 | MX: Chiapas, Motozintla | X / X |
| 631 | *Arremon brunneinucha* | MVZ | 188247 | MX: Chiapas, Motozintla | X / X |
| 632 | *Arremon brunneinucha* | MVZ | 188248 | MX: Chiapas, Motozintla | X / X |
| 633 | *Arremon brunneinucha* | MVZ | 188249 | MX: Chiapas, Motozintla | X / X |
| 634 | *Arremon brunneinucha* | MVZ | 187234 | GT: Quetzaltenango, Volcán Lacandón | X / X |
| 635 | *Arremon brunneinucha* | MVZ | 187735 | GT: Quetzaltenango, Volcán Zunil | X / X |
| 636 | *Arremon brunneinucha* | MVZ | 187736 | GT: Quetzaltenango, Volcán Zunil | X / X |
| 637 | *Arremon brunneinucha* | MVZ | 187737 | GT: Quetzaltenango, Volcán Zunil | X / X |
| 638 | *Arremon brunneinucha* | MVZ | 187738 | GT: Quetzaltenango, Volcán Zunil | X / X |
| 639 | *Arremon brunneinucha* | MVZ | 187739 | GT: Quetzaltenango, Volcán Zunil | X / X |

| | | | | | |
|---|---|---|---|---|---|
| 640 | *Arremon brunneinucha* | MVZ | 187235 | GT: Suchitepéquez, Volcán Atitlán | X / X |
| 641 | *Arremon brunneinucha* | MVZ | 187236 | GT: Suchitepéquez, Volcán Atitlán | X / X |
| 642 | *Arremon brunneinucha* | MVZ | 187237 | GT: Suchitepéquez, Volcán Atitlán | X / X |
| 643 | *Arremon brunneinucha* | MVZ | 187740 | GT: Zacapa, La Unión | X / X |
| 644 | *Arremon brunneinucha* | MVZ | 187741 | GT: Zacapa, La Unión | X / X |
| 645 | *Arremon brunneinucha* | MVZ | 187742 | GT: Zacapa, La Unión | X / X |
| 646 | *Arremon brunneinucha* | MVZ | 187743 | GT: Zacapa, La Unión | X / X |
| 647 | *Arremon brunneinucha* | MVZ | 187744 | GT: Zacapa, La Unión | X / X |
| 648 | *Arremon brunneinucha* | KU | 109451 | ES: Santa Ana, Cerro Montecristo | X / X |
| 649 | *Arremon brunneinucha* | KU | 109459 | ES: Santa Ana, Cerro Montecristo | X / X |
| 650 | *Arremon brunneinucha* | KU | 109469 | ES: Santa Ana, Cerro Montecristo | X / X |
| 651 | *Arremon brunneinucha* | KU | 109837 | ES: Santa Ana, Cerro Montecristo | X / - |
| 652 | *Arremon brunneinucha* | KU | 95314 | ES: San Vicente, Volcán San Vicente | X / - |
| 653 | *Arremon brunneinucha* | KU | 95492 | ES: San Vicente, Volcán San Vicente | X / - |
| 654 | *Arremon brunneinucha* | KU | 95315 | ES: San Vicente, Volcán San Vicente | X / - |
| 655 | *Arremon brunneinucha* | KU | 95396 | ES: San Vicente, Volcán San Vicente | X / - |
| 656 | *Arremon brunneinucha* | CUMV | 57177 | HO: El Paraíso | X / X |
| 657 | *Arremon brunneinucha* | LSUMZ | 60988 | HO: Uyuca | X / X |
| 658 | *Arremon brunneinucha* | LSUMZ | 60987 | HO: Uyuca | X / X |
| 659 | *Arremon brunneinucha* | FMNH | 481775 | NI: Estelí | X / X |
| 660 | *Arremon brunneinucha* | FMNH | 481660 | NI: Estelí | X / X |
| 661 | *Arremon brunneinucha* | FMNH | 481657 | NI: Estelí | X / X |
| 662 | *Arremon brunneinucha* | FMNH | 481658 | NI: Estelí | X / X |
| 663 | *Arremon brunneinucha* | UWBM | 69090 | NI: Granada | X / X |
| 664 | *Arremon brunneinucha* | UWBM | 69092 | NI: Granada | X / X |
| 665 | *Arremon brunneinucha* | UWBM | 69131 | NI: Granada | X / X |
| 666 | *Arremon brunneinucha* | UWBM | 69408 | NI: Granada | X / X |
| 667 | *Arremon brunneinucha* | LSUMZ | 72032 | Costa Rica | X / X |
| 668 | *Arremon brunneinucha* | LSUMZ | 16053 | Costa Rica | X / X |
| 669 | *Arremon brunneinucha* | LSUMZ | 28316 | Panamá | X / X |
| 670 | *Arremon brunneinucha* | LSUMZ | 28322 | Panamá | X / X |
| 671 | *Arremon brunneinucha* | MSB | 41807 | Perú | X / X |
| 672 | *Arremon brunneinucha* | MSB | 41984 | Perú | X / X |
| 673 | *Arremon torquatus* | MSB | 42559 | Outgroup | X / X |
| 674 | *Arremon aurantiirostris* | MVZ | 188242 | Outgroup | X / X |
| 675 | *Pipilo chlorurus* | MVZ | 182530 | Outgroup | X / X |
| 676 | *Spizella passerina* | MVZ | 182532 | Outgroup | X / X |

**Table S2.** Effective coverage for the ddRAD datasets of montane birds of Nuclear Central America.

| Species (dataset) | Initial number of individuals | Final number of individuals (after filtering) | Effective per-sample coverage | | Mean number of sites per locus |
|---|---|---|---|---|---|
| | | | Mean (stdev) | Range | |
| *Lampornis viridipallens – L. sybillae* | 164 | 139 | 106.0x (40.8x) | 20.9x – 267.9x | 206.8 |
| *Henicorhina leucophrys* | 83 | 81 | 74.2x (19.7x) | 35.4x – 123.7x | 250.1 |
| *Basileuterus belli* | 89 | 89 | 74.4x (20.4x) | 38.0x – 129.7x | 213.8 |
| *Myioborus miniatus* | 85 | 82 | 50.3x (47.2x) | 15.6x – 193.9x | 243.6 |
| *Chlorospingus flavopectus* | 152 | 151 | 69.7x (57.2x) | 18.5x – 247.9x | 228.9 |
| *Arremon brunneinucha* | 91 | 88 | 60.7x (26.0x) | 21.8x – 135.7x | 239.4 |

**Table S3.** Total number of unlinked SNPs used in phylogenetic and genetic structure analyses of montane birds of Nuclear Central America.

| Species (dataset) | Phylogenetic analysis | | Genetic structure analysis | |
|---|---|---|---|---|
| | Number of individuals | Number of SNPs | Number of individuals | Number of SNPs |
| *Lampornis viridipallens – L. sybillae* | 139 | 10,617 | 137 | 10,460 |
| *Henicorhina leucophrys* | 81 | 12,102 | 76 | 13,308 |
| *Basileuterus belli* | 89 | 14,309 | 86 | 14,828 |
| *Myioborus miniatus* | 82 | 17,849 | 78 | 18,395 |
| *Chlorospingus flavopectus* | 151 | 14,635 | 146 | 14,643 |
| *Arremon brunneinucha* | 88 | 9,364 | 83 | 10,382 |